DESIGN AND DEVELOPMENT OF HIGHLY EFFICIENT NANO FLUIDIC FLAT PLATE SOLAR COLLECTOR

KANIZ FARHANA

DOCTOR OF PHILOSOPHY

UNIVERSITI MALAYSIA PAHANG

UNIVERSITI MALAYSIA PAHANG

DECLARATION OF THESIS AND COPYRIGHT

Author's Full Name : KANIZ FARHANA

Date of Birth : 30TH OCTOBER 1983

Title : DESIGN AND DEVELOPMENT OF HIGHLY EFFICIENT NANO FLUIDIC FLAT PLATE SOLAR COLLECTOR

Academic Session : SEM 1 2019/2020

I declare that this thesis is classified as:

- ☐ CONFIDENTIAL (Contains confidential information under the Official Secret Act 1997)*
- ☐ RESTRICTED (Contains restricted information as specified by the organization where research was done)*
- ☑ OPEN ACCESS I agree that my thesis to be published as online open access (Full Text)

I acknowledge that Universiti Malaysia Pahang reserves the following rights:

1. The Thesis is the Property of Universiti Malaysia Pahang
2. The Library of Universiti Malaysia Pahang has the right to make copies of the thesis for the purpose of research only.
3. The Library has the right to make copies of the thesis for academic exchange.

Certified by:

_____ _____

(Student's Signature) (Supervisor's Signature)

BL0075009 ASSOC. PROF. DR. KUMARAN KADIRGAMA

_____ _____

New IC/Passport Number Name of Supervisor
Date: Date:

NOTE : * If the thesis is CONFIDENTIAL or RESTRICTED, please attach a thesis declaration letter.

SUPERVISOR'S DECLARATION

I hereby declare that I have checked this thesis and in my opinion, this thesis is adequate in terms of scope and quality for the award of Doctor of Philosophy.

_____

(Supervisor's Signature)

Full Name   : TS. DR. KUMARAN KADIRGAMA

Position   : ASSOCIATE PROFESSOR

Date   :

_____

(Co-supervisor's Signature)

Full Name   : TS. DR. MUHAMAD BIN MAT NOOR

Position   : SENIOR LECTURER

Date   :

STUDENT'S DECLARATION

I hereby declare that the work in this thesis is based on my original work except for quotations and citations which have been duly acknowledged. I also declare that it has not been previously or concurrently submitted for any other degree at Universiti Malaysia Pahang or any other institutions.

_____

(Student's Signature)

Full Name   : KANIZ FARHANA

ID Number   : PMM16021

Date   :

DESIGN AND DEVELOPMENT OF HIGHLY EFFICIENT NANO FLUIDIC
FLAT PLATE SOLAR COLLECTOR

KANIZ FARHANA

Thesis submitted in fulfillment of the requirements
for the award of the degree of
Doctor of Philosophy

Faculty of Mechanical and Automotive Engineering Technology

UNIVERSITI MALAYSIA PAHANG

NOVEMBER 2019

ACKNOWLEDGEMENTS

ABSTRACT

The increase in demand for energy along with the depletion of conventional energy sources requires the improved utilization of renewable energy resources. Moreover, the unfavourable response of existing energy urges to take necessary action rapidly. Therefore, it is desired to generate an alternative source of energy or renewable energy for the industries. Among all renewable energy resources, solar energy is the most advantageous alternative to conventional energy sources owing to its inexhaustibility and green property. Generally, solar energy is harvested using different solar collectors. Solar collectors are devices that convert solar radiation into heat or electricity. However, the efficiency of the solar collector specifically flat plate solar collector is still not adequate. Thus, to form an optimum designed of a flat plate solar collector and by reintroducing the working fluid with the new transport medium; the efficiency of the collector can be improved. The competent step to enhance the efficiency of the solar collector is to redesign the flat plate solar collector considering the number and diameter of the header and riser tubes of flat plate solar collector. Secondly, replacing the working fluid inside the header and riser tubes with ethylene glycol-based Al_2O_3 and CNC nanofluids flowing through them. And finally, analysing the thermal performance of these new transport mediums in flat plate solar collector. This study is carried out in different phases viz. computational numerical simulations to design flat plate solar collector; measurement and evaluation of distinctive thermo-physical properties of Al_2O_3 and CNC nanofluids including stability, thermal conductivity, viscosity, specific heat, density and pH; implementation of nanofluids in the solar collector and finally, numerical simulation based on the experimental design and experimental properties of nanofluids. Experiment executed with a fixed flow rate and in the steady-state condition under solar irradiation. In results, the optimum 8-23-12 (number of riser tubes-diameter of header-diameter of riser) design of header and riser tubes of solar collector selected based on the statistical analysis of numerical simulations. From the thermo-physical point of view, thermal conductivity increased in a maximum of 13.4% and 11.5% for Al_2O_3 and CNC nanofluids respectively. Furthermore, the highest of 36% and 19% viscosity obtained with the augmentation of Al_2O_3 and CNC nanoparticle into the base fluid at $30^{\circ}C$ temperature respectively but decreased with the raising of temperature. Moreover, decrement of specific heat occurred due to an increment of volume concentrations of nanofluids. However, specific heat capacity enhanced by the progressive gradient of temperature. On the other hand, contraction of the density of nanofluids obtained with an improvement of temperature and of 3.8% decreased in maximum at $80^{\circ}C$ temperature. Al_2O_3 nanofluids showed the pH range of 2 to 4 and CNC nanofluids were within 5 to 7.5 scale of pH. The experimental study has implied that up to 2.48% and 8.46% efficiency of solar collector enhanced by using 0.5% Al_2O_3 and 0.5% CNC nanofluids respectively. And the most significant result is that of about 5.8% efficiency can be improved in flat plate solar collector by CNC/water-EG nanofluid. In addition, all types of nanofluids performed better convection heat transfer and quick heat diffusion characteristics with laminar fluid flow behaviour. Applying CNC/water-EG nanofluid enhances the efficiency of a flat-plate solar collector to consume the limitless solar energy to create an alternative source of energy for the industries.

ABSTRAK

Permintaan yang semakin menaik bagi sumber tenaga ditambah dengan pengurangan sumber tenaga konvensional memerlukan penggunaan sumber tenaga boleh diperbaharui yang lebih baik. Selain itu, tindak balas yang tidak baik daripada tenaga yang sedia ada memerlukan tindakan segera yang perlu diambil. Oleh itu, sumber tenaga boleh diperbaharui merupakan alternatif penting kepada industri. Di antara semua sumber tenaga boleh diperbaharui, tenaga suria adalah alternatif yang paling menguntungkan jika dibandingkan dengan sumber tenaga konvensional kerana sifatnya yang tidak habis serta mesra alam. Secara amnya, tenaga solar diperolehi menggunakan pengumpul suria yang berbeza. Pengumpul suria merupakan peranti yang menukarkan radiasi matahari menjadi haba atau tenaga. Walau bagaimanapun, kecekapan pengumpul suria terutamanya jenis plat rata masih tidak mencukupi. Bagi meningkatkan kecekapan pengumpul suria, reka bentuk optimum pengumpul suria plat rata dan cecair kerja dengan medium pengangkutan baru harus diperkenalkan. Langkah yang kompeten untuk meningkatkan kecekapan pengumpul suria adalah dengan mereka bentuk semula pemungut plat rata dengan mengambil kira bilangan dan diameter kepala dan riser tiub pengumpul suria plat rata. Kedua, menggantikan cecair kerja di dalam kepala dan tiub riser dengan nanofluid yang berasaskan etilena glikol Al_2O_3 dan CNC mengalir melalui mereka. Akhir sekali, prestasi haba medium pengangkutan baru di dalam pengumpul suria plat rata ini dianalisis. Kajian ini dijalankan dalam fasa yang berlainan. simulasi berangka komputasi untuk reka bentuk pengumpul suria plat rata; pengukuran ciri-ciri fizikal terma-fizikal nanofluid Al_2O_3 dan CNC termasuk kestabilan, kekonduksian terma, kelikatan, haba tertentu, ketumpatan dan pH; pelaksanaan nanofluid dalam pengumpul suria dan akhirnya, simulasi berangka berdasarkan sifat eksperimen nanofluid. Eksperimen dilaksanakan dengan kadar aliran yang tetap di bawah sinaran suria. Hasilnya, reka bentuk optimum 8-23-12 (bilangan tiub riser-diameter kepala-diameter riser) jenis kepala dan riser tiub pengumpul suria dipilih berdasarkan analisis statistik simulasi berangka. Dari sudut termo-fizikal, kekonduksian terma meningkat sebanyak 13.4% dan 11.5% bagi Al_2O_3 dan CNC nanofluid masing-masing. Tambahan pula, kelikatan tertinggi sebanyak 36% dan 19% diperolehi dalam penambahan Al_2O_3 dan nanopartikel CNC pada suhu 30^oC tetapi kemudian menurun dengan peningkatan suhu. Selain itu, pengurangan haba tertentu berlaku disebabkan peningkatan kepekatan jumlah nanofluid. Walaubagaimanapun, kapasiti haba tertentu dipertingkatkan oleh kecerunan suhu yang progresif. Sebaliknya, penurunan ketumpatan nanofluid diperoleh dengan peningkatan suhu dan 3.8% penurunan diperolehi pada suhu 80^oC. Al_2O_3 nanofluid menunjukkan julat pH 2-4 dan nanofluid CNC berada dalam lingkungan 5 hingga 7.5 skala pH. Kajian eksperimental menunjukkan bahawa kecekapan pengumpul suria sebanyak 2.48% dan 8.46% ditingkatkan dengan menggunakan 0.5% Al_2O_3 dan 0.5% nanofluid CNC. Keputusan yang paling ketara adalah kira-kira 5.8% kecekapan boleh ditingkatkan bagi pengumpul suria plat rata jenis CNC/air-EG nanofluid. Di samping itu, semua jenis nanofluid melakukan pemindahan haba perpecahan yang lebih baik dan ciri-ciri penyebaran haba yang cepat dengan aliran bendalir laminar. Penggunaan nanofluid CNC/air-EG dapat meningkatkan kecekapan pengumpul suria plat rata bagi mengumpul tenaga solar tanpa had sebagai sumber tenaga alternatif kepada industri.

TABLE OF CONTENT

LIST OF TABLES

LIST OF FIGURES

xiii

LIST OF SYMBOLS

ρ	Density (kg/m^3 or g/m^3)
ϕ	Volumetric concentration of particles (%)
C_p	Specific heat (J/kg-K or J/g-K)
D	Characteristic linear dimension (m)
k	Thermal conductivity (W/m-K)
μ	Viscosity (kg/m. s or cP)
w	Mass fraction
Q_u	Energy gain (kW)
$\dot{m}$	Mass flow rate (kg/s)
I_t	Incident solar radiation (W/m^2)
A_c	Area of the solar collector (m^2)
η	Efficiency (%)
T	Temperature (K or ^{o}C)
v	Characteristic velocity (m/s)
Q	Volumetric flow rate (m^3/s)
A	Cross-sectional area of the tube (m^2)
τ	Shear stress/stress tensor
γ	Shear rate
U	Velocity vector
p	Pressure (kg/m. s^2)
g	Gravitational acceleration (m/s^2)
h	Sensible enthalpy (joule)
∇	Advection operator
R_e	Reynolds number
N_u	Nusselt number
P_r	Prandtl number

Subscripts

s	Solid
f	Fluid
nf	Nanofluid
p	Particle
bf	Base fluid

LIST OF ABBREVIATIONS

ASHRAE	The American Society of Heating, Refrigerating and Air Conditioning Engineers
Al_2O_3	Aluminium Oxide
Al	Aluminium
Ar	Argon
BBD	Box–Behnken design
CFD	Computational fluid dynamics
CNC	Crystal nano-cellulose
CO_2	Carbon Dioxide
CSR	Controlled shear rate
CTAB	Cetyl Trimethyl Ammonium Bromide
Cu	Copper
CuO	Copper Oxide
DC	Direct current
DI	Deionized
DOE	Design of experiment
DSC	Differential scanning calorimetry
DW	Distilled water
DWCNT	Double-Walled Carbon Nanotube
EDX	Energy dispersive x-ray spectroscopy
EG	Ethylene glycol
ELS	Electrophoretic light scattering
Fe_2O_3	Ferric Oxide
FESEM	Field emission scanning electron microscopy
FLIR	Forward-looking infrared
FPSC	Flat plate solar collector
FTIR	Fourier transform infrared spectroscopy
ICDD	International centre for diffraction data
IEP	Isoelectric point
Ipm	Inches per minute
L	Litre

Max	Maximum
MgO	Magnesium Oxide
Min	Minimum
MWCNT	Multi-Walled Carbon Nanotube
NPs	Nanoparticles
N_2	Nitrogen
PWE	Pulse wire evaporation
RH	Relative humidity
RSM	Response surface methodology
SC	Solar collector
SDBS	Sodium Dodecyl Benzene Sulphonate
SiO_2	Silicon Dioxide
SWCNT	Single-Walled Carbon Nanotube
TEM	Transmission electron microscopy
TiO_2	Titanium Dioxide
W	Water
WD	Working distance
ZnO	Zinc Oxide
ZrO_2	Zirconium Dioxide

CHAPTER 1

INTRODUCTION

1.1 Background

Energy is a fundamental component of people's everyday life and industry as well. Today fossil energy is the most concerning issue owing to its depletion and impact on the environment. Therefore, it urges the necessity to generate an eco-friendly alternative source of energy to fulfill the demand for energy (Chu, Cui, & Liu, 2017). This chapter commences with the background of the study and the problem statement followed by the research objectives, the scope of the study, the contribution of the research and finally, organization of the thesis.

The consumption and the production of energy (fossil fuels) are increasing with time being which results in the decreasing of the reserve of energy day-to-day (Japan International Cooperation Agency, 2016). For this unavoidable situation, the industries are now facing a great crisis of energy. The performance of the industries which are situated mostly in developing countries is declining because of the deficiency and discontinuation of energy (fossil fuels) supply (Shah, Syed, & Shaikh, 2013). Both the energy crisis and energy consumption of industries have a great impact on the economic growth of any country (Khurshid & Anwar, 2013). Generally, the industries produce CO_2 as a by-product during production when they consume fossil energy as the main energy supply. Not only that, the emission of CO_2 is directly related to fossil energy consumption (Alkaya & Demirer, 2014). CO_2 is the major part of greenhouse gas which leads directly to global warming and that is the most concerning affair nowadays (Ruzmaikin & Byalko, 2015). As a matter of fact, alternative or renewable energy is one of the sustainable solutions to resolve these above problems without the confusion of any serious environmental impacts (Zaman & Abd-el Moemen, 2017). Renewable energies are the alternative sources of the traditional fossil fuels and obtained from those resources which

are essentially inexhaustible and abundant in nature. Different types of renewable energies such as solar, wind, hydropower, biofuel, geothermal, marine, etc are available all around in the environment (Pazheri, Othman, & Malik, 2014). These renewable energies can act as the best alternative source of energy to fulfill the energy demands in industry or everywhere (Ahmed et al., 2013; Ozdil, Tantekin, & Erbay, 2016).
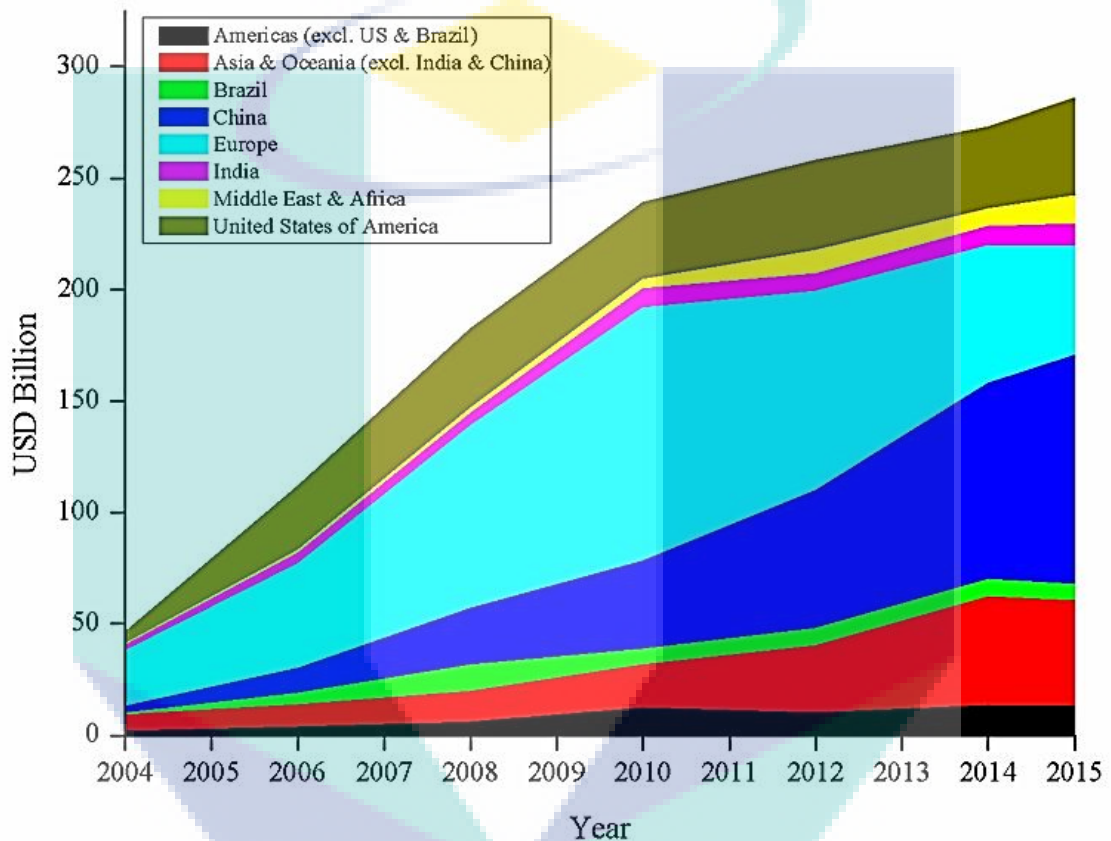
Figure 1.1   Worldwide renewable energy investment
Source: International Renewable Energy Agency (2017)

At present, many countries in the world already took different strategic policies to establish renewable energy as one of the main energy supplies and started their investment in it for the last few years as shown in Figure 1.1. For instance, Germany started a renewable energy journey from 2000, in that year they produced 7% electric renewable energy and in 2013, 24% electric renewable energy accumulated to their national gross electricity production (Bundesamt., 2014). In another example, Denmark has taken a pledge to enact 100% renewable energy replacement by the year 2050 (Renewable Energy Policy Network, 2014). Among all other renewable energies, solar energy already applied in different industries such as mining (Nasirov & Agostini, 2018),

2

oil (Halabi, Al-Qattan, & Al-Otaibi, 2015), textile (Muneer, Maubleu, & Asif, 2006) as an alternative source of energy by different solar energy converting systems; as solar cells have attracted much attention being the exhaustion of non-renewable energy resources as well as their contribution to the global warming. Moreover, solar energy has a great opportunity to be supplied in industries because it is inexhaustible, plentiful, clear and free from pollution attributes. Therefore, the investment in solar energy is also increasing rapidly by the global economy as shown in Figure 1.2. Generally, solar energy applied in two ways: solar thermal and photovoltaic systems. The common applications are hot water, steam, drying and dehydration, sterilization, washing, cleaning, food, plastic, building, pasteurization, business concerns, and textile industries. Solar energy should be applied directly or as the power supply to a project (Liu et al., 2019; Mekhilef, Saidur, & Safari, 2011). Flat plate solar collector is one of the important solar thermal devices used to harvest solar energy to heat the water (Ghorbani, Mehrpooya, & Sadeghzadeh, 2018).
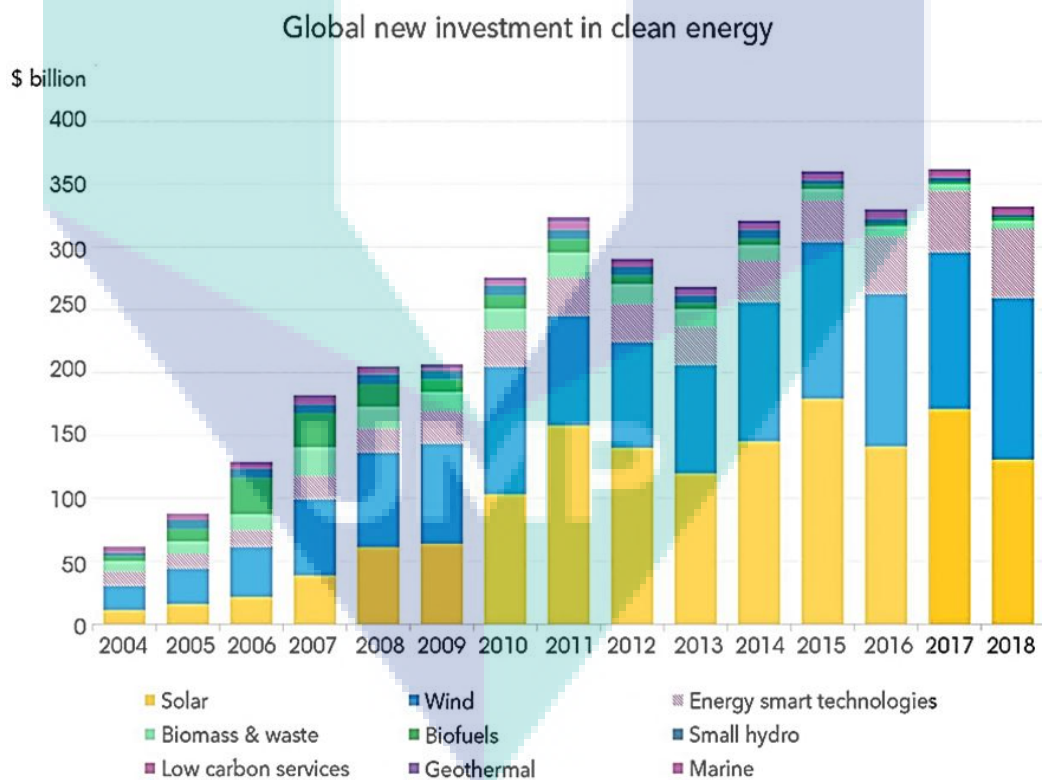
Figure 1.2   Global investment in solar energy

Source: BloombergNEF (2019)

Fundamentally, working fluid or transport medium is an important element of a flat plate solar collector that circulates through inside the header and riser tubes. Not only that, this working fluid can transfer the heat which absorbed from solar emissions helping to increase the efficiency of flat plate solar collectors (Jamil, Sidik, & Yazid, 2016). Many studies stated the efficiency of flat plate solar collector can be improved by changing this working fluid with the most recent promising is nanofluids (Tong et al., 2019; Zayed et al., 2019). Nanofluid is the fluid with nano-sized solid particles which may be metallic or non-metallic solid particles can change the transport properties and heat transfer characteristics of the base fluid (Panchal, 2015).
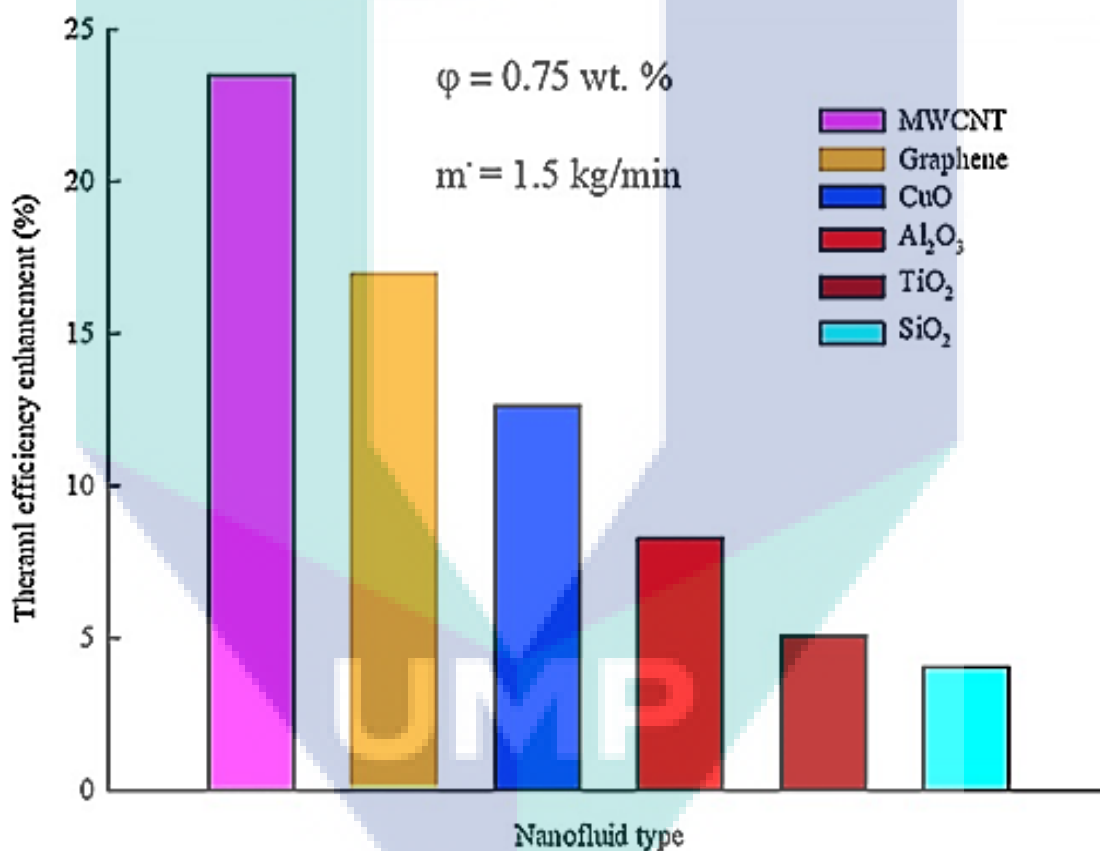
Figure 1.3   Thermal efficiency enhancement of flat plate solar collectors for different nanofluids

Source: Verma, Tiwari, and Chauhan (2017)

Nanofluids in solar collectors exhibit the enhancement of thermal conductivity, heat transfer coefficient and efficiency of solar collectors. Thermal conductivity and heat transfer coefficient increase with an increase in volume fraction and the mass flow rate of nanofluids (Nagarajan et al., 2014). In a study, Verma, Tiwari, and Chauhan (2017)

experimentally investigated the thermal performance of flat plate solar collectors with different nanofluids and concluded with thermal efficiency enhancement of flat plate solar collectors at the various percentage as shown in Figure 1.3.
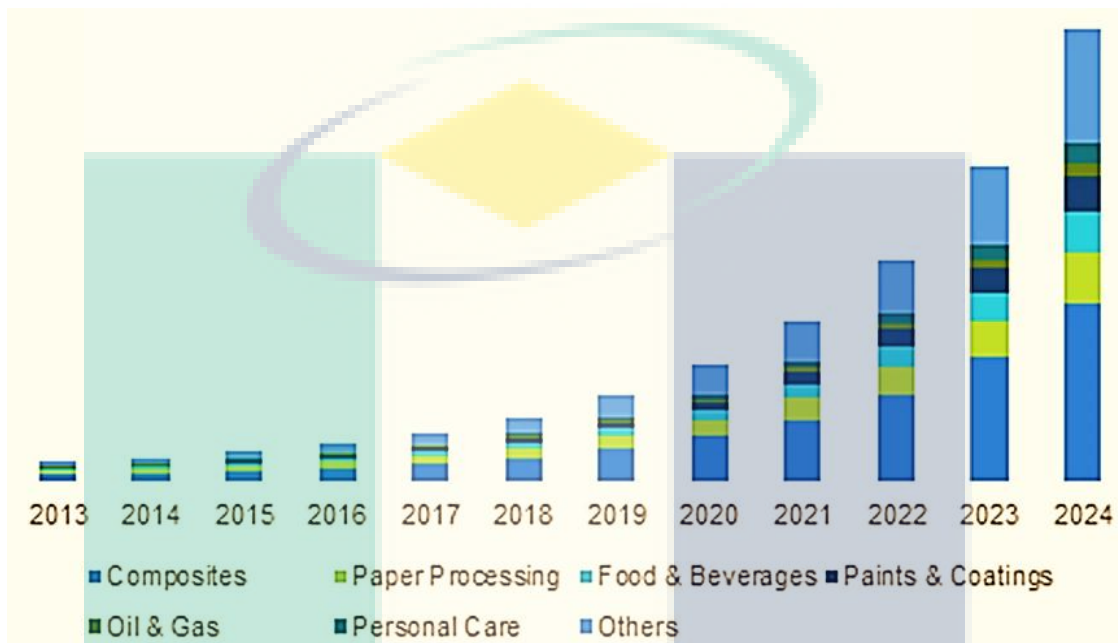
Figure 1.4   U. S. nano-cellulose market from the year 2013 -2024
Source: OpenPR (2019)

Though nanoparticles are the most auspicious and important invention for today's science and engineering field; it also has some adverse effects such as possible toxicity of nanoparticles towards the environment which poses the potentiality of hazardous substances for plants and human health as well. Moreover, researchers investigated that there should be an ecological problem when plants would be captivated by nanoparticles and as a consequence, human beings should be attacked (Dietz & Herth, 2011; Hossain et al., 2016; Huang, Wu, & Aronstam, 2010). Therefore as an alternative, over the last few years nano-cellulose has attracted more attention of the researchers due to some of their notable characteristics such as biodegradability, low density, superior strength, rigidity, transparency, available in surroundings and most importantly eco-friendly property (Abitbol et al., 2016; Theivasanthi et al., 2017). Hence, the demand for nano-cellulose is increasing periodically in various application fields such as paper processing, composites, food, paints, etc; for instance, the market size of nano-cellulose of the United States of America has been presented in Figure 1.4.

1.2 Problem Statement

Flat plate solar collector is one of the simplest solar devices for harvesting solar energy and this device already used for water heating purposes in industries (Muneer et al., 2008). Structurally the working fluid inside the header and riser tubes of flat plate solar collector plays a significant role to transfer the heat which is harvested from solar radiation for the enhancement of efficiency (Jamil, Sidik, & Yazid, 2016). However, solar energy converting systems suffer from low efficiency; hence harvesting solar radiation with a high-efficiency technology is a vital issue nowadays (Vezmar et al., 2014). The literature stated different numbers and the diameter of the header and rise tubes used in flat plate solar collector in different studies as these two tubes are the most important parts of flat plate solar collector. There is no optimum number and diameter of header and riser tubes in flat plate solar collectors which can facilitate the working fluid to improve the internal energy by absorbing solar energy. Therefore, there is an opportunity to investigate the optimum designing model of header and riser tubes of flat plate solar collectors. Besides that, solar systems (collectors) efficiency should be increased by changing the working fluid or transport medium with some new transport medium and recently some studies (Kasaeian et al., 2015; Noghrehabadi, Hajidavaloo, & Moravej, 2016) concluded that nanofluid plays a vital role to enhance the efficiency of solar systems. Already it revealed that the application of different (metal/non-metal) nanofluids can increase solar energy efficiency (Hussein, 2016; Verma & Tiwari, 2015). However, there is a gap to research the performance of inorganic (Al_2O_3) and organic crystal nano-cellulose (CNC) nanofluids dispersed into a different base fluid for the efficiency enhancement of flat plate solar collector system. The efficiency of this newly optimum design of flat plate solar collectors can be analysed using Al_2O_3 and CNC nanofluids flowing through inside it.

1.3 Research Objectives

Because of the low energy efficiency of solar collector devices, several essential techniques are initiated to enhance their efficiency to build an improved alternative energy system. One of the impressive methods to increase efficiency is to use nanofluids in the replacement of working fluids in solar collectors. Therefore, in order to make an energy-efficient flat plate solar collector, the following objectives need to be determined:

1.   To design an optimum model of flat plate solar collector by arranging the header and riser tubes of the collector.

2.   To evaluate the thermo-physical properties of nanofluids for the new design and new transport medium of solar collector comparing with the existing one.

3.   To analyse the thermal performance of Al_2O_3 and CNC nanofluids using the new design of flat plate solar collector.

1.4   Scope of the Study

Designing of header and riser tubes of flat plate solar collector and computational numerical simulation using the software. Afterword, selecting the designing model (arrangement of header and riser tubes) of flat plate solar collector by simulation statistical analysis. Using Al_2O_3 and CNC nanoparticles dispersed into a mixture of water and ethylene glycol-based fluid and selecting the mixture ratio of water and ethylene glycol is 60: 40. Preparing different volume concentrations of nanofluids within a range of 0.1% to 0.5% by the two-step method. Stabilization of nanofluids by the ultrasonication process using the sonication processor. Measuring different thermo-physical properties of nanofluids such as stability, thermal conductivity, viscosity, specific heat, density, and pH. Selecting the temperatures range of 30^oC to 80^oC to measure the thermo-physical properties of the nanofluids. Selecting the volume concentrations (0.3% and 0.5% volume concentration of both Al_2O_3 and CNC nanofluids) for experimental application by evaluating the thermo-physical properties of nanofluids. Preparing the actual experimental setup, running the experiment and reading the data under direct solar radiation in a steady-state condition. Measuring the surface temperature by using the thermographic camera during the experiment. Computing the non-dimensional numbers such as Reynolds number, Nusselt number, and Prandtl number. Finally, simulating the Prandtl number based on the experimental designing model of flat plate solar collector and the experimental thermo-physical data of nanofluids.

1.5　Contribution of the Research

It is important to understand the current research topics outlined for several reasons. This study contributes to the theoretical, methodological and experimental knowledge of energy efficiency enhancement of flat plate solar collector as follows:

1. Optimum design of flat plate solar collector formed for providing energy supply to the industries as an alternative source of energy and the influence of the arrangement of header and riser tubes of flat plate solar collector identified.

2. Preparation of stable inorganic and organic nanofluids for solar collector purposes.

3. Increase the efficiency of the current flat plate solar collector.

1.6　Organization of the Thesis

This thesis is organized into five chapters. Chapter 1 provides the background of the study, problem statement, research objectives, scope of the study, the contribution of the research and organization of the remaining chapters.

Chapter 2 presents a literature review on the discussion of the solar collector which includes flat plate solar collector, designing of flat plate solar collector, computational fluid dynamics, and mathematical formulation of nanofluids and solar collectors. In the second phase, it reviews on the nanotechnology which covered by nanomaterials, nanofluids, preparation methods of nanofluids, the stability of nanofluids, thermo-physical properties of nanofluids, application and advantages of nanofluids.

Chapter 3 describes the details of the process flow chart for this study. This chapter also describes the methodology that is employed to obtain a new approach to enhance the energy efficiency of flat plate solar by implementing nanofluids applied to a new designing model of flat plate solar collector.

Chapter 4 illustrates the expected results that were obtained after the experiment conducted and the analysis of the data by different software.

Chapter 5 presents the conclusion of this research work and some recommendations for further works that can be conducted in the future.

CHAPTER 2

LITERATURE REVIEW

2.1 Introduction

This chapter reviews the literature of solar collectors and nanotechnology comprehensively; especially the designing of flat plate solar collectors and the thermal properties of nanofluids have been reviewed. Because an optimum design with nanofluids can improve the thermal performance (energy gain and efficiency) of flat plate solar collectors. In this chapter, the discussion covers the aspects of solar collector which involves flat plate solar collector, solar collector design, computational fluid dynamics, and mathematical expressions; nanotechnology which consists of nanomaterials and nanofluids, preparation method of nanofluids, stability of nanofluids, various thermo-physical properties of nanofluids, applications and advantages of nanofluids in different subchapters.

2.1 Solar Collector

The solar collector (SC) is the most important part of the solar energy harvesting and water heating system. SC might be defined as an eco-friendly heat exchanger device converting thermal energy in solar thermal applications and electrical energy directly in photovoltaic applications. In the case of thermal application, solar devices absorb the solar radiant energy incident on its surface; transform it into heat and transfer the heat to the working fluid flowing through them (Chang et al., 2015; Melchior et al., 2008). Consequently, the higher the heat transfer to the fluid, the higher the outlet temperature and hence, improve the collector efficiency. SCs are different types such as flat plate, evacuated tube, direct absorption, parabolic trough, concentrating solar collector, cylindrical, transpired, hybrid photovoltaic thermal, etc. (Hussein, 2016) as shown in

Table 2.1 in which solar collectors mainly categorised into non-concentrating and concentrating types.

Table 2.1 Different types of solar collector

Category	Types of collectors	Functioning parameters	Important information
Non-concentrating or stationary	Flat plate	Water systems	Absorber- flat
		Air systems	Indicative temperature range 30ºC–80ºC
	Evacuated tube	Without heat pipe	Absorber- flat
		With heat pipe	Indicative temperature range 50ºC–200ºC
	Direct absorber	-	Absorber- flat
			Indicative temperature very low
	Compound parabolic	-	Absorber- flat
			Indicative temperature 60ºC–240ºC
Concentrating	Non-tracking	Flat receiver with booster mirror	Absorber- additional reflector with conventional absorber
			Thermal efficiency higher than the same collection area of flat plate collector
		Tabor–Zeimer circular cylinder	Absorber- triangular pipe
			Thermal efficiency greater than conventional flat plate collector
		Compound parabolic	Absorber- flat
			Non-imaging group of concentrators
	One-axis tracking	Fixed-mirror solar concentrator	Absorber- tubular
			Efficiency 40-50%
		Cylindrical Parabolic	Absorber- tubular
			Better performance
		Linear Fresnel lens/reflector	Absorber- tubular
			Downward-facing grooms show better performance
	Two-axes tracking	Parabolic dish solar concentrator	Absorber- point
			High collective and quality thermal efficiencies
		Circular Fresnel lens	Absorber- large surface
			Used for a solar furnace
		Hemispherical bowl mirror	Absorber- point
			Lesser concentration than paraboloids

Non-concentrating solar collectors such as flat plate, evacuated tube, direct absorber, and compound parabolic are mainly functioned with water, air and heat pipes. On the other hand, concentrating solar collectors are non-tracking, one-axis tracking and two-axes tracking with various primary functioning parameters such as mirror, cylinder, and lens (Ghaderian & Sidik, 2017; Jesko, 2008; Tiwari & Tiwari, 2017) has been portrayed in Table 2.1. Many researchers study the efficiency improvement of the

collector by changing different components or equipment or design as well as the setting of solar collectors. However, the most effective method and the latest technology is the nanofluid application in the solar collector as a working fluid in the place of conventional fluids. Nanofluids exhibit a much better heat transfer coefficient performance than conventional fluids (Eastman et al., 1996; Yılmaz & Söylemez, 2014). The performance of different solar collectors based on nanofluids depicted in Table 2.2. The overall thermal performance (efficiency and outlet temperature) of all types of solar collectors has been improved using nanofluids. Moreover, economically advanced solar collectors can be prepared by using a very low volume concentration of nanofluids.

Table 2.2   Summary of previous studies based on the thermal performance of nanofluids in solar collectors

References	Solar collector	Performance
Said et al. (2015)	Flat plate	Maximum water output temperature 65ºC
He, Zeng, and Wang (2015)	Flat plate	Maximum outlet temperature 68ºC
Said, Saidur, and Rahim (2016)	Flat plate	Maximum outlet temperature 72.5ºC
Meibodi et al. (2015)	Flat plate	Maximum efficiency increased by 8%
Arıkan, Abbasoğlu, and Gazi (2018)	Flat plate	Enhanced efficiency
He et al. (2013)	Direct absorption	Increased highest temperature up to 25.3%
Gorji and Ranjbar (2016)	Direct absorption	Output temperature enhanced
Wenjing, Zou, and Li (2017)	Direct absorption	The performance of the collector system increased
Gorji and Ranjbar (2017)	Direct absorption	Achieved the highest thermal and exergy efficiency of the collector
Ghaderian and Sidik (2017)	Evacuated tube	The highest temperature attained at 345 K
Sabiha et al. (2015)	Evacuated tube	Maximum output temperature around 72ºC
Mahendran et al. (2012)	Evacuated tube	Temperature raised by 19.0% higher than water
Chougule, Pise, and Madane (2012)	Evacuated tube	Exhibited better performance even in a very low 0.015% concentration and economical as well
Ghaderian et al. (2017)	Evacuated tube	The average output temperature increased by 14% approximately
Kasaeian, Daneshazarian, and Pourfayaz (2017)	Parabolic trough	Highest output temperature of 338.3 K and thermal efficiency by 74.9%

2.2   Flat Plate Solar Collector

The concept developed on flat plate solar collector (FPSC) is relatively simple and widest in an application such as water heating, space heating, domestic use, commercial use, and industrial use (Struckmann, 2008). Generally, the solar radiation absorbing surface of FPSC is nearly as large as the collector. It is classified into liquid type collectors where the liquid is the heat transfer fluid and air type collectors as air is the heat transfer fluid (Amrutkar, Ghodke, & Patil, 2012; Klevinskis & Bucinskas, 2011). FPSC is the most primitive and firstly in 1958, Hottel & Woertz worked on flat plate solar collectors (Hottlel & Whillier) and after that many researchers did many studies on it to establish, analysis and to improve the thermal efficiency of this collector. It consists of glass, absorber, riser and header pipes, insulator, a back sheet, aluminium rails. To protect the absorber clear and strengthened glass is used and it can allow the sunlight through to the absorber. The absorber is made with aluminium and ultrasonically welded with riser pipe to transfer the heat to the working fluid. The riser pipe and the header pipe are fixed together to form a harp-shaped heat exchanger through them the working fluid can circulate (Jamil, Sidik, & Yazid, 2016). Figure 2.1 is the typical flat plate solar collector specifically on header and riser tubes. Moreover, in the early 2012 calendar year, the study on the performance of FPSC especially on the heat transfer coefficient started (Muhammad et al., 2016). The thermal performance of FPSC based on various nanofluids presented in Table 2.3. Many studies performed to enhance the thermal performance of FPSC with various nanofluids such as MWCNT, TiO_2, SiO_2, Al_2O_3, CuO, Cu, MgO, ZnO dispersed into water base fluid mostly rather Meibodi et al. (2015) and Arıkan, Abbasoğlu, and Gazi (2018) used water/ethylene glycol based fluid. The size of particles was in a range of 10 to 50 nm, but Arıkan, Abbasoğlu, and Gazi (2018) used 0.196 μm (Al_2O_3) and 68.12 μm (ZnO) sized nanoparticles in their study. Most of the studies utilized the two-step method while very few used surfactants. The range of volume concentration of nanofluids was from 0.01% to 4%. The range of mass flow rate was about 0.01 to 0.5 kg/s. The studies in Table 2.3 concluded that the better enhancement of energy gain, efficiency, outlet temperature, and heat transport properties of FPSC achieved using nanofluids. Besides, few kinds of literature mentioned smaller size nanoparticles perform better than larger one. On the other hand, some studies showed that economically effective collector could be prepared using nanofluids.
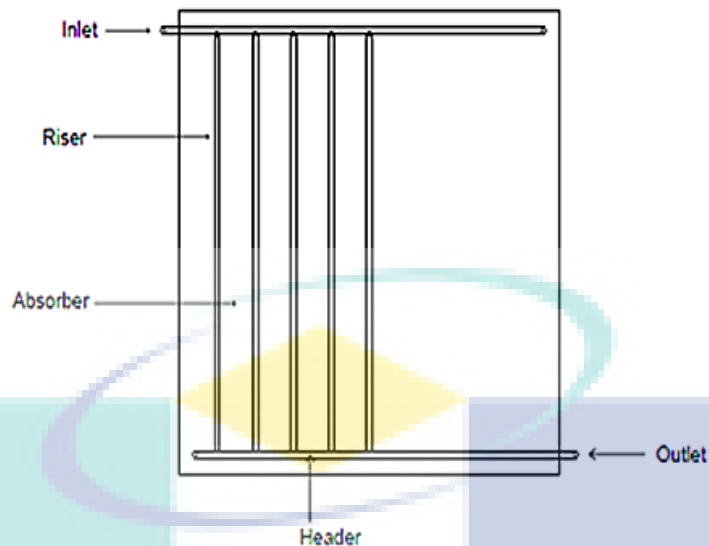
Figure 2.1   Flat plate solar collector

Source: Kong et al. (2015)

2.3   Designing of Flat Plate Solar Collector

To get the optimum output from a flat plate solar collector, it is necessary to design it. Several types of research have been done for designing FPSC by changing different arrangements such as shapes of pipes, coating, materials of heat pipes, etc. By literature review, the different experiments conducted by different specification parameters and properties of FPSC. The specification parameters of various flat plate solar collectors have been illustrated in Table 2.4. The absorber area, absorber thickness, number of header and riser tubes, diameter and thickness of header and riser tubes, back insulation thickness, thickness and number of glazing of FPSC has been depicted in Table 2.4. Moreover, the materials of frame, absorber, glazing, insulation, header and riser tube have been also presented in Table 2.4.

Previously many kinds of literature did the study on the designing of FPSC experimentally and numerically such as Fan et al. (2019) experimentally investigated the thermal performance of FPSC by changing the flat absorber to V-corrugated absorber with multi-channels. The authors remarked that V-corrugated absorber can improve thermal efficiency and optical properties as well as can reduce the pressure drop and pumping power consumption significantly. Besides, Sivakumar et al. (2012) studied the performance of FPSC by changing the design parameters such as the number of riser tubes and the arrangement of riser tubes in a zigzag pattern from the existing FPSC

system. The performance showed that the efficiency of the collector increased with the number of tubes and zigzag arrangement of tubes (Z-configuration) which was higher than that of the conventional collector. Consecutively, once again Sivakumar et al. (2013) experimentally investigated the performance of flat plate solar collectors by changing the heat pipe materials. In this experiment stainless steel tubes with epoxy-polyether coating and aluminium tubes with copper oxide coating used. The maximum efficiency produced around 41-47% as well as cost reduced by 30%.

On the other hand, Selmi, Al-Khawaja, and Marafia (2008) simulated and analysed the problem of FPSC with water flow by considering the solar radiation and modes of mixed convection between the tube surface, glass cover, sidewalls and insulation of the collectors. The authors concluded that there was a good agreement between the simulated and experimental data of the outlet temperature of the water. In a study of Gertzos, Pnevmatikakis, and Caouris (2008) examined the thermal behaviour of flat plate-integrated collector storage solar water heater numerically and experimentally. They revealed that numerical prediction was highly accurate when validated with experimental results. In addition, Martinopoulos et al. (2010) numerically investigated the behaviour of polymer solar collector and compared with the experimental data. They considered the solar irradiation, convection and heat transfer in the circulating fluid and between the parts of the collectors. Reasonably a good agreement was found by the authors regarding the collector efficiency and the temperature distribution during operation between numerical and experimental data. Besides, Basavanna and Shashishekar (2013) numerically studied the outlet temperature of triangular tube absorber FPSC and concluded that outlet temperature increased by changing this tube configuration.

The information summarised in Table 2.4 showed different types of design specification parameters of FPSC. By critical observing, it was found that there was some variation in the measurement of header and riser tube, as these two tubes are very important for transferring the heat which absorbed from solar emission. The diameters of the header tube and riser tubes were varying from 22 mm to 25.4 mm and 10 mm to 12.5 mm respectively. Moreover, the number of risers was in a range from 7 to 15. There was not any typical arrangement of header and riser tubes in FPSC as they are the most important parts of FPSC to aid the collector by absorbing and transferring the heat.

Table 2.3   Summary of previous studies on the basis of the thermal performance of FPSC

Authors	Nanofluid	Particle size (nm)	Method	Surfactant	Volume concentration	Mass flow rate	Important findings
Yousefi, Veisy, et al. (2012)	MWCNT/water	10-30 outer diameter	Two-step	Triton X-100	0.2, 0.4%	0.0167-0.05 kg/s	MWCNT nanofluid increases efficiency without surfactant
Alim et al. (2013)	TiO_2, Al_2O_3, SiO_2, CuO/water	-	-	-	1-4%	1-4 L/min	Heat transfer properties and convective heat transfer coefficient increased surprisingly
Moghadam et al. (2014)	CuO/water	40	Two-step	-	0.4%	1-3 kg/min	Collector efficiency increases of 16.7%
Meibodi et al. (2015)	SiO_2/water-EG	~40	Two-step	-	0.5, 0.75, 1%	0.018, 0.032, 0.045 kg/min	Maximum thermal efficiency increases of 8%
Said, Saidur, and Rahim (2016)	Al_2O_3/water	13, 20	Two-step	-	0.1%	0.5-1.5 kg/min	Smaller size nanoparticles show a higher performance in the first and second laws of energy
He, Zeng, and Wang (2015)	Cu/ water	25, 50	Two-step	SDBS	0.01, 0.02, 0.04, 0.1, 0.2% wt	140 L/h	Highest temperature and heat gain increased up to 12.24% and 24.52% respectively
Noghrehabadi, Hajidavaloo, and Moravej (2016)	SiO_2/water	~12	Two-step	-	1%	0.35-2.8 L/min	Increased efficiency of the collector with an increase in mass flow rate and better than pure water
Verma, Tiwari, and Chauhan (2016)	MgO/water	~40	Two-step	CTAB	0.25, 0.5, 0.75, 1.00, 1.25, 1.5%	0.5, 1.0, 1.5, 2.0, 2.5 Ipm	Collector efficiency enhanced, and economically compact collector should be made by reducing surface area
Arıkan, Abbasoğlu, and Gazi (2018)	Al_2O_3, ZnO/W-EG	Al_2O_3 – 0.196 μm, ZnO-68.12 μm	Two-step	-	0.25%	0.05, 0.7, 0.09 kg/s.	Collector efficiency increased and Al_2O_3 nanofluid performed higher efficiency than ZnO nanofluid

Table 2.4   Summary of previous studies based on the specification parameters of FPSC

Specification parameters of FPSC	References						
	Gunjo, Mahanta, and Robi (2017)	Moghadam et al. (2014)	Said et al. (2013)	Said et al. (2015)	Shojaeizadeh et al. (2014)	Cruz-Peragon et al. (2012)	Yousefi, Veisy, et al. (2012)
				Value			
Absorber area	1.65 m^2	1.51 m^2	1.51 m^2	1.84 m^2	1.51 m^2	0.21 m^2	1.51 m^2
Absorber thickness	0.0005 m	-	-	-	-	2 mm	-
Header pipe	Diameter-0.025 m; thickness-0.0007 m	Diameter-22 mm; thickness-0.9 mm	-	Diameter- 22 mm; thickness-0.6 mm	Diameter-22 mm; thickness-0.9 mm	Inner diameter-20 mm	Diameter-22 mm; thickness-0.9 mm
Riser pipe	Diameter-0.0125 m; thickness-0.0007 m	Diameter-10 mm; thickness-0.9 mm	Inner diameter-0.01 m	Diameter-10 mm; thickness-0.45 mm number- 8	Diameter-10 mm; thickness-0.9 mm	Inner diameter-10 mm; number-15	Diameter-10 mm; thickness-0.9 mm
Back insulation thickness	0.04 m	-	-	-	-	10+7 mm	-
Center to center tube distance	0.1125 m	-	-	-	-	30 mm	-
Glass/glazing thickness	0.03 m	4 mm	4 mm	4 mm	4 mm	4 mm	4 mm
Number of glass/glazing	1	-	1	-	-	-	-
Spacing between glass and absorber plate	0.03 m	-	-	-	-	-	-
Frame	-	-	-	Aluminium alloy	-	-	-
Absorber	-	-	-	Aluminium	-	Copper	Copper
Riser tube material	-	Copper	-	Copper	Copper	-	Copper
Header tube material	-	Copper	-	Copper	Copper	-	Copper
Glazing	-	-	-	Tempered glass	-	-	-
Insulation	Glass wool	-	-	Glass wool	-	-	Polyurethane

Table 2.4   Continued

Specification parameters of FPSC	References			
	Sundar et al. (2018)	Eltaweel and Abdel-Rehim (2019)	Meibodi et al. (2015)	Arıkan, Abbasoğlu, and Gazi (2018)
				Value
Absorber area	2 m^2	2 m^2	1.59 m^2	Length-170 cm, width-90 cm, thickness-0.5 cm
Absorber thickness	0.6 mm	-	-	-
Header pipe	Diameter-25.4 mm	-	-	-
Riser pipe	Inner diamter-10 mm (9)	Number 7	-	-
Back insulation thickness	100 mm	-	-	-
Center to center tube distance	0.15 mm	-	-	-
Glass/glazing thickness	4 mm	4 mm	-	0.5 cm
Number of glass/glazing	-	-	-	-
Spacing between glass and absorber plate	-	-	-	-
Frame	-	-	-	-
Absorber	Copper	Copper	-	-
Riser tube	Copper	-	-	-
Header tube	Copper	-	-	-
Glazing	Toughened glass	-	-	-
Insulation	Rock wool pads	-	-	Glass wool

2.4 Computational Fluid Dynamics

Computational fluid dynamics or CFD is the analysis of systems involving fluid flow, heat transfer and associated phenomena such as chemical reactions by means of computer-based simulation. The technique is very powerful and spans in a wide range of industrial and non-industrial application areas such as aerodynamics, hydrodynamics, power plant, turbomachinery, electrical and electronic engineering, chemical process engineering, the external and internal environment of buildings, marine engineering, environmental engineering, hydrology and oceanography, meteorology and biomedical engineering. CFD codes are structured around the numerical algorithms that can tackle fluid flow problems. CFD codes contain three main elements: (i) a pre-processor, (ii) a solver and (iii) a post-processor (Blazek, 2015; Versteeg & Malalasekera, 2007).

The cornerstone of CFD is the fundamental governing equations of fluid dynamics- the continuity, momentum, and energy equations. There are the mathematical statements of these fundamental physical principles upon which all of fluid dynamics based:

i.   Mass is conserved;

ii.   F = ma (Newton's second law);

iii.   Energy is conserved (Blazek, 2015; Wendt, 2008).

CFD Governing Equations

CFD approach usages the numerical calculation by solving mass, momentum and energy conservation governing equation equations as follows:

Continuity equation

$$\frac{\partial \rho}{\partial t} + \nabla . (\rho U) = 0 \qquad\qquad 2.1$$

Momentum equation

$$\frac{\partial}{\partial_t}(\rho U) + \nabla . (\rho U U) = -\nabla p + \nabla . \tau + \rho g \qquad\qquad 2.2$$

Energy equation

$$\frac{\partial}{\partial t}(\rho h) + \nabla.(\rho U C_p T) = \nabla.(k\nabla T) \qquad\qquad 2.3$$

Before going to practical operations; computer-based numerical simulation can be done repeatedly by creating a virtual design model to reduce the cost of any project. Numerical simulations can be done by CFD systems of different objects such as fluid flow, heat transfer and chemical reactions as well (Baukal Jr, Gershtein, & Li, 2000; Versteeg & Malalasekera, 2007). Many engineering problems (Safari, Ghamari, & Nasiritosi, 2003), as well as various numerical simulations, have been performed on solar energy to replace the fossil energy successfully (Villar et al., 2009). Considerable numbers of articles have been published on CFD simulations in the case of flat plate solar collectors (Farajzadeh, Movahed, & Hosseini, 2018; Gertzos, Pnevmatikakis, & Caouris, 2008; Gunjo, Mahanta, & Robi, 2016; Ranjith & Karim, 2016). In a study, Gunjo, Mahanta, and Robi (2017) validated experimental values of outlet water and absorber plate temperature with numerical values using CFD software of a solar flat plate collector with straight riser and header arrangement. Different operating parameters such as solar insolation, ambient temperature, inlet water temperature and mass flow rate used and found that the developed model could predict outlet water and absorber plate temperature of heating system with reasonable accuracy. Besides, Selmi, Al-Khawaja, and Marafia (2008) studied the problem of water flow in FPSC simulating with CFD software. CFD modelling has been done on solar irradiation and the modes of mixed convection and radiation heat transfer. They revealed a good agreement between experimental and simulated results. In another study, numerical simulation of flat plate solar collector has been done by CFD solver such as Gunjo, Mahanta, and Robi (2017) validated experimental values of outlet water and absorber plate temperature with numerical values using CFD of FPSC with straight riser and header tube arrangement.

2.5   Mathematical Formulations of Nanofluids and Solar Collector

Nanofluid Preparation

Nanofluids can be prepared by calculating the quantity of nanoparticles for required volume concentrations using the following (Eq. (2.4)) (Sundar et al., 2018):

$$\phi = \left[\frac{\frac{w}{\rho_p}}{\frac{w}{\rho_p}+\frac{w_{bf}}{\rho_{bf}}}\right] \times 100 \qquad\qquad 2.4$$

Where ϕ is the volume concentration of nanofluids (%); w is the mass and ρ stands for the density of nanoparticles. The subscripts p and bf stand for nanoparticles and base fluid respectively.

Solar Collector Efficiency Calculation

The useful energy gain of the working fluid of solar collector can be calculated by the following (Eq. (2.5)) (Kalogirou, 2013):

$$Q_u = \dot{m}\,C_p(T_{out} - T_{in})\;\text{(kW)} \qquad\qquad 2.5$$

Where Q_u is the useful energy gain, $\dot{m}$ is the mass flow rate of the working fluid, C_p is the specific heat of the working fluid, T_{out} and T_{in} are the outlet and inlet temperature of FPSC respectively. The thermal efficiency of the solar collection is given by the below (Eq. (2.6)) (Kalogirou, 2013):

$$\eta = \frac{Q_u}{I_t A_c}\;(\%) \qquad\qquad 2.6$$

Where, I_t is the incident solar radiation, A_c is the area of solar collector.

2.6   Nanotechnology

Nano is a popular emerging area of science and technology nowadays. It has attracted the attention of researchers from all segments of science such as physics, chemistry, biology, and engineering. Nano has even entered popular culture. It's used as a buzzword in contemporary books, movies, and television commercials. The prefix 'nano' is derived from the Greek word Nanos which means dwarf. One nanometre (nm) is equal to one-billionth of a meter, 10^{-9} m (Kuno, 2005).

The conceptual basement of nanotechnologies were first introduced in 1959 by the physicist Richard Feynman, in his lecture 'There's plenty of room at the bottom' (Feynman, 1960) and afterward a researcher at the University of Tokyo (Japan International Cooperation Agency) used it to point out to the strength to engineering materials specifically at nanometre size and originated the term 'Nanotechnology' (Taniguchi, 1974).

2.6.1 Nanomaterials

A nanomaterial is an object which should have at least one dimension in the nanometer scale. Generally, nanomaterials are constructed from larger pieces of materials to very small structures defined as 'top-down' techniques. However, they might be produced by 'bottom-up' techniques. The scientists and the researchers expect that nanomaterials will provide the ways of improving performance in a wide range of products such as silicon-based electronics, displays, paints, batteries, micro-machined silicon sensors and catalysts (Filipponi, Sutherland, & Center, 2010; Society, 2004). Nanomaterials can be classified into four and Figure 2.2 shows the schematic view of nanomaterials.

- 3D-system confined in three dimensions e.g. structures typically composed of consolidated equiaxed crystallites.

- 2D-system confined in two dimensions e.g. filamentary structures where the length is substantially greater than the cross-sectional dimensions.

- 1D-system confined in one dimension e.g. layered or laminate structures.

- 0D-zero dimensional structures e.g. nano-pores and nanoparticles (Pokropivny et al., 2007).
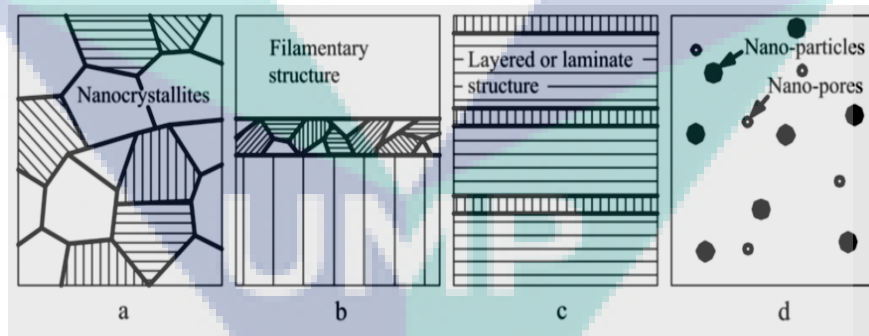
Figure 2.2   Schematic classification of nanomaterials: (a) three-dimensional structures, (b) two-dimensional, (c) one-dimensional, and (d) zero-dimensional structures

Source: Pokropivny et al. (2007)

2.6.2 Nanofluids

Nanofluids are newly invented fluids of fluid engineering by dispersing unique and nanometre-sized particles which were discovered and coined in 1995 by Choi. It was invented to make stable suspension with these nanometre-sized (<100 nm) solid

substances into the base conventional industrial heat transfer fluid such as water, ethylene glycol or engine oil (Chol, 1995; Pourmohamadian et al., 2019). Nanoparticles have unique characteristics equivalent to their bulk stages and their characteristics should be changed with decreasing in dimensions at the atomic level. Nanoparticles enable unique properties such as physio-chemical, optical and biological properties which can be manipulated suitably in the intended application (Feynman, 2011; Hayat et al., 2015).

The researchers and scientists have experimented and identified different types of metallic nanoparticles such as Al, Fe, Cu, Ag, and Au; non-metallic nanoparticles such as CuO, SiC, Al_2O_3, ZnO, semiconductors (TiO_2), carbon nanotubes (SWCNT, DWCNT, MWCNT) and composites materials such as nanoparticles core polymer shell composites; while most of them are chemically stable and functionalized nanoparticles. Generally, nanoparticles produced by physical and chemical synthesis techniques (Nagarajan et al., 2014; Panchal, 2015; Zakomirnyi et al., 2018). In addition to this, over the last few years crystal nano-cellulose (CNC) attract more attention to the researchers due to some of their notable properties such as biodegradability, impressive mechanical properties, lower density, plentiful in nature and most importantly eco-friendly aspect as well (Abitbol et al., 2016; Theivasanthi et al., 2017). Thermal conductivity and heat transfer coefficient increased significantly by adding a tiny number of nanoparticles into the base fluids as well as further enhancement occurred due to the increasing amount of volume fraction of nanoparticles in base fluids. Moreover, nanofluid exhibits the enhancement of heat transfer, improved suspension stability, high surface volume, fewer particles clogging and anomalous increase in thermal conductivity while the heat transfer or heat transfer coefficient directly related to thermal conductivity. Water and ethylene glycol have been utilized in many nanofluid related research studies as a base fluid. However, nanofluids are not only interesting area for increasing the heat transfer but also improving other properties such as rheological behaviour and mass transfer properties (Ganvir, Walke, & Kriplani, 2016; Ghanbarpour et al., 2015). This heat transfer enhancement enormously depends on the size, shape, density, surface energy, and thermophysical properties of nanoparticles. The thermal conductivity of metallic nanoparticles is much higher than the non-metallic nanoparticles. Moreover, smaller size and cylindrical shape exhibit better performance (Nadooshan, Eshgarf, & Afrand, 2018; Noghrehabadi, Hajidavaloo, & Moravej, 2016). The application of nanofluids recognized in various sections by the researchers such as heat exchanger, solar cells, solar collectors, cooling devices, heat

pipes, engine ultrahigh cooling systems, energy supply, microelectronics and biomechanics (Akbar & Mustafa, 2015; Liu et al., 2016; Olia et al., 2019; Sajid & Ali, 2019).

2.6.3 Preparation Method of Nanofluids

One or Single-step Method

One or single-step method also known as pulse wire evaporation (PWE) is a famous method for producing nanofluid. There are four key apparatus in the PWE method: a capacitor bank, a high-voltage DC power supply, a high voltage gap switch and a condensation or evaporation chamber. In this method, a pulsed high voltage (300 V) is driven through a thin wire, and as a result, a non-equilibrium overheating induces the wire which makes the wire to evaporate within few microseconds into the plasma. This plasma is then cooled by using Ar or N_2 inert gas which condenses the plasma into nanosized particles or powder.
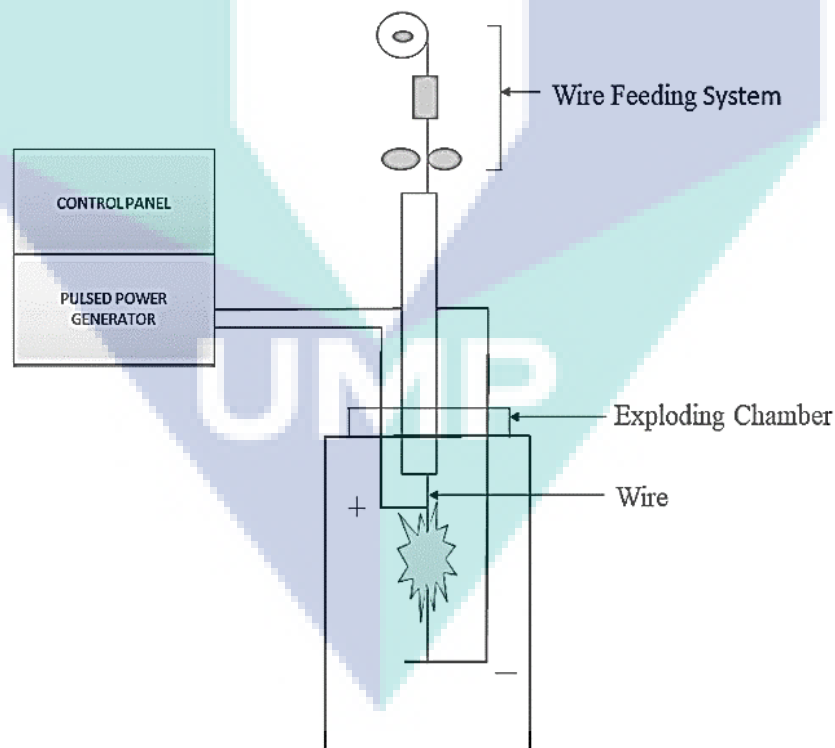
Figure 2.3   Schematic view of pulsed-wire evaporation

Source: Lee et al. (2003); Park et al. (2012)

Heat transfer fluid is then poured into the exploding chamber at a required volume concentration to be mix with the nanoparticles. This method is prevalent to prepare a low-cost nanofluid (Kim, Lee, & Kim, 2001; Lee et al., 2003). Figure 2.3 shows the schematic view of the PWE set-up. In this method, the size of the particles depends on the heat applied to the wire and the applied pressure of the inert gas (Lee et al., 2006; Park et al., 2012).

Two-step Method
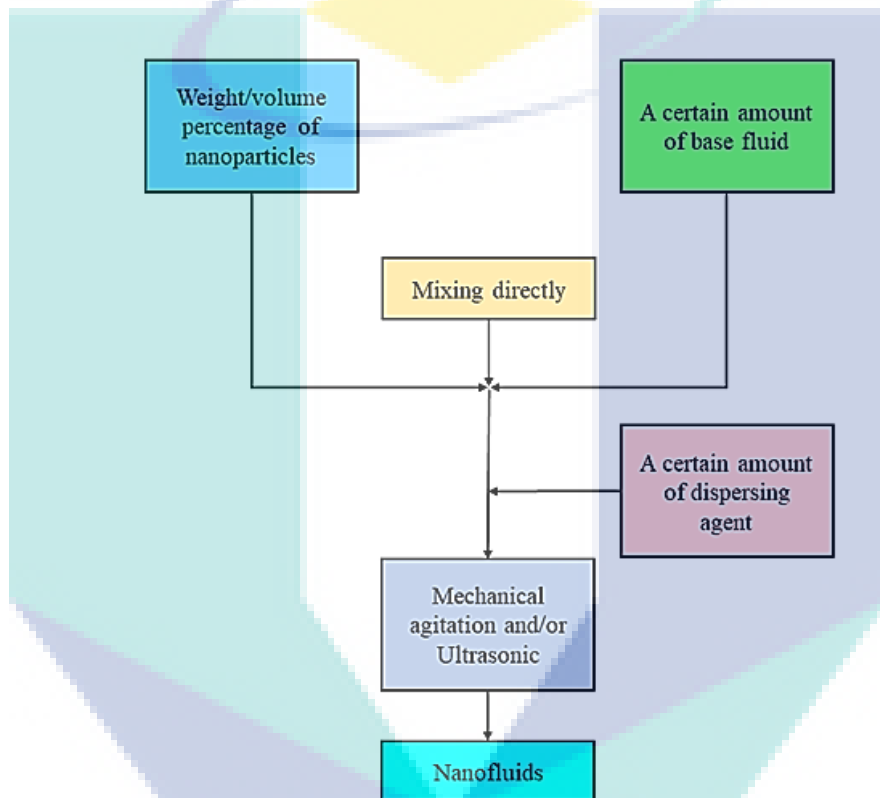
Figure 2.4   Two-step method preparation process of nanofluid
Source: Sun et al. (2016)

In the two-step method, the nanopowder or nanoparticle in dry form is produced via chemical, mechanical or physical processes such as sol-gel, milling, grinding, inert gas condensation, vapor phase, sputtering, laser ablation or flame synthesis. The produced nanopowder is then suspended into the base fluids by using magnetic stirring, mechanical mixing, electromechanical agitation or ultrasonication. A dispersing agent may be used to disperse nanoparticle in the fluid further. This process is very suitable for the mass production of both mono and hybrid nanofluids. As such, this method is economically advantaged for industrial scaled production (Farzaneh et al., 2016; Li et al., 2009; Wang & Chiang, 2013). Figure 2.4 portrays the preparation process of mono and/or hybrid

nanofluid using the two-step method (Sun et al., 2016). Generally, the single-step method of nanofluid preparation is much better for small scale production while the two-step method is very cheap for mass-scale production (Sidik et al., 2016). Most of the researchers used the two-step method for nanofluids preparation and Table 2.5 presents the summary of some two-step method related studies. The authors mentioned in Table 2.5 used the two-step methods to conduct their research studies.

Table 2.5   Summary of the preparation method of nanofluids related studies

References	Nanofluid	Preparation method
Xu, Bandyopadhyay, and Jung (2016)	Al_2O_3/water-EG	Two-step
Azmi et al. (2016)	Al_2O_3/water-EG	Two-step
Stephen et al. (2018)	Al_2O_3/DW	Two-step
Kim et al. (2019)	Al_2O_3/DW	Two-step
Kaaliarasan Ramachandran et al. (2017)	CNC/water-EG	Two-step
Kadirgama et al. (2018)	CNC/water-EG	Two-step

2.6.4   Stability of Nanofluids

Preparing a homogeneous suspension is still a technical challenge due to strong Van der Waals interactions between nanoparticles invariably favouring the formation of aggregates. Balamurugan and Sajith (2017) experimentally investigated that the stability of nanofluids is very important particularly long-term stability of nanofluids. The authors revealed that to improve the lubricity of diesel, a long term stable nanofluids required along with an optimum concentration of nanoparticles. In a study, Mukherjee and Paria (2013) concluded that long term stability and stability after a long working cycle should pay intense attention for both research and real-life application. To obtain stable nanofluids some physical or chemical treatments are necessary. Moreover, the stability of nanofluids mostly depends on the preparation methods, nanoparticle characteristics, type of base fluids, surfactants, pH, ultra-sonication process, etc. The duration period of the stability of nanofluids has been found in different time phases in various studies as depicted in Table 2.6. Different nanofluids exhibited the maximum duration in more than six months while thirty hours were in a minimal period of stability (Table 2.6). A few studies used surfactant or pH had been controlled for the stability of nanofluids represented in Table 2.6.

Table 2.6   Summary of previous studies on the basis of the stability of nanofluids

References	Nanoparticles	Base fluid	Surfactant/ pH	Duration of stability
Suganthi, Vinodhan, and Rajan (2014)	ZnO	EG and water-EG	Ammonium citrate	Saturated for thirty hours
Khedkar, Sonawane, and Wasewar (2012)	CuO	EG and water	Polyvinylpy rrolidone	Good stable
Rashin and Hemalatha (2014)	CuO	EG	-	More than six days
Khdher et al. (2016)	Al_2O_3	EG	-	For several days
Sundar et al. (2012)	Fe_3O_4	EG	-	Stable up to eighty days
Asadzadeh, Esfahany, and Etesami (2012)				
Kaaliarasan Ramachandran et al. (2017)	CNC	Water-EG	-	Stable more than one month
Kadirgama et al. (2018)	CNC	Water-EG	-	High stability, more than two months
Kim et al. (2019)	Al_2O_3	DW	-	Good dispersion
De Robertis et al. (2012)	Cu	EG	-	Stable up to sixty days

Methods of Stabilization

Stable nanofluid with uniform dispersion is an important requirement for improving the heat transfer of nanofluids. There are a few important methods for the preparation of stable nanofluids (Mukherjee & Paria, 2013; Trisaksri & Wongwises, 2007):

1.   Addition of surfactant in the base fluid

2.   Surface modification techniques

3.   Acid treatment of the base fluid

4.   Ultrasonic mixing of nanopowder in the base fluid

In a study, Mahbubul et al. (2015) experimentally investigated the ultrasonication duration performance on the dispersion and thermal behaviour of Al_2O_3-water nanofluids. The author revealed that ultrasonication has a significant effect on the colloidal suspension and thermo-physical properties of nanofluids. The stable nanofluids prepared using the longer duration of ultrasonication. Better thermo-physical properties achieved by a higher ultrasonication period and ultrasonication was more effective on temperature as well. Moreover, larger duration ultrasonication of nanofluids exhibits good thermal

properties, better colloidal dispersion, smaller aggregation size of nanoparticles, higher zeta potential value of stability and decrement of viscosity. Among all these stabilization methods, ultrasonication is the most widely used stabilization method as many studies used this method that has been portrayed in Table 2.7. The authors conducted the ultrasonication process to stabilize the nanofluids during their research studies. They did the ultrasonication process in different time frames and found good results of the stability of nanofluids.

Table 2.7   Summary of stabilization method related studies

References	Nanofluid	Stabilization method
Xu, Bandyopadhyay, and Jung (2016)	Al_2O_3/water-EG	Ultrasonication
Azmi et al. (2016)	Al_2O_3/water-EG	Ultrasonication
Stephen et al. (2018)	Al_2O_3/DW	Ultrasonication
Kim et al. (2019)	Al_2O_3/DW	Ultrasonication
Kaaliarasan Ramachandran et al. (2017)	CNC/water-EG	Ultrasonication
Kadirgama et al. (2018)	CNC/water-EG	Ultrasonication

Stability Evaluation Methods

Angayarkanni and Philip (2015) and Kumar and Arasu (2017) mentioned different types of stability evaluation methods such as:

- Light scattering method

- Zeta potential method

- Sedimentation and centrifugation method

- Spectral analysis

Zeta potential method is very important for nanoparticle suspensions. Because the stability of colloidal suspension is closely related to the zeta potential values (Delgado et al., 2007). The mutual repulsion forces between the equivalent charged particles create a relation between the colloidal suspension of nanoparticles and zeta potential. Thus, the high surface charged nanoparticles do not have a tendency to agglomerate and vice-versa (Vandsburger, 2009). Many studies used zeta potential methods to evaluate the stability of nanofluids (Ghadimi & Metselaar, 2013; Marsalek, 2014; Sarsam et al., 2016; Xu, 2008; Zawrah et al., 2016).

2.6.5 Thermo-physical Properties of Nanofluids

Generally, nanofluids are associated with different thermo-physical properties such as thermal conductivity, viscosity, specific heat, and density exhibited dramatical changes in these properties. The concise scenario of different thermo-physical properties of nanofluids has been illustrated in Table 2.10. Moreover, the potential of hydrogen (pH) is another important property of nanofluids which influences the stability of nanofluids; as a result, the thermal conductivity of nanofluids is altered. Almost all of the research studies in Table 2.10 illustrated different thermo-physical scenarios such as enhancement of thermal conductivity, improved viscosity, reduced specific heat, increased density, and influenced pH individually by using different nanoparticles dispersed into the base fluid.

Nanofluid is a novel outcome of nanotechnology applied in a thermal fluid system. It is of great potential for improving system performance intensely. Compared to conventional working fluids such as water, kerosene, ethylene glycol, and microfluidics; nanofluid has been shown to exhibit higher thermal conductivities. Nanofluids have higher thermal conductivity and a single-phase heat transfer coefficient than their base fluids. As the volume concentration of nanoparticles dispersed into the base fluid increases; the enhancement of thermal conductivity of nanofluids increases considerably. Moreover, thermal conductivity depends on various parameters such as the shape and size of nanoparticles, the dispersion medium, stability, and temperature (Esfahani & Toghraie, 2017; Suganthi & Rajan, 2017). Further, nanofluids do not block flow channels and induce only a very small pressure drop during flow, which is beneficial for heat transfer applications. The vigorous Brownian motion of suspended nanoparticles in base fluids makes nanofluids more stable compared to microfluidics (Angayarkanni & Philip, 2015; Rashidi et al., 2014). Ideal nanofluids possess better thermo-physical properties such as thermal conductivity, electrical conductivity, thermal diffusivity, convective heat transfer coefficient, and viscosity than the base fluids. Among those, the thermal conductivity and viscosity heavily affect the heat transfer property of nanofluid (Hassan et al., 2013). The enhancement of the thermal conductivity of different objects using nanofluids depicted in Table 2.8. Most of the studies used Al_2O_3 nanoparticles and water as base fluid. The two-step method utilized almost all studies to prepare nanofluids and for the stabilization ultrasonication process applied. The average particle size was

below 100 nm. The maximum percentage of volume concentration and weight was 6% and 9% respectively.

Measurement of thermal conductivity of nanofluids can be carried out using different methods. The most common techniques for this purpose are the transient ones including (Tawfik, 2017):

1. Transient hot-wire method

2. Thermal constants analyzer techniques

3. The steady-state parallel plate method

4. 3-ω method

5. Temperature oscillation method

6. Micro-hot strip method

7. Optical beam deflection techniques

The transient hot-wire method is the most widely used method to measure the thermal conductivity of nanofluids and it is a standard transient dynamic approach based on the measurement of the temperature increment in a defined distance from a linear heat source (hot wire) ingrained in the test sample. In this method, a metallic wire (hot wire) functions as the probe which is inserted into the nanofluids to measure thermal conductivity. This probe acts as both a heat source and a thermometer. Based on Fourier's law, the standard mathematical model of this method prepared. Fourier's law narrates the fluid of higher thermal conductivity corresponds to a lower temperature rise with a heated wire. A constant heat supply is fixed to this hot wire with a constant heat flux at a time interval. The heat dissipated in the probe increases the temperature of the probe as well as that of the nanofluids. This temperature rise depends on the thermal conductivity of the materials in which the hot-wire is placed (Davis, 1984; Vadasz, 2010). Despite this technique is effortless, fast responsive and cost-effective to measure the thermal conductivity of nanofluids; its accuracy can be altered by the sedimentation and/or agglomeration of nanoparticles (Paul et al., 2010).

Table 2.8   Enhancement of thermal conductivity with nanofluids related studies

References	Base fluid	Method	NPs size (nm)	Dispersion technique	Volume concentration	Observation	Thermal conductivity
Chandrasekar, Suresh, and Bose (2010)	Al_2O_3/water	Two-step	43	Ultrasonication	0.33-5%	Thermal conductivity and viscosity	Enhanced
Xu, Bandyopadhyay, and Jung (2016)	Al_2O_3/DW-EG	Two-step	29.7	Magnetic stirring and ultrasonication	3, 5, 7, 9% wt	Thermal properties	Improved
Ilyas et al. (2017)	Al_2O_3/oil	Two-step	40	Functionalization process and ultrasonication	0.5-3% wt	Advanced cooling system	Increased
Chougule and Sahu (2015)	Al_2O_3/DW	Two-step	<100	Functionalization acid treatment method and ultrasonication	0.15, 0.45, 0.60, 1%	Horizontal circular tuba in transition regime	Enhanced
Azmi et al. (2016)	Al_2O_3/W-EG	Two-step	13	Mechanical mixing and ultrasonication	0.6, 0.8, 1.0%	Under turbulent flow in a tube	Increased
Xia et al. (2016)	Al_2O_3/DI-water	Two-step	5	Mechanical agitation and ultrasonication	0.1, 0.5, 1.0%	Micro-channel heat sinks	Better behavior
Lelea and Laza (2014)	Al_2O_3/water	-	13, 28, 36, 47	-	-	Tangential micro tube heat sink with multiple inlets	Improved
Stephen et al. (2018)	Al_2O_3/DW	Two-step	70-90	Ultrasonication	0.09, 0.12%	Compact loop heat pipe	Better thermal performance
Kadirgama et al. (2018)	CNC/W-EG	Two-step	-	Ultrasonication	0.1, 0.5, 0.9, 1.3%	Turning machining	Improved

Table 2.8   Continued

References	Base fluid	Method	NPs size (nm)	Dispersion technique	Volume concentration	Observation	Thermal conductivity
Murshed, Leong, and Yang (2008)	Al_2O_3/ DI-water	Two-step	-	Ultrasonication	1-5%	Thermal conductivity and viscosity	Enhanced
Rezaei Gorjaei and Shahidian (2019)	Al_2O_3/ water	Three-step	-	Ultrasonication and magnetic stirring	0.5, 1%	Twisted tape inside the curved tube	Wall temperature enhanced
Bahrevar, Jahanfarnia, and Shayesteh (2018)	Al_2O_3/ DI-water	Two-step	13	Non-ionic surfactant and sonication	1-4.5%	Direct absorption solar collector	Improved outlet temperature
K Ramachandran et al. (2017)	CNC/ W-EG	Two-step	-	Ultrasonication	0.1, 0.5, 0.9%	Thermal conductivity and viscosity	Increased effective thermal conductivity
Mashaei, Shahryari, and Madani (2016)	Al_2O_3/ water	-	-	-	2, 4, 6%	Numerical analysis on cylindrical heat pipe	Best thermal-hydraulic performance
Kim et al. (2019)	Al_2O_3/ DW	Two-step	40	Ultrasonication	0.5, 1.0, 2.0% wt	Compact heat exchanger	Increased
Agarwal et al. (2016)	CuO/water, EG, engine oil	Two-step	66, 55	Ultrasonication	0.25, 0.5, 0.75, 1, 1.25, 1.5, 1.75, 2%	Synthesis, characterization, thermal conductivity and sensitivity	Enhanced
Kole and Dey (2012)	ZnO/EG	Two-step	<50	Ultrasonication	0.005, 0.0375%	Thermophysical and pool boiling	Enhanced
Muraleedharan et al. (2016)	Al_2O_3/ Therminol-55	Two-step	30-40	Ultrasonication	0.025, 0.05, 0.075, 0.1, 0.2, 0.3%	Concentrating solar collector	Enhanced
Said, Saidur, and Rahim (2016)	Al_2O_3/ DI-water	Two-step	13-20	High-pressure homogenizer	0.1%	Flat plate solar collector	Excellent performance

Viscosity (dynamic) is a very important property of nanofluids as the viscosity of nanofluids increases than the base fluid due to the loading of nanoparticles into it. Viscosity increases linearly with increasing volume fractions of nanofluids. But viscosity decreases when the temperature of nanofluids increased. Aggregation also influence the viscosity of nanofluids (Turgut et al., 2009; Wang, Chen, & Witharana, 2013). In a study, Pourmohamadian et al. (2019) investigated that the viscosity of nanofluids significantly decreases with increasing temperature and slightly increases with an increment mass fraction of nanoparticles. Not only that viscosity of nanofluids also depends on the several other factors such as size and shape of nanoparticles, base fluid properties, pH of nanofluids, temperature, synthesis of nanoparticles, stable dispersion methods and stability of nanofluids (Jeong et al., 2013; Koca, Doganay, & Turgut, 2017; Li, Zhu, & Wang, 2009); whereas Bashirnezhad et al. (2016) mentioned that most of the experimental studies investigated and reported the effects of two or three important parameters including temperature, volume concentration on viscosity of nanofluids. Moreover, surfactants used to make stable nanofluids which also affect the viscosity of nanofluids such as Kaggwa et al. (2019) studied the effect of surfactants on viscosity and revealed that various types of surfactants significantly increased the viscosity of nanofluid individually prepared on different base fluid. In addition, Nguyen et al. (2007) concluded that the particle-size plays an important role in high concentration and viscosity of nanofluids.

On the other hand, Koca et al. (2018) stated that viscosity of nanofluids increases with decreasing particle sizes but in several cases, viscosity also increases with increasing particle size. Generally, viscometer is used to measure the viscosity of nanofluids and viscometer depends on how the flow is maintained or initiated (Macosko & Larson, 1994) as shown in Table 2.9. Viscometers are mainly two types e.g. drag flow type and pressure-flow type. Generally, drag flow meter viscometers are very simple. Besides that, they are good for low viscosity and transparent liquid, homogeneous shear, suitable for high temperature, high shear rate and pressure, and specifically best for the non-Newtonian fluids. On the other hand, pressure flow type viscometers are complex structures and tough to clean. These are preferable for high shear and rate but not suitable for dynamic viscosity and non-Newtonian fluids. Moreover, there is another type of viscometer called ultrasonic which is good for a high viscous fluid with a small amount (Table 2.9).

Table 2.9   Classification of viscometer

Geometry/Type	Basic characteristics
Drag flow type	
Rotating concentric cylinders	Good for low viscosity and high shear rates
Rotating cone and plate	Homogeneous shear, best for non-Newtonian fluids and normal stresses
Rotating parallel disks	Same as cone-and-plate but inhomogeneous shear
Sliding parallel plates	Simple design, homogeneous shear, and good for high viscosity
Falling body	Very simple, good for high temperature and pressure
Rising bubble	Suitable for transparent fluids
Oscillating body	Needs instrument constant and good for low viscous liquid metals
Pressure flow type	
Long capillary	Simple, very high shears and range
short capillary	Simple, reliable, but not suitable for absolute viscosity and non-Newtonian fluids
Slit pressure flow	Same as capillary, but difficult to clean
Axial annulus pressure flow	Better shear uniformity, but more complex, eccentricity problem
Others/Miscellaneous	
Ultrasonic	Good for high viscosity fluids and small sample volume

Specific heat is one of the most important criteria of nanofluids and it depends on the volume concentrations of nanofluids. Increasing volume concentrations decreases the specific heat of nanofluids (Zhou & Ni, 2008). Similarly, Namburu et al. (2007) experimentally investigated the specific heat of SiO_2/water-ethylene glycol (60: 40) nanofluids with a volume concentration range of 0-10%. The authors concluded that the specific heat of SiO_2 nanofluids decreases as the volume concentrations of nanofluids increase and about 12% decreases than the base fluids at 10% volume concentration of SiO_2 nanofluid. However, the specific heat of nanofluids increases with an increase in temperature and it does not depend on the particle-size of nanofluids as well (Satti, Das, & Ray, 2016). Differential scanning calorimetry (DSC) is a highly sensitive technique can be used to measure the specific heat capacity (C_p) of both solid and fluids (Kodre et al., 2014; O'neill, 1966).

The density is one of the most important physical properties of the nanofluid as it plays a major role in heat transfer exchange. In heat gain, the mass flow rate usually derived from the volume flow rate directly which defines the density value (Teng & Hung, 2014). Furthermore, density shows interesting behaviour in volumetric concentrations

(Vallejo et al., 2018) as well as influences various important factors of nanofluids such as pumping power, friction factor, Reynolds number, etc (Shoghl, Jamali, & Moraveji, 2016). Moreover, base fluid performs an important role in the density of nanofluids (Sharifpur, Yousefi, & Meyer, 2016). In a study, Vajjha, Das, and Mahagaonkar (2009) investigated that density is also temperature sensitive characteristic of nanofluids. The increasing temperature decreases the density of nanofluids. Besides, Mahbubul, Saidur, and Amalina (2013) concluded that the density and viscosity of nanofluids increased with the augmentation of nanoparticles into base fluids and decreased with the rising of temperature. Density is an influential property of nanofluids which affects the pumping power, friction factor, Reynolds number and so on. Many studies utilized the digital density meter to evaluate the density of nanofluids (Mahian et al., 2013; Said et al., 2013).

The potential of hydrogen (pH) of nanofluids is another important property but very few studies have been conducted on it. There is a very good relation between the pH and stability of the nanofluids as stability depends on the pH which discussed by Lee, Kim, and Kim (2006) in a study. The authors demonstrate that the greater distance between the pH and isoelectric point of particles produces more stable colloidal particles (CuO/water) which modify the thermal conductivity of nanofluids. Not only that but also thermal conductivity of nanofluids depends on the stability and stability associated with the pH of nanofluids such as Wang and Zhu (2009) experimentally studied that the stability and enhancement of thermal conductivity are interrelated, as better dispersed nanofluids accelerate higher thermal conductivity. The increment of thermal conductivity well depends on the stability and the state of surface charge of nanofluids (Huang et al., 2009). Furthermore, increased thermal conductivity enhances the heat transfer more in the application. In addition, Wamkam et al. (2011) investigated that pH induces of zeta potential and stability on heat transfer fluids (ZrO_2 and TiO_2). The authors revealed the thermal conductivity increased significantly near to the isoelectric point of particles which indicates that the stability of nanofluids is influenced by the pH. Moreover, low pH values of nanofluids improve the dispersion behaviour of nanoparticles and decrease the sedimentation of particles in the base fluids; as a result, effective thermal conductivity increased (Gowda et al., 2010). In addition, pH also influences the efficiency of any device or machine greatly (Goudarzi et al., 2015).

Table 2.10   Summary of different thermo-physical performance of nanofluids related studies

References	Nanofluids	Thermo-physical properties				
		Thermal conductivity	Viscosity	Specific heat	Density	pH
Kadirgama et al. (2018)	CNC/W-EG	Increased	Enhanced	-	-	-
Kaaliarasan Ramachandran et al. (2017)	CNC/W-EG	Increasing trend	Increasing pattern	-	-	-
Kole and Dey (2012)	ZnO/EG	Enhanced in maximum 40%	Increased	-	-	-
Lee et al. (2012)	ZnO/EG	The maximum increase of 23%	Increment of viscosity	-	-	-
Turgut et al. (2009)	TiO_2/water	Enhanced	Increased linearly with particle concentration but decreases with increase in temperature	-	-	-
Longo and Zilio (2011)	Al_2O_3, TiO_2/water	Increased	Significantly increased	-	-	-
Jeong et al. (2013)	ZnO/water	Maximum 18% increased	Significantly increased	-	-	-
O'Hanley et al. (2012)	Al_2O_3, SiO_2, CuO/water	-	-	Decreased with increasing volume fractions of NPs	-	-
Agarwal et al. (2016)	CuO/water, EG, engine oil	Enhanced	Increased	-	Increased	-
Singh et al. (2017)	Al_2O_3, SiO_2, CuO/ water emulsion-vegetable oil	Increased	-	Declined	-	-

Table 2.10   Continued

References	Nanofluids	Thermo-physical properties				
		Thermal conductivity	Viscosity	Specific heat	Density	pH
Vajjha and Das (2009)	Al_2O_3, CuO, ZnO/W-EG	Enhanced	-	-	-	-
Chandrasekar, Suresh, and Bose (2010)	Al_2O_3/water	Increased	-	-	Increased	-
Vajjha, Das, and Mahagaonkar (2009)	Al_2O_3, Sb_2O_5:SnO_2, ZnO/ W-EG	-	-	-	Enhanced	-
Xu, Bandyopadhyay, and Jung (2016)	Al_2O_3/DW-EG	Improved	-	-	Improved	Increased
Namburu et al. (2007)	Al_2O_3, TiO_2, SiO_2, ZnO, CuO/ W-PG	-	-	Decreased	-	-
Kaggwa et al. (2019)	C, Al_2O_3, CuO/W-EG	-	Increased	-	-	-
Gowda et al. (2010)	Al_2O_3, CuO/DI-water, EG	Enhanced	-	-	-	Influenced
Wang and Zhu (2009)	Al_2O_3, CuO/water	Increased	-	-	-	Improved
Lee, Kim, and Kim (2006)	CuO/water	Improved	-	-	-	Increased
Said et al. (2016)	Al_2O_3/water	Effective	-	-	-	Influenced

2.6.6 Applications and Advantages of Nanofluids

The application area of nanofluid is boundless such as industrial, commercial, residential and transportation sectors and so on. Nanofluid should be applied in different electronics products to cool such as air cooling systems, liquid cooling systems and two-phase cooling systems (Lee, 2009). It might be exposed in other electronic devices such as in ceramic lenses, cell phone displays and microscale fluidic devices (Topnews, 2009). Nanofluid has been applied in the domestic refrigerator also (Bi, Shi, & Zhang, 2008). The efficiency of the solar water heating system can be increased by applying nanofluids (Tyagi, 2008). In the heat exchanger, nanofluid could be used to increase its energy efficiency (Elcock, 2007). It should be applied in the transformer to enhance thermal conductivity and dielectric properties of the mineral oil (Davidson, 2009). To cool and to heat the buildings nanofluids can be employed in the conventional heat exchanger (Yu et al., 2007). Nanofluid should be used in defense to cool power electronics and directed energy weapons as well as in another military system such as military vehicles, submarines, and high-power laser diodes, etc. (Xiang-Qi & Mujumdar, 2008). It can be applied in the biomedical industry especially for cancer and tumor cell treatment (Sridhara et al., 2009). To get the best antibacterial behaviour and sustainable antibacterial activities of nanofluids are already evaluated (Lingling et al., 2008). Nanofluid can be employed in a nuclear reactor to heat transfer enhancement as well as economic performance improvement (Saadati, Hadad, & Rabiee, 2018). Nanofluid might be applied to increase the efficiency of the fuel cell (Choi, 1995).

Nanofluids have many beneficial faces. The absorbed solar energy should be maximized by nanofluids depending on the size, shape, material and volume concentrations of nanoparticles. Nanofluids increase the effective thermal conductivity of the heat transfer fluids or working fluids which results in the enhancement of heat transfer coefficient. The mixing fluctuation and turbulence of the fluid are intensified and increased significantly by the nanoparticles. The dispersion of nanoparticles flattens the transverse temperature gradient of the fluid. The properties such as viscosity, specific heat, thermal conductivity, and density may be varied easily by changing the volume fraction of nanoparticles which should be suitable for different industrial applications. Nanofluids have a high thermal capacity which makes them easy to store a large quantity of heat which obviously reduces the energy losses and increases the efficiency of the

system. Nanofluids can pass through pumps and pipes without clogging and fouling. Therefore, it is very demandable in microchannel applications. Nanoparticles dispersed quickly in the base fluids, thus, it reduces the fraction and corrosion that occur in the pipelines and pumps (Hussein, 2016; Pordanjani et al., 2019; Ravisankar et al., 2014).

2.7 Summary

The theoretical background of flat plate solar collector and nanofluids have been viewed in this chapter. FPSC is one of the most important solar collectors for harvesting solar energy to heat the water. The diameter of the header and riser tubes as well as the number of riser tubes were varied which had been used by different research studies. Thereby, to achieve an optimum designing model of the arrangement of header and riser tubes in flat plate solar collectors, CFD numerical simulations has been considered. Moreover, nanofluid is the most promising engineering fluid as it has outstanding thermo-physical properties such as stability, thermal conductivity, viscosity, specific heat, density, and pH. Therefore, it has been preferred to implement the nanofluids in the selected newly design FPSC under direct solar radiation to monitor the efficiency enhancement performance of the collector. Almost all studies used water as the base fluid, thus there is an opportunity to work with water/ethylene glycol as the base fluid for the efficiency enhancement of FPSC. The two-step method has been privileged to prepare nanofluids at various volume concentrations. Moreover, to obtain good stable nanofluids ultrasonication has been preferred. Besides to evaluate the thermo-physical behaviour of nanofluids such as stability, thermal conductivity, viscosity, specific heat, density, and pH properties have been selected.

CHAPTER 3

METHODOLOGY

3.1 Introduction

This chapter describes the overall research plan and research methodology which covers the design of the experimental setup, equipment utilized throughout the experiment; different software and technique that has been used in this study. The accumulation of several stages helps to complete the methodology of this study such as (i) designing of flat plate solar collector (arrangement of header and riser tubes), (ii) nanofluids characterization, preparation and stabilization, (iii) measurement of different thermo-physical properties of nanofluids, (iv) implementation of nanofluids in FPSC and finally, (v) numerical simulation on actual experimental design and properties of nanofluids successively.

3.2 Methodology Flow Chart

This chapter aims to explain the technique and the design of the experimental research methodology employed in this study. The flowchart is the process flow of the research from the beginning until completion. The purpose of the flow chart is to display the sequence of activities in a process graphically to the viewers to make them understandable. The flow chart of the research methodology has been portrayed in both Figure 3.1 and Figure 3.2; as in this study, the entire experimental work has been done in mainly three segments. Therefore, three types of process flow with an overall process flow has been prepared, as shown in Figure 3.1 and Figure 3.2.
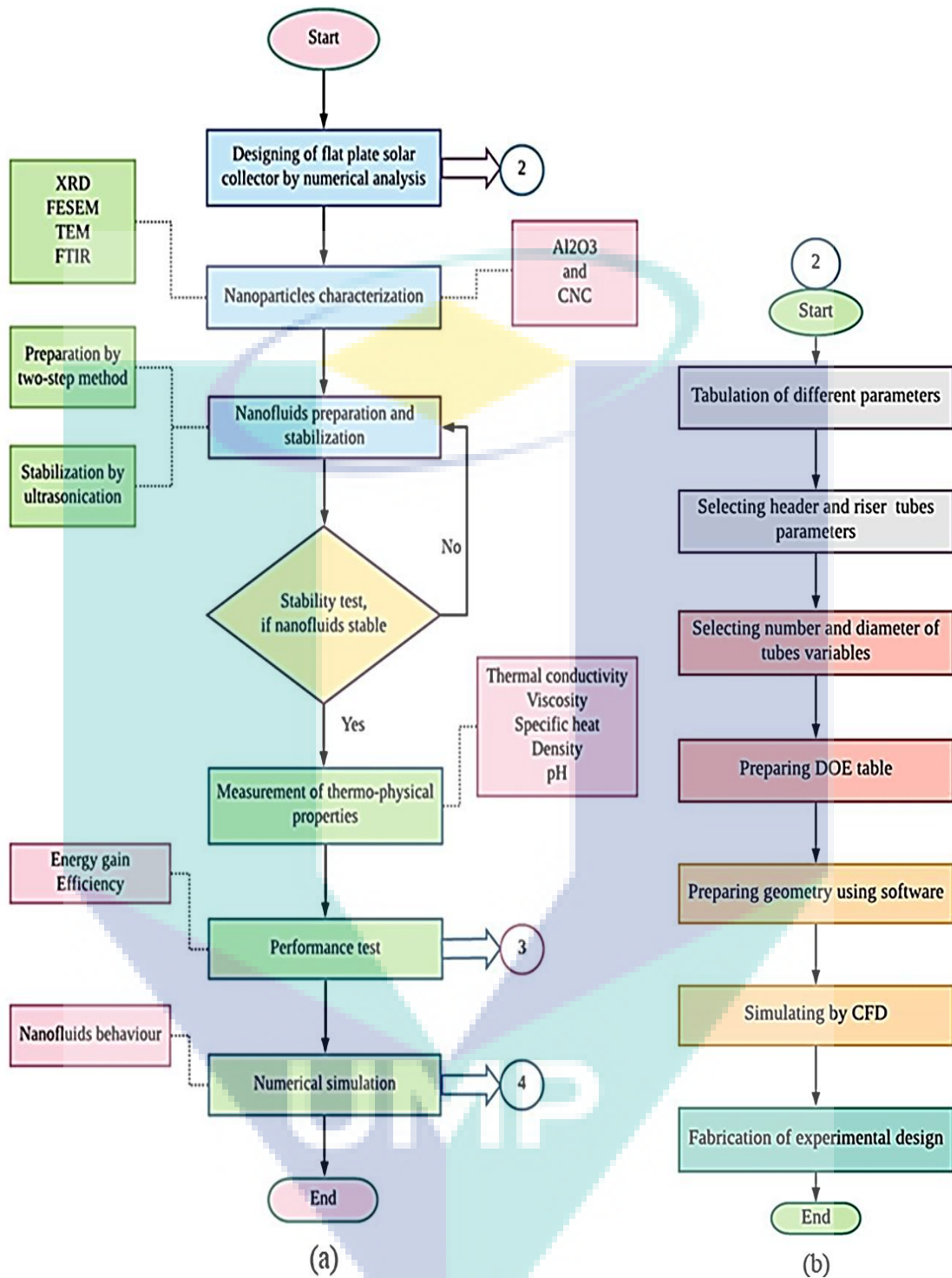
Figure 3.1   Flow chart of research methodology (a) overall process and (b) designing process of the FPSC
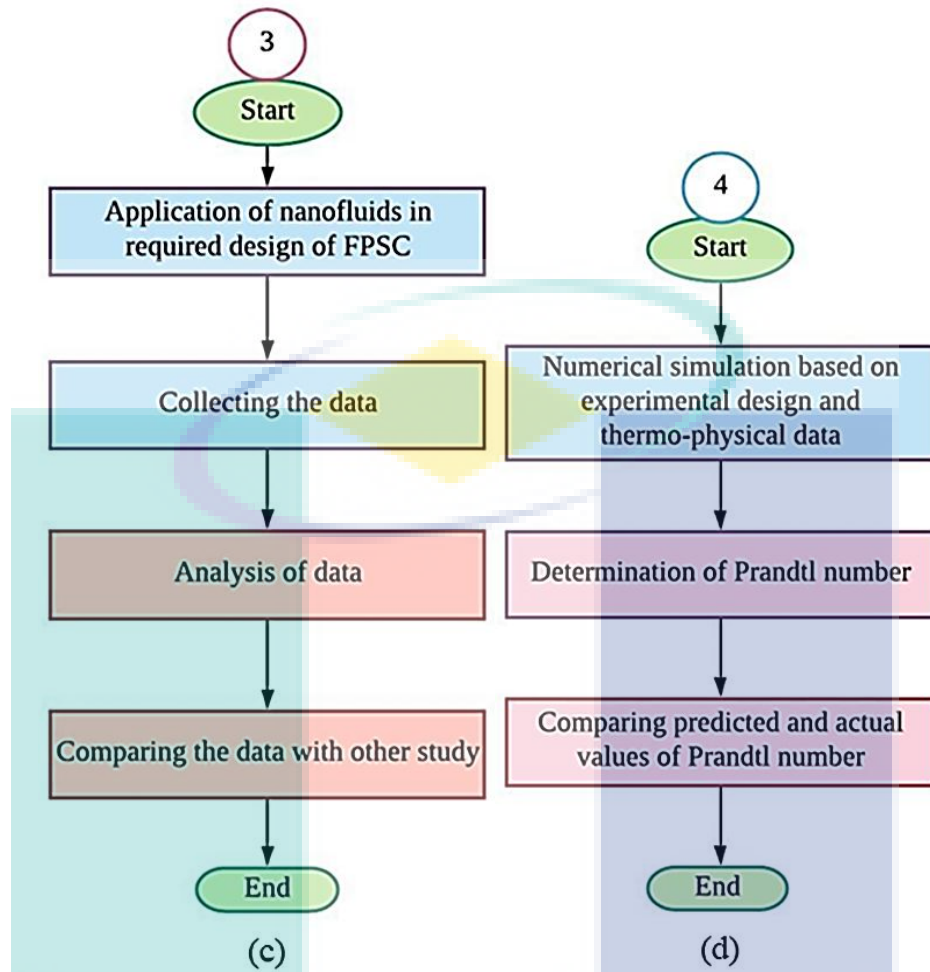
Figure 3.2   Flow chart of research methodology (c) performance test process and (d) numerical simulation process

The overall experimental work has been done into different segments throughout this research study. The study started with computational numerical simulation of the arrangement of header and riser tubes of FPSC using CFD numerical simulation with different fluids and nanofluids. Afterward selecting, preparing and setting the designing model of FPSC has been done to carry out the experiment. Bulk 0.3% and 0.5% volume concentrations of both Al_2O_3 and CNC nanofluids prepared to apply in FPSC by analysing different thermo-physical properties such as stability, thermal conductivity, viscosity, specific heat, density, and pH of the sample nanofluids. Thermographic camera used to measure the surface temperature during the experiment. The experiment conducted under direct solar emission in a steady-state condition. And finally, all the data has been transferred to the computer to calculate the efficiency of FPSC and further analysis. The overall schematic view of this experimental works has been portrayed in Figure 3.3.

3.3 Designing of Flat Plate Solar Collector

Designing of Geometry

The models are designed and developed using different software. The specification parameters of FPSC presented in Table 3.1 which illustrates the diameter, number, thickness, and materials of header and riser tubes. The diameter of the header and riser tubes was varied in this study. The number of header tubes was fixed with two, but it varied for riser tubes. Besides, the thickness of both tubes was fixed and both tubes made off with similar material in copper, as copper is an excellent thermal conductor among the engineering material (Pops, 1993). Table 3.1 has been prepared based on Table 2.4 (Chapter 2) to make the design of experiment (DOE) table. To prepare the DOE table the even number of diameter and number of the tubes (header and riser) has been selected. DOE table (Table 3.2) has been created following the response surface methodology (RSM) using software based on Table 3.1. Box–Behnken design model (BBD) of RSM has been selected and the designing statistical approach of geometries has been shown in Table 3.2. Three types of variables such as the number of the risers (8, 12, and 16), the diameter of the header (22 mm, 23 mm, and 24 mm) and the diameter of the riser (10 mm, 11 mm, and 12 mm) have been portrayed in Table 3.2. Three-dimensional combined geometry of header and riser tube has been generated by using software following the variables as depicted in Table 3.2 and thirteen geometries have been prepared as well. Different geometries of the combination of header and riser tube of FPSC has been portrayed in Figure 3.4. All models have an equal number of header tubes, but the number of riser tubes varied such as eight, twelve and sixteen accordingly. A total of thirteen number of the designing models has been prepared and these have been categorised into three groups.

Table 3.1   Designing specification parameters of FPSC

Specification parameters	Values and properties
Diameter of header tube	22-25.4 mm
Diameter of riser tube	10-12.5 mm
Thickness of header tube	0.6 mm
Thickness of riser tube	0.45 mm
Number of header tube	2
Number of riser tube	7-15
Header tube material	Copper
Riser tube material	Copper
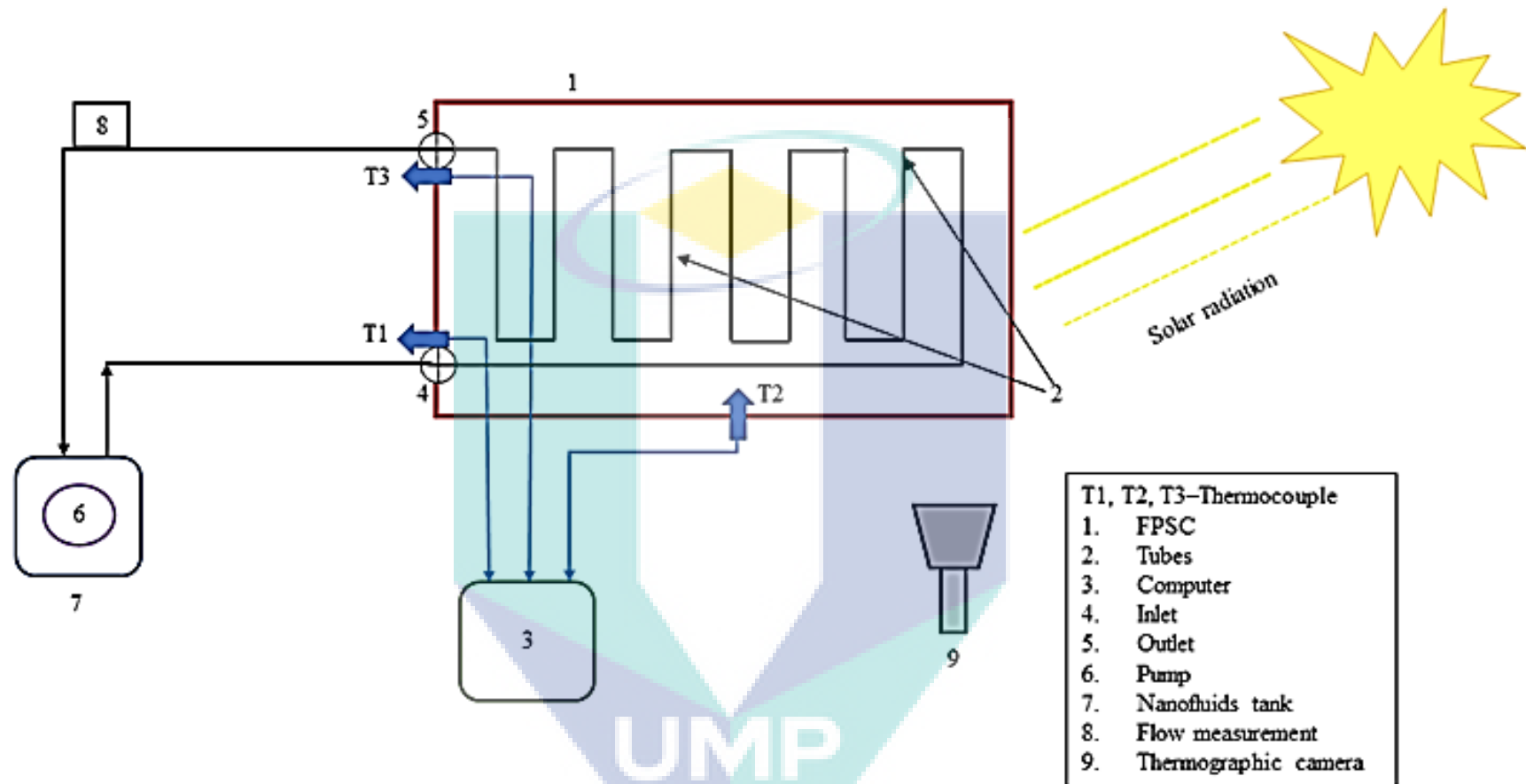
Figure 3.3   Schematic diagram of experimental setup

Table 3.2   Table of design of experiment (DOE) for the geometries of FPSC

Serial no.	Number of riser tubes	Diameter of header tube (mm)	Diameter of riser tube (mm)
1	8	23	10
2	12	22	12
3	8	24	11
4	16	24	11
5	16	22	11
6	12	23	11
7	12	22	10
8	12	24	12
9	16	23	12
10	8	22	11
11	12	24	10
12	8	23	12
13	16	23	10

In the first group, designing models that consist of eight riser tubes were in four numbers. Second group, the models made of twelve rise tubes was in five number and lastly, the designing models that consists of sixteen riser tubes was in four number also. All the designs have been identified according to the number of riser tubes-diameter of header-diameter of riser that is 8-23-10. Afterward, all these designing models have been imported to CFD for computational numerical simulations one after another. The modelling part has been commenced with the designmodeler. Thereafter, one by one step such as meshing, setup, solution, and results has been performed in CFD numerical simulations for all the designing models. The systematic analysis of designing of FPSC in CFD simulation has been portrayed in Figure 3.5.

3.4   Modelling of Flat Plate Solar Collector

DesignModeler

The geometries have been imported to the designmodeler in analysis systems fluid flow fluent of ANSYS workbench R15.0 in a suitable form for computational simulations. The geometry has been edited in fluid form in modelling option with geometry type design modeler and automatic shared topology method as shown in Figure 3.6. All riser tubes within a defined categorised geometry showed the same number of faces, edges, and vertices; and the two header tubes also showed the similarities in faces, edges, and vertices between them. But the number of faces, edges, and vertices differ for header and riser tubes in geometry. Not only that, the number of faces, edges, and vertices of riser

tubes in all types of geometry was similar while it only varied for header tubes in different categorised geometry; for instance, all eight riser tubes geometries showed the different number of faces, edges, and vertices compared with the twelve and sixteen riser tubes geometries for header tubes. The faces of eight riser tubes, twelve riser tubes, and sixteen riser tubes were 28, 40, and 52 respectively for header tubes. Besides, the edges of eight riser tubes, twelve riser tubes, and sixteen riser tubes were 78, 114, and 150 of header tubes accordingly. And finally, the vertices of eight riser tubes, twelve riser tubes, and sixteen riser tubes were 52, 76, and 100 for header tubes respectively. Whereas the faces, edges, and vertices for all types of geometries were 4, 6, and 4 for riser tube respectively. Moreover, the volume and the surface area depending on the diameter of the riser tubes. The volume was 0.00012133 m^3, 0.00014807 m^3, and 0.00017747 m^3 for the diameter of 10 mm, 11 mm, and 12 mm of riser tubes respectively. On the other hand, the surface area was 0.05095 m^2, 0.056302 m^2, and 0.061657 m^2 for the diameter of 10 mm, 11 mm, and 12 mm of riser tubes accordingly.
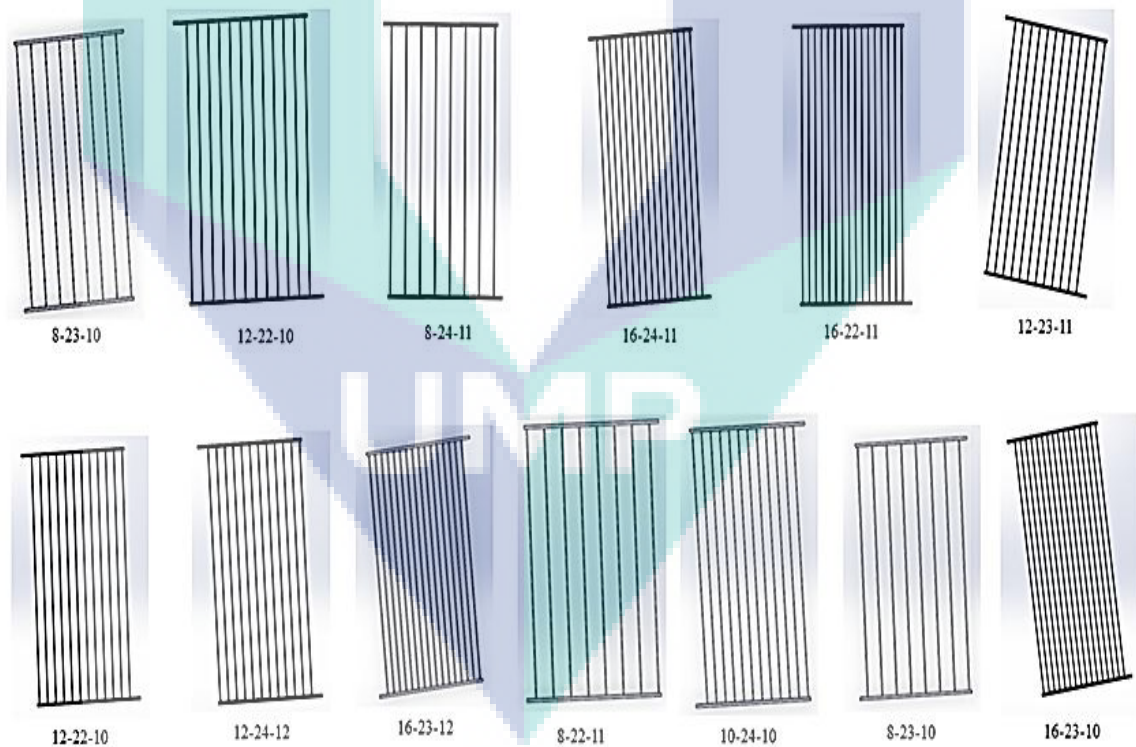
Figure 3.4   Different geometries of designing models of flat plate solar collector
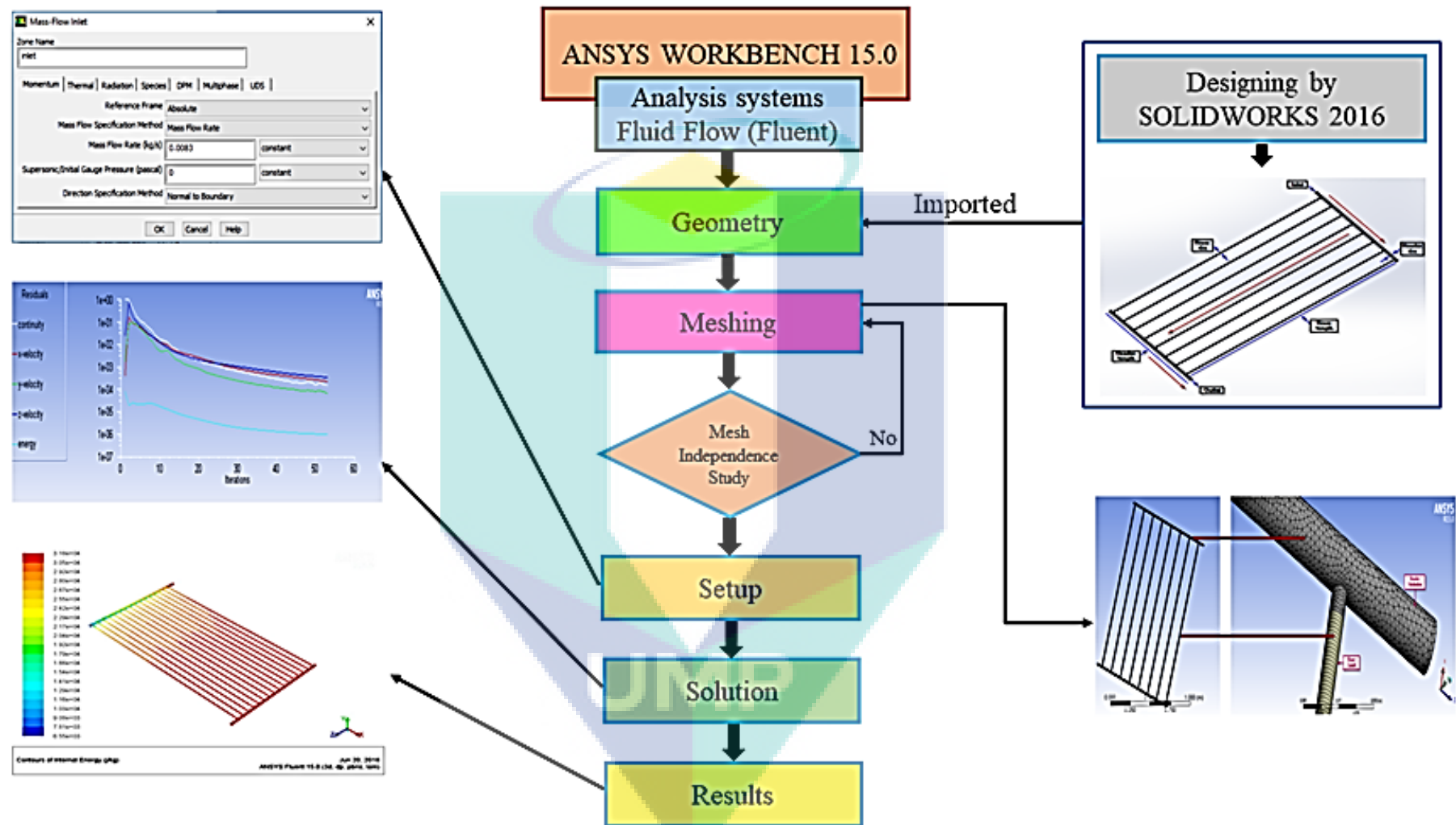
Figure 3.5   Schematic diagram of systematic analysis of designing of flat plate solar collector
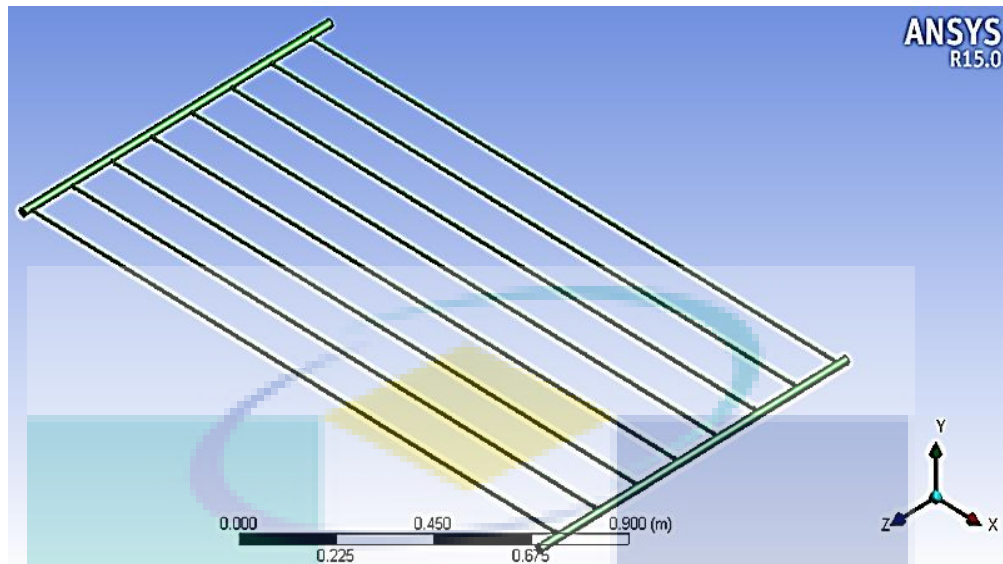
Figure 3.6   Edited geometry of designing model in designmodeler of CFD simulation

Meshing

Meshing is the most important and critical component of CFD modelling (Pointer, 2004). Meshing quality depends on meshing techniques. Meshing elements and the grid of cells are subjected to solve the fluid flow equations (Madenci & Guven, 2015). Automatically, tetrahedrons and cutcell meshing have been done in the three-dimensional computational domain with physics preference CFD and solver preference fluent. Figure 3.7 shows the 3D meshed model of the header and riser tube. The common mesh sizing parameters for all models has been depicted in Table 3.3. In addition, mesh independence test studied by changing mesh sizing relevance center such as coarse, medium and fine.

Mesh metric (Skewness and Aspect Ratio) and smoothness determine the quality of the mesh. The overall range of skewness is from zero to one. Whereas the maximum skewness must be below 0.98 otherwise solutions should simply fall in divergence error. The ratio between the longest length to shortest edge called aspect ratio and 1.0 defines the best aspect ratio as it determines the cell is nicely square of any shape. Smoothness describes the change of cell to cell gradually and it must not be more than 20%. In addition, nodes and elements quantity are very sensitive since it has a significant effect on the ultimate results and computational time. Higher meshing elements will allow better outputs but longer computational time (Madenci & Guven, 2015; Noor, Wandel, & Yusaf, 2013). Table 3.4 illustrates the volume of the nodes, elements and mesh metric of all

47

models. The maximum, minimum, average and standard deviation of skewness and aspect ratio has been portrayed in Table 3.4.

Table 3.3   Parameters of mesh sizing

Sizing	Setting
Advanced size function	Curvature
Relevance centre	Coarse
Initial size seed	Active assembly
Smoothing	Medium
Transition	Slow
Span angle center	Fine
Curvature normal angle	Default (18.0º)
Growth rate	Default (1.20)
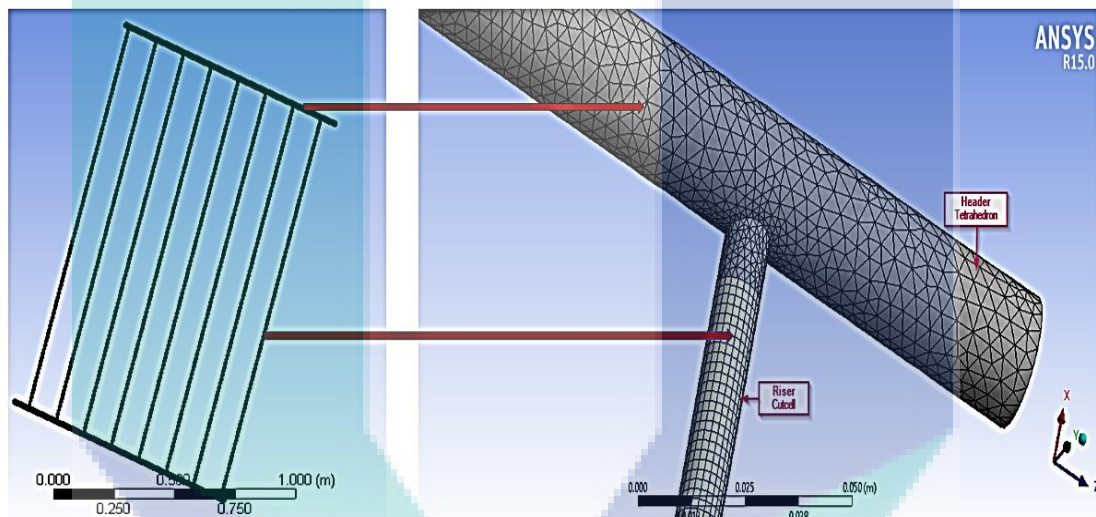
Figure 3.7   Meshing of geometry

Setup

In the setup of CFD simulations, double precision option and serial processing option is selected in the fluent launcher window. Afterward, mesh checking has been done following the selection of models. Pressure-based, absolute-velocity and time-steady solver has been selected. Energy equation and Viscous-Laminar model used for CFD simulations (Hawwash et al., 2018; Noor, Wandel, & Yusaf, 2013). Prior to select models, Reynolds number and flow behaviour have been identified empirically by the (Eq. (3.1)) (Reynolds, 1883):

$$R_e = \frac{\rho D v}{\mu} \qquad\qquad 3.1$$

Table 3.4   Statistics of meshing of all geometries

Features	Final outcomes of meshing statistics												
	8-23-10	**12-22-12**	**8-24-11**	**16-24-11**	**16-22-11**	**12-23-11**	**12-22-10**	**12-24-12**	**16-23-12**	**8-22-11**	**12-24-10**	**8-23-12**	**16-23-10**
Nodes	707390	861324	626092	1231866	1245222	914026	1017219	845529	1129621	640159	985951	584387	1368710
Elements	757895	901217	678046	1246642	1266808	948547	1049480	888232	1153447	699596	1015053	642160	1372751
Mesh metric	Skewness	Skewness	Skewness	Skewness	Skewness	Skewness	Skewness	Skewness	Skewness	Skewness	Skewness	Skewness	Skewness
Min	1.4735568286E-03	8.76845680711E04	8.8508405578E-04	2.7288680380E-04	5.2210933558E-04	5.6278280284E-04	1.6799775534E-04	5.8549523064E-04	8.4099908265E-04	1.1370100408E-03	5.2396208161E-04	6.2235639386E-04	6.5606347454E-04
Max	0.83219643901701	0.89820106198574	0.88367718076568	0.85563479481068	0.89323563385607	0.84765385639137	0.92350058235923	0.82155792240312	0.87798385806018	0.89674518779307	0.89367632653518	0.84235324700740	0.89572713219681
Average	0.25925241137696	0.27397640833837	0.25335915388694	0.30057457495214	0.28138667812897	0.33801886459001	0.32581427830475	0.30217801227277	0.26555692117667	0.25336486512380	0.31347810843584	0.28356991332943	0.33996067429118
Standard deviation	0.1287443188215	0.14780946103553	0.13478519529395	0.16646092397526	0.15191328423617	0.18529803675810	0.19132201413270	0.15623043978635	0.14269122633034	0.14103092840439	0.17262495606620	0.14804336998967	0.19074271121957
Mesh metric	Aspect ratio	Aspect ratio	Aspect ratio	Aspect ratio	Aspect ratio	Aspect ratio	Aspect ratio	Aspect ratio	Aspect ratio	Aspect ratio	Aspect ratio	Aspect ratio	Aspect ratio
Min	1.0699	1.0823	1.085	1.1558	1.1681	1.087	1.1039	1.1099	1.1014	1.1597	1.126	1.1417	1.1536
Max	32.349	18.936	22.63	15.937	30.11	18.645	70.933	9.7782	23.934	33.493	28.469	11.842	36.243
Average	2.17352423990135	2.0649138304286	2.06671314763306	2.25239560338895	2.17052231719406	2.28645544785871	2.53010228446462	2.13075199835179	2.18936588824634	2.13415194183508	2.24951186154806	2.11631239488611	2.54828219932092
Standard deviation	1.44980636716343	0.64376714161980	0.65295450510789	0.91833498257666	0.78650301796948	1.10578508056881	2.69645272955209	0.69671019151943	0.77043414845259	0.73351103964240	1.27306433356882	0.7039438448611	2.07617636285241

49

After that, the properties of fluids have been created/changed in the fluent fluid material page from a fluent database in the material window of the setup of CFD simulations. The theoretical values of different properties of materials have been fixed here. These theoretical values have been collected and calculated using the following (Eq. (3.2), (3.3), (3.4), and (3.5)) and Table 3.5 illustrates the theoretical different properties of fluids and nanofluids. In the case of boundary conditions, mass-flow-inlet and pressure-outlet type were selected for inlet and outlet respectively. The mass flow rate was 0.0083 kg/s (Ranjith & Karim, 2016; Said et al., 2015). The temperature was constant in both inlet and outlet and that was 300 K (26.85°C). The fluid domain was wall type with stationary wall motion and no-slip shear condition and finally, reference values are computed form inlet.

i.   The density of nanofluid defined as Drew and Passman (2006):

$$\rho_{nf} = \phi\rho_s + (1-\phi)\rho_f \qquad\qquad 3.2$$

ii.   Thermal equilibrium defines the specific heat of nanofluids (Choi, 1995):

$$C_{p,nf} = \frac{\phi(\rho C_p)_s + (1-\phi)(\rho C_p)_f}{\rho_{nf}} \qquad\qquad 3.3$$

iii.   Thermal conductivity of nanofluids calculated by the following equation (Suresh et al., 2011):

$$\frac{k_{nf}}{k_f} = \frac{k_s + 2k_f + 2\phi(k_s - k_f)}{k_s + 2k_f - \phi(k_s - k_f)} \qquad\qquad 3.4$$

iv.   The viscosity of the suspension defined as (Suresh et al., 2012):

$$\mu_{nf} = \mu(1 + 2.5\phi) \qquad\qquad 3.5$$

Table 3.5   Physical properties of required fluids and nanofluids

Physical properties	Water	Ethylene glycol	60% Water + 40% EG	TiO$_2$	Crystal nano-cellulose
Density (kg/m^3)	998.2	1111.4	1050	2640	1050
Specific heat (J/kg-K)	4182	2415	3600.648	1270.424	2450.324
Thermal conductivity (W/m-K)	0.6	0.252	0.260	0.91	0.31
Viscosity (kg/m. s)	0.001003	0.0157	0.0022	0.00495	0.00495

Solution

Solution calculation is performed based on pressure-velocity coupling with simple scheme and spatial discretization. Under spatial discretization least-squares cell-based gradient, second-order pressure, second-order upwind momentum, and second-order upwind energy have been fixed. Solution control parameters (Under-relaxation factors) for computational simulations are described in Table 3.6. CFD simulations have been initialized by the standard solution initialization method. Moreover, relative to cell zone reference frame was fixed and computation is done from the inlet. And in the end, the calculation has been run with a hundred number of iterations.

Table 3.6   Solution control parameters

Parameters	Setting values
Under-relaxation factors	
Pressure	0.3
Density	1
Body forces	1
Momentum	0.7
Energy	1
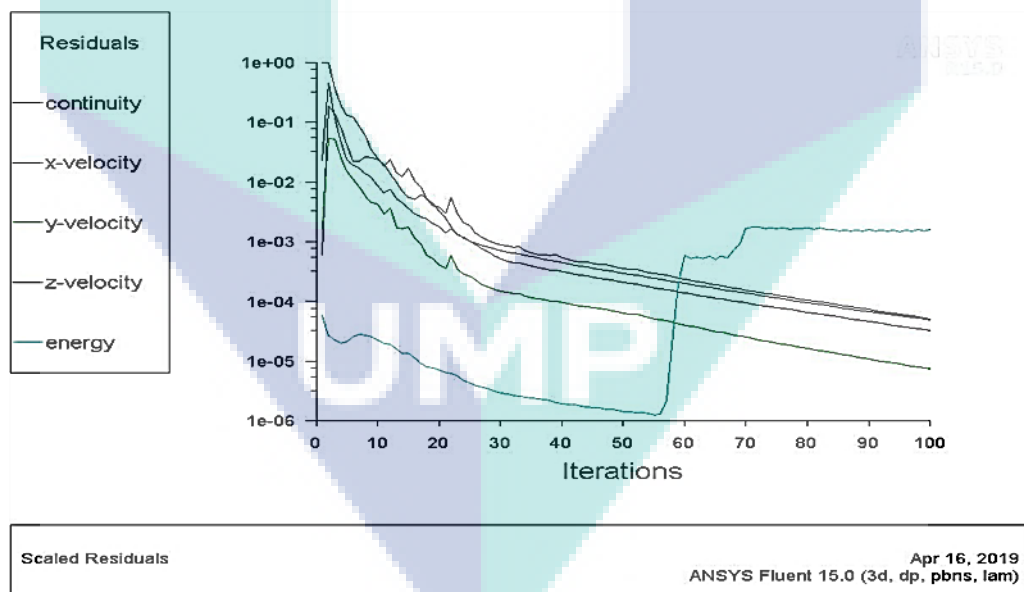
Figure 3.8   Discontinuation of energy equation converge solution

About all designing models showed convergence equation of solution with all parameters but a few designs performed divergence equation with some parameters as shown in Figure 3.8. The energy residual of fluent flow suddenly changed the direction of the movement during solution calculation as well as in the final stage of calculation, it was not in parallel with other residuals. Moreover, the converged solution equation of the CFD simulations is relatively similar for all the designing models. All the residuals such as continuity, velocity, and energy are in the equal state during the solution calculations.

Results

The results of computational simulations can be analysed both in data interpretation and graphical images. In this study, both have been performed. For graphical presentation, the contour selected in the graphics and animation section in the post-processing results of CDF simulations. Here contour of temperature specifically internal energy has been analysed; for instance, Figure 3.9 describes the contour of the internal energy of CFD simulation of fluent flow. The numerical data has been obtained by computing all the surfaces of the geometry in the contours of temperature (Internal energy) in the post-processing results of CFD simulations.
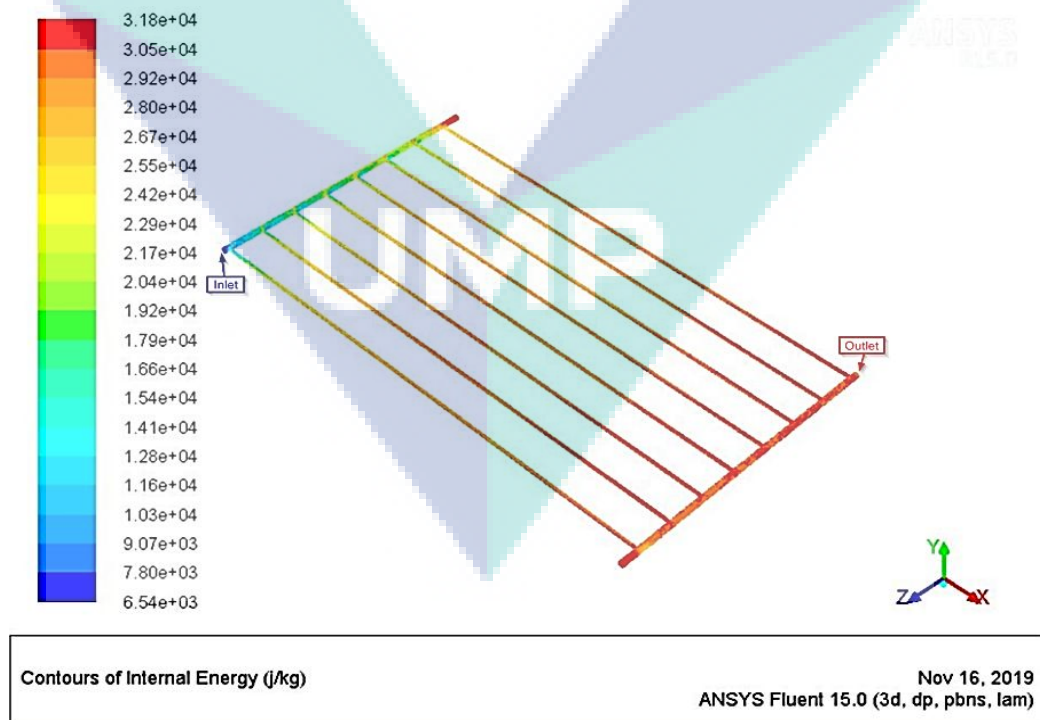
Figure 3.9   Contour of internal energy of CFD simulation

3.5   Nanoparticles and Base fluid

3.5.1   Selection of Nanoparticles and Base fluid

Aluminium Oxide (Al₂O₃) Nanoparticles

One of the main advantages of metal oxide nanoparticles such as CuO, TiO_2, ZnO, SiO_2, etc is that they are already oxidized; therefore they are very resistant to further oxidation and thus chemically stable (Fernández- García & Rodriguez, 2011). Besides that, in a study, Suganthi and Rajan (2017) mentioned that some important factors need to be considered of nanoparticles before going to prepare nanofluids for heat transfer applications including thermal properties, compatibility with base fluids, chemical stability, cost, availability, and toxicity. Moreover, the authors determined that metal oxide nanoparticles have a low density for that amount of material used will be low for a defined volume concentration; perform higher thermal conductivity and specific heat as well. Several kinds of literature studied the thermal behaviour of Al_2O_3 nanofluids and concluded with the thermal property enhancement upon the loading of Al_2O_3 nanoparticles, as shown in Table 2.8 (Chapter 2). In addition, Al_2O_3 is highly chemically and thermally stable nanofluid (Kim, 2008; Lei et al., 2009). Al_2O_3 nanofluid has the lowest precipitation rate and greatest emulsification stability among all other nanofluids and precipitation rate increased with time as well (Lin, Wang, & Chen, 2011). Moreover, Suganthi and Rajan (2017) also mentioned that Al_2O_3 nanoparticles have been investigated extensively due to its high thermal conductivity and low density. Therefore, in this study aluminium oxide (Al_2O_3) anhydrous nanoparticle has been used and it was procured from Bendosen Laboratory Chemicals.

Crystal Nano-Cellulose (CNC) Nanoparticles

Crystal nano-cellulose (CNC) is a newly invented nanoparticle and there is not enough research literature on it especially on the mechanical engineering field. CNC is a renewable and eco-friendly nanoparticle, as it exists in nature abundantly. A few studies have been conducted with CNC nanofluids to evaluate its thermal properties and thermal application as well; such as Kaaliarasan Ramachandran et al. (2017) investigated the effective thermal conductivity and relative viscosity of CNC dispersed in ethylene glycol-water mixture base fluid as a heat transfer through a combined experimental-theoretical approach using statistical response surface methodology. The authors found that the

thermal conductivity and relative viscosity has a rising trend with volume fractions and temperature. Besides, they also concluded as thermal conductivity linearly increases with an increase volume concentration of nanofluids whereas viscosity has a proportional relation with volume concentration but inverse relation with temperature. Similarly, in this study CNC nanoparticle used and was purchased from Blue Goose Biorefiners Inc. company with a weight concentration of 8.0% w/w. The specification of CNC nanoparticles was provided by the company as presented in Table 3.7.

Table 3.7   Specification parameters of CNC

Parameter	Value
Crystallinity index	80%
Crystal length	100-150 nm
Crystal diameter	9-14 nm
Hydrodynamic diameter	150 nm

Base fluid

Ethylene glycol (EG) is a colourless, odourless, hygroscopic, non-volatile liquid with lower viscosity and a higher boiling point ($198^{o}C$) (Yue et al., 2012). Besides, EG is a non-flammable and low toxic substance as well as it is superior to higher volumetric energy density. Moreover, it is completely soluble with water and with other polar solvents (Kim et al., 2011; Zhang et al., 2019). The sources of EG are plentiful and have a wide range of application potentiality; therefore, the study on composing newly applied methods concerned with energy, environment, and technology has been expanding for the last two decades (An & Chen, 2016; Serov & Kwak, 2010). Water has been used in many research studies as the base fluid for nanofluid applications and it is observed in Table 2.8 (Chapter 2) that most of the studies conducted with water as base fluid. Nanofluids based on water performed good thermal properties and good efficiency as well. However, water-based nanofluids have one important drawback is corrosion (Prajitno & Syarif, 2014). In addition to this, Bubbico et al. (2015) experimentally analysed the corrosion behaviour on metal surfaces (copper, aluminium and stainless steel) using different water-based TiO_2, Al_2O_3, SiC, and ZrO_2 nanofluids. The authors revealed that the metal surfaces are affected by nanofluids chemical corrosion. On the other hand, Zhang et al. (2018) experimentally investigated the corrosion behaviour of ethylene glycol on stainless steel and revealed that a layer of Al-alcohol products reduces the corrosion rate of that metal. Thereby, EG with distilled water (W: EG 60: 40) has been

selected as the base or working fluids with considering the thermal performance and corrosion effect of nanofluids.

3.5.2 Characterization Techniques

The nanoparticles of both Al_2O_3 and CNC were characterized by using different characterization equipment such as X-ray diffraction (XRD), Field-emission scanning electron spectroscopy (FESEM), Transmission electron microscopy (TEM), Fourier transform infrared spectroscopy (FTIR), as previously many studies utilized this equipment to characterise the nanoparticles (Baghbanzadeh et al., 2012; Nikkam et al., 2014; Suresh et al., 2011; Wei et al., 2017) and Figure 3.10 show the FESEM image of Al_2O_3 and CNC nanoparticles respectively.
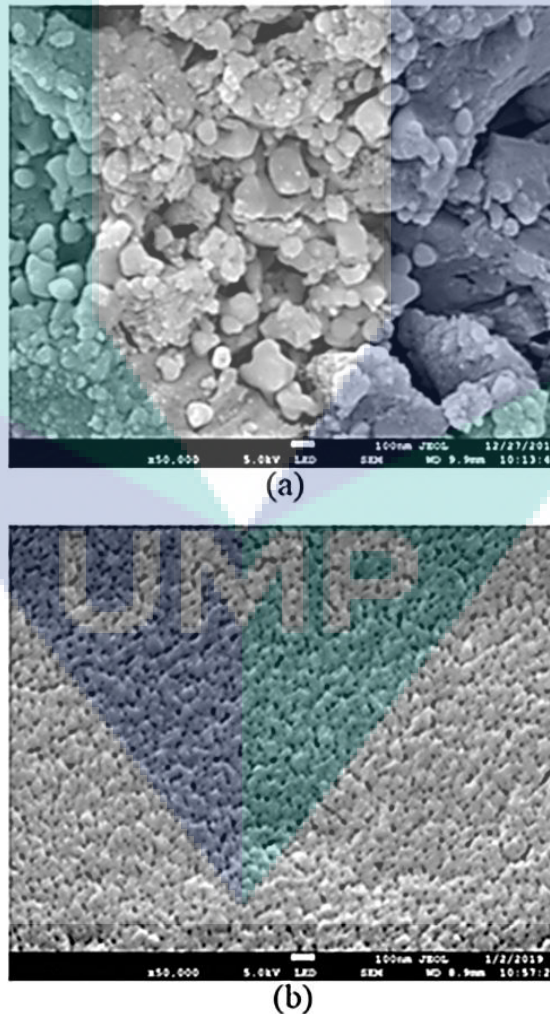
Figure 3.10   FESEM image of (a) Al_2O_3 and (b) CNC in film form (Magnification x50,000; WD 9.9 for Al_2O_3 and WD 8.9 mm for CNC)

3.6   Preparation Method and Stabilization of Nanofluids

In this study, the two-step method has been selected to prepare nanofluids as similar to many previous studies such as Kaaliarasan Ramachandran et al. (2017) and Azmi et al. (2016). Here, sample nanofluids prepared in the primary stage to measure the various thermo-physical properties of nanofluids with different volume fractions at a range of temperatures from 30°C to 80°C. Al_2O_3 and CNC nanoparticles and a mixture of water-ethylene glycol (60: 40) base fluid used. Nanoparticles (Al_2O_3 and CNC) were dispersed into the base fluid (W: EG 60:40) after weighing with high precision (0.0001 g) electronic balance with different volume fractions such as 0.1%, 0.3%, and 0.5%. 200 ml sample nanofluids prepared at various volume concentrations. The required mass of nanoparticles in a dry form corresponding to the volume concentration was calculated using (Eq. (2.4)) (Sundar et al., 2018) in chapter 2.

Then the mixers were mixed/blended using a magnetic stirrer at a range of 400-500 rpm (Favorit, PLT Scientific SDN BHD, Malaysia) until proper mixing or blending appeared. Afterward, ultrasonication has been done by the processor of ultrasonication. Here probe sonication processor used until not any aggregation of nanoparticles observed in the suspension. Moreover, some volume fraction of nanofluids needs two hours to find the solution without aggregation while some nanofluids showed less than two hours to obtain a homogeneous dispersion. Sonication of nanofluids is very necessary to prepare stable nanofluids. Nanoparticles dispersed into the base fluids uniformly and avoiding agglomeration/aggregation of nanoparticles (Abbasi et al., 2013). The preparation method of sample nanofluids as shown in Figure 3.11. One portrayal of the nanofluids (all volume fractions) that have been captured immediately after preparing the sample nanofluids. Afterword the prepared nanofluids (all volume fractions) has been retained for a period to observe the sedimentation phenomena of the nanofluids.

3.7   Measurement of Thermo-physical Properties

Different thermo-physical properties such as stability, thermal conductivity, viscosity, specific heat, density, and potential of hydrogen (pH) have been evaluated using respective standard procedures.
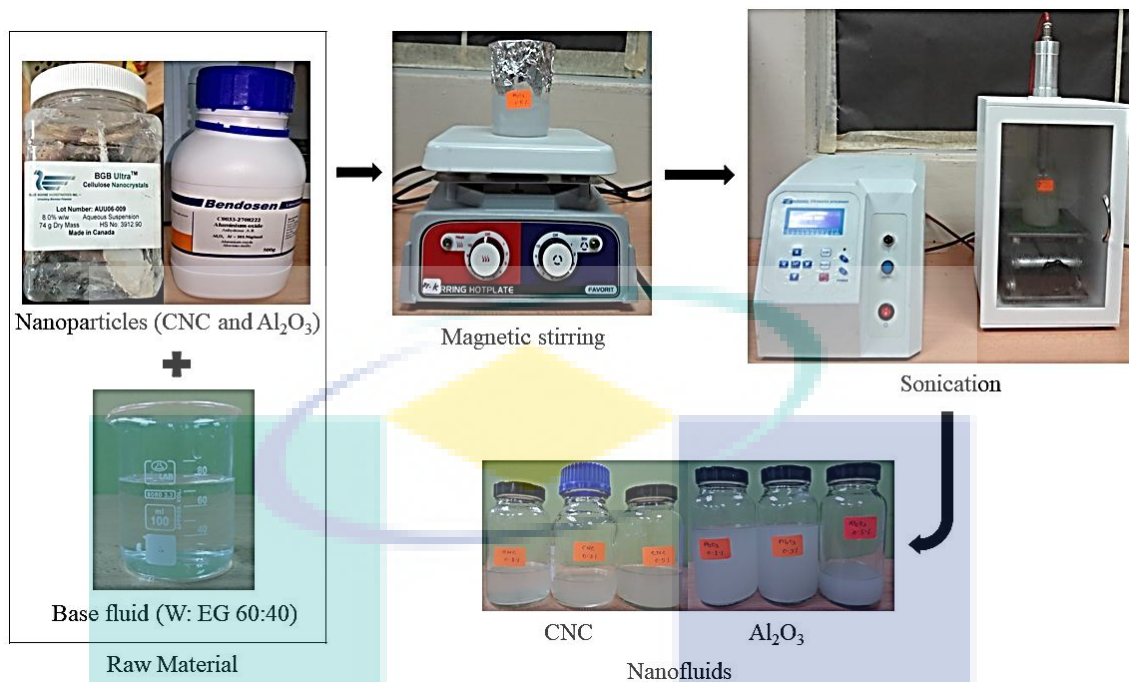
Figure 3.11   Preparation process of nanofluids

3.7.1   Measurement of Stability

The stability of Al_2O_3 and CNC nanofluids has been measured by qualitative and quantitative methods. In the case of the quantitative method, litesizer 500 zeta potential (Anton Paar, Austria) equipment used to measure the stability of both nanofluids (all volume concentrations). Prior to zeta potential measurements of all samples were sonicated for 10 minutes. ELS (electrophoretic light scattering) Omega Cuvette measurement cell used to evaluate the electro kinetic potential in colloidal dispersion. The zeta potential values obtained in the millivolt (Agarwal et al., 2016) with the electrophoretic mobility by the Smoluchowski equation. Figure 3.12 shows the zeta-potential equipment to measure the stability of nanofluids (both Al_2O_3 and CNC) at various volume concentrations. Sedimentation observation (Qualitative method) has been done by naked eyes to examine the stability of Al_2O_3 and CNC nanofluids at various volume concentrations similarly with Kadirgama et al. (2018) conducted the qualitative method to measure the stability of nanofluids in thermal analysis of SUS 304 stainless steel using nano-cellulose/ethylene glycol based nanofluids study.

Figure 3.12   Stability measurement equipment (Zeta-potential)

3.7.2   Measurement of Thermal Conductivity

Thermal conductivity of the base fluid, Al_2O_3, and CNC nanofluid at 0.1%, 0.3%, and 0.5% volume concentrations were measured by KD2 Pro Thermal Property Analyser as shown in Figure 3.13 (Decagon Devices, Inc., USA) followed the standard method entitled "ASTM D7896-14 Standard Test Method for Thermal Conductivity, Thermal Diffusivity and Volumetric Heat Capacity of Engine Coolants and Related Fluids by Transient Hot Wire Liquid Thermal Conductivity Method". The transient hot-wire method was the operating principle of that device. KD2 Pro consists of a handheld controller and a sensor. Here 60 mm long with 1.3 mm diameter single-needle KS-1 sensor used in accordance with the test sample to measure thermal conductivity. This sensor can measure the thermal conductivity between 0.002-2.00 W/m-K with an accuracy of ±5%. The experiment was performed at a temperature range of 30ºC to 80ºC (controlled condition). Memmert water bath with an accuracy of 0.1ºC used to maintain the temperature by the electric current supplied. The sensor is inserted into the test sample bottle and the bottle is immersed into the water bath. To prevent the bending of the sensor, it must be installed in a vertical position with the cap of the bottle. Before starting the actual sample measurement, the sensor was validated by measuring the thermal conductivity of glycerine (k= 0.282 W/m-K at 20ºC); the solution provided by the manufacturer. Moreover, the thermal conductivity measurement verified by measuring the base fluid (60% water and 40% ethylene glycol) and compared with predetermined values of ASHRAE Standard (American Society of Heating, Refrigerating and Air Conditioning Engineers).
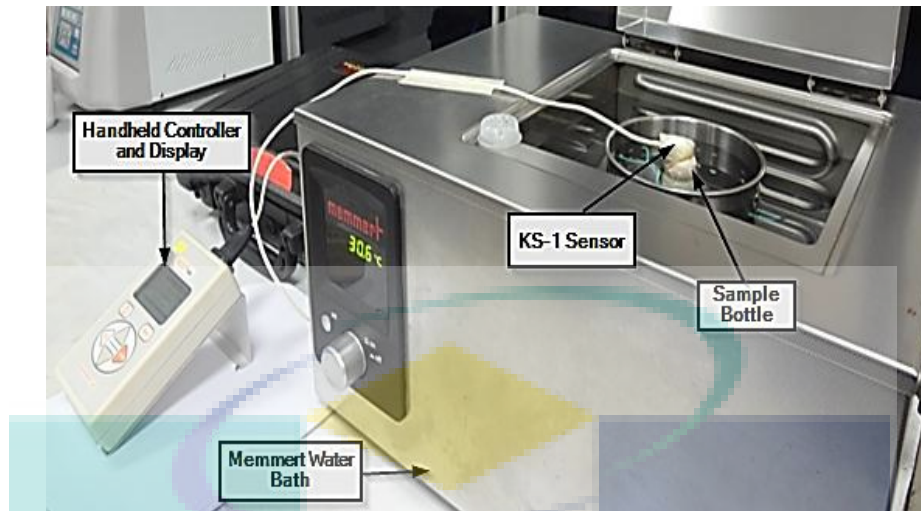
Figure 3.13   Equipment of thermal conductivity measurement (KD2-Pro Thermal Property Analyser)

The maximum deviation between the actual and ASHRAE Standard data of base fluid was 3.2%. The deviation result determines the authenticity of the analyser which can perform the measurement. Each reading was measured with 15-minute interval time for the consistency of the data. To ignore the experimental error repeated measurement readings have been taken and average did for every concentration of the nanofluid samples. Previously many researchers used KD2 Pro Thermal Property Analyser to measure the thermal conductivity of nanofluids in experimental studies (Azmi et al., 2014; Chiam et al., 2017; Esfe et al., 2015; Samylingam et al., 2018).

3.7.3   Measurement of Dynamic Viscosity

In this study, the dynamic viscosity of CNC nanofluids with various volume concentrations was measured at a temperature range of 30ºC to 80ºC by Brookfield RST, Coaxial cylinder rheometer (Figure 3.14) (United States). And the dynamic viscosity of Al_2O_3 nanofluids measured at the same range of temperature by Malvern Panalytical (model Kinexus lab+) (Figure 3.15) manufactured by Malvern Panalytical Ltd, United Kingdom. At first, the viscosity of base fluid measured and compared the obtained values with the prementioned data of the ASHRAE Standard. To minimize the experimental error at least twenty times viscosity reading monitored and averaged it. The experiment performed under steady-state conditions. The rotational measurement under controlled shear rate (CSR) method used and shear rate 260 (1/s). Previously many studies used Brookfield RST and Malvern Panalytical in order to measure the viscosity of nanofluids.

The method of measuring the viscosity follows the standard method of "ASTM D2196-10 which is known as the standard test methods for rheological properties of non-Newtonian materials by the rotational (Brookfield type) viscometer" (Azmi et al., 2016; Sun, Deluca, & Mattison, 2005).
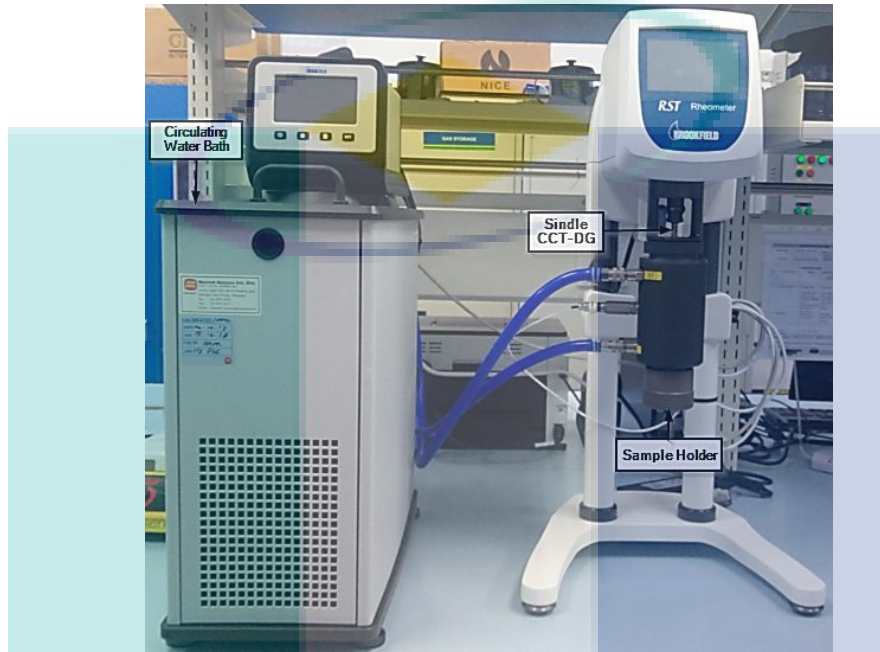
Figure 3.14   Viscosity measurement equipment (Brookfield RST rheometer) of CNC nanofluids

Figure 3.15   Viscosity measurement equipment (Malvern Panalytical) of Al_2O_3 nanofluids

3.7.4 Measurement of Specific Heat

In this study, the specific heat (C_p) of nanofluids (both Al_2O_3 and CNC) at various volume concentrations has been measured using the Linseis DSC1000 (Differential scanning calorimetry-Germany) following the standard method entitled as "ASTM E1269-11(2018) Standard Test Method for Determining Specific Heat Capacity by Differential Scanning Calorimetry". Here the weight of all nanofluid samples was fixed at 13 mg weighing by electrical balance and which has been loaded in aluminium crucibles. Figure 3.16 shows the specific heat measurement tools and the settings of Linseis DSC1000 have been depicted in Table 3.8. This equipment gives the highest possible accuracy of specific heat (C_p) by using modulated heating rate temperature profiles. This method defines a steady change in heat flow at of the samples and the system can observe the heat uptake superiorly than a linear heating system (Demetzos, 2008). Besides, specific heat (C_p) measurement could be affected by the mass value of the materials and the heating rate owing to the use of DSC (Clas, Dalton, & Hancock, 1999).

Table 3.8   Setting of adjusted parameters of DSC

Parameters	Settings
Temperature	25-80°C
Sampling interval	0.1 s
Preheat temperature	25°C
High-temperature differential scanning (HDSC)	250 µV
Temperature modulation: Period:	60 s/amplitude: 3 K
Gas	Nitrogen (20 sccm/min)

3.7.5 Measurement of Density

In this study, the density of Al_2O_3 and CNC nanofluids has been measured with different volume concentrations at a temperature range of 30°C to 80°C using digital density meter similar to previous research studies (Mahian, Kianifar, & Wongwises, 2013; Said, Kamyar, & Saidur, 2013). Here KEM (model DA-640) density meter manufactured by Kem Kyoto Electronics Co. Ltd. used. This meter has density (gm/cm^3) measuring range of 0.0000-3.000 with ±0.0001 (gm/cm^3) accuracy and density (gm/cm^3) repeatability is 0.00005. The ambient condition for using this meter is about temperature range of 5°C-35°C and humidity 85% RH or below. The method for measuring the density follows the method named "ASTM D4052-18 which is acknowledged as the Standard

test method for density, relative density and API gravity of liquids by digital density meter".
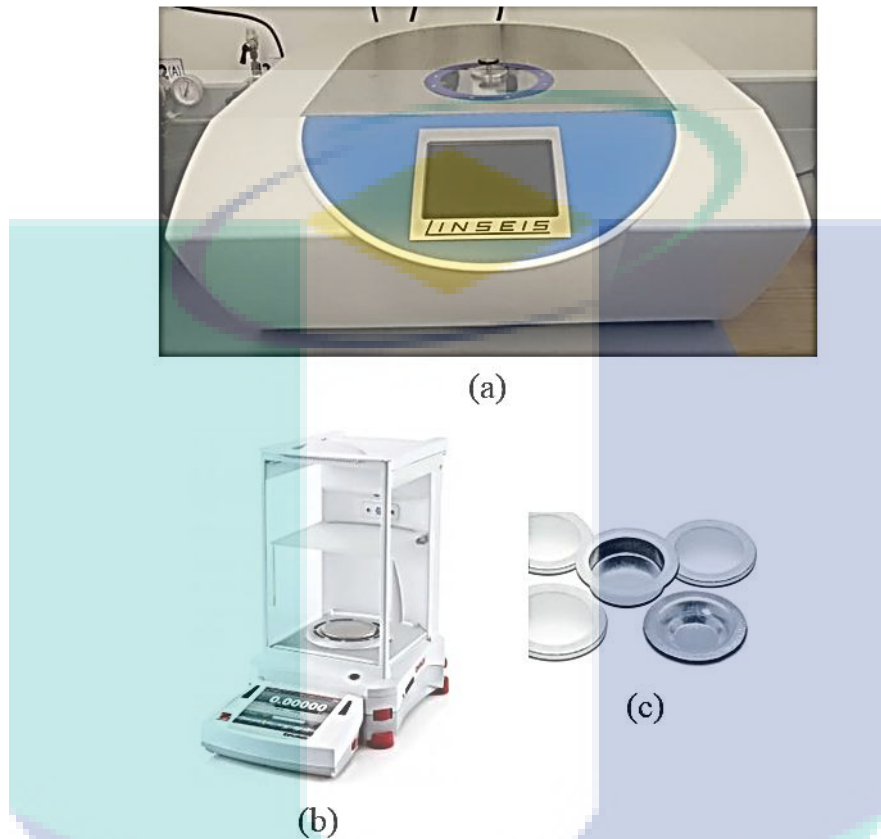
Figure 3.16   Equipment of specific heat measurement (a) DSC Linseis 1000, (b) electric balance, and (c) aluminium crucible

3.7.6   Measurement of the Potential of Hydrogen (pH)

For the measurement of the potential of hydrogen (pH) of Al_2O_3 and CNC nanofluids with different volume concentration pH meter used. A considerable number of experimental studies utilized the pH meter to assess the pH of the nanofluids (Li et al., 2008; Xian-Ju & Xin-Fang, 2009). In this study, Mettler Toledo pH meter used (model five easy) to measure the pH of Al_2O_3 and CNC nanofluids along with base fluid. The pH measurement range of pH meter was 0-14 with the accuracy of ±0.1 and pH resolution was 0.01. The method for evaluating the pH follows the electrometric method that is APHA 4500H+ B. The basic principle of this electrometric method is to determine the activity of the hydrogen ions by potentiometric measurement using standard and reference electrode.

3.8 Application of Nanofluids in Required Flat Plate Solar Collector

Two types of volume concentrations have been preferred based on the results of thermo-physical properties of both (Al_2O_3 and CNC) nanofluids such as 0.3% and 0.5% to apply in required flat plate solar collector. Here nanofluids have been prepared following the same method as previous nanofluid samples which were prepared to evaluate the thermal properties. The experiment has been run during day time (sunny day); from 10.00 am to 2.00 pm and the location was University Malaysia Pahang. Many studies such as Arıkan, Abbasoğlu, and Gazi (2018); Meibodi et al. (2015) did their experiment without assuming the humidity and wind speed, thereby following them wind speed and humidity did not be considered in this study. Figure 3.17 portrays the actual experimental setup and the list of apparatus of the actual experimental setup of the FPSC with properties has been depicted in Table 3.9. Forward-looking infrared (FLIR) thermal camera has been used to measure the surface temperature of copper tubes which works by sensing infrared radiation. To avoid the error data of surface temperature repeated measurement has been done and averaged it. The measurement parameters of the FLIR thermographic camera have been listed in Table 3.10. Prior to starting the measurement of temperature by FLIR thermal camera, FLIR has been calibrated by sensing the temperature of hot water. Ten reading has been taken and calculated the average of the maximum temperatures of boiling water around 84.94°C to ignore the error data. Figure 3.18 shows the calibration of the FLIR thermal camera to sense the temperature of boiling water by infrared thermal radiation. Before applying the nanofluids in FPSC, the flow rate of the submersible pump has been checked with water by adjusting the flow control of the pump. The highest and lowest flow rates were 950 and 650 ml/min respectively.

Table 3.9   List of apparatus of the actual experimental setup of FPSC

Sr. no	Name of the apparatus	Characteristics	Number of apparatus
1	Frame	Wooden	One
2	Tubes	Copper; outer diameter 12.7 mm; inner diameter 12.5 mm; length 1m	Ten
3	Thermocouples	Sensing element: coiled bimetallic	Three
4	Pump (Dolphin PA500)	Electrical submersible filter	One
5	Bucket	Plastic	One

Table 3.10   Measurement parameters of the FLIR thermal camera

Setting of parameters	Values of parameters
Copper	Emissivity, ε 0.78
Reflected temperature	30ºC
Distance	1 meter
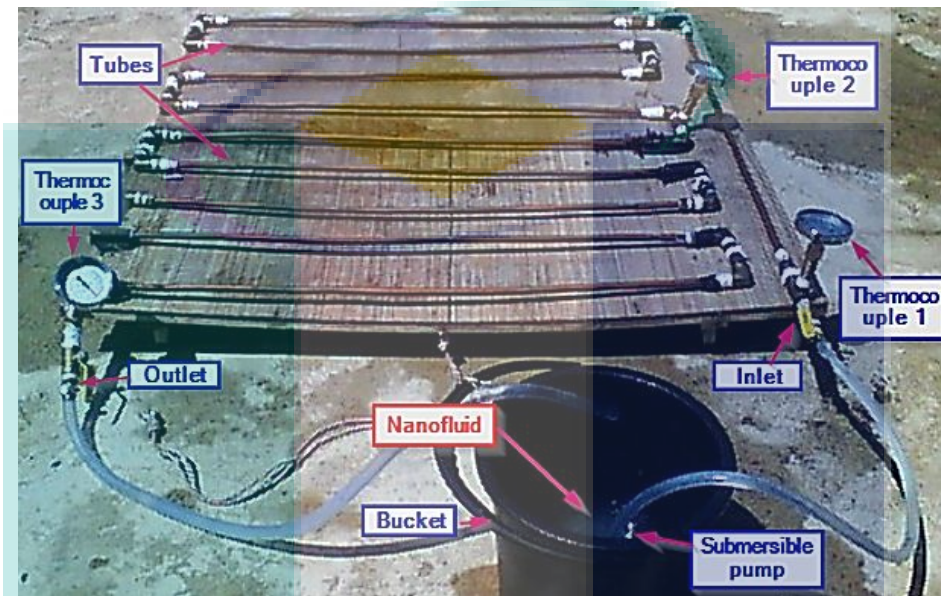
Figure 3.17   The actual experimental setup of FPSC
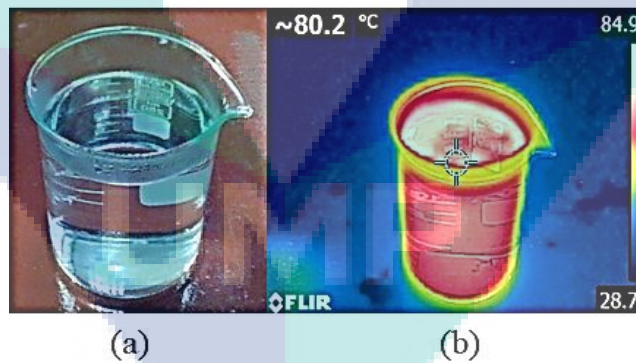
Figure 3.18   Calibration of FLIR thermal camera (a) hot water and (b) thermographic view of hot water

At the beginning of the running of this experiment, the inlet and outlet thermocouples showed the unprecedented data of temperature difference between them. To deter this error reading, three types of observation have been done. After starting equipment, the data of temperature has been checked after 10 minutes, 30 minutes, and 60 minutes consecutively; and the stable temperature difference was observed between

the inlet and outlet of the equipment at every individual time. Thus, the optimum time has been fixed (30 minutes) to take data after repeated tests done with each nanofluid. Data observed every 30 minutes. Figure 3.19 portrays the whole process flow of the experimental work to analyse the enhancement of efficiency of the FPSC applying Al_2O_3 and CNC nanofluids successively. However, the temperature difference between inlet and outlet has been evaluated at the lowest and highest flow rate of the pump. The flow rate does not have any significant effect on it. Around 2000 ml of bulk nanofluids have been prepared for each type of nanoparticles (Al_2O_3 and CNC). The volume concentrations prepared by 0.3% and 0.5% of both Al_2O_3 and CNC nanofluids. These four-volume concentrations of nanofluids have been loaded in bucket one after another and the lowest flow rate has been set in the pump. Minimum three and a maximum of ten reading has been taken with these four-volume concentrations of nanofluids. Afterward, calculated the average of these data. This experimental work has been done in the steady-state condition under direct solar radiation.

Energy Gain of FPSC

The energy gain has been calculated following the (Eq. (2.5)) in chapter 2:

$$Q_u = \dot{m}\, C_p (T_{out} - T_{in})$$

Where,

Q_u= Energy gain (kW) by the FPSC

$\dot{m}$ = Mass flow rate (kg/s) of the nanofluids and base fluid

C_p= Specific heat (J/kg-K) of the nanofluids and base fluid

T_{out}= Outlet temperature (ºC) of the nanofluids and base fluid

T_{in}= Inlet temperature (ºC) of the nanofluids and base fluid

Efficiency of FPSC

The efficiency of the solar collector has been computed using the (Eq. (2.6)) of chapter 2:

$$\eta = \frac{Q_u}{I_t A_c}$$

Where,

η= Efficiency (%) of the FPSC

Q_u= Energy gain (kW) by the FPSC

I_t= Solar radiance (W/m^2)

A_c= Surface area (m^2) of FPSC

3.9   Numerical Simulation for Fluid Behaviour

At the final phase of the methodology, again computational numerical simulation has been done with actual experimental design and experimental thermo-physical data of the base fluid and nanofluids (both Al$_2$O$_3$ and CNC). The simulation method has been followed according to the previous steps stated earlier in this chapter. The volume concentrations of both nanofluids were 0.3% and 0.5%. The modelling has been performed as follows:

Geometry

The three-dimensional geometry of the actual experimental design has been created by designing software. The outer and inner diameters of the tube were 12.7 mm and 12.5 mm respectively while the total length of the tubes was 12.325 m. Afterward, the geometry has been imported to CFD ANSYS R15.0 workbench for CFD simulations. The geometry edited in fluid form in designmodeler like the previous method as shown in Figure 3.20.

Meshing

Meshing has been done according to the previous method. However, here automatically only cutcell meshing has been done in the computational fluid domain as portrayed in Figure 3.21. Besides that, mesh independence test performed by changing mesh sizing relevance center such as coarse, medium and fine. In this study, a fine relevance center has been selected to obtain a flawless solution calculation.
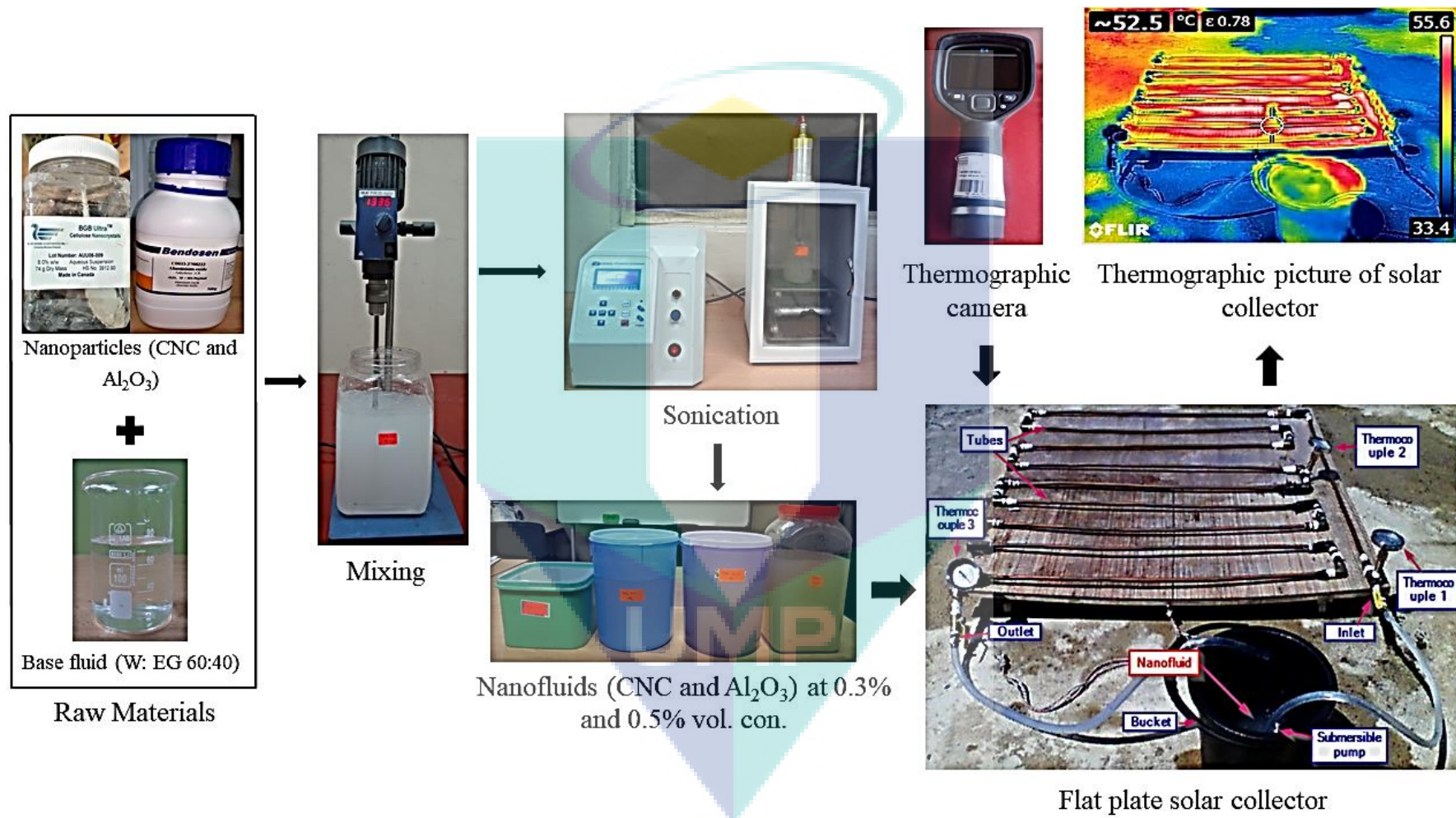
Figure 3.19   Summary of the process flow of the experimental work
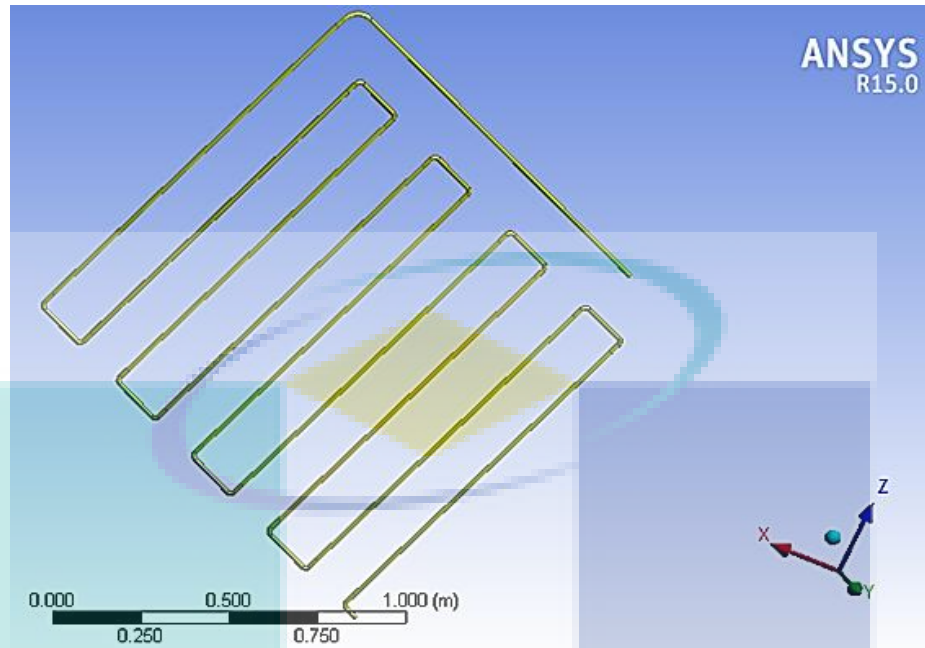
Figure 3.20   Geometry of actual designing model in the fluid form of CFD simulation
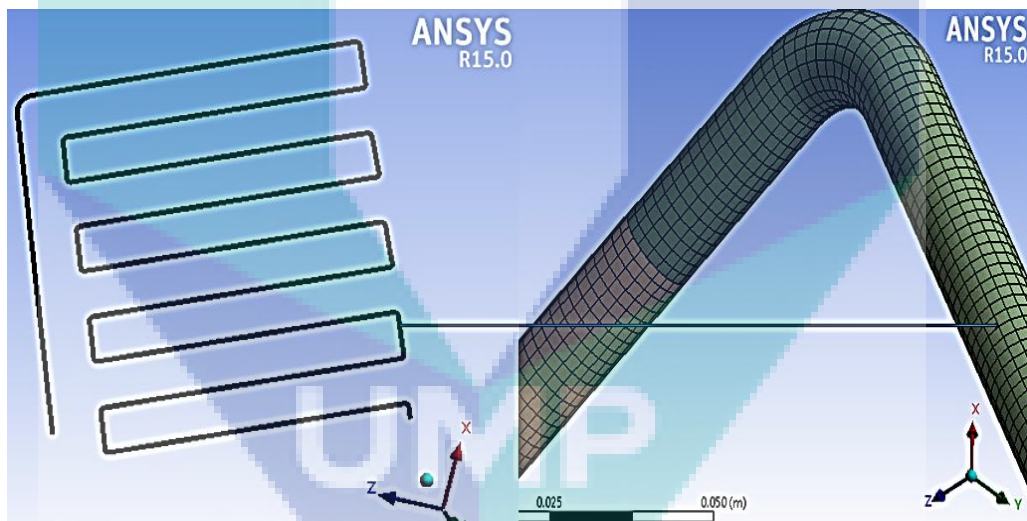
Figure 3.21   Meshing of the geometry of the experimental design

Setup

In this study, the energy equation and Viscous-Laminar model along with other parameters have been set following the previous method. But the actual experimental properties of materials and the boundary conditions have been preferred. Simulations have been done for individual actual experimental properties of the base fluid, Al_2O_3 nanofluids, and CNC nanofluids (at 0.3% and 0.5% volume concentrations of both

nanofluids). Table 3.11 shows the experimental properties of the base fluid, Al_2O_3 nanofluids, and CNC nanofluids while Table 3.12 presents the actual boundary conation parameters for CFD simulations. Here, mass-flow-inlet and pressure-outlet type boundary conditions of inlet and outlet have been selected respectively which were like the preceding study. Moreover, wall type boundary condition has been selected for the wall-fluid domain in which thermal condition has been fixed with the surface temperature.

Solution

Solution calculation has been executed following the same criterion as earlier stated in this study such as the solution method was pressure-velocity coupling with the simple scheme and spatial discretization. Besides, solution control panel parameters were also similar, and solution initialized with standard initialization method. A hundred iterations were preferred for CFD simulations and Figure 3.22 shows the converge of the solution of 0.3% Al_2O_3 nanofluid (mentioned properties were at 30°C temperature) such as an example. Similarly, all solutions such as base fluid, Al_2O_3, and CNC nanofluids have been calculated using their experimental properties accordingly.

Table 3.11   Properties of different fluids to be included in CFD simulations

Temperature	Parameters	Experimental properties			
		Density (kg/m³)	Specific heat (J/kg-K)	Thermal conductivity (W/m-K)	Viscosity (kg/m. s)
At 30°C temperature	Base fluid	1050.5	830	0.407	0.00208
	0.3% Al_2O_3	1050.1	110	0.443	0.00324
	0.5% Al_2O_3	1051.7	180	0.454	0.00327
	0.3% CNC	1051.1	1260	0.414	0.00258
	0.5% CNC	1050.6	2080	0.41	0.00223
At 50°C temperature	Base fluid	1039.0	880	0.433	0.00133
	0.3% Al_2O_3	1039.2	650	0.462	0.00213
	0.5% Al_2O_3	1040.5	380	0.462	0.00265
	0.3% CNC	1039.9	1090	0.443	0.00164
	0.5% CNC	1039.3	1910	0.491	0.00146
At 70°C temperature	Base fluid	1021.7	680	0.463	0.00116
	0.3% Al_2O_3	1026.3	900	0.524	0.00152
	0.5% Al_2O_3	1026.9	870	0.528	0.00186
	0.3% CNC	1025	1420	0.496	0.00117
	0.5% CNC	1026	3940	0.475	0.00115
At 80°C temperature	Base fluid	1011.8	530	0.452	0.00121
	0.3% Al_2O_3	1009.4	910	0.539	0.00148
	0.5% Al_2O_3	1010	980	0.55	0.00127
	0.3% CNC	1015.7	1619	0.567	0.00132
	0.5% CNC	1013.6	5290	0.525	0.00117

Table 3.12   Actual boundary conditions

Parameters	Mass flow rate (kg/s)	Inlet temperature (K)	Outlet temperature (K)	Surface temperature (K)
Base fluid	0.0108	314.81	315.81	320.51
0.3% Al_2O_3		313.55	315.55	319.81
0.5% Al_2O_3		316.35	318.25	321.62
0.3% CNC		316.05	317.95	320.74
0.5% CNC		315.55	316.75	321.73

Result

The Prandtl number of both Al_2O_3 and CNC nanofluids (at 0.3% and 0.5% volume fractions) and also the base fluid at a temperature range of 30°C to 80°C have been identified in the post-processing results of ANSYS Fluent of CFD simulations. Figure 3.23 displays the graphical presentation of the Prandtl number of 0.3% Al_2O_3 nanofluid (for instance) simulated based on the actual experimental designing model and actual experimental properties of the nanofluid. The CFD simulation data of Prandtl number has been obtained by computing the wall-fluid domain surfaces of the geometry in the contours of properties (Molecular Prandtl Number) in the post-processing results of CFD simulations.
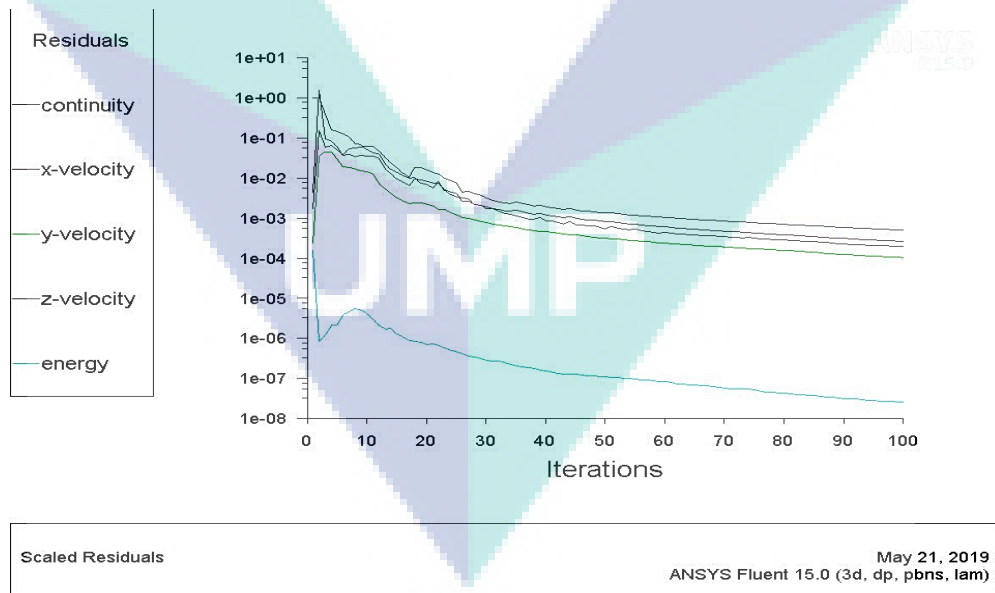
Figure 3.22   Converged solution of CFD simulation of 0.3% Al_2O_3 nanofluid
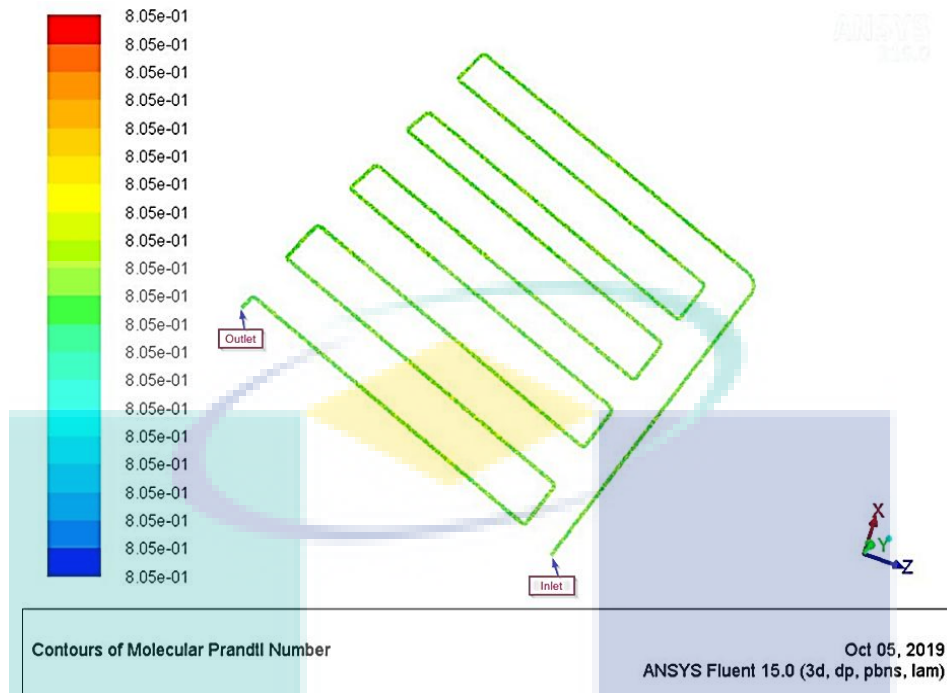
Figure 3.23   Contour of Prandtl number of 0.3% Al_2O_3 nanofluid

3.10   Summary

The research methodology flow chart has been discussed broadly in this chapter. CFD simulations to design flat plate solar collector specifically the arrangement of header and riser tubes of FPSC; nanofluids characterization, preparation and stabilization; measurement of different thermo-physical properties of nanofluids; and lastly, the application of nanofluids in solar collector have been described precisely. At the end of this chapter, the final computational simulation done based on the experimental design of FPSC and the experimental properties of the nanofluids. The next chapter covers the analysis of the resulting data.

CHAPTER 4
RESULTS AND DISCUSSION

4.1   Introduction

The main purpose of this chapter is to discuss the enhancement of thermal performance (energy gain and efficiency) of flat plate solar collector by applying nanofluids (Al_2O_3 and CNC nanoparticle dispersed into water and ethylene glycol mixture base fluid). Therefore, designing of the solar collector (arrangement of header and riser tubes) performed; thermo-physical properties of nanofluids analysed and discussed in accordance with other studies; the efficiency of solar collector has been calculated by applying nanofluids in required design of solar collector and finally, the non-dimensional numbers have been computed to identify the behaviour of nanofluids.

4.2   Design Analysis of Flat Plate Solar Collector

The results of computational simulations can be analysed both in numerical data or graphical views (contour plot). In CFD post-processing, blue colour defines the lowest value and red is the highest value (Sorokes, Hardin, & Hutchinson, 2016). FPSC has been selected based on the analysis of internal energy (J/kg). The numerical values of the internal energy of fluids and nanofluids flowing through inside the header and riser tubes of FPSC have been depicted in Table 4.1. In this study, the internal energy of the fluids such as water, ethylene glycol, a mixture of water/ethylene glycol (60: 40) as base fluid, and the nanofluids such as TiO_2 and CNC observed flowing through the designing models of FPSC. The models were 8-22-11, 8-23-10, 8-23-12, 8-24-11, 12-22-10, 12-22-12, 12-23-11, 12-24-10, 12-24-12, 16-22-11, 16-23-10, 16-23-12, and 16-24-11. Computational simulations revealed that these parameters exhibited the similarities scenario in the maximum phase of internal energy for all designing models of FPSC. But there were some differences in minimum values of internal energy of these flowing fluid parameters. Therefore, it stated that the number and diameter of the header and riser tubes of FPSC

do not affect the internal energy of FPSC. Internal energy only depends on the properties of the fluid flowing through inside them. Figure 4.1, Figure 4.2, and Figure 4.3 represent the contours of the internal energy of eight riser tubes (8-23-12) model, twelve riser tubes (12-23-11) designing model, and sixteen riser tubes (16-24-11) model of FPSC. Though the contours of internal energy of all designs were similar, therefore, these three contours have been presented as the model of their respective associations. According to Mazumder (2012), this colour of contours presents the development of the solution. From blue colour to red colour shows the gradual development of the solution. Moreover, Figure 4.4, Figure 4.6, and Figure 4.8 show the inlet contour of these three models as well as Figure 4.5, Figure 4.7, and Figure 4.9 are the outlet contour of internal energy. Inlet contours present no development of internal energy whereas outlet contours show fully developed solutions of fluid flows inside the tubes. The conservation of the solutions has been presented in Figure 4.10 and the graphical view of all these conversed solutions was almost similar. The results were consistent for all designs although mesh or grid independence test has been conducted.

Figure 4.1　　Contour of internal energy of model 8-23-12
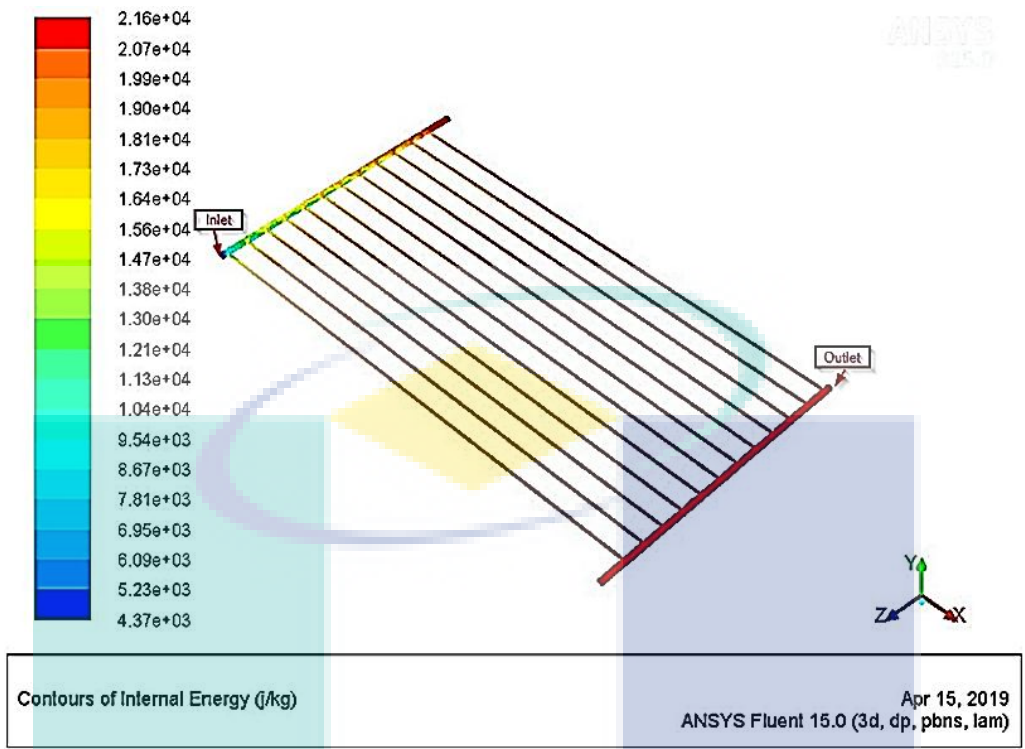
Figure 4.2   Contour of internal energy of designing model 12-23-11
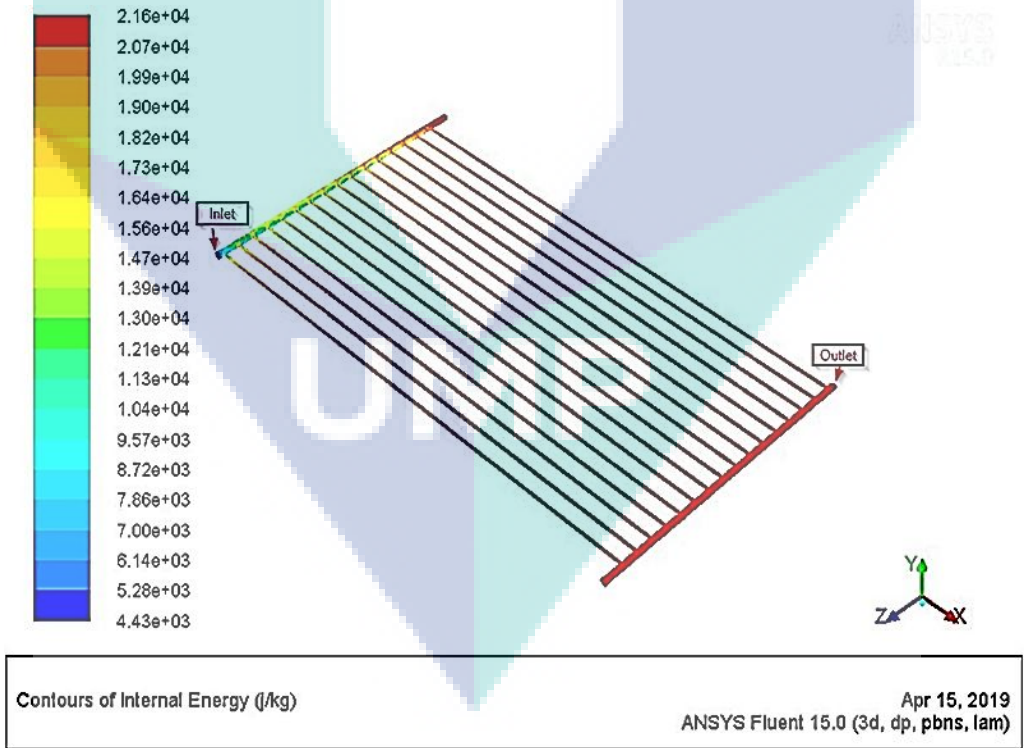
Figure 4.3   Contour of internal energy of model 16-24-11

In addition, all residuals such as continuity, velocity, and energy of a fully developed solution showed the continuation during the calculation of fluent flow which defined as converged solution as shown in Figure 4.10. The continuity and velocity residuals were reverse to the energy residual at the beginning of the calculation. After a certain number of calculations, all the residuals (continuity, velocity, and energy) moved in a similar direction. Moreover, the continuity and velocity residuals performed a bit zigzag pattern trend in the primary stage of calculation but finally, they were in even condition. However, the energy residual showed the almost even condition consistently.

Table 4.1   Numerical values of the internal energy of fluids and nanofluids

Designing models	Parameters	Internal energy	
		Min (J/kg)	Max (J/kg)
8-22-11	Water	7555.765	36909.2
	Ethylene glycol	4359.228	21281.57
	60%Water+40%Ethylene glycol	N/A	N/A
	TiO_2	2288.478	11204.88
	Crystal nanocellulose	4414.128	21588.86
8-23-10	Water	7519.131	36909.19
	Ethylene glycol	4343.408	21281.56
	60%Water+40%Ethylene glycol	N/A	N/A
	TiO_2	2288.026	11204.88
	Crystal nanocellulose	4375.026	21588.86
8-23-12	Water	7602.524	36909.1
	Ethylene glycol	4365.053	21281.57
	60%Water+40%Ethylene glycol	6543.348	31769.23
	TiO_2	2311.612	11204.88
	Crystal nanocellulose	4421.486	21588.86
8-24-11	Water	7328.505	36909.19
	Ethylene glycol	4286.926	21281.54
	60%Water+40%Ethylene glycol	6381.715	31769.23
	TiO_2	2242.375	11204.38
	Crystal nanocellulose	4316.959	21588.84
12-22-10	Water	7582.486	36909.2
	Ethylene glycol	4353.318	12181.58
	60%Water+40%Ethylene glycol	6537.199	31769.24
	TiO_2	2310.3	11204.38
	Crystal nanocellulose	4388.4	21588.87
12-22-12	Water	7584.952	36909.21
	Ethylene glycol	4376.075	21281.57
	60%Water+40%Ethylene glycol	6560.45	31769.24
	TiO_2	2311.537	11204.88
	Crystal nanocellulose	4436.216	21588.87
12-23-11	Water	7496.358	36909.2
	Ethylene glycol	4342.002	21281.58
	60%Water+40%Ethylene glycol	6493.067	31769.24
	TiO_2	2259.208	11204.88
	Crystal nanocellulose	4369.304	21588.87
12-24-10	Water	7496.358	36909.2
	Ethylene glycol	4342.002	21281.58

Table 4.1   Continued

Designing models	Parameters	Internal energy	
		Min (J/kg)	Max (J/kg)
	60%Water+40%Ethylene glycol	6513.174	31769.24
	TiO$_2$	2261.074	11204.88
	Crystal nanocellulose	4369.304	21588.87
12-24-12	Water	7615.049	36909.2
	Ethylene glycol	4374.993	21281.58
	60%Water+40%Ethylene glycol	6546.11	31769.24
	TiO$_2$	2311.431	11204.88
	Crystal nanocellulose	4434.519	21588.87
16-22-11	Water	7601	36909.2
	Ethylene glycol	4364.763	21281.57
	60%Water+40%Ethylene glycol	6542.221	31769.24
	TiO$_2$	2311.612	11204.88
	Crystal nanocellulose	4426.937	21588.87
16-23-10	Water	N/A	N/A
	Ethylene glycol	N/A	N/A
	60%Water+40%Ethylene glycol	6413.789	31769.23
	TiO$_2$	2311.472	11204.23
	Crystal nanocellulose	4433.686	21588.87
16-23-12	Water	7375.112	36909.2
	Ethylene glycol	N/A	N/A
	60%Water+40%Ethylene glycol	6303.268	31769.24
	TiO$_2$	2306.632	11204.88
	Crystal nanocellulose	3740.407	21588.86
16-24-11	Water	7600.43	36909.2
	Ethylene glycol	4370.075	21281.72
	60%Water+40%Ethylene glycol	6553.69	31769.23
	TiO$_2$	2311.864	11204.88
	Crystal nanocellulose	4426.148	21588.87

Besides that, these residuals (continuity, velocity, and energy) remained parallel with each other. However, some designs are not compatible with all kinds of fluent flow which define the discontinuation of the energy equation of solutions (Gunjo, Mahanta, & Robi, 2017). The list of designs and parameters of the defective energy equation of the solution has been presented in Table 4.2. Here, all these parameters showed the divergence energy equation during the simulations with four designing models indexed in Table 4.2. Divergence of the solution might be happened owing to meshing statistics mesh metric parameters such as skewness and/or aspect ratio of designing models such as designing model 8-22-11 performed slightly higher skewness (0.896), model 8-23-10 showed higher standard deviation of aspect ratio (1.44), designing model 16-23-10 exhibited both greater skewness (0.895) and higher standard deviation of aspect ratio (2.07), and finally, model 16-23-12 showed marginally higher skewness (0.877) (Data from Table 3.4; in chapter 3) (Madenci & Guven, 2015).
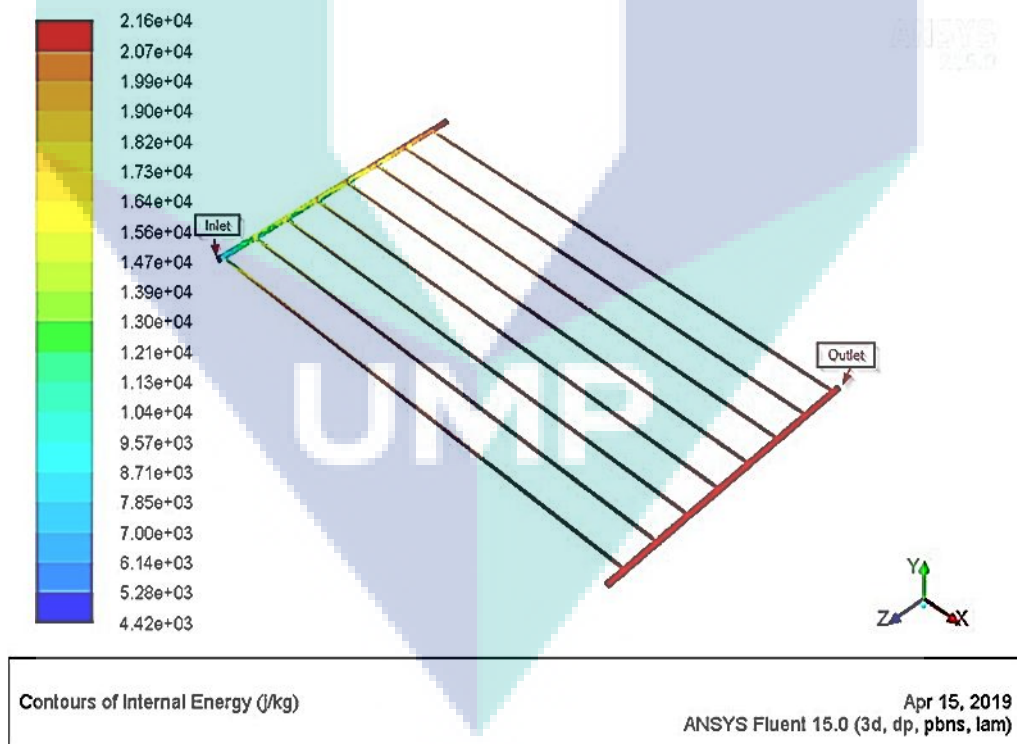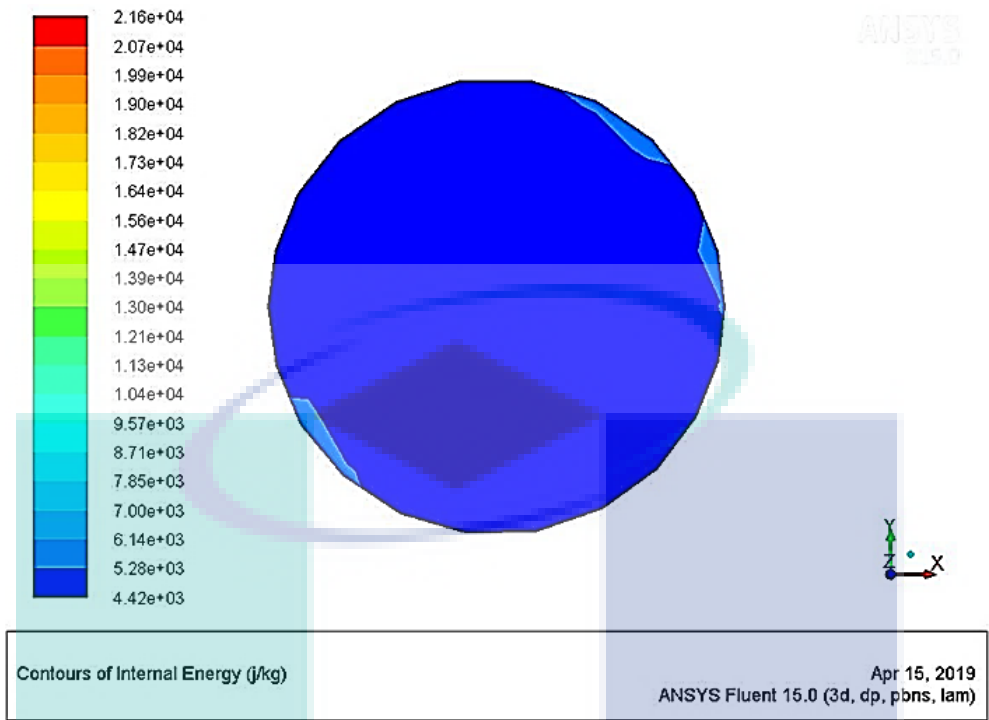
Figure 4.4   Inlet contour of internal energy of model 8-23-12
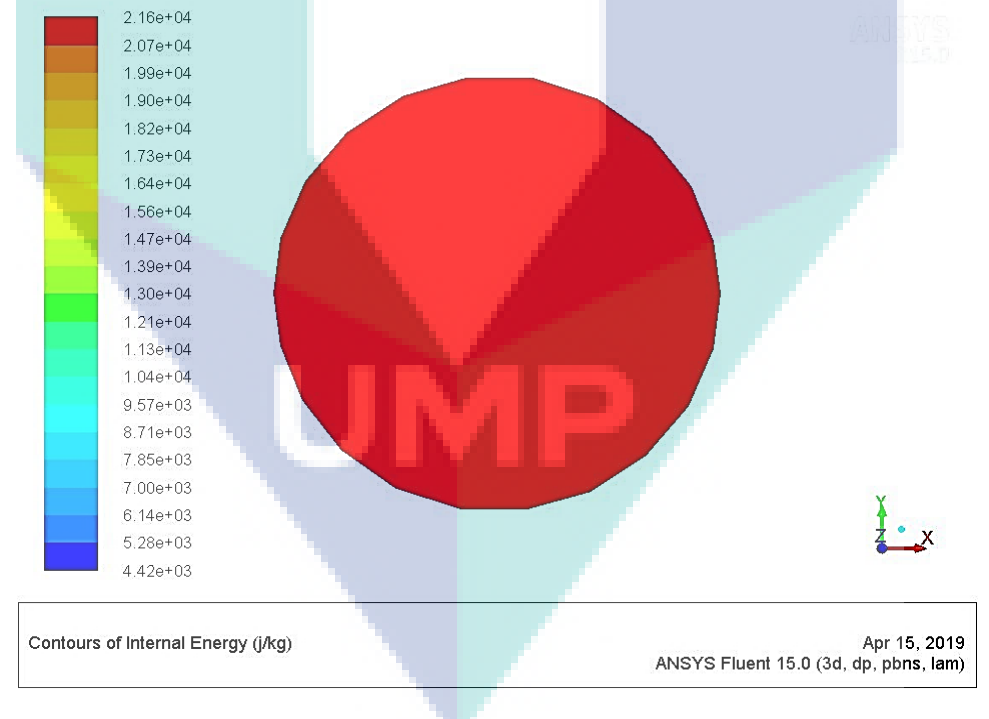
Figure 4.5   Outlet contour of internal energy of designing model 8-23-12
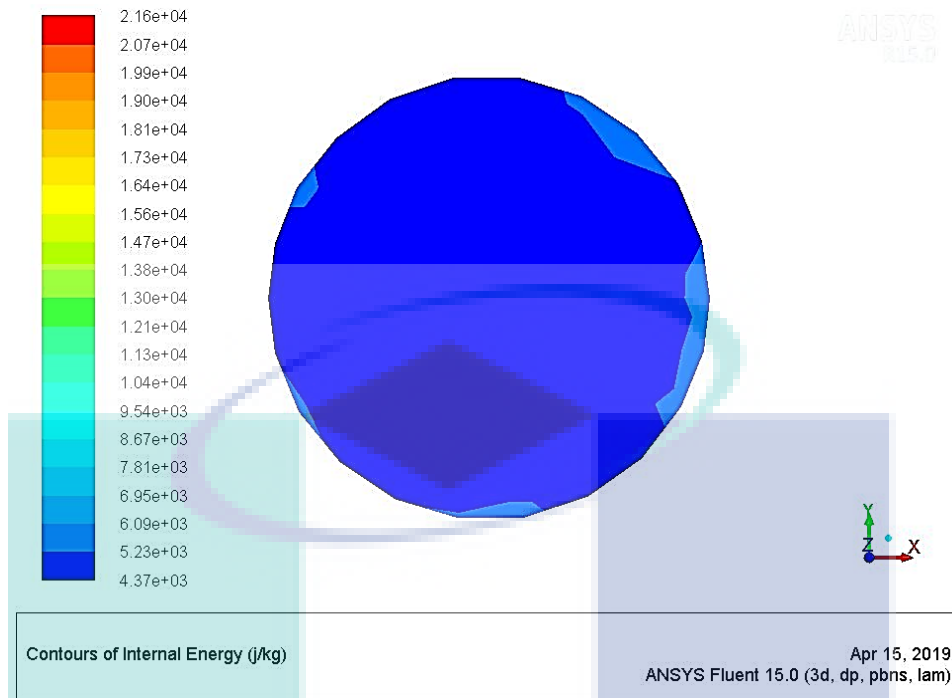
Figure 4.6   Inlet contour of internal energy of model 12-23-11
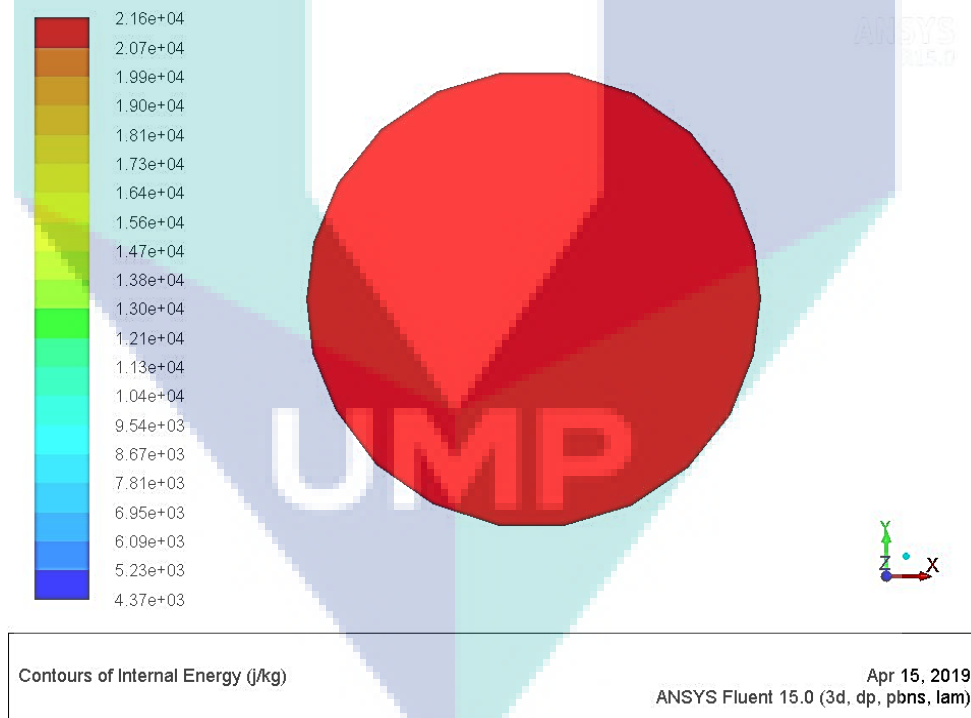
Figure 4.7   Outlet contour of internal energy of designing model 12-23-11
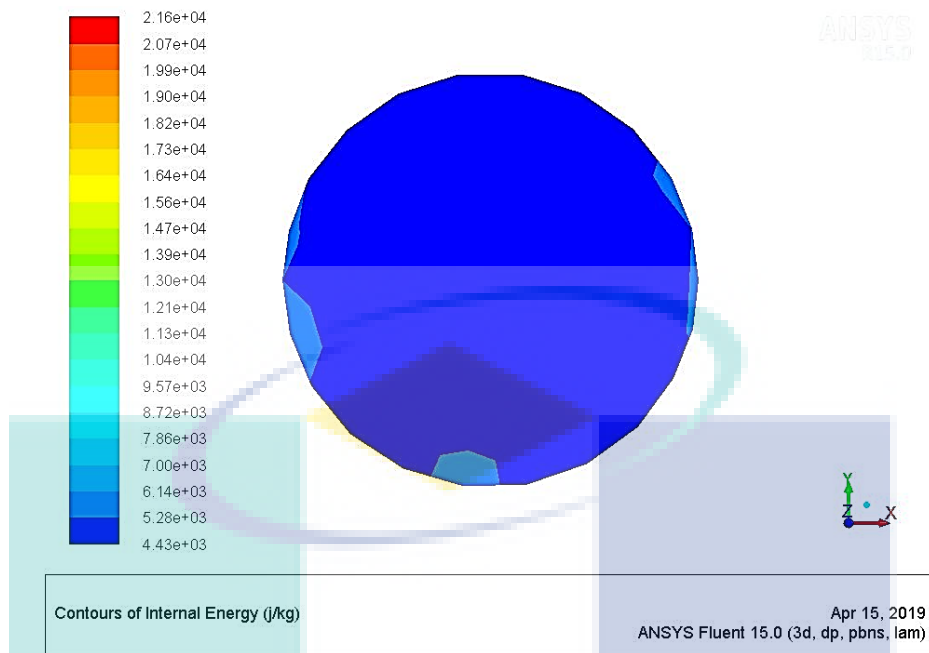
Figure 4.8   Inlet contour of internal energy of model 16-24-11
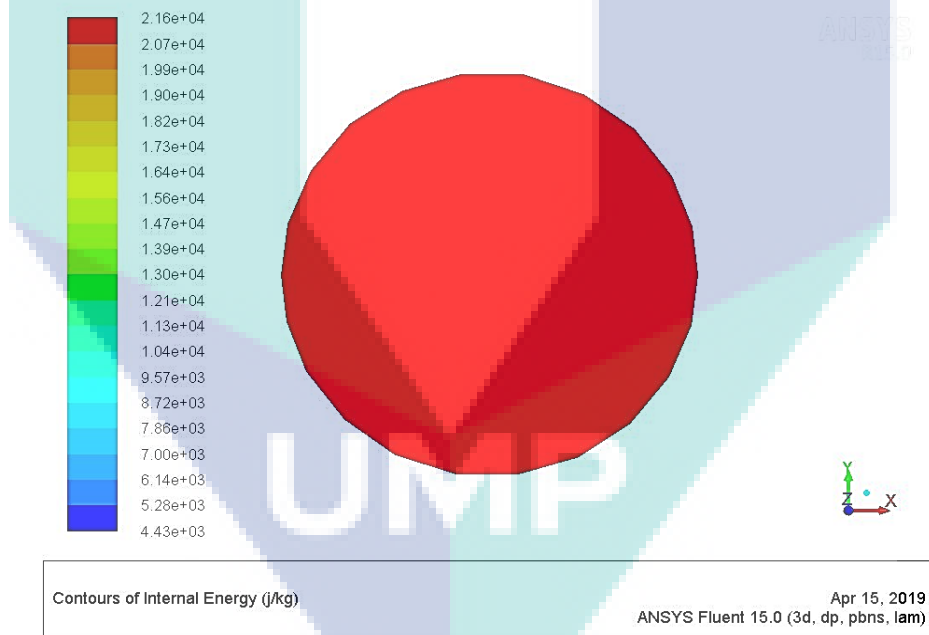
Figure 4.9   Outlet contour of internal energy of designing model 16-24-11

The designing models such as 8-22-11, 8-23-12, 8-23-12, and 8-24-11 contained the minimum number of tubes that can be very compatible with the economic point of view to fabricate a designing model of FPSC. However, the designing model of geometry 8-22-11 and 8-23-10 showed some divergence energy equation with a specific parameter such as 60%water+40%ethylene glycol fluid; thereby these two designs were not

preferred; as mesh metric statistics of simulations are the possible reason of divergence error.
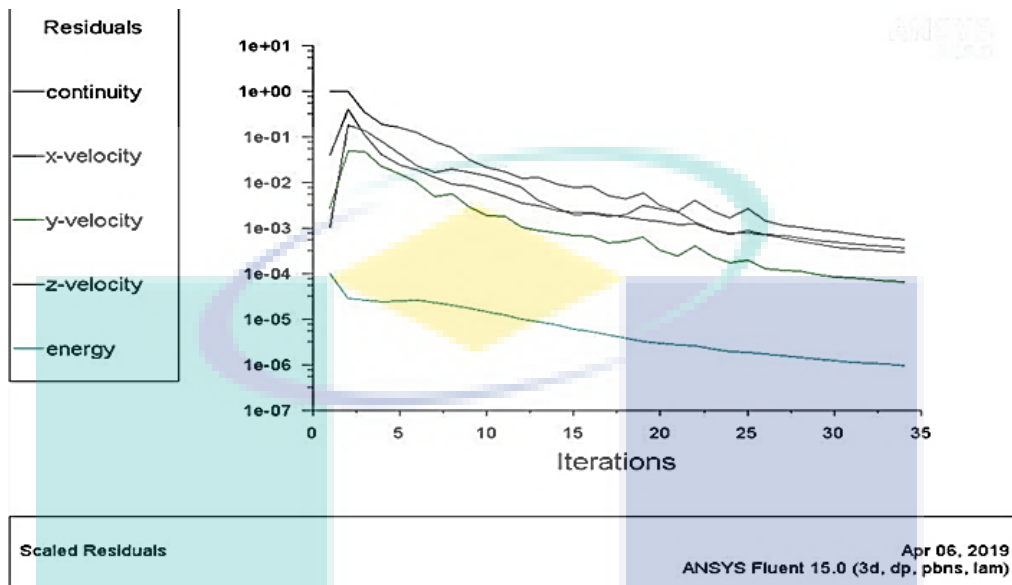
Figure 4.10   Converged solution of fluent flow in CFD simulations

Table 4.2   Table of defective energy equation of converge solution

Designing models	Parameters	Criteria of solution
8-22-11	60%Water+40%Ethylene glycol	
8-23-10	60%Water+40%Ethylene glycol	
16-23-10	Ethylene glycol	Divergence of solution
	Water	
16-23-12	Ethylene glycol	

Thus, the deigning model preferred from the other two designing models by analysing the data of mesh metric skewness. The maximum skewness of model 8-24-11 was 0.883 whereas it was 0.842 of designing model 8-23-12 as the lowest value of mesh metric skewness performs better solution of convergence energy equation (Madenci & Guven, 2015); even though the aspect ratio of model 8-24-11 (0.652) was marginally less than the model 8-23-12 (0.703). Hence, the designing model of 8-23-12 (number of riser tube-diameter of header-diameter of riser) has been selected for the actual experimental designing model of flat plate solar collector from these two designing models to conduct this study.

4.3   Characterization of Nanofluids

Different characteristics such as crystallinity, morphology, and size of the nanoparticles have been carried out by XRD, FESEM, and TEM analysis followed by FESEM EDX to evaluate the elemental properties of nanoparticles. Besides, the FTIR test has been performed to identify the molecular components and structures of the nanofluids.

Al_2O_3 Nanofluids

The Al_2O_3 nanoparticles were characterized by X-ray diffraction (XRD) data analysis to determine the crystallinity of it. The crystallinity of a material is a very important identification as it makes the material strong. Figure 4.11 represents the x-ray diffraction pattern of Al_2O_3 solid nanoparticles. By this Figure 4.11, alumina phase was identified at 2θ values of 19.4^o, 37.7^o, 45.8^o, and 66.8^o corresponds to the diffraction from the (1 1 1), (3 1 1), (4 0 0), and (4 4 0) crystal planes respectively; agreement with the standard XRD pattern (ICDD, PDF no. 01-074-2206 (Al_2O_3) 5.3333 Aluminum Oxide). Moreover, this Al_2O_3 XRD pattern is very much similar to Karunakaran, Anilkumar, and Gomathisankar (2011) study to determine the crystallinity of Al_2O_3 nanoparticles by X-ray diffraction.

The morphological shape and size of nanoparticles are very important parameters as they influence the thermo-physical properties of nanofluids to a great extent. The size and morphological shape of Al_2O_3 nanoparticles were determined by field emission scanning electron microscopy (FESEM) as shown in Figure 4.12. FESEM has done with 70,000x magnification and 9.9 mm working distance (WD) parameters. The size of Al_2O_3 nanoparticles was below 80 nm. The shape of the particles identified in both spherical and nearly spherical. However, the cluster of nanoparticles was also spotted in the FESEM image (Figure 4.12).

The elemental composition of nanoparticles analysed by means of FESEM EDX with 60 µm, 20 µm and 10 µm scale electron image as shown in Figure 4.13, Figure 4.14, and Figure 4.15 respectively. All these EDX spectrum images show the presence of aluminium (Al) and oxygen (O) atoms in Al_2O_3 nanoparticles. Table 4.3 depicts the EDX results of the elemental proportion of Al_2O_3 nanoparticle based on the numerical data of all-electron images (60 µm, 20 µm, and 10 µm scale) (Gupta, Singh, & Katyal, 2018). The standard deviation of the oxygen atom was smaller than the aluminium atom of Al_2O_3 nanoparticles in both weight% and atomic% aspects.
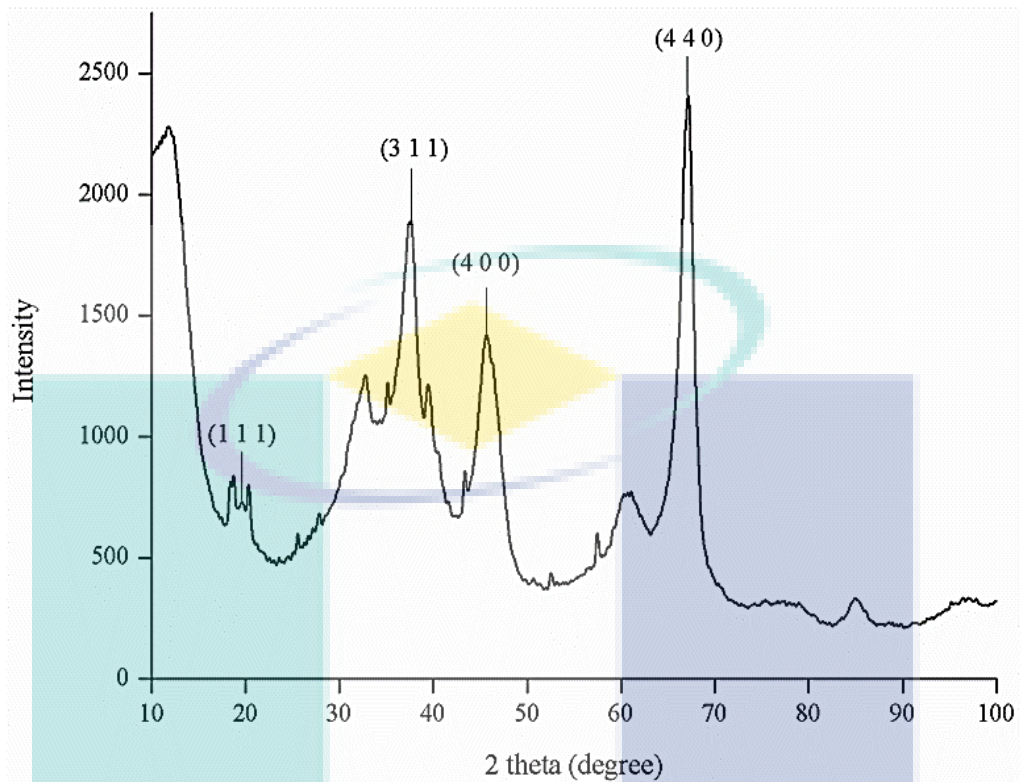
Figure 4.11   XRD pattern of Al$_2$O$_3$ nanoparticles
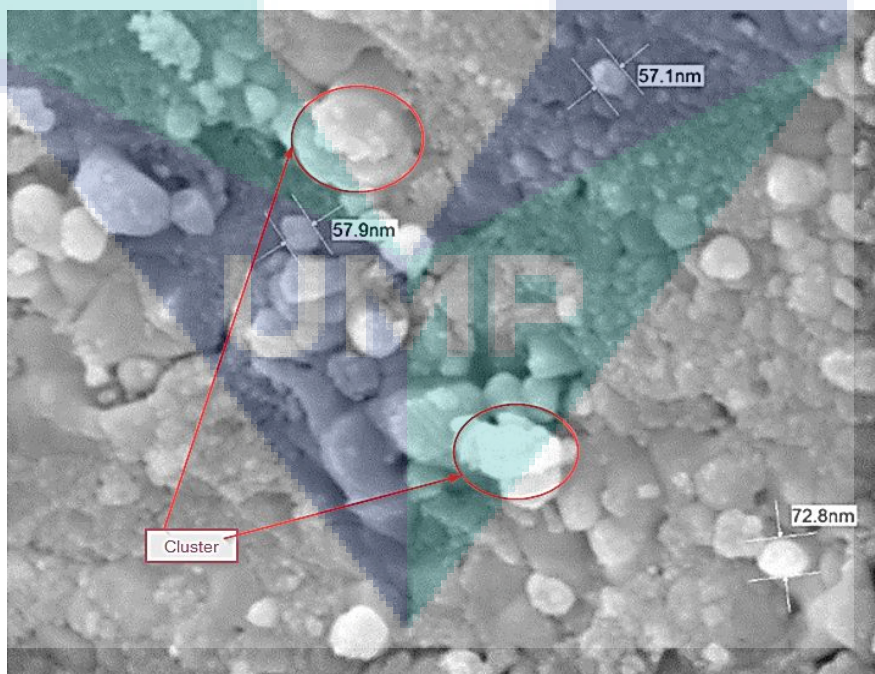
Figure 4.12   FESEM morphology of Al$_2$O$_3$ nanoparticles (Magnification x70,000; WD 9.9 mm)
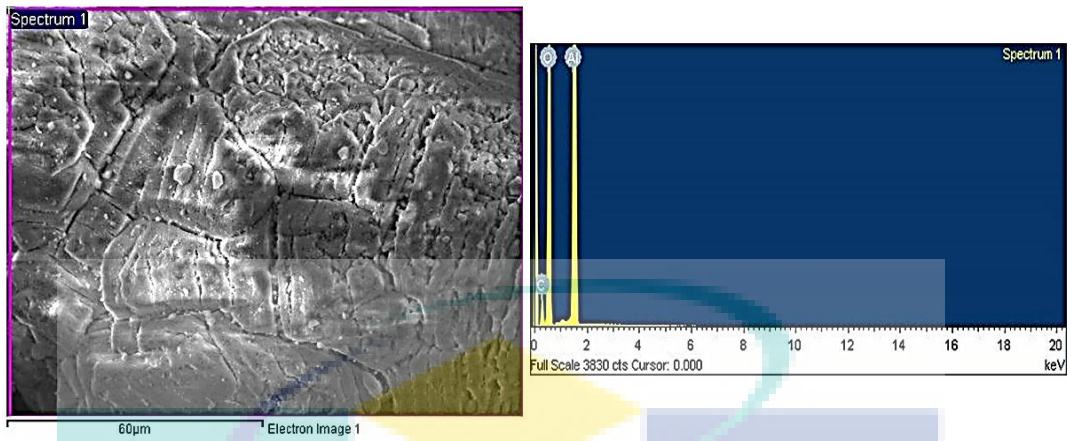
Figure 4.13   EDX spectrum of Al$_2$O$_3$ nanoparticles with a 60 μm scale electron image

Figure 4.14   EDX spectrum of Al$_2$O$_3$ nanoparticles with a 20 μm scale electron image

Figure 4.15   EDX spectrum of Al$_2$O$_3$ nanoparticles with a 10 μm scale electron image

Table 4.3   Quantification results of Al_2O_3 nanoparticles

Element	Weight %	Standard deviation	Atomic %	Standard deviation
Oxygen, O	49.49	5.34	59.73	3.36
Aluminium, Al	45.90	9.41	32.85	8.35

In addition, the shape and size of solid nanoparticles into the base fluid that is in nanofluid form can also be measured by transmission electron microscopy (TEM) (Baghbanzadeh et al., 2012) image as shown in Figure 4.16. Moreover, the dispersion of nanoparticles into the base fluid should be defined precisely by the TEM image. Figure 4.16 illustrates that most of the nanoparticles of Al_2O_3 nanofluids were nearly spherical and nearly elongated geometry in morphological shape. Nanoparticles were also better uniform in shape and size. Besides that, the nanoparticles were dispersed evenly into base fluids but often agglomerated into small aggregation.
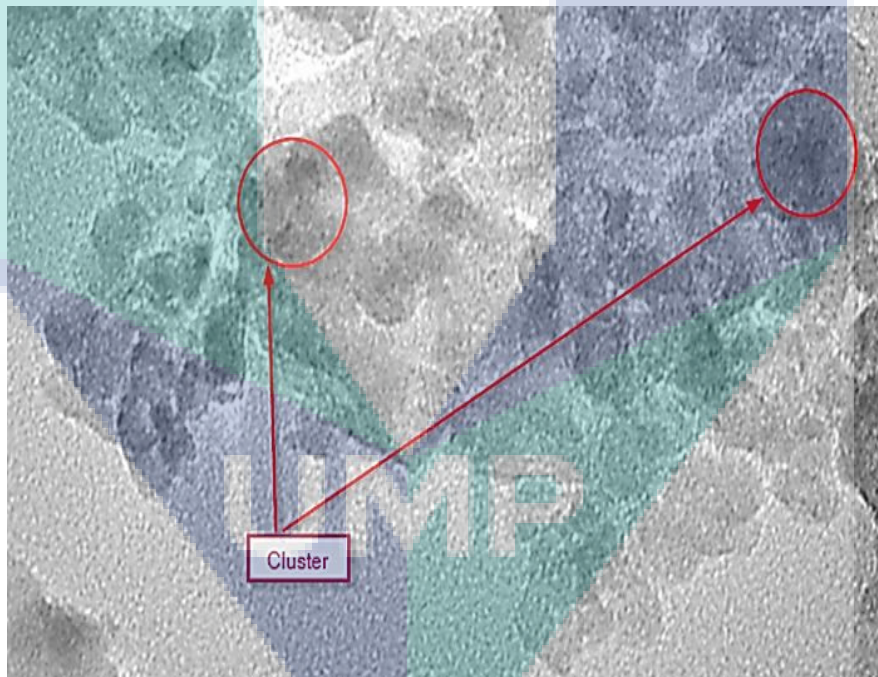
Figure 4.16   TEM morphology of Al_2O_3 nanofluids (Magnification x100,000)

CNC Nanofluids

The crystallinity of CNC nanoparticles identified by the X-ray diffraction as shown in Figure 4.17. CNC nanoparticle determined at 2θ angles of 16.6^o and 22.9^o which corresponds to the crystal planes of (1 1 0), and (2 0 0) respectively; agreement with the

standard XRD pattern (ICDD, PDF no. 00-056-1718 ($C_6H_{10}O_5$)n Cellulose-1ß). Besides, this XRD pattern of CNC nanoparticles matched with the pattern of cellulose nanocrystal produced from sugarcane bagasse and characterization studied by Kumar et al. (2014). This PDF no. 00-056-1718 of ICDD defines it as the cellulose of containing beta-glucose monomer unit in the polymer chain.
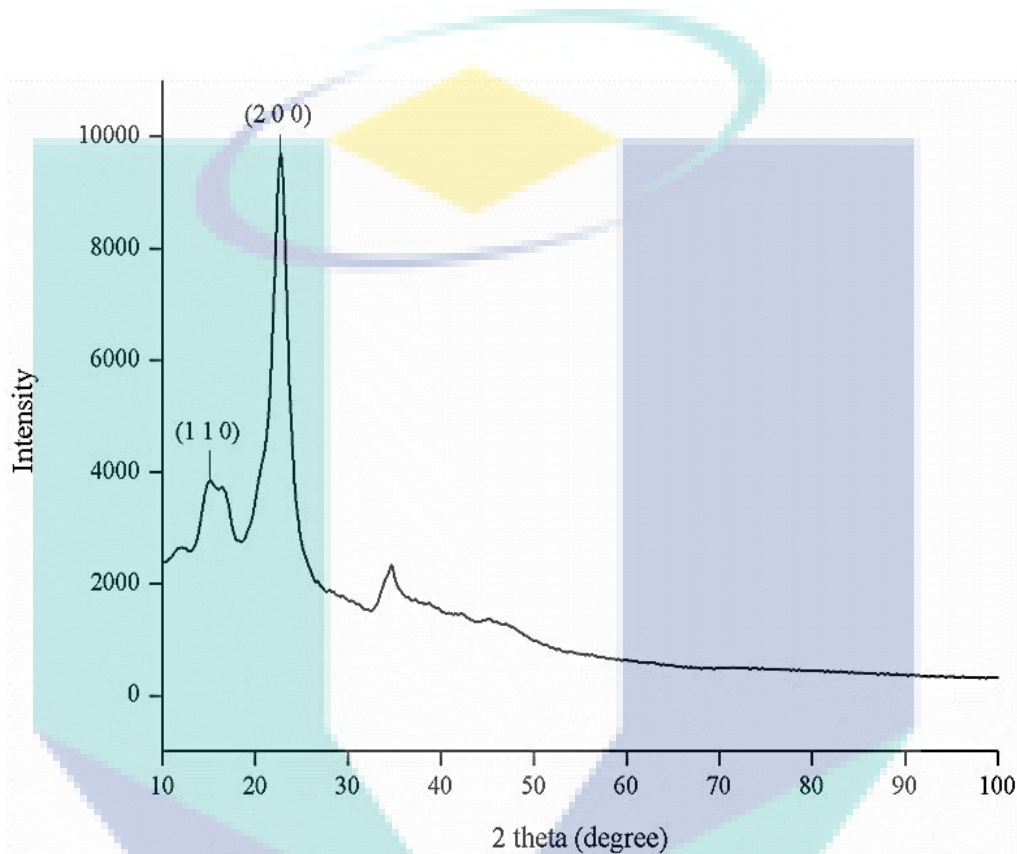
Figure 4.17   XRD pattern of CNC nanoparticles

Apparently, CNC nanoparticles were in gel form and it was not possible to evaluate it morphologically using FESEM as FESEM cannot measure the sample within the presence of water. Therefore, CNC nanoparticles have been prepared into two dried forms such as film and powder to analyse it in FESEM. Figure 4.18 shows the morphology of CNC nanoparticles in film form (Figure 4.18 (a)), and in powder form (Figure 4.18 (b)). The size and shape of nanoparticles could not be measured using FESEM as there were no individual nanosized particles observed in Figure 4.18 even though the samples were dried. Figure 4.18 showed the CNC nanoparticles clung with each other. However, the elemental analysis has been done using FESEM EDX. EDX did with 60 µm (Figure 4.19), 20 µm (Figure 4.20), and 10 µm (Figure 4.21) scale electron morphology similar to Al_2O_3 nanoparticles. These EDX spectrums showed that the clear

appearance of carbon (C) and oxygen (O) atoms in CNC nanoparticles. In addition, Table 4.4 illustrates the elemental chemical fraction of CNC nanoparticles with standard deviation (Awang et al., 2019). The standard deviation of weight% and atomic% parameters of oxygen and carbon elements of CNC nanoparticles were similar.
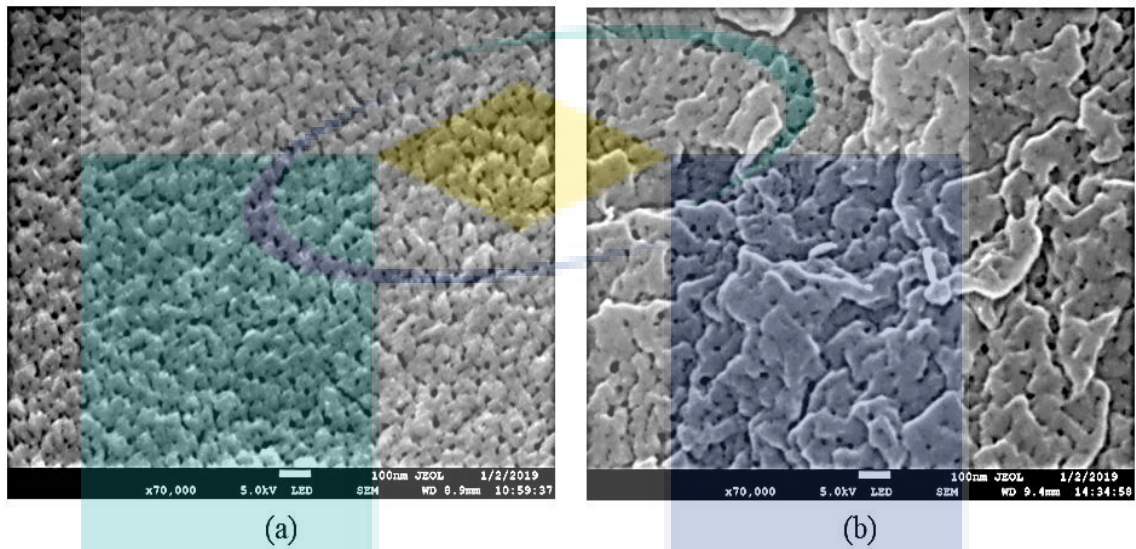
Figure 4.18   FESEM micrograph of CNC nanoparticles (a) film form (Magnification x70,000; WD 9.3 mm) and (b) powder form (Magnification x70,000; WD 9.4 mm)
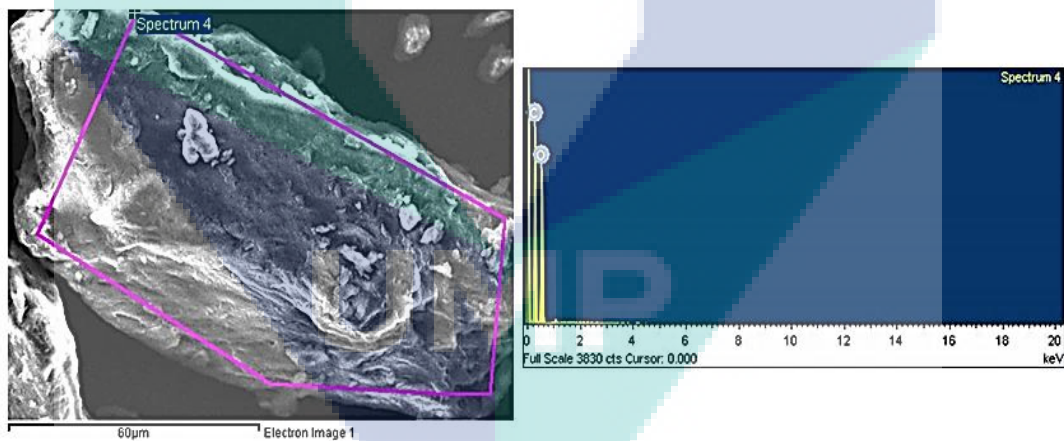
Figure 4.19   EDX spectrum of CNC nanoparticles with a 60 μm scale image

Table 4.4   Quantification results of CNC nanoparticles

Element	Weight %	Standard deviation	Atomic %	Standard deviation
Carbon, C	47.22	1.19	54.37	1.18
Oxygen, O	52.78	1.19	45.63	1.18

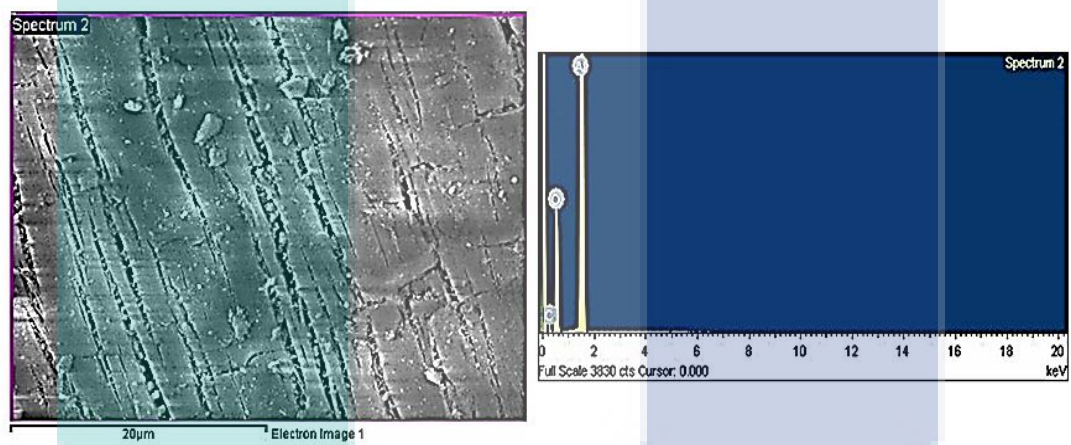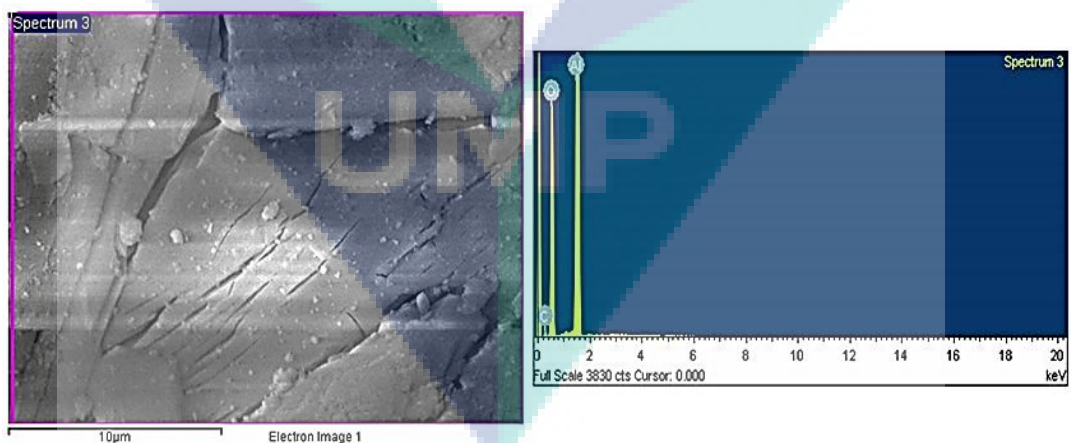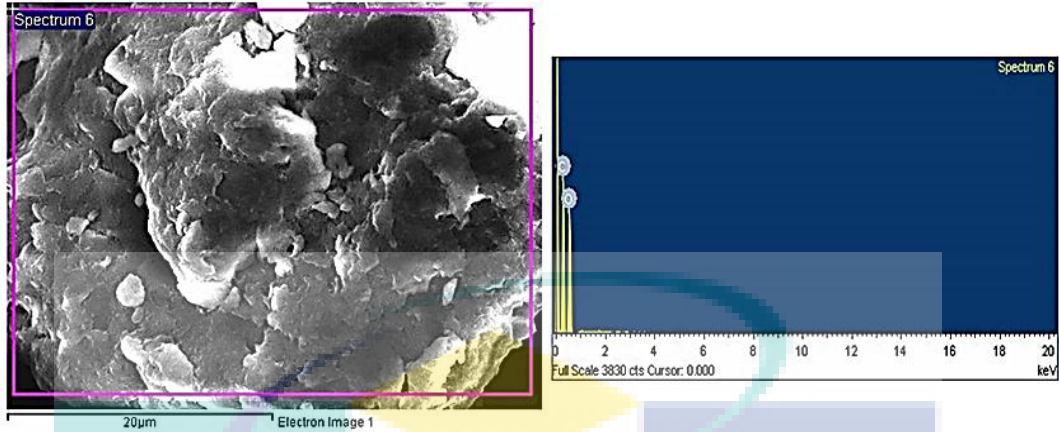Figure 4.20   EDX spectrum of CNC nanoparticles with a 20 µm scale image
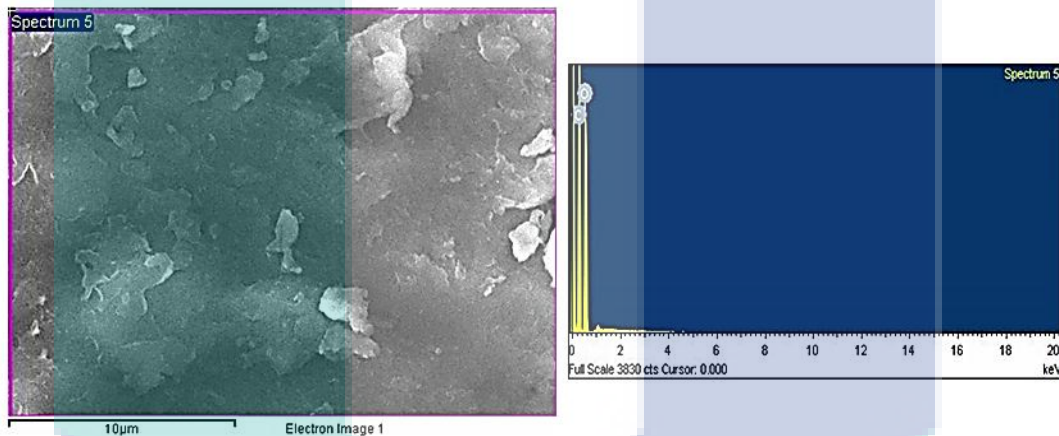
Figure 4.21   EDX spectrum of CNC nanoparticles with a 10 µm scale image

The TEM micrograph of CNC nanoparticles (powder form) and CNC nanofluids showed in Figure 4.22 and Figure 4.23 respectively. The size and shape of the CNC nanoparticles determined by Figure 4.22. In this micrographic view, it was observed that the size of the CNC nanoparticles was less than 50 nm. The shape of nanoparticles was in both elongated and nearly spherical geometry. On the other hand, Figure 4.23 represents the dispersion phenomenon of CNC nanofluids into the base fluid. The dispersion was not enough fairly even as some aggregation of nanoparticles was observed due to strong Van der Waals forces between the nanoparticles (Rance et al., 2010).
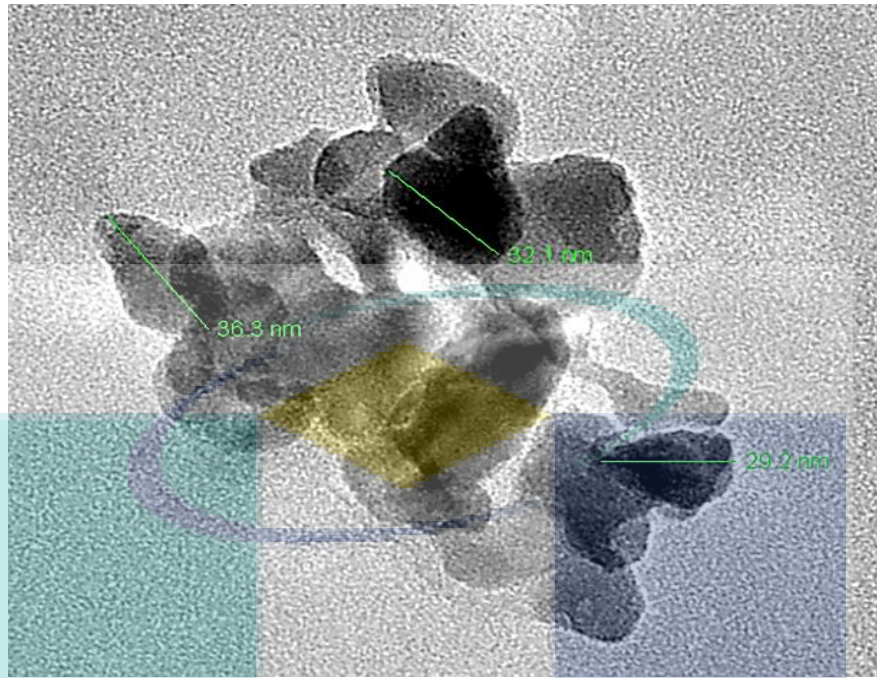
Figure 4.22   TEM morphology of CNC nanoparticles (Magnification x62,000)
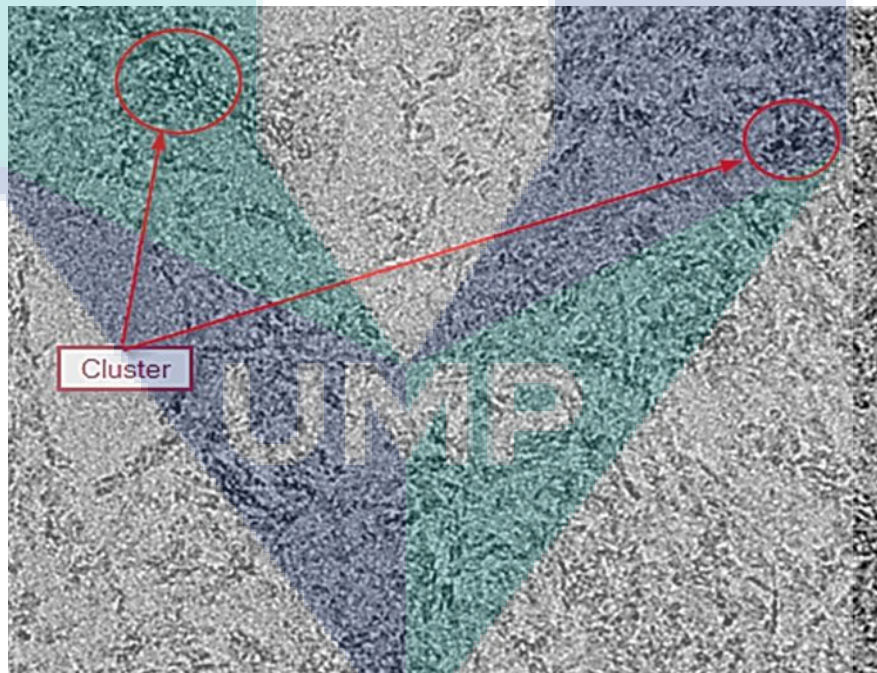
Figure 4.23   TEM micrograph of CNC nanofluids (Magnification x50,000)

Chemical Characterization of Nanofluids

The chemical composition and molecular structures of Al_2O_3 and CNC nanofluids were identified by transmission Fourier transform infrared (FTIR). The spectra in FTIR

were recorded in the range of 500 to 4000 cm^{-1}. FTIR test has been performed for both types of nanofluids. Figure 4.24 shows the FTIR spectra of Al_2O_3 and CNC nanofluids. In the case of Al_2O_3 nanofluids, the broadband around 3200 cm^{-1} was referred to stretching and bending O-H vibration which means the presence of the hydroxy group. The band identified at 1400 cm^{-1} correlate to the stretching vibration of Al-OH bands. The strong band near to 500 cm^{-1} corresponds to the Al-O bond. The medium to weak bond at about 2100 cm^{-1} assigned to C≡C bonds (Al-Abadleh & Grassian, 2003; Tabesh, Davar, & Loghman-Estarki, 2018). Similarly, from CNC nanofluid points of view, the peak about 3300 cm^{-1} is attributed to the O-H bond, indicating the appearance of hydroxy groups. The peak at 2951cm^{-1} wave number indicates a stretching vibrating band of C-H groups. The band observed at 2115 cm^{-1} attributed to C≡C bonds. The peak found at 1640 cm^{-1} is assigned to O-H stretching vibration of absorbed water and peak observed at 1412 cm^{-1} correspond to -CH_2 stretch vibrating bond. Besides that, the peak near 1031 cm^{-1} indicates the deformation in the cellulose of the C-O-H bond (Bai et al., 2019).
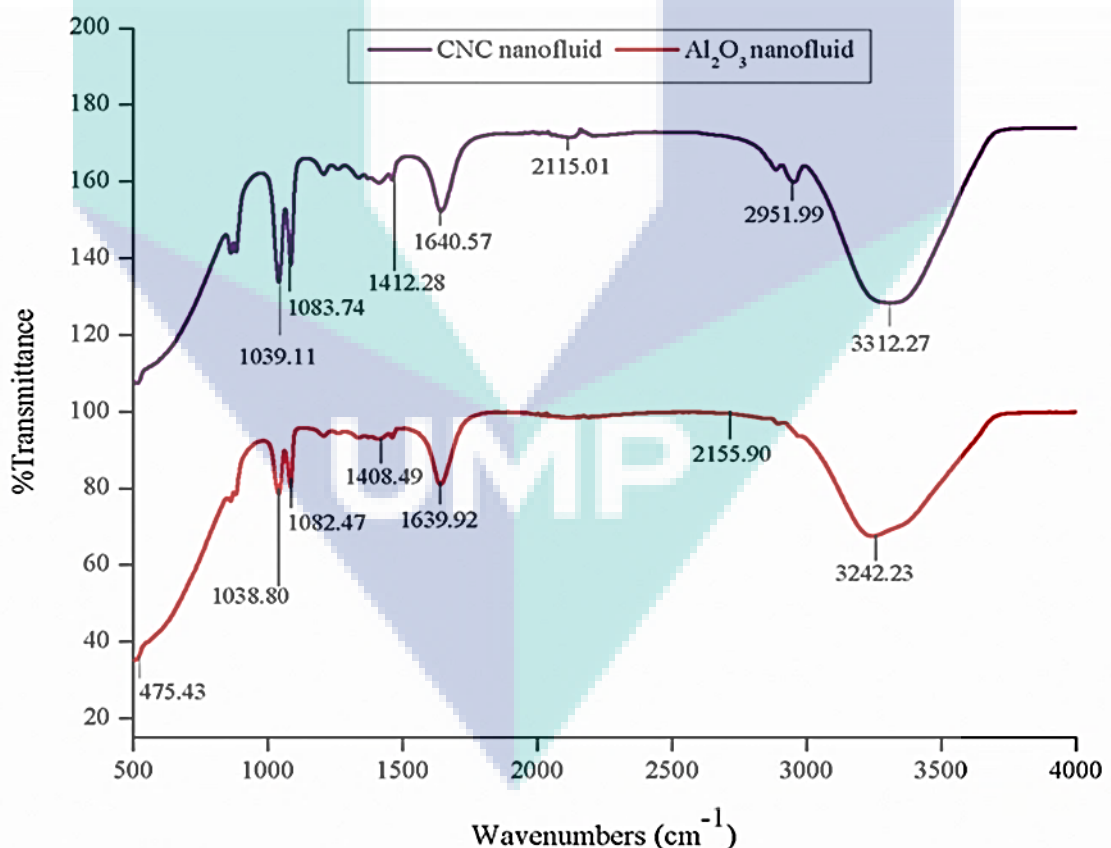
Figure 4.24   FTIR spectra of nanofluids (Al_2O_3 and CNC)
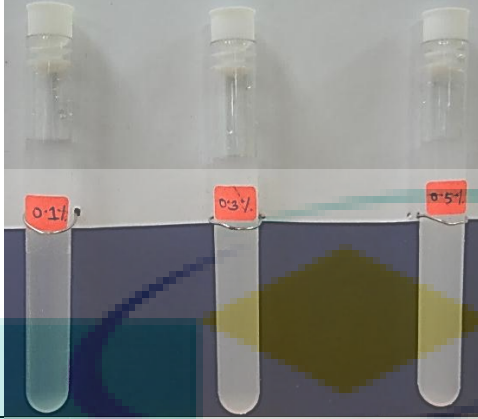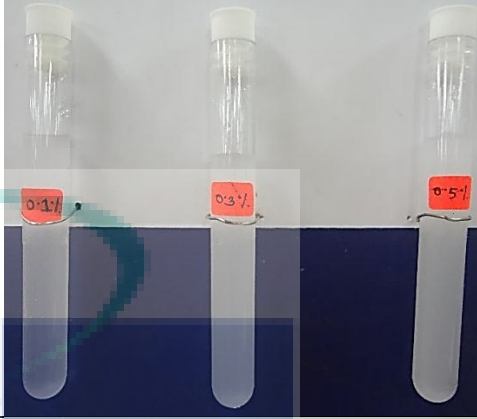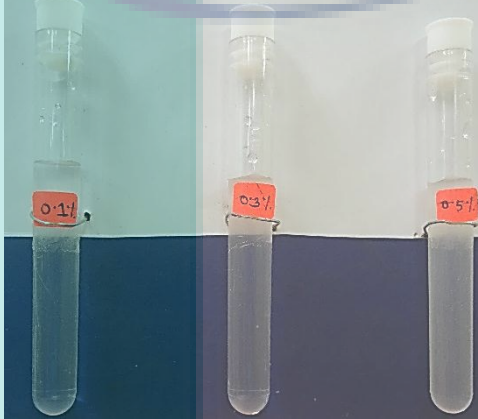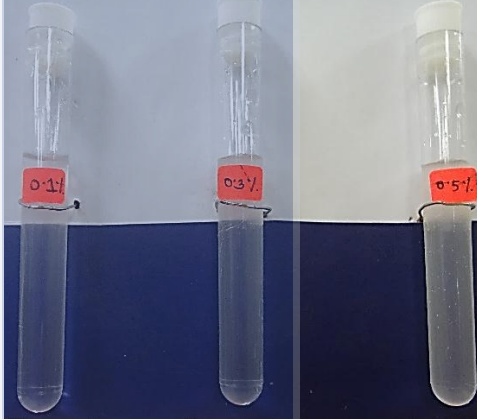
4.4 Analysis of Thermo-physical Properties

4.4.1 Stability Analysis

Both the qualitative and quantitation methods applied to evaluate the stability of Al_2O_3 and CNC nanofluids. In case of sedimentation observation (Qualitative method), the stability of Al_2O_3 and CNC nanofluids have been examined at various volume concentrations which is similar with Kaaliarasan Ramachandran et al. (2017) experimental study on effective thermal conductivity and relative viscosity of CNC/W-EG nanofluids through a combined experimental and statistical approach. The authors evaluated the stability of nanofluids by sedimentation observation. In this study, the observation has been done every day. No aggregation of Al_2O_3 and CNC nanoparticles occurred at the bottom of the test tube after one week of the preparation of the nanofluids as shown in Table 4.5. This observation demonstrates the moderate to good stability of both nanofluids meanwhile the numerical values of stability have been investigated by quantitative methods.

Long term physical and chemical stability of nanofluids is one of the fundamental requirements for its proper usage in heat transfer applications (Ghadimi, Saidur, & Metselaar, 2011). Moreover, Sharma and Gupta (2016) remarked that the stability of nanofluids should be at least in years rather than corresponding to the lifetime of the heat transfer equipment or basic maintenance period of the system. Because of strong Van der Waals interactions of nanoparticles create cluster/aggregation causing non-homogeneity of nanofluids. In addition, Yu et al. (2012) mentioned that the nanoparticle cannot be aggregate at a significant rate which is defined as the stability of nanofluids. The frequency of collisions caused by Brownian motion and the cohesion during the collision between the nanoparticles determined the rate of aggregation of nanoparticles. On the other hand, the sedimentation of nanoparticles degrades the thermo-physical properties such as thermal conductivity, density, viscosity, specific heat capacity; especially the stability of nanofluids has a significant effect on thermal conductivity directly or indirectly (Korada & Hamid, 2017). Aggregation of nanoparticles within the nanofluids can block the tubes which are responsible for discontinuation of heat transfer and resulting deflation of advantages of nanofluids in heat transfer (Sharma & Gupta, 2016).

Table 4.5   Evaluation of qualitative stability measurement of nanofluids

Nanofluids	After preparation	After seven days
Al₂O₃		
CNC		

From the quantitative method point of view, measurement of the zeta potential of nanofluids is one of the techniques used to evaluate the stability of nanofluids by analyzing electrophoretic behaviour (Ghadimi, Saidur, & Metselaar, 2011). The measured value of zeta potential above ±30 mV is considered to be a good stable nanofluid (Yu & Xie, 2012). The absolute zeta potential values of all nanofluids are presented in Figure 4.25. The highest zeta potential value is about 36.1 mV of 0.3% Al₂O₃ nanofluids followed by 0.5% Al₂O₃ nanofluid with 33.6 mV, while 0.1% showed the absolute value of zeta potential is less than 30 mV. On the other hand, the zeta potential values of the three-volume concentrations of CNC nanofluids were below 30 mV. Meanwhile, the Al₂O₃ nanofluids showed positive charge and CNC exhibited negativity potential behaviour. The zeta potential that means the stability trend of Al₂O₃ nanofluids was rising with the addition of nanoparticles into the base fluid. But stability turned to downward movement at 0.5% volume concentration of Al₂O₃ nanofluid, nevertheless zeta potential was above the benchmark of stable suspension. In the case of CNC nanofluids,

the trend was also in upward but changed in downward at 0.5% volume concentration of CNC nanofluid in the negative electrical field (Figure 4.25).
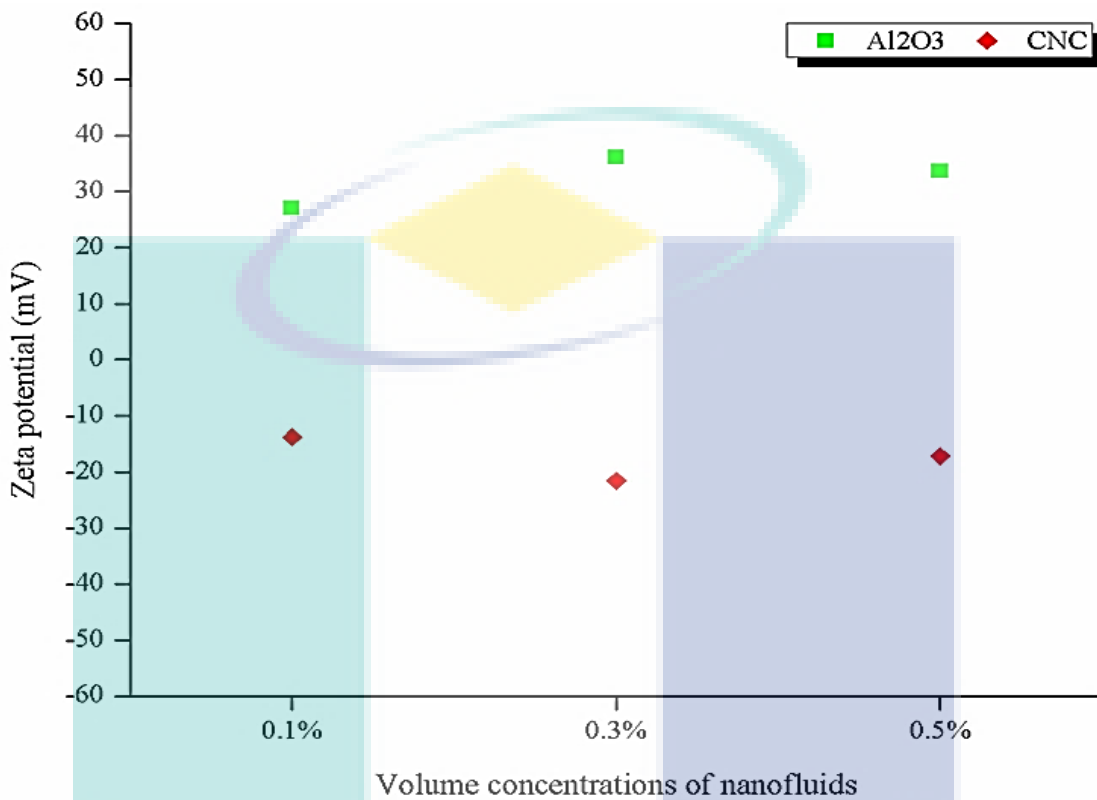
Figure 4.25   Quantitative analysis of the stability of nanofluids

4.4.2   Thermal Conductivity Analysis

The thermal conductivity of the base fluid (60% water and 40% EG), Al_2O_3 and CNC nanofluids with different volume concentrations (0.1%, 0.3%, and 0.5%) measured at four different temperatures such as 30°C, 50°C, 70°C, and 80°C temperature. The thermal conductivity of working fluids increased anomalously due to adding nanoparticles into base fluids. Figure 4.26 shows the enhancement of thermal conductivity of nanofluids (Al_2O_3 and CNC) at 0.1%, 0.3%, and 0.5% volume concentrations comparing with base fluid. Despite the increment phenomena of thermal conductivity; 0.1% CNC, nanofluid exhibited a slight decrement of thermal conductivity at the temperature of 50°C and 70°C. However, Al_2O_3 exhibited the increment of thermal conductivity consistently. Moreover, the thermal conductivity increases with an increase in temperature as well. The average enhancement percentage of thermal conductivity of both Al_2O_3 and CNC nanofluids presented in Table 4.6. Maximum thermal conductivity

achieved at 80°C for both types of nanofluids at all volume concentrations. Among them, 0.1% Al_2O_3 nanofluid performed the highest thermal conductivity enhancement at 80°C temperature while 0.3% CNC nanofluid maximized the thermal conductivity at 80°C temperature. Moreover, Figure 4.26 also illustrates that the enhancement of thermal conductivity is not linear with linearly increased volume concentration percentage of nanoparticles at any temperature. At 80°C temperature thermal conductivity of 0.3% and 0.5%, Al_2O_3 nanofluids were smaller than 0.1% Al_2O_3 nanofluid but it should be higher. On the other hand, thermal conductivity at 30°C temperature of 0.3% and 0.5% CNC nanofluids was decreasing than the 0.1% volume fraction of CNC nanofluid even though thermal conductivity of all volume fraction of CNC nanofluids was higher than the base fluid. In addition, the thermal conductivity of 0.3% CNC nanofluid was greater than 0.5% CNC nanofluid at 70°C and 80°C temperature. This similar phenomenon also observed by Wei, Zou, and Li (2017). The authors found thermal conductivity enhancement is not even with an increase in volume concentration at a temperature of 20°C.

Besides, Kaaliarasan Ramachandran et al. (2017) studied the thermal properties of water-ethylene glycol-based CNC nanofluids and found the addition of CNC nanoparticles can improve thermal conductivity and viscosity as well. It was also observed that the increasing temperature enhances the thermal conductivity of CNC nanofluids. Similarly, Azmi et al. (2016) experimentally studied and concluded the enhancement of thermal conductivity of Al_2O_3/W-EG nanofluid at various concentrations (0.2%, 0.8%, and 1%) under turbulent flow. The thermal conductivity enhancement pattern can be discussed in accordance with the theory of Brownian motion. The collision between the particles strengthened at higher temperature generating an increment of Brownian diffusion which reinforces the enhancement of thermal conductivity. Moreover, the reason for thermal conductivity enhancement can be discussed by the experimental study of Wen and Ding (2004). The authors studied that the nanoparticles in the base fluid increase the thermal conductivity by reducing thermal boundary layer thickness causing convection heat transfer enhancement. Not only that, the migration of nanoparticles in the based fluid is one of the roots of heat transfer enhancement which forms non-uniform distribution of thermal conductivity and viscosity field due to Brownian motion, shear action and spatial gradient in viscosity (Ding & Wen, 2005).
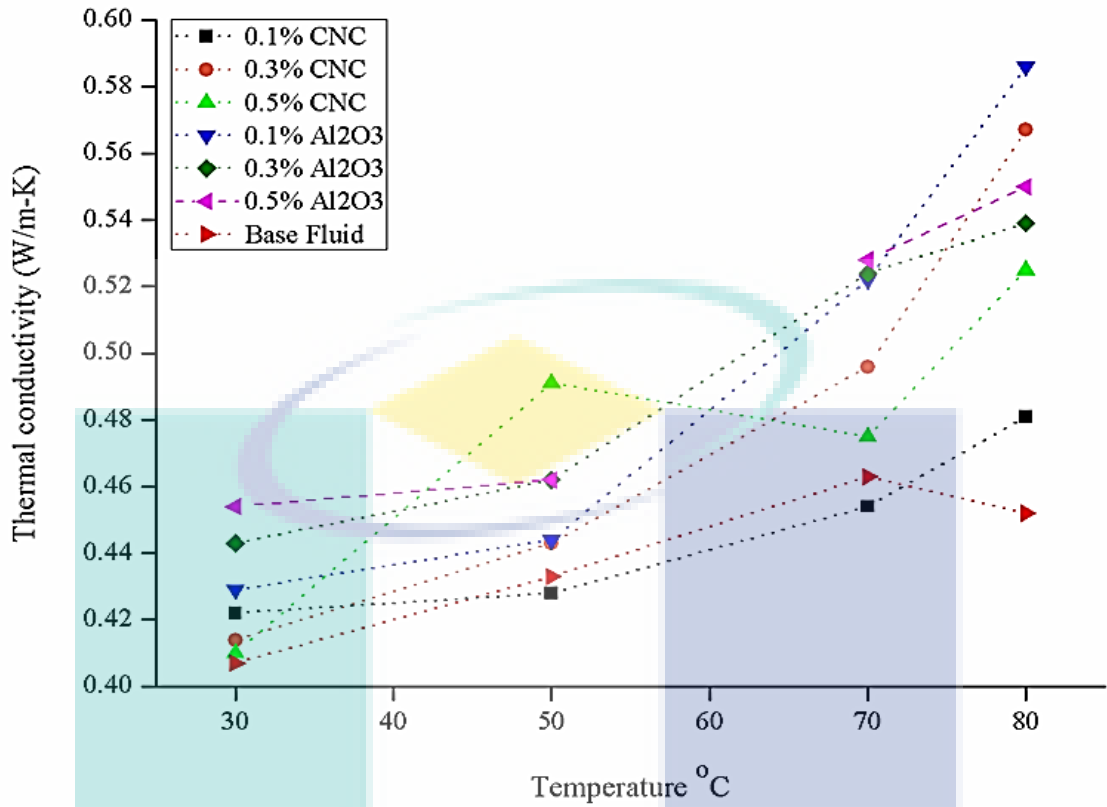
Figure 4.26   Thermal conductivity of Al₂O₃ and CNC nanofluids at various temperatures
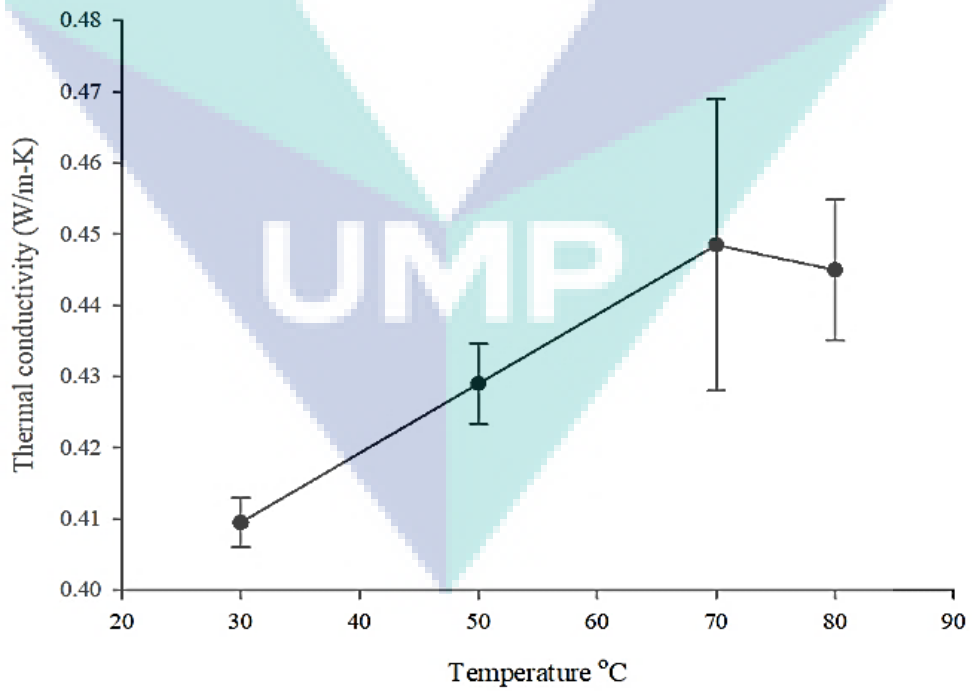
Figure 4.27   Graphical presentation of error difference of thermal conductivity of experimental and ASHRAE Standard data of base fluid

Prior to the experiment with nanofluids, the thermal conductivity of the base fluid (W: EG 60:40) measured to evaluate the measurement accuracy of KD2 Pro Thermal Property Analyser. The error percentage between resulting data and ASHRAE standard of base fluid has been analysed and shown in Figure 4.27 which defines the good agreement with the measurement accuracy of the thermal conductivity equipment as well as the thermal conductivity characteristic of the experimental base fluid. The maximum error deviation found at 70°C followed by at 80°C temperature; whereas the deviation at 50°C and 30°C temperature was less accordingly.

Table 4.6   The average enhancement of thermal conductivity for different volume concentrations of nanofluids at different temperatures (^{o}C)

Nanofluids	Al$_2$O$_3$			CNC		
Volume concentrations	0.1%	0.3%	0.5%	0.1%	0.3%	0.5%
Temperature (^{o}C)	Percentage enhancement (%)					
At 30°C	2.2	3.6	4.7	1.5	0.7	0.3
At 50°C	1.1	2.9	2.9	-0.5	2	5.8
At 70°C	5.9	6.1	6.5	-0.9	3.3	1.2
At 80°C	13.4	8.7	9.8	2.9	11.5	7.3

4.4.3 Dynamic Viscosity Analysis

At first the measurement of viscosity has been done for base fluid (60: 40 W: EG); afterward viscosity of nanofluids (Al$_2$O$_3$ and CNC) with different volume concentrations (0.1%, 0.3%, and 0.5%) determined at four distinct temperatures such as 30°C, 50°C, 70°C, and 80°C temperature. Earlier, the deviation of experimental viscosity data and ASHRAE Standard data of the base fluid has been analysed and portrayed in Figure 4.29. The maximum standard deviation of about 0.27 found at the 80°C temperature of the base fluid and other deviations were very less at 30°C, 50°C, and 70°C temperature. The viscosity of nanofluids increases due to the improvement of the internal shear stress and afterward increasing volume concentration affects this shear stress more significantly (Jabbari, Rajabpour, & Saedodin, 2017). The intermolecular interactions between the particles decrease at low temperatures. At higher temperature, the molecules obtain higher kinetic energy which facilitates to enhance fluid motion and reduce the viscosity (Li et al., 2015). In this study, viscosity increases with increasing volume fractions of nanoparticles but decreases when the temperature increased, and this phenomenon is similar to many previous studies (Azmi et al., 2016; Kaaliarasan Ramachandran et al., 2017; K Ramachandran et al., 2017).

In this study, the viscosity of Al_2O_3 enhanced due to adding nanoparticles into the base fluid and further increased linearly with increasing volume fractions of nanofluids. The maximum viscosity obtained at 30°C temperature of 0.5% volume concentration Al_2O_3 nanofluid. But the highest viscosity gained for CNC nanofluid at 0.3% volume concentration at 30°C temperature. Surprisingly viscosity of 0.5% CNC nanofluid was lower than 0.3% CNC nanofluid at 30°C temperature as shown in Figure 4.28, although this viscosity value of CNC nanofluids was higher comparing with base fluid. The viscosity trend of 0.3% and 0.5% CNC nanofluids along with base fluid exhibit upward trend at 80°C temperature; though viscosity trend of CNC nanofluids (all volume concentrations) and base fluid is downward with raising the temperature up to 70°C temperature and the trend supposed to be in the similar direction as well. Perhaps this viscosity phenomenon of CNC nanofluids in this study supports the recommendation of Nguyen et al. (2008) viscosity of nanofluid study. Moreover, 0.1% of CNC nanofluid exhibited the same performance at 70°C and 80°C temperature.
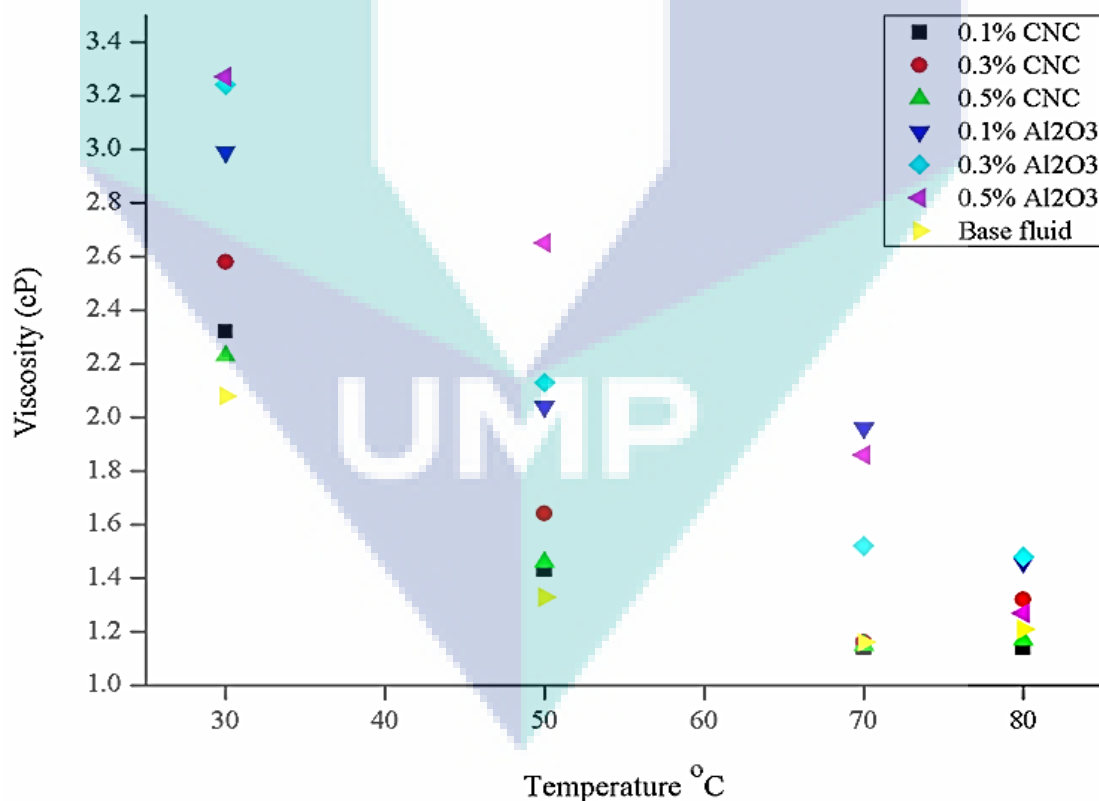
Figure 4.28   Temperature dependence of viscosity of Al_2O_3 and CNC nanofluids

On the other hand, the viscosity of Al_2O_3 nanofluids with various volume concentrations decreased gradually with the gradient of temperature (Figure 4.28).

However, the lowest viscosity observed at 80°C temperature at 0.5% volume fraction Al_2O_3 nanofluid. According to Newtonian fluid theory, shear stress (τ) and shear rate (γ) are straight and viscosity remains constant as defined Newtonian fluid (Bagnold, 1954). In this study, the nanofluids (both Al_2O_3 and CNC) at various volume concentrations showed the non-Newtonian behaviour as shear viscosity increases with increasing shear stress at every individual temperature (Yapici et al., 2014).
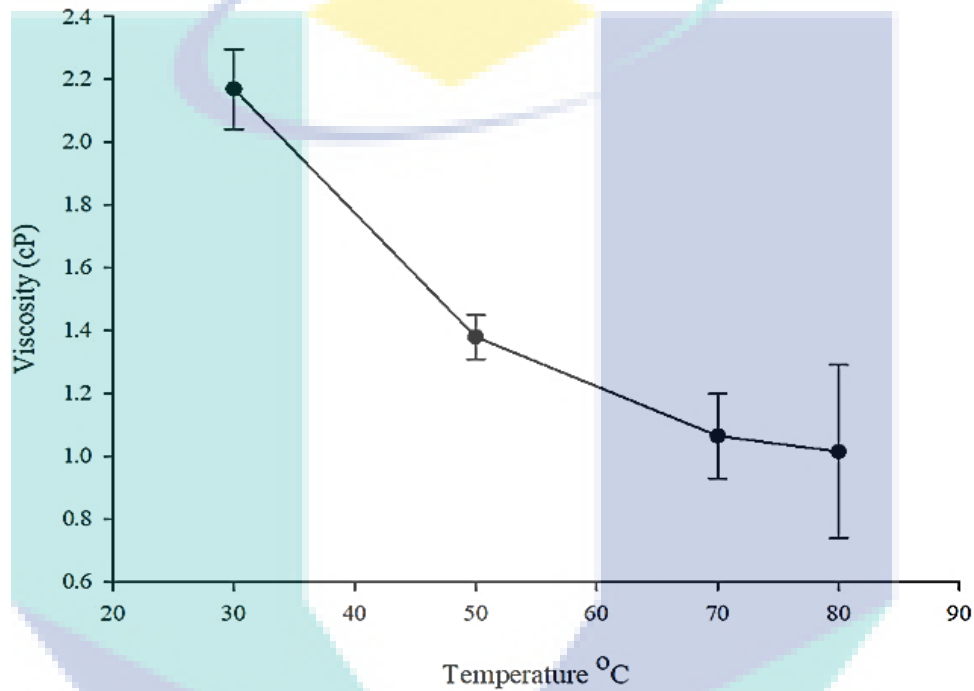
Figure 4.29   Variation of error of dynamic viscosity of experimental and ASHRAE Standard data of base fluid

4.4.4   Specific Heat Analysis

The resulting data of specific heat capacity (C_p) of the base fluid, Al_2O_3, and CNC nanofluids are shown in Figure 4.30. Insufficient numerical and experimental studies had been conducted to determine the specific heat capacity of nanofluids at different temperature and volume concentrations. In a study, O'Hanley et al. (2012) studied the specific heat capacity of nanofluids at various volume concentrations with different types of nanofluids (water-based alumina, silica, copper-oxide). The authors also used a set of different size (diameter) of nanoparticles. They revealed specific heat capacity decreased due to the increase of volume fractions of nanofluids. In another study, Singh et al. (2017) concluded the specific heat decreases with an increase of nanoparticle concentrations at

room temperature and the specific heat value is minimum at the highest temperature for all nanofluids. In addition, Sekhar and Sharma (2015) found that the increasing volume concentration of nanofluids (water-based aluminium oxide) decline the specific heat capacity of nanofluids owing to the increase of thermal diffusivity of nanofluids. They also mentioned the increment of temperature causes the decrement of effective specific heat capacity of nanofluids. On the other hand, Zhou and Ni (2008) and Sekhar and Sharma (2015) experimentally studied that effective specific heat corresponds to nanoparticle diameter. Effective specific heat improved owing to the higher diameter of nanoparticles; as thermal conductivity increases with an increase in particle diameter. Figure 4.30 portrays the scenario of specific heat of base fluid, Al_2O_3, and CNC nanofluids (all volume concentrations). The adding of Al_2O_3 nanoparticles into the base fluid causes the loss of specific heat capacity and increases with an increase in the mass fraction of nanoparticles into the base fluid. Moreover, 0.5% Al_2O_3 nanofluid showed a higher specific heat capacity than the 0.3% volume concentration nanofluid but the specific heat was in the negative potential. In this study, specific heat was in increasing trend due to the increasing temperature of Al_2O_3 nanofluid at all volume concentrations along with base fluid. But 0.1% of Al_2O_3 nanofluid achieved the highest specific heat at 70^oC temperature. Maximum specific heat achieved at 80^oC temperature for Al_2O_3 nanofluid at 0.5% volume concentration.

In the case of CNC, all volume concentrations of nanofluid exhibited the negative potentiality of specific heat capacity at a range of temperatures from 30^oC to 80^oC. Moreover, negativity increases with an increasing volume concentration of CNC nanofluids and with the improvement of temperature as well. 0.5% CNC nanofluids performed the highest specific heat capacity at 80^oC temperature. Whereas, 0.3% of CNC nanofluid performed the lowest specific heat capacity at 50^oC temperature. Moreover, 0.3% of CNC nanofluid showed lower specific heat than 01% CNC at 30^oC and 50^oC temperature. In addition, the CNC nanofluids at all volume concentrations showed fewer negativity results at 50^oC temperature than at 30^oC temperature. Furthermore, Das, Gupta, and Mekjian (2003) studied the negative specific heat in a thermodynamic model and reported that mechanical instability leads to the negative value of specific heat. Besides, the smaller specific heat of solid particles compared to that of base fluid obviously will decrease the specific heat of the nanofluid mixture. The declining will be continued at the increment of the volumetric loading of particles (Murshed, 2012). Moreover, literature

stated, there is good relation between specific heat and thermal conductivity, especially with thermal diffusivity as nanofluids can diffuse heat much better than base fluid such as Vajjha and Das (2012) studied that among three of nanofluids (Al_2O_3, SiO_2, CuO) CuO showed the highest thermal diffusivity at a defined temperature due to its lowest specific heat and high thermal conductivity values.
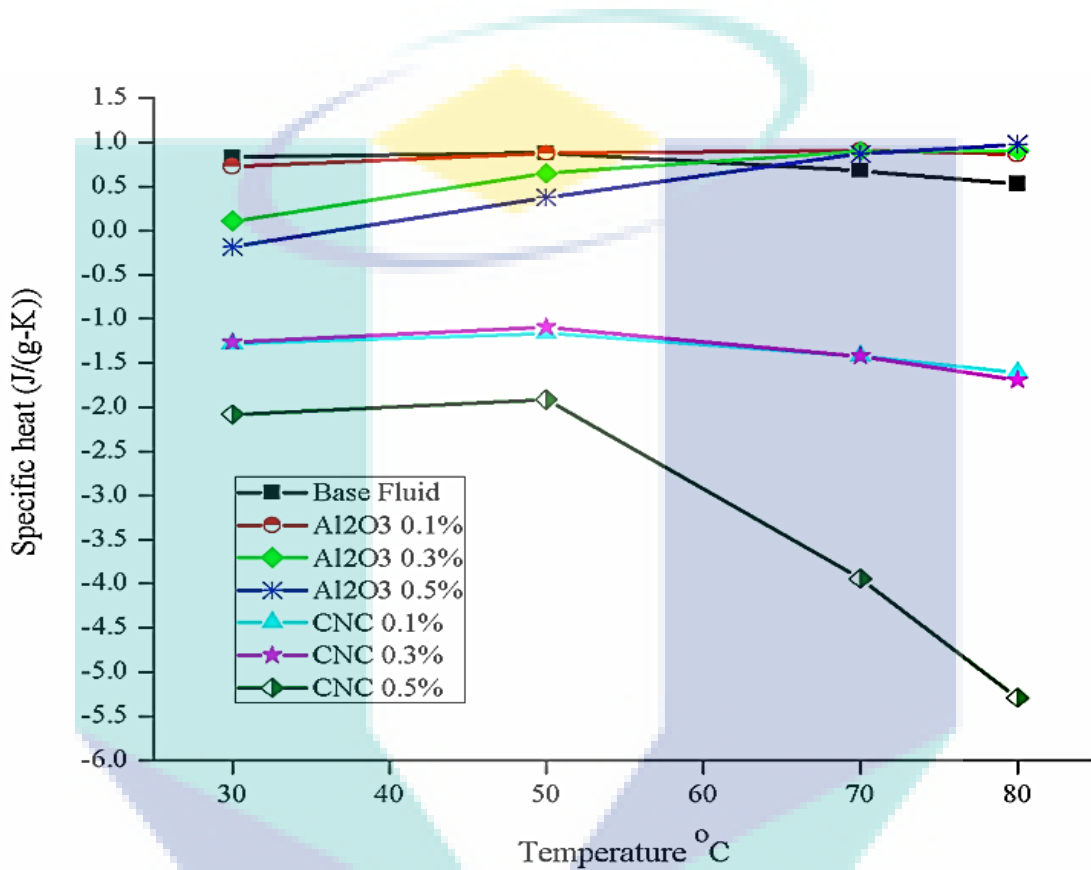
Figure 4.30   Evaluation of specific heat of Al_2O_3 and CNC nanofluids correlated with temperature

4.4.5 Density Analysis

Generally, the density of nanofluids is equivalent to the volume ratio of nanoparticles and base fluid. Base fluid performs an important role in the density of nanofluids. Density is also temperature sensitive characteristic of nanofluids. The increasing temperature decreases the density of nanofluids (Vajjha, Das, & Mahagaonkar, 2009). Prior to the experimental density analysis of nanofluids, the experimental and ASHRAE Standard density data of base fluid has been investigated and has been shown in Figure 4.32. The resulting data of the density of the base fluid is in good agreement with ASHRAE Standard data and the maximum deviation is only about 0.77% (Figure 4.32). The standard deviation of these two values (experimental and ASHRAE Standard)

of base fluid illustrates that the maximum deviation found at 80℃ temperature and the deviation is gradually decreasing since the temperature is degrading. In this study, the density of the base fluid and nanofluids (Al$_2$O$_3$ and CNC) with different volumetric concentrations measured at a temperature range of 30℃ to 80℃ and obtained data portrayed in Figure 4.31. According to obtained data, density increased with an increase in volume concentrations of both (Al$_2$O$_3$ and CNC) nanofluids (Shoghl, Jamali, & Moraveji, 2016) and decreases with an increase in temperature (Vajjha, Das, & Mahagaonkar, 2009).
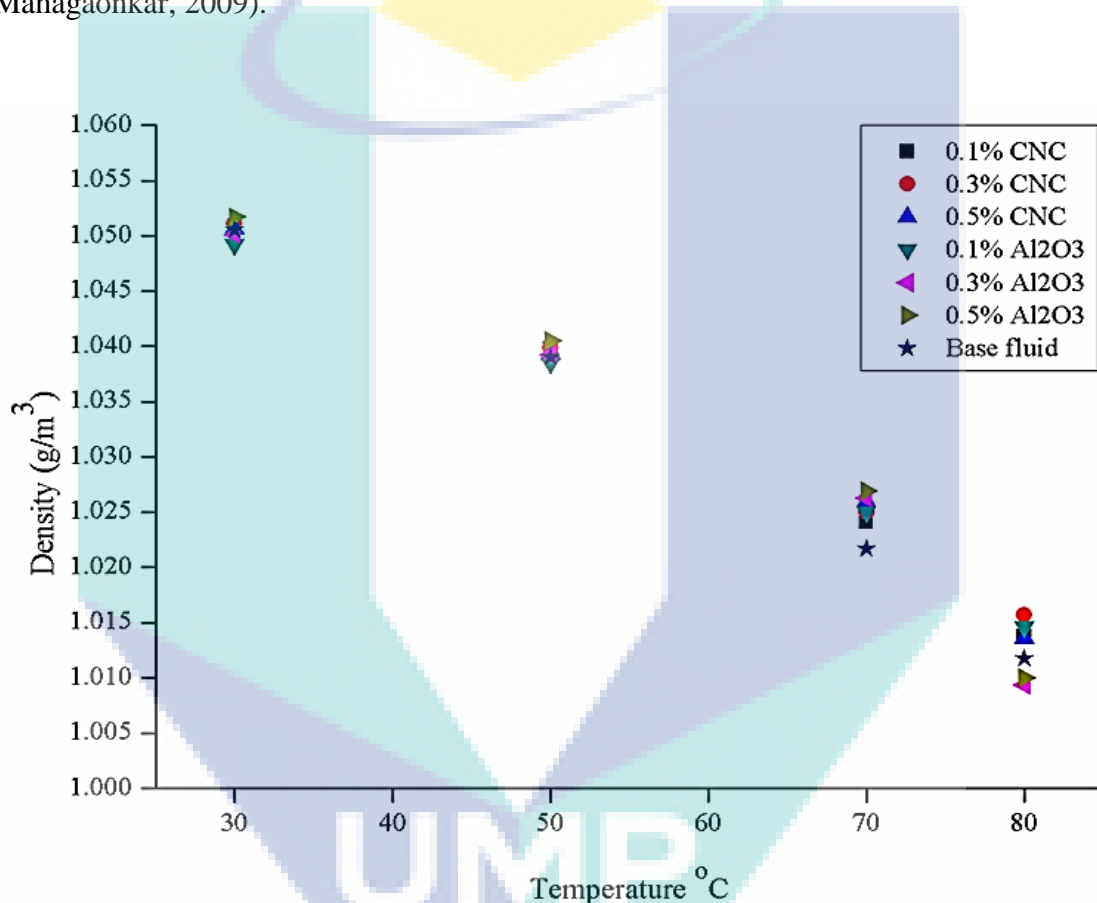
Figure 4.31   Density measurement of nanofluids (Al$_2$O$_3$ and CNC) at different temperatures

All the volume fraction of both Al$_2$O$_3$ and CNC nanofluids exhibited the highest density at 30℃ and the smallest density at 80℃ temperature continuously. Furthermore, 0.5% Al$_2$O$_3$ nanofluid showed the maximum density at 30℃ temperature and minimum density found for 0.3% volume fraction Al$_2$O$_3$ nanofluid at 80℃ temperature. Nevertheless, Al$_2$O$_3$ nanofluids showed the increment trend of density with an augmentation of nanoparticles into the base fluids among all volume concentrations, but the density of 0.1% Al$_2$O$_3$ nanofluid is slightly below than the base fluid at 30℃ and 50℃

temperature. Similarly, 0.3% of Al_2O_3 nanofluid exhibited a bit less density at 30°C temperature than the base fluid. In the case of CNC nanofluids, the highest density observed for 0.3% volume fraction at 30°C temperature while minimum density obtained at 80°C temperature for 0.5% volume concentration. Moreover, the density of 0.5% CNC nanofluid was slightly lower than 0.3% CNC nanofluid at 30°C, 50°C and 80°C temperature whereas it was only greater at 70°C temperature (Figure 4.31).
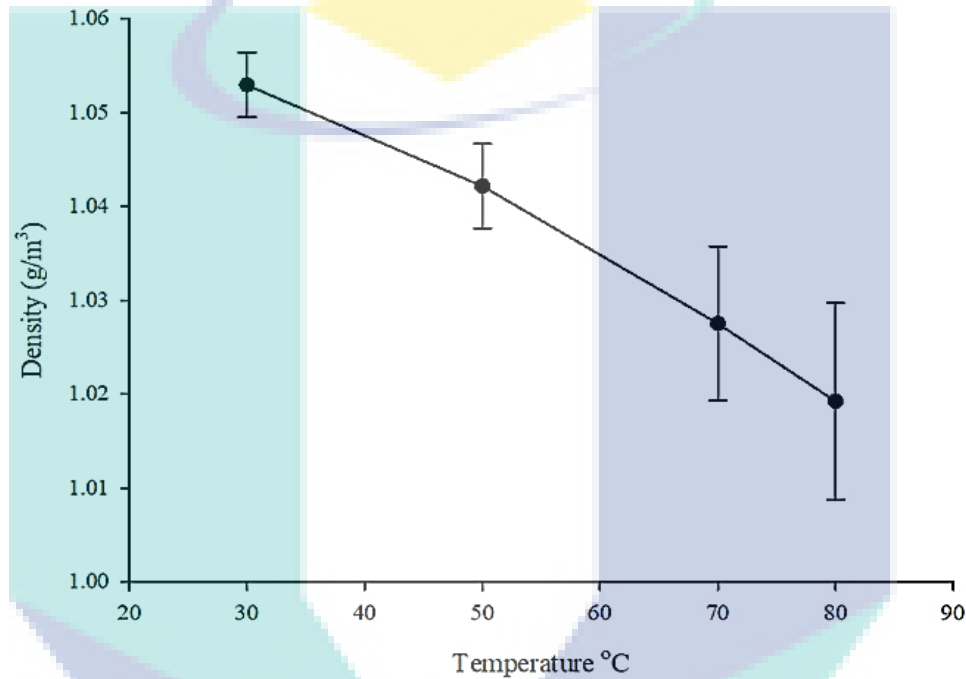
Figure 4.32   Density error of base fluid (Experimental and ASHRAE Standard data)

4.4.6   The potential of hydrogen (pH) Analysis

The potential of hydrogen (pH) is one of the most important factors of nanofluids as the stability of nanofluids depends on it. The increment of thermal conductivity well depends on the stability and the state of surface charge of nanofluids (Huang et al., 2009). Moreover, surface charge states directly affect on the stability of nanofluids suspension and conferred the strong correlation between the hydrodynamic size of nanoparticles and the co-efficient of stability of the nanofluids (Lee, Kim, & Kim, 2006). The more distance between the pH of nanofluids and the pH of isoelectric point (IEP) causes more stable nanofluids and increases efficiency as well (Goudarzi et al., 2015). The pH affects the thermal conductivity of nanofluids considerably and it can be enhanced significantly by altering the pH of the nanofluids (Gowda et al., 2010). Moreover, Wamkam et al. (2011)

have studied the pH effects of stability and zeta-potential on heat transfer nanofluids and exhibited the improvement of thermal conductivity significantly of nanofluids near to the isoelectric point that indicates the stability of nanofluids were affected by the pH values. In another study, Wang and Zhu (2009) experimentally investigated of pH of two water-based nanofluids and mentioned that an optimum pH value can improve the highest thermal conductivity of nanofluids. Besides that, literature stated the pH value of different nanoparticles is not equivalent and has a dependency on temperature, volume concentration and particle size (Adio, Sharifpur, & Meyer, 2015; Yousefi, Shojaeizadeh, et al., 2012). In addition, Jia-Fei et al. (2009) revealed that the small size of nanoparticles performs significantly fluctuations of pH values from 5 to 7. Besides that, low pH value performs good heat transfer property of nanofluids. Because in low pH condition, hydration forces among the particles increases in the suspension which results in the mobility enhancement of nanofluids in the suspension to lead the heat transport process (Xie et al., 2002). On the contrary, Goudarzi et al. (2015) experimentally concluded that higher the pH value of nanofluids increases more efficiency than lower pH values. In addition, Said et al. (2016) experimentally revealed that the controlled pH of nanofluids influence the efficiency of solar collector remarkably. In this study, the pH values of Al_2O_3 and CNC nanofluids with various volume concentrations at a temperature range of 30^oC to 80^oC along with base fluid has been demonstrated in Figure 4.33. Base fluid showed a pH scale from slightly acidic to slightly alkaline at 30^oC, 50^oC, 70^oC, and 80^oC temperature. The pH values of Al_2O_3 nanofluids (all volume concentrations) was in acidic range of pH scale at 30^oC to 80^oC temperature. Moreover, pH values of Al_2O_3 nanofluids was decreasing owing to increasing temperature. In this context, 0.3% Al_2O_3 nanofluid showed the highest pH value at 30^oC temperature while 0.5% Al_2O_3 nanofluid performed the lowest pH value strong acidic phase at 80^oC temperature. On the other hand, the pH of CNC nanofluids (all volume concentrations) was in decreasing trend with respect to temperature enhancement and the pH was within marginally acidic to lightly alkaline scale. Maximum pH found at 30^oC temperature for 01% and 0.5% CNC nanofluids while 0.3% CNC nanofluid portrayed at 50^oC temperature. The minimum pH obtained at 80^oC temperature which defines raising temperature progressively made the nanofluids slightly alkaline to light acidic. However, 0.1% of CNC nanofluid showed the lowest pH at 50^oC temperature.
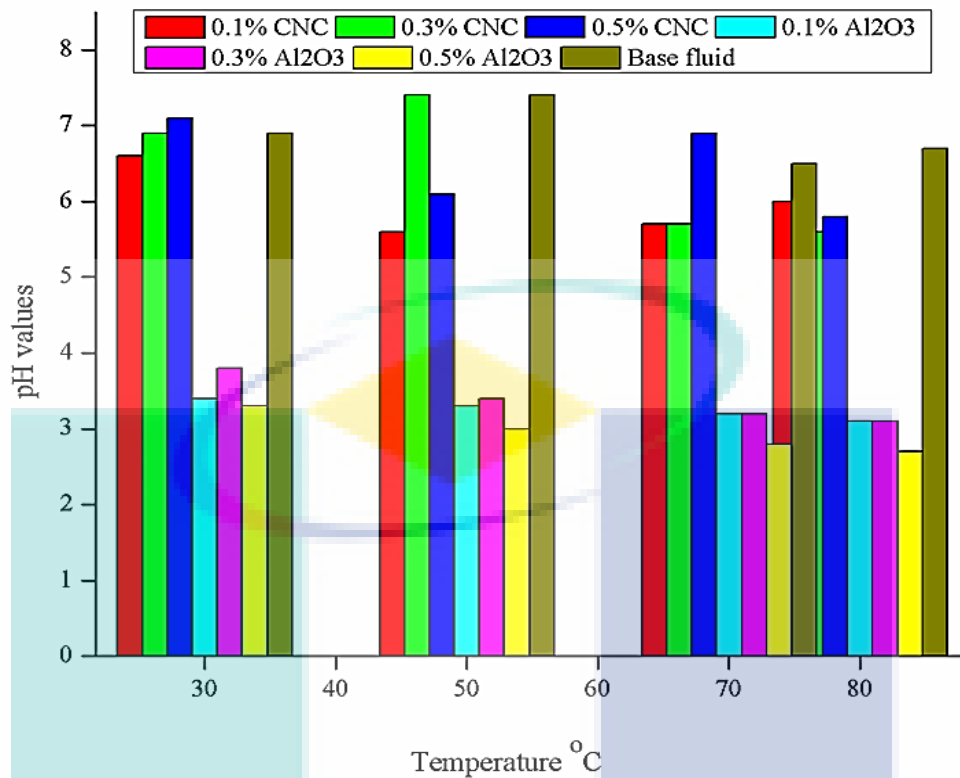
Figure 4.33   pH of different concentrations of Al_2O_3 and CNC nanofluids

4.5   Experimental Result Analysis of Flat Plate Solar Collector

In this study, 0.3% and 0.5% volume fraction of nanofluids (both Al_2O_3 and CNC) have been selected and used in FPSC by analysing the thermo-physical properties of nanofluids. 0.1% volume concentration of nanofluids (both Al_2O_3 and CNC) has been abandoned because of some inconsistent results of thermo-physical properties. Thermal conductivity is the most important property of heat transfer application. 0.1% CNC nanofluid showed the uncertain enhancement of thermal conductivity with increasing temperature since thermal conductivity was smaller than base fluid at 50°C and 70°C temperature. The maximum thermal conductivity obtained of 2.9% only at 80°C temperature. Even though 0.1% of Al_2O_3 nanofluid exhibited the highest thermal conductivity enhancement of 13.4% at 80°C temperature, there was a big void of thermal conductivity enhancement of nanofluid between at the adjacent temperature. In the case of viscosity, 0.1% Al_2O_3 nanofluid showed good agreement with the raising of temperature while 0.1% CNC nanofluid was not in better condition with temperature increment. 0.1% CNC nanofluid performed the equal result of viscosity at 70°C and 80°C temperature. From the specific heat point of view, 0.1% Al_2O_3 exhibited irregular enhancement with increasing temperature. Specific heat capacity of 0.1% Al_2O_3

nanofluid was higher at 70°C than at 80°C temperature but it supposed to be smaller. Besides, the specific capacity of 0.1% CNC nanofluid decreased at 50°C temperature than at 30°C rather it should be higher. From the pH standpoint, 0.1% CNC nanofluid showed irregular behaviour with the increasing temperature. But 0.1% of Al$_2$O$_3$ nanofluid performed the continues decreasing trend with respect to temperature. And finally, the stability of 0.1% volume concentration nanofluid (both Al$_2$O$_3$ and CNC) was not good in zeta potential scale as stability is the fundamental requirement of proper utilization of nanofluid in the heat transfer application.

The inlet and outlet temperature have been monitored in a repeated manner for individual nanofluids and averaged the data, as shown in Table 4.7. The difference between the outlet and inlet temperature of 0.3% and 0.5% volume concentration of nanofluids (both Al$_2$O$_3$ and CNC) was higher than the base fluid illustrated in Table 4.7. The resulting data referred that the adding of nanoparticles into the base fluid increased thermal conductivity which enhanced the outlet temperature of FPSC. Maximum outlet temperature obtained by 0.5% Al$_2$O$_3$ nanofluid and maximum inlet temperature also found at 0.5% volume concentration of Al$_2$O$_3$ nanofluid. The temperature difference between 0.3% and 0.5% Al$_2$O$_3$ nanofluids was relatively the same, even though 0.5% of Al$_2$O$_3$ nanofluid showed a higher thermal conductivity enhancement in thermo-physical property analysis. On the other hand, 0.5% CNC nanofluid performed lower temperature differences than 0.3% CNC nanofluid between outlet and inlet of FPSC. In thermo-physical property analysis, it was observed that 0.3% CNC exhibited higher thermal conductivity than 0.5% CNC nanofluid which defines good agreement of CNC nanoparticles between the sample and bulk application.

Table 4.7   Experimental data of temperature ($^{\circ}$C) of nanofluids

Parameters	Outlet temperature ($^{\circ}$C)	Inlet temperature ($^{\circ}$C)
Base fluid	42.66	41.66
0.3% Al$_2$O$_3$	42.4	40.4
0.5% Al$_2$O$_3$	45.1	43.2
0.3% CNC	44.8	42.9
0.5% CNC	43.6	42.4

Energy Gain and Efficiency of Flat Plate Solar Collector

The energy gain and efficiency of FPSC has been calculated (Kalogirou, 2013) using the data presented in Table 4.8. The scenario of specific heat of base fluid, 0.3% and 0.5% volume fraction nanofluids (both Al_2O_3 and CNC) at 30ºC, 50ºC, 70ºC, and 80ºC temperature depicted in Table 4.8. The mass flow rate of all fluids was fixed with 0.0108 kg/s. The outlet and inlet temperature of FPSC recorded in Table 4.8 in a repeated form for the individual specific heat of base fluid, 0.3% and 0.5% volume fraction of nanofluids (both Al_2O_3 and CNC) at a temperature range of 30º to 80ºC.

In this study, solar radiance has been considered as a constant value which was 830 W/m^2; this value has been selected from the experimental work of solar collectors performed by Gaos et al. (2017). The authors found the maximum average value of solar radiance was 830 W/m^2 during the evaluation of the performance of the solar collector. Besides, the area of the solar collector was 0.97526 m^2 which has been calculated manually using the actual measurement of tubes as shown in Table 4.9. The inner and outer diameter (mm) of header and riser tubes was the equivalent and the total number of tubes was ten (Table 4.9).

Table 4.8   Table of required data for experimental calculations

Parameters	C_p (J/kg-K)	$\dot{m}$ (kg/s)	T_{out} (ºC)	T_{in} (ºC)
Base fluid	830 at 30ºC	0.0108	42.66	41.66
0.3% Al_2O_3	110 at 30ºC		42.4	40.4
0.5% Al_2O_3	180 at 30ºC		45.1	43.2
0.3% CNC	1260 at 30ºC		44.8	42.9
0.5% CNC	2080 at 30ºC		43.6	42.4
Base fluid	880 at 50ºC		42.66	41.66
0.3% Al_2O_3	650 at 50ºC		42.4	40.4
0.5% Al_2O_3	380 at 50ºC		45.1	43.2
0.3% CNC	1090 at 50ºC		44.8	42.9
0.5% CNC	1910 at 50ºC		43.6	42.4
Base fluid	680 at 70ºC		42.66	41.66
0.3% Al_2O_3	900 at 70ºC		42.4	40.4
0.5% Al_2O_3	870 at 70ºC		45.1	43.2
0.3% CNC	1420 at 70ºC		44.8	42.9
0.5% CNC	3940 at 70ºC		43.6	42.4
Base fluid	530 at 80ºC		42.66	41.66
0.3% Al_2O_3	910 at 80ºC		42.4	40.4
0.5% Al_2O_3	980 at 80ºC		45.1	43.2
0.3% CNC	1690 at 8ºC		44.8	42.9
0.5% CNC	5290 at 80ºC		43.6	42.4

Table 4.9   Actual measurements of the tubes of FPSC

Properties	Parameters
Inner diameter (mm)	12.5
Outer diameter (mm)	12.7
Number of tubes	10
Total length (m)	12.325

The energy gain (kW) performing as heat transfer and the efficiency (%) of FPSC have been tabulated in Table 4.10. The energy gain by 0.3% and 0.5% Al$_2$O$_3$ nanofluids was the lowest than the base fluid at 30°C temperature in FPSC. But 0.3% and 0.5% CNC nanofluids exhibited higher energy gain than base fluid. Consequently, the efficiency of FPSC at 0.3% and 0.5% Al$_2$O$_3$ nanofluids was lower than base fluid but it was higher at 0.3% and 0.5% CNC nanofluids than base fluid. At 50°C temperature, energy gain increased at 0.3% Al$_2$O$_3$ nanofluid than the base fluid while it was still low for 0.5% Al$_2$O$_3$ nanofluid. The efficiency of FPSC also behaved similarly with energy gain. Alternatively, 0.3% and 0.5% CNC nanofluids exhibited higher energy gain and efficiency in both than base fluid. However, the energy gain and efficiency of FPSC have increased enough by 0.3% and 0.5% volume fraction nanofluids (both Al$_2$O$_3$ and CNC) at 70°C and 80°C temperature than the base fluid.

The energy gain and efficiency scenario of FPSC has been presented in Figure 4.34, and Figure 4.35. Figure 4.34 presents the gradual enhancement of energy gain of 0.3% Al$_2$O$_3$ and 0.5% Al$_2$O$_3$ nanofluids at a temperature range of 30°C to 80°C temperature; while 0.3% CNC and 0.5% CNC nanofluids do not exhibit the linearity of energy gain increment at the same temperature range. Both volume concentrations (0.3% and 0.5%) of CNC shows the decrement of energy gain at 50°C temperature. Moreover, the base fluid performs the discontinuation trend of energy gain in this system. In addition, Figure 4.35 illustrates the progressive enhancement of efficiency of Al$_2$O$_3$ nanofluids (both of 0.3% and 0.5% volume fractions) whereas CNC nanofluids at both volume concentrations and base fluid do not maintain the gradual improvement of efficiency of solar collector. Besides, the maximum efficiency of 2.48% and 8.46% achieved by 0.5% Al$_2$O$_3$ and 0.5% CNC at 80°C temperature respectively; while there is a big difference between these two values of efficiency. On the other hand, the base fluid shows a maximum efficiency of 1.17% at 50°C temperature.

Table 4.10   Resulting data of energy gain and efficiency of flat plate solar collector

Parameters	Energy gain, Q_u(kW)	Efficiency %
Base fluid at 30ºC	8.964	1.10
0.3% Al₂O₃ at 30ºC	2.376	0.29
0.5% Al₂O₃ at 30ºC	3.6936	0.46
0.3% CNC at 30ºC	25.8552	3.20
0.5% CNC at 30ºC	26.9568	3.33
Base fluid at 50ºC	9.504	1.17
0.3% Al₂O₃ at 50ºC	14.04	1.73
0.5% Al₂O₃ at 50ºC	7.7976	0.96
0.3% CNC at 50ºC	22.3668	2.76
0.5% CNC at 50ºC	24.7536	3.06
Base fluid at 70ºC	7.344	0.91
0.3% Al₂O₃ at 70ºC	19.44	2.40
0.5% Al₂O₃ at 70ºC	17.8524	2.21
0.3% CNC at 70ºC	29.1384	3.60
0.5% CNC at 70ºC	51.0624	6.31
Base fluid at 80ºC	5.724	0.71
0.3% Al₂O₃ at 80ºC	19.656	2.42
0.5% Al₂O₃ at 80ºC	20.1096	2.48
0.3% CNC at 80ºC	34.6788	4.28
0.5% CNC at 80ºC	68.5584	8.46
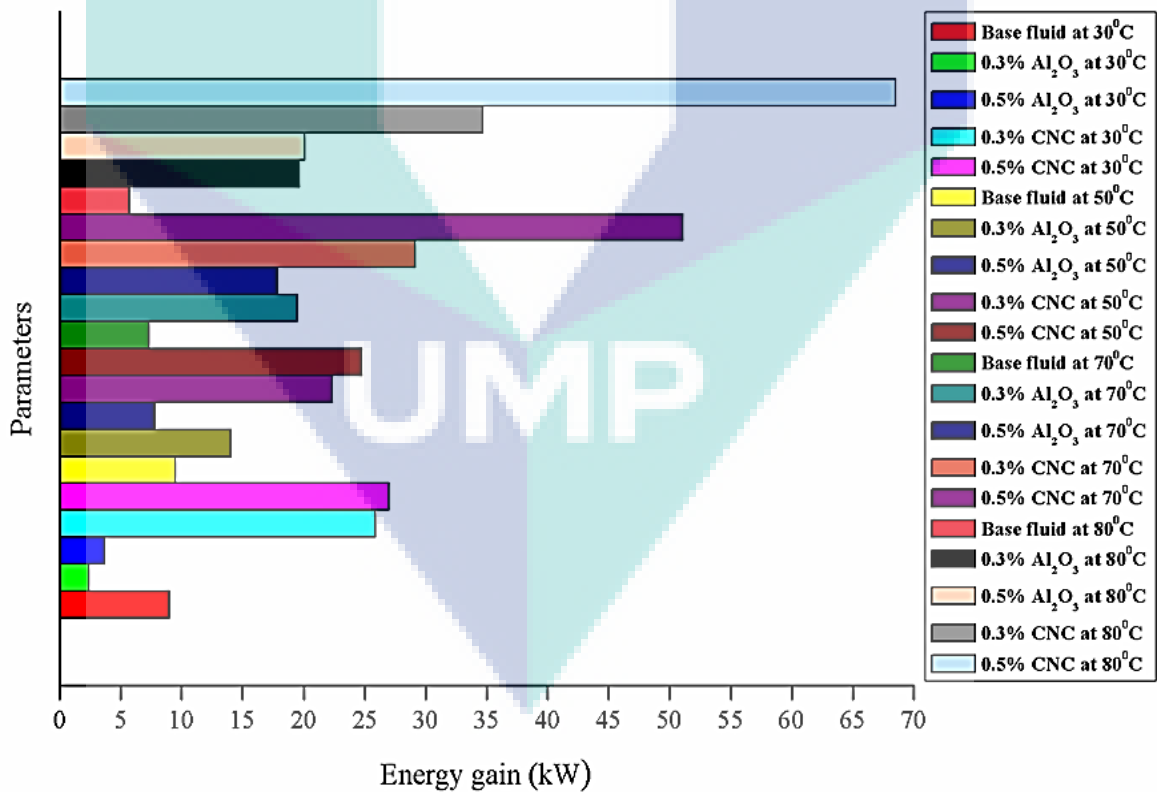
Figure 4.34   Energy gain of flat plate solar collector
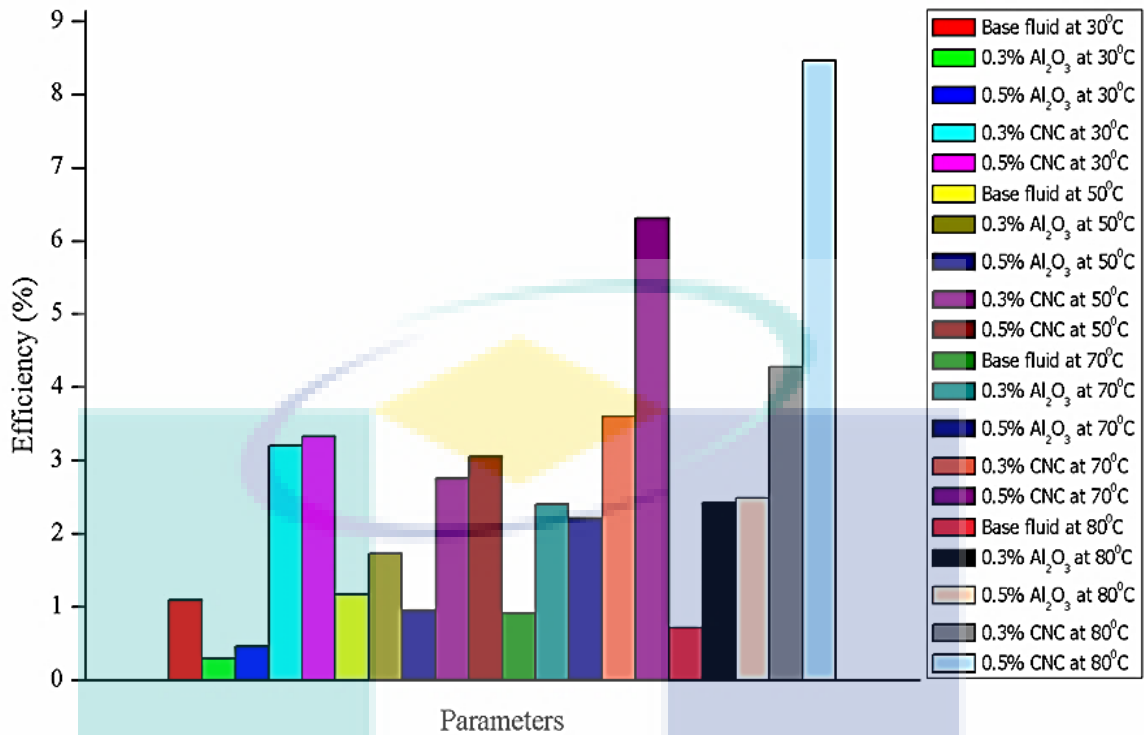
Figure 4.35   Improvement of efficiency of flat plate solar collector

The outlet temperature of nanofluid improved due to use the nanoparticles into the base fluid (Said et al., 2015). Nanoparticles enhance the thermal conductivity of the base fluid by the migration of it into base fluid owing to Brownian motion and shear action. Another way, nanoparticles can improve thermal conductivity by reducing the boundary layer thickness into the base fluid (Wen & Ding, 2004). The improved thermal conductivity causes the enhancement of heat transfer, as a result, the outlet temperature of FPSC improved. Not only that, when the temperature increased the thermal conductivity also increased resulting in higher outlet temperature. The energy gain equation showed that the energy gain is directly proportional to the mass flow rate. But the mass flow rate was fixed in this study. Therefore, energy gain depends on the specific heat and temperature differences and directly proportional to them. The energy gain calculated based on the different specific values at different temperatures of base fluid and nanofluids (Al_2O_3 and CNC) as shown in Table 4.8. However, the outlet temperature was fixed for the specific heat at different temperatures. The energy gain calculation revealed that higher the specific heat of base fluid and CNC nanofluids performed higher energy gain than the Al_2O_3 nanofluids in FPSC. The efficiency of FPSC increased according to the energy gain of FPSC. The maximum energy gain and efficiency achieved of FPSC when the value of specific heat considered at 80°C temperature. In this study,

the pH value of Al_2O_3 nanofluids was smaller which aided the nanofluids in the mobility enhancement in the suspension to improve the heat transfer process in FPSC. Besides, the pH of CNC nanofluids was higher which lead to enhance the efficiency of the system (Goudarzi et al., 2015).

In addition, the size and shape of nanoparticles influence on the thermal conductivity, heat transfer and efficiency of a system to a great extent (Suganthi & Rajan, 2017). Here the size of the Al_2O_3 nanoparticles was mostly below 80 nm and CNC nanoparticles were below 50 nm. Generally smaller sized nanoparticles improve the thermal conductivity of nanofluids resulting in enhanced heat transfer and efficiency. Moreover, Al_2O_3 nanoparticles were both in spherical and nearly spherical shaped in FESEM morphology (Figure 4.12). Both these shapes of Al_2O_3 nanoparticles have an impact on the thermal conductivity increment of nanofluids. Afterward, increased thermal conductivity dominates heat transfer (energy gain) and efficiency of FPSC. Furthermore, here both elongated and nearly spherical shaped CNC nanoparticles found in the TEM image (Figure 4.22) which influenced the thermal conductivity of nanofluids greatly as well as heat transfer and efficiency of the FPSC system.

Not only that but also stability has a great effect on thermal conductivity (Ganvir, Walke, & Kriplani, 2016). The stability of Al_2O_3 nanofluids especially 0.3% and 0.5% volume concentration were good in the quantitative method (Zeta potential). TEM micrograph (Figure 4.16) referred to the good dispersion of nanoparticles into the base fluid. These stable nanofluids improved the thermal conductivity of nanofluids occurring heat transfer enhancement and improved efficiency as stability is the primary requirement of nanofluids in the heat transfer application system. On the contrary, CNC nanofluids performed the initial stage of instability in the quantitative method (Zeta potential) and well-dispersed suspension in TEM morphology (Figure 4.23). Even though thermal conductivity improved but the temperature differences were less specifically at 0.5% volume concentration CNC nanofluid.

In this study, CNC nanoparticles used to enhance the efficiency of the FPSC system. Earlier any study did not be conducted with this nanoparticle for the efficiency enhancement of the FPSC system. Therefore, it was very difficult to compare the efficiency enhancement of FPSC with other studies. Many studies conducted with Al_2O_3 and other nanoparticles dispersed into water stated in Table 2.3 (Chapter 2) used for the

FPSC system to improve the efficiency previously (Said, Saidur, & Rahim, 2016; Verma, Tiwari, & Chauhan, 2016). Currently, there are a few studies conducted with a mixture of water and ethylene glycol (60: 40) as the base or working fluid for FPSC. This is due to the stability of nanoparticles in the water-EG mixture. Not all nanofluids stable in water/EG base fluid. It is different compared with water where nanoparticle easily stable specifically Al_2O_3 nanoparticles. A comparison illustration of efficiency enhancement of FPSC using Al_2O_3 and CNC nonfluids with the experimental study of Meibodi et al. (2015) prepared as shown in Table 4.11. The authors investigated the thermal efficiency of FPSC using SiO_2/water-EG nanofluids with 0%, 0.5%, 0.75% and 1% volume fraction of nanofluids at three mass flow rates including 0.018, 0.032, and 0.045 (kg/s). They concluded that the enhancement of the thermal efficiency of FPSC was 4 to 8% in maximum. Moreover, they remarked thermal efficiencies associated with the concentration of 0.75% and 1% were very close to compare with each other. The efficiency enhancement of FPSC using CNC/water-EG is higher than Al_2O_3/water-EG and SiO_2/water-EG nanofluids has been portrayed in Table 4.11. Even though the Al_2O_3 nanofluids exhibit lower efficiency enhancement, stability of Al_2O_3 nanofluids was good.

Table 4.11   Comparison of the efficiency of FPSC with a different research study

Nanofluids	Efficiency (%)	
	Experimental results	Meibodi et al. (2015)
CNC/water-EG	8.46	-
SiO_2/water-EG	-	8
Al_2O_3/water-EG	2.48	-

4.6   Analysis of Numerical Simulation for Fluid Behaviour

Several non-dimensional numbers such as Reynolds number, Nusselt number, and Prandtl number have been computed based on experimental data as well as the numerical data has been derived from CFD simulations. Numerical simulation performed based on actual experimental design, the experimental data of nanofluids and the actual boundary conditions of nanofluids. The geometry preparation, different steps of modelling such as edited geometry in designmodeler, meshing, setup (Viscous-Laminar method and physical properties) and solution calculation have been followed the same as the previous method.

4.6.1   Reynolds Number

Reynolds number depends on both viscosity and density of fluids (Reynolds, 1883). Here the viscosity of Al_2O_3 nanofluids (all volume concentrations) performed good behaviour with increased temperature. The decreasing trend of viscosity with respect to temperature is dissimilar with Reynolds number enhancement. The Reynolds number of 0.3% and 0.5% volume fraction of Al_2O_3 nanofluids increased with respect to temperature. But the base fluid and CNC nanofluids (0.3% and 0.5% volume fractions) upward trend of Reynolds number up to at 70^oC temperature, as the viscosity of these nanofluids, were in downward trend up to at 70^oC temperature. The viscosity of the base fluid and CNC nanofluids was higher at 80^oC temperature, thus Reynolds number was higher at this point of these fluids. In addition to this, the density of all Al_2O_3 and CNC (all volume fractions) was declining with the improvement of temperature. But the Reynolds number defining equation showed that higher the density higher the Reynolds number of fluids.
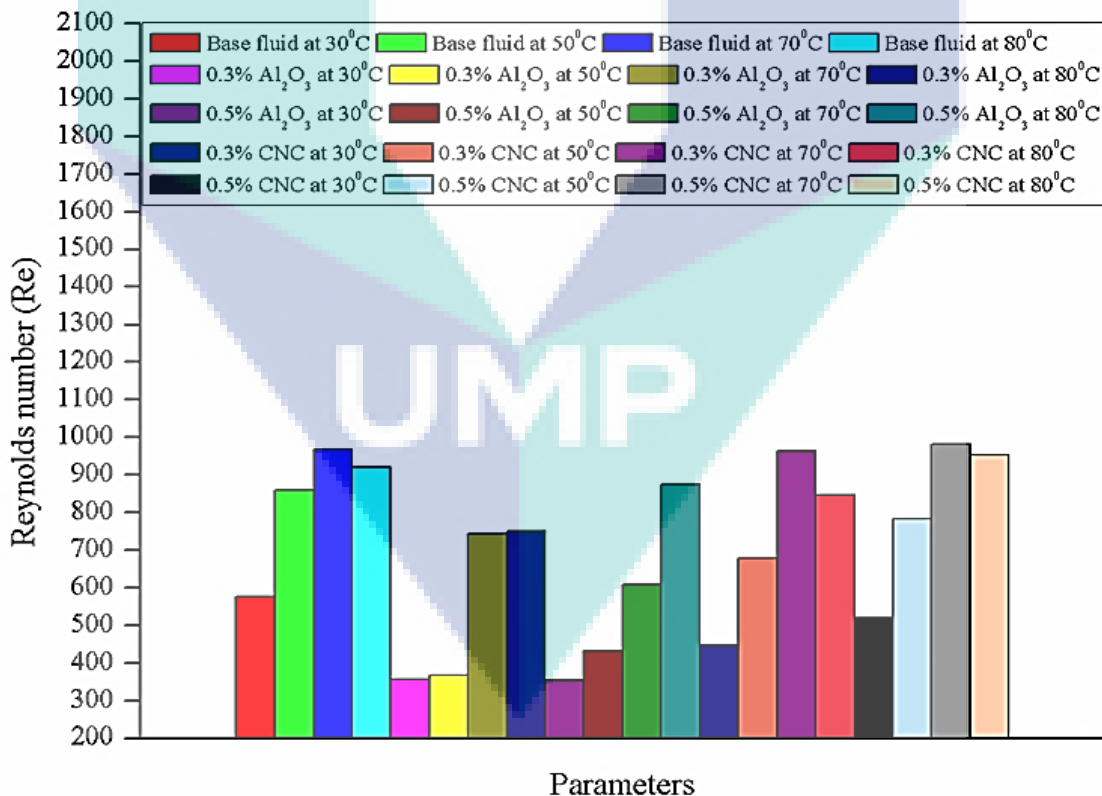
Figure 4.36   Reynolds number of the fluids

The calculative Reynolds number of the experimental fluids has been shown in Figure 4.36 and all of these values were below 2100 number which defines laminar flow behaviour of the experimental base fluid and nanofluids at different volume concentrations (Rodi, 2017). Figure 4.36 defined that the trend of Reynolds number was gradually rising for 0.3% and 0.5% Al_2O_3 nanofluids within a range of temperatures from 30°C to 80°C. Whereas the base fluid, 0.3% and 0.5% CNC nanofluids exhibited the increasing trend of Reynolds number until at 70°C temperature. Afterward, the trend of Reynolds number of these parameters was declining at 80°C temperature. Besides that, the higher temperature of all types of fluids showed a very higher Reynolds number value compared with the lower temperature.

4.6.2 Nusselt Number

The Nusselt number has been computed (Patankar, 2018) with the aid of Table 4.12. Surface temperature is a very important parameter to calculate the Nusselt number and the surface temperature of base fluids, 0.3% Al_2O_3, 0.5% Al_2O_3, 0.3% CNC and 0.5% CNC nanofluids measured during the experiment and presented in Figure 4.37, Figure 4.38, Figure 4.39, Figure 4.40, and Figure 4.41 respectively. The surface temperature of base fluids, 0.3% and 0.5% volume concentration of nanofluids (both Al_2O_3 and CNC) tabulated in Table 4.12 and averaged it. The average surface temperature of fluids was within a range of 46°C to 49°C temperature, while the maximum surface temperature recorded at 0.5% CNC nanofluid of about 48.58°C and the minimum was at 0.3% Al_2O_3 nanofluid around 46.66°C temperature.

Table 4.12   Surface temperature (°C) of nanofluids and base fluid

Base fluid	0.3% Al_2O_3	0.5% Al_2O_3	0.3% CNC	0.5% CNC
50.2°C	51.0°C	46.1°C	53.1°C	43.9°C
48.3°C	35.2°C	50.8°C	40.3°C	50.5°C
50.1°C	49.1°C	50.6°C	49.9°C	47.2°C
43.8°C	47.9°C	55.7°C	47.00C	39.7°C
43.4°C	45.0°C	41.6°C	51.0°C	51.7°C
50.7°C	52.2°C	42.3°C	43.4°C	50.5°C
51.4°C	43.7°C	43.2°C	53.1°C	53.4°C
42.6°C	49.5°C	54.6°C	45.3°C	39.7°C
45.6°C	46.2°C	47.3°C	41.6°C	48.9°C
47.5°C	46.8°C	52.5°C	51.2°C	48.1°C
Average	Average	Average	Average	Average
47.36°C	46.66°C	48.47°C	47.59°C	48.58°C

Table 4.13   Table of Nusselt number (Nu) of different fluids

Types of fluids	Temperature ($^{\circ}$C)	Nusselt number (Nu)
Base fluid	30°C	3.39
(W:EG 60:40)	50°C	3.18
	70°C	2.97
	80°C	3.04
0.3% Al_2O_3	30°C	5.50
	50°C	5.27
	70°C	4.65
	80°C	4.52
0.5% Al_2O_3	30°C	6.78
	50°C	6.66
	70°C	5.83
	80°C	5.60
0.3% CNC	30°C	8.98
	50°C	8.39
	70°C	7.50
	80°C	6.55
0.5% CNC	30°C	5.08
	50°C	4.24
	70°C	4.38
	80°C	3.97

The Nusselt number of base fluids, 0.3% and 0.5% volume fraction of nanofluids (both Al_2O_3 and CNC) presented in Table 4.13. The maximum Nusselt number of 0.3% and 0.5% volume concentration of nanofluids (both Al_2O_3 and CNC) obtained at 30°C and minimum achieved at 80°C temperature. The base fluid showed the highest Nusselt number at 30°C and the smallest at 70°C temperature. Figure 4.42 represents the phase of the Nusselt number during experimental work. Here, 0.3% Al_2O_3, 0.5% Al_2O_3, and 0.3% CNC nanofluids showed uninterrupted decreasing trend of Nusselt number from 30°C to 80°C temperature. On the other hand, 0.5% CNC nanofluid performed asymmetrical downward trend of Nusselt number within the equal range of temperature. Nusselt number of 0.5% CNC nanofluid was higher at 70°C temperature than at 50°C temperature. Besides, the trend of base fluid was declining up to 70°C temperature and it was in the upward direction at 80°C temperature. However, the experimental Nusselt number of these fluids (base fluid and nanofluids at various volume fractions) was greater than one. The higher Nusselt number (Nu>>1) depicts the more effective convection heat transfer of the fluids layer (Mostafazade Abolmaali & Afshin, 2019).
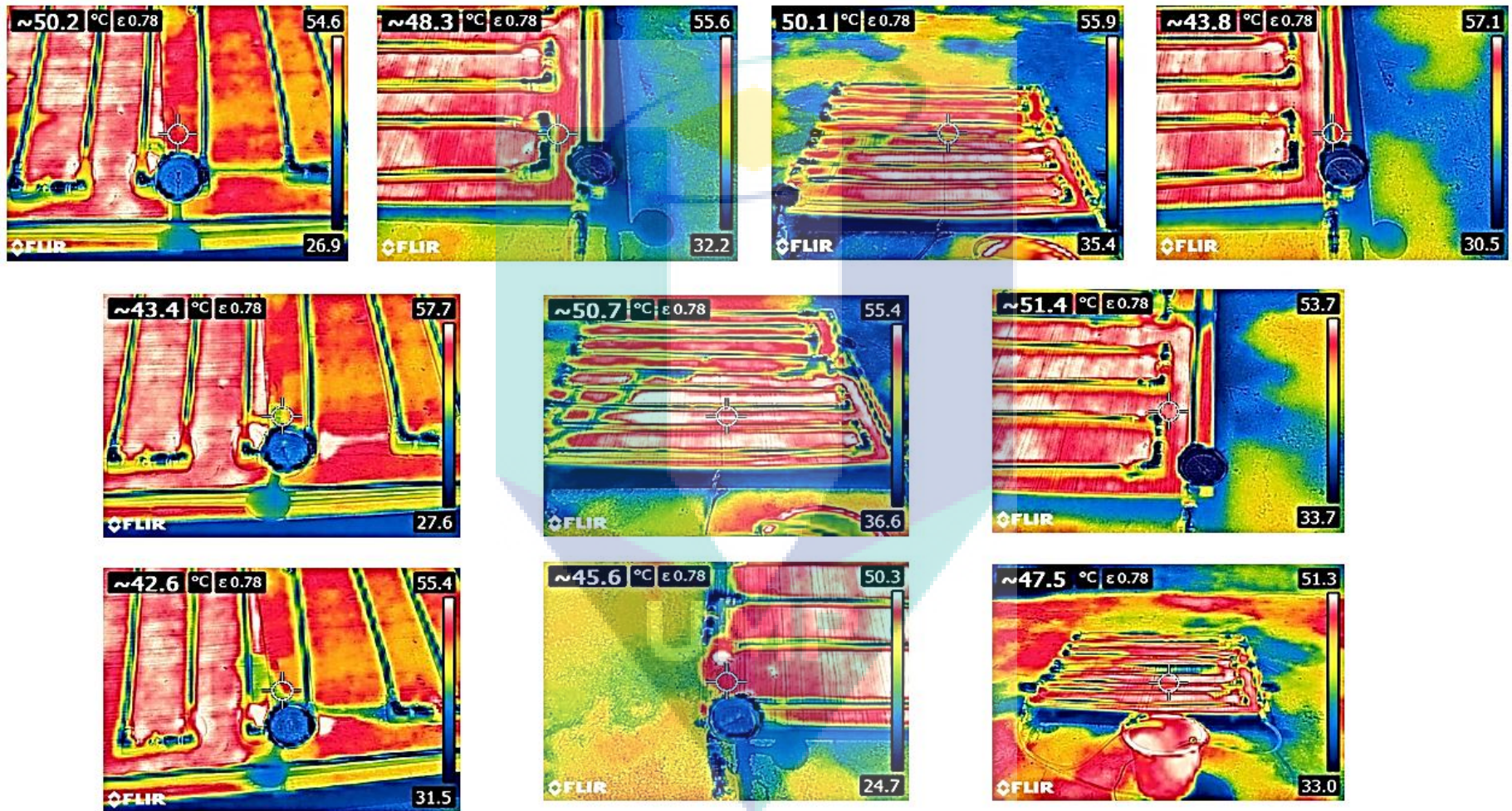
Figure 4.37   Thermal images of the surface temperature of the base fluid
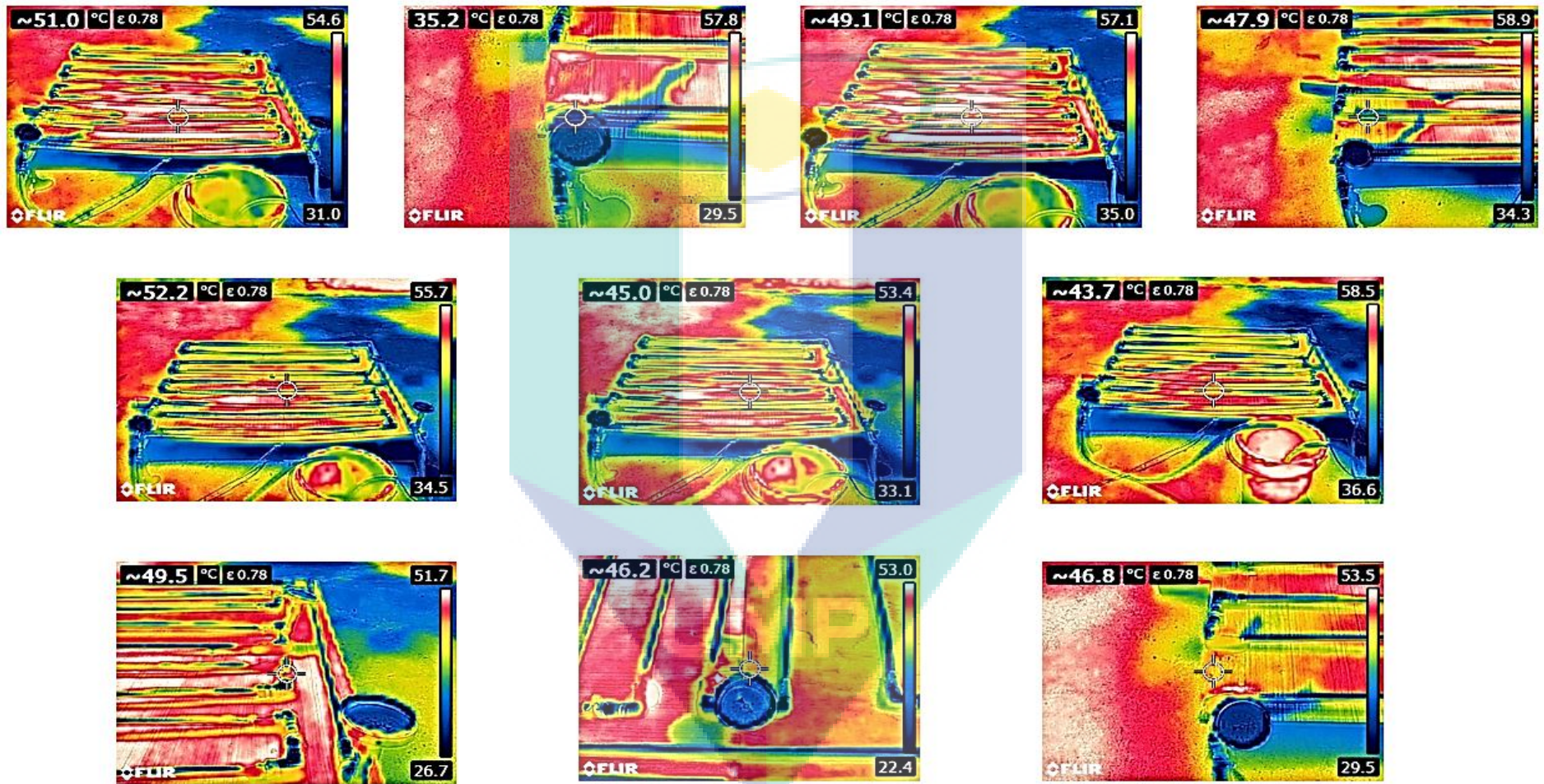
Figure 4.38   Thermal images of the surface temperature of 0.3% Al_2O_3 nanofluid
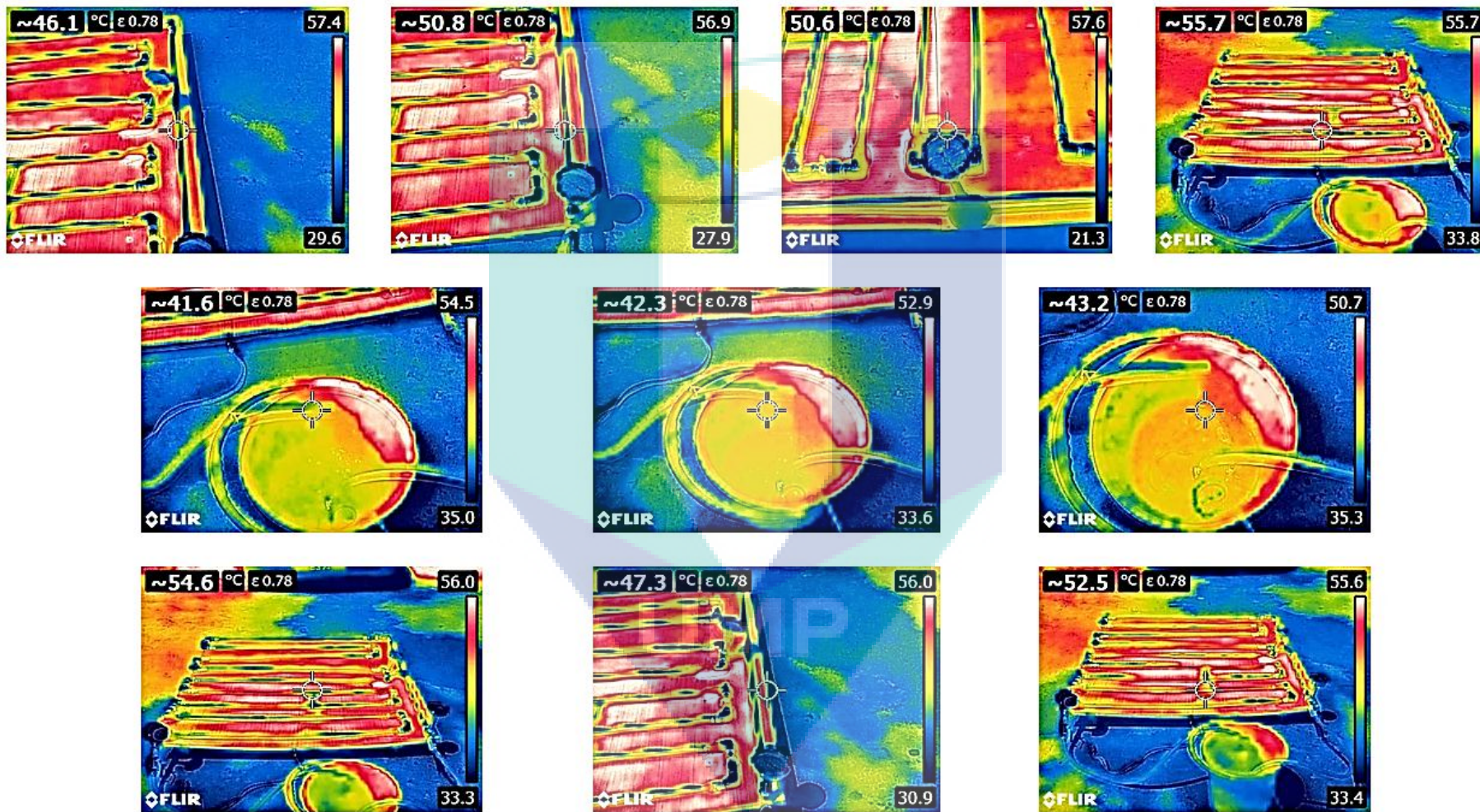
Figure 4.39   Thermal images of the surface temperature of 0.5% Al_2O_3 nanofluid
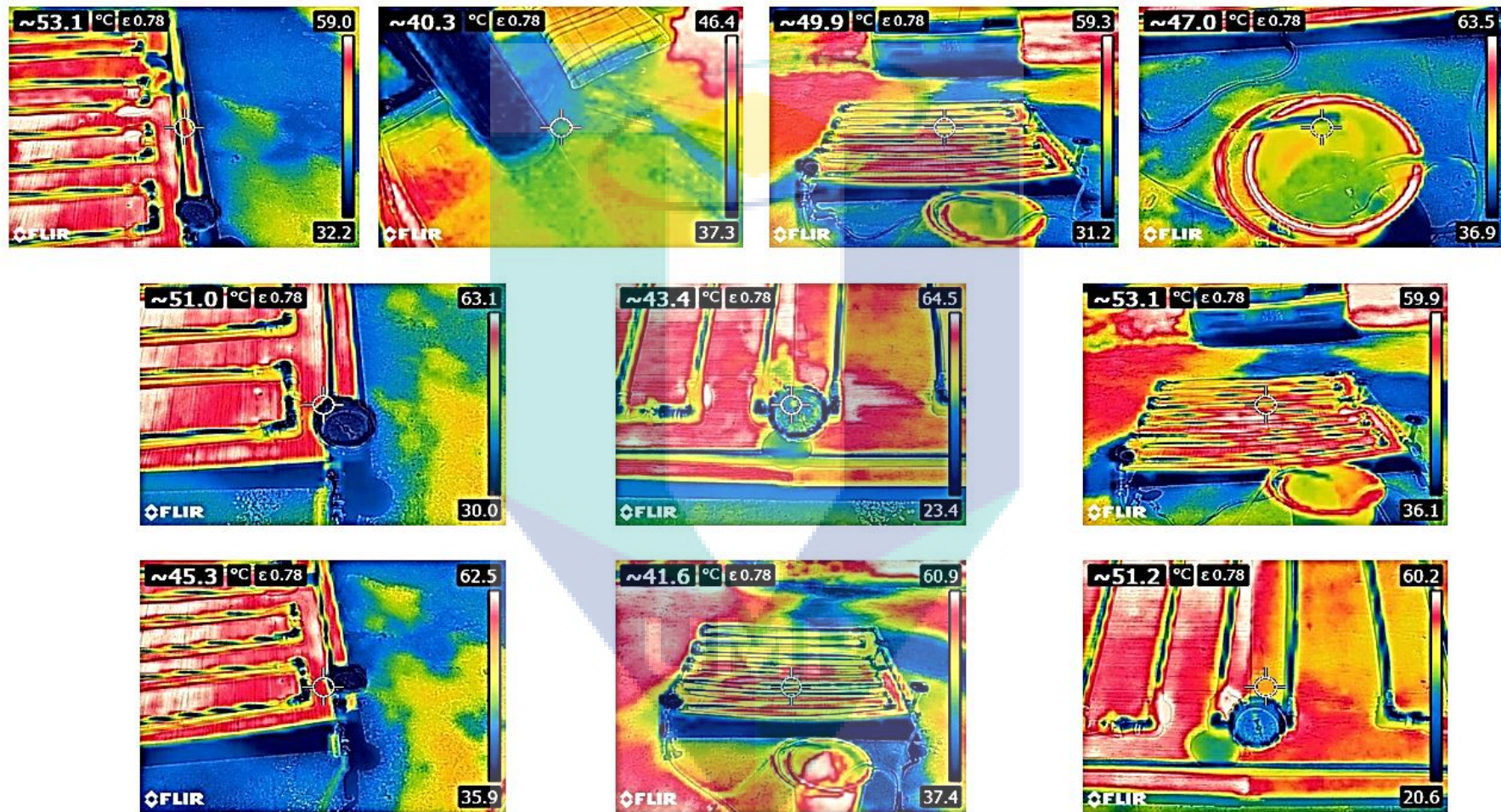
Figure 4.40   Thermal images of the surface temperature of 0.3% CNC nanofluid
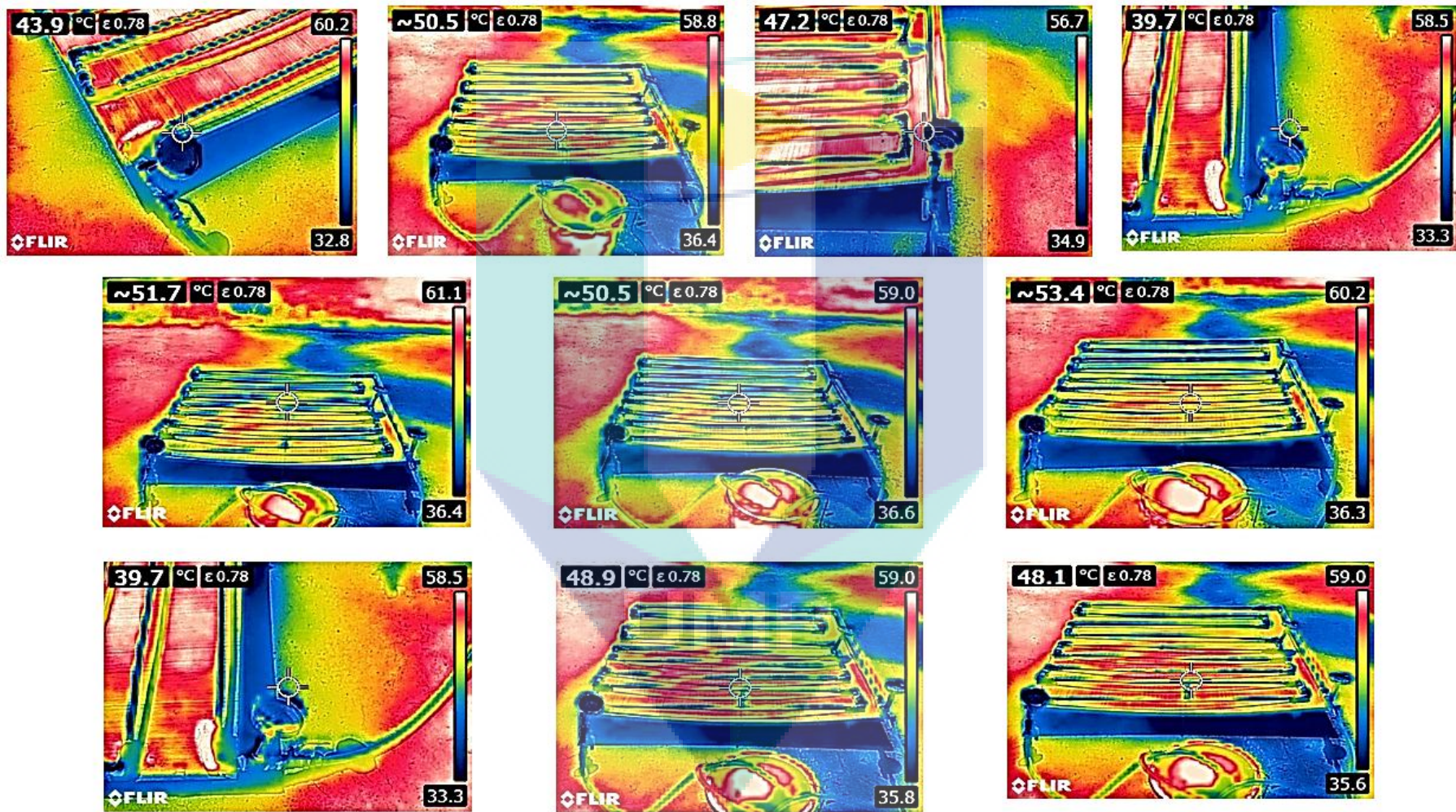
Figure 4.41   Thermal images of the surface temperature of 0.5% CNC nanofluid
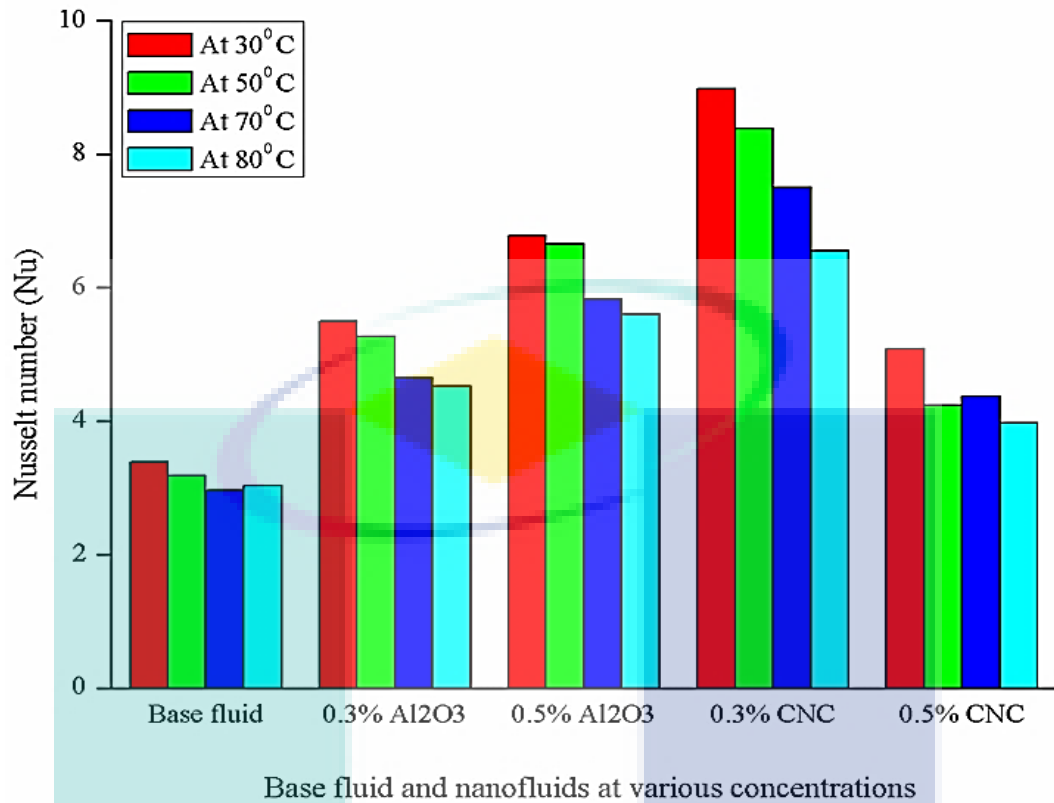
Figure 4.42   Nusselt number of the base fluid and nanofluids

4.6.3   Prandtl Number

The predicted and actual Prandtl number of the base fluid, 0.3% and 0.5% volume fraction of nanofluids (both Al_2O_3 and CNC) at a range of temperatures from $30^{\circ}C$ to $80^{\circ}C$ tabulated in Table 4.14. Prandtl number of both actual and predicted of all these fluids was higher than one (Pr>>1) at a temperature range of $30^{\circ}C$ to $80^{\circ}C$ except 0.3% Al_2O_3 nanofluid. The Prandtl number (both predicted and actual) of 0.3% Al_2O_3 nanofluid at $30^{\circ}C$ temperature was less than one (Pr<<1) as shown in Table 4.14. The greater Prandtl number determines the momentum diffusivity dominates the behaviour (Patankar, 2018). Besides, a large Prandtl number is responsible for quick heat diffusion in liquid metal. On the contrary, smaller Prandtl number defines that the heat diffuses rapidly compared to the momentum (velocity) which describes the thickness of the thermal boundary layer for the liquid metals is much higher than the velocity boundary layer (Raju, Nath, & Pati, 2018). Moreover, the resultant actual and predicted data depicts a very good agreement between them as shown in Figure 4.43.

Table 4.14   Table of Prandtl number (Pr) of fluids

Types of fluids	Temperature (ºC)	Prandtl number	
		Predicted	Actual
Base fluid	30ºC	4.24	4.24
(W:EG 60:40)	50ºC	2.70	2.70
	70ºC	1.70	1.70
	80ºC	1.41	1.42
0.3% Al_2O_3	30ºC	0.805	0.805
	50ºC	2.97	2.97
	70ºC	2.61	2.55
	80ºC	2.50	2.56
0.5% Al_2O_3	30ºC	1.29	1.29
	50ºC	2.18	2.18
	70ºC	3.06	3.06
	80ºC	2.26	2.62
0.3% CNC	30ºC	7.85	7.85
	50ºC	4.04	4.04
	70ºC	3.35	3.35
	80ºC	3.77	3.77
0.5% CNC	30ºC	11.31	11.31
	50ºC	5.67	5.68
	70ºC	9.53	9.53
	80ºC	11.79	11.79

Figure 4.43   Distribution of Prandtl number of fluids

4.7   Summary

In this chapter, the designing (arrangement) of header and riser tubes of flat plate solar collector specifically the influence of number and diameter of tubes has been evaluated; characterization of nanoparticles and nanofluids have been discussed; different thermo-physical properties of nanofluids such as, stability, thermal conductivity, viscosity, specific heat, density, and pH have been described; the energy gain and efficiency of FPSC have been analysed; and finally the predicted and experimental values of different non-dimensional numbers such as Reynolds number, Nusselt number, and Prandtl number have been computed and evaluated to identify the fluid behaviour. The next chapter covers the conclusion and recommendation of this research study.
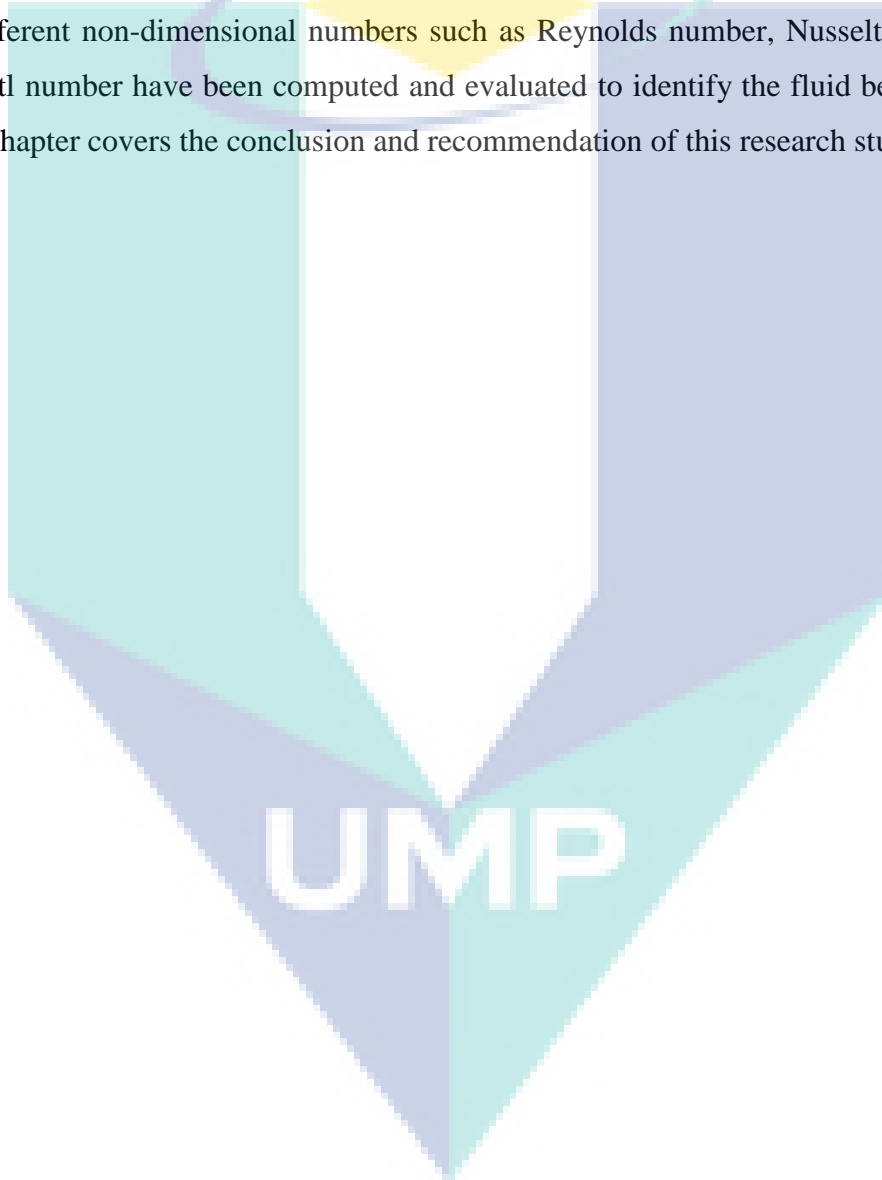
CHAPTER 5

CONCLUSION AND RECOMMENDATIONS

5.1   Conclusion

In this present study, the energy gain and the efficiency of flat plate solar collector enhanced by using Al_2O_3 and CNC nanofluids (at 0.3% and 0.5% volume concentrations of both nanofluids) flowing through inside the tubes (header and riser) under direct solar radiation. Nanofluids play the role of working fluids. Therefore, the works done throughout the study can be summarised and discussed as followings:

Objective 1: Designing of Flat Plate Solar Collector

Riser and header tubes are the most important parts of solar collectors which are fixed together to form a harp-shaped heat exchanger through them the working fluid can circulate. Different studies used diverse types of flat plate solar collector especially the diameter and number of the tubes. To obtain an optimum designing model (arrangement of header and riser tubes) of flat plate solar collector; simulation has been done and found that the number and diameter of the tubes (header and riser) do not affect the internal energy of flat plate solar collector. Internal energy only depends on the properties of the inside working fluids. Therefore, the design has been selected based on simulation statistical analysis. Optimum designing model is 8-23-12 which defines the number of riser tubes is 8; the diameter of the header is 23 mm while the diameter of the riser tube is 12 mm.

Objective 2: Evaluation of Thermo-physical Properties of Nanofluids

Nanoparticles (Al_2O_3 and CNC) have been procured and nanofluids were prepared by a two-step method at three different volume concentrations such as 0.1%, 0.3% and

0.5% followed by the ultrasonication process. The crystallinity of nanoparticles defined by XRD analysis. The particle morphology and size have been evaluated by FESEM and TEM; whereas elemental analysis done by FESEM EDX. Besides, molecular components and structures of nanofluids identified by FTIR. Afterward, different thermo-physical properties of Al_2O_3 and CNC nanofluids such as stability, thermal conductivity, viscosity, specific heat, density, and pH evaluated using different standard measurement methods and equipment.

The Al_2O_3 and CNC nanofluids (at 0.1%, 0.3%, and 0.5% volume concentrations) were stable evaluated by qualitative method. Whereas in the quantitative method, the zeta potential values of these nanofluids such as Al_2O_3 nanofluids at 0.3% and 0.5% volume concentrations exhibited good stability and 0.1% of Al_2O_3 nanofluid showed moderate performance. Besides, the absolute zeta potential values of CNC nanofluids (all volume concentrations) exhibited the initial stage of instability.

Thermal conductivity increased significantly due to loading nanoparticles into the base fluid. The augmentation of nanoparticles and the improvement in temperature increases thermal conductivity undoubtedly. Al_2O_3 nanofluids exhibited of about 13.4% maximum increment of thermal conductivity at 80°C temperature while CNC nanofluids performed maximum enhancement of thermal conductivity of 11.5% at 80°C temperature.

Dynamic viscosity increased owing to the adding of nanoparticles into the base fluid. Al_2O_3 nanofluids show the gradual enhancement of viscosity within an increment of loading nanoparticles into the base fluid. On the other hand, CNC nanofluids do not perform the progressive increment trend with an increase in volume concentrations. Dynamic viscosity increased by about 36% and 19% in maximum at 30°C temperature for Al_2O_3 and CNC nanofluids respectively. However, the dynamic viscosity of Al_2O_3 nanofluids at 0.1%, 0.3%, and 0.5% volume concentrations decreases with the raising of temperature and the lowest dynamic viscosity obtained at 80°C temperature; whereas CNC nanofluids (all volume concentrations) exhibit the lowest dynamic viscosity at 70° C temperature.

The specific heat capacity of Al_2O_3 nanofluids decreases with an augmentation of nanoparticles into the base fluid but it increases with the improvement of temperature. However, 0.1% volume concentration of Al_2O_3 nanofluid shows the highest specific heat

capacity at 70°C temperature. Moreover, 0.5% of Al_2O_3 nanofluid exhibits the negative specific heat at only at 30°C temperature. In the case of CNC nanofluids, specific heat capacity is negative for all volume concentrations of nanofluids. Though specific heat increases with increasing temperature, it declines at 50°C temperature for CNC nanofluids at all volume concentrations. The maximum specific heat was 5290 (J/kg-K) for CNC at 80°C temperature and minimum 110 (J/kg-K) for Al_2O_3 nanofluids at 30°C temperature respectively.

Al_2O_3 and CNC nanofluids (all volume concentrations) exhibit the decreasing trend of density with the improvement of temperature progressively. The density of nanofluids decreased at a maximum of 3.8% at 80°C temperature for Al_2O_3 nanofluid. In addition, Al_2O_3 nanofluids (all volume concentrations) exhibit acidic pH range whereas CNC nanofluids (all volume concentrations) perform slightly acidic to neutral in pH scale.

Objective 3: Thermal Performance of Flat Plate Solar Collector

Finally, experimental resulting data showed the maximum outlet temperature achieved by 0.5% volume concentration of Al_2O_3 nanofluid of about 45.1°C temperature. As a result, the energy gain and efficiency of flat plate solar collector improved too. However, nanofluids exhibit the distinctive value of specific heat capacity at individual temperature; therefore, distinct energy gain obtained of solar collector and efficiency of solar collector varied according to energy gain as well. The maximum efficiency of the flat plate solar collector obtained around 2.48% for 0.5% Al_2O_3 and 8.46% for 0.5% CNC nanofluid. Therefore, about 5.8% efficiency can be improved using CNC/water-EG nanofluid in a flat plate solar collector.

The behaviour of nanofluids has been evaluated by various non-dimensional numbers such as Reynolds number, Nusselt number, and Prandtl number. At first, the calculative data of Reynolds number revealed that the flows of all types of nanofluids were laminar. Secondly, the data of Nusselt number showed the more effective convection heat transfer of nanofluids and finally, the Prandtl number defined that the quicker heat diffusion occurred in liquid metal and the momentum diffusivity dominates the behaviour. Moreover, there was a very good agreement between the predicted and experimental data of the Prandtl number as well.

In conclusion, the efficiency of the optimum designed flat plate solar collector has been improved significantly by using ethylene glycol based inorganic (Al_2O_3) and organic (crystal nano-cellulose) nanofluids successively. Among these two nanoparticles organic (crystal nano-cellulose) shows much better thermal performance in flat plate solar collector with appropriate fluid behaviour; though both inorganic (Al_2O_3) and organic (crystal nano-cellulose) nanofluids exhibited a few inconsistent thermo-physical properties.

5.2 Recommendations

The numerical simulations and experimental work presented in this study have shown the efficiency improvement of the flat plate solar collector by using nanofluids. However, a variety of studies should be addressed in future work as follows:

1. A mixture of two or more nanofluids can be applied in solar collectors to investigate the thermal performance of it. In addition, newly invented synthetic nanoparticles can be applied to a solar collector to determine its performance. Besides, by changing the base fluid ratio or other base fluids can be considered too.

2. The accurate reason can find out for the increment of thermal conductivity and specific heat.

3. The experiment can be done under turbulent flow by selecting appropriate parameters.

4. The flow process can be evaluated under controlled heat flux.

5. The experiment can be performed with an absorber plate that is welded with header and riser tubes.

REFERENCES

Abbasi, S. M., Rashidi, A., Nemati, A., & Arzani, K. (2013). The effect of functionalisation method on the stability and the thermal conductivity of nanofluid hybrids of carbon nanotubes/gamma alumina. *Ceramics International, 39*(4), 3885-3891.

Abitbol, T., Rivkin, A., Cao, Y., et al. (2016). Nanocellulose, a tiny fiber with huge applications. *Current opinion in biotechnology, 39*, 76-88.

Adio, S. A., Sharifpur, M., & Meyer, J. P. (2015). Factors affecting the pH and electrical conductivity of MgO–ethylene glycol nanofluids. *Bulletin of Materials Science, 38*(5), 1345-1357.

Agarwal, R., Verma, K., Agrawal, N. K., Duchaniya, R. K., & Singh, R. (2016). Synthesis, characterization, thermal conductivity and sensitivity of CuO nanofluids. *Applied Thermal Engineering, 102*, 1024-1036.

Ahmed, F., Al Amin, A. Q., Hasanuzzaman, M., & Saidur, R. (2013). Alternative energy resources in Bangladesh and future prospect. *Renewable and Sustainable Energy Reviews, 25*, 698-707.

Akbar, N. S., & Mustafa, M. (2015). Ferromagnetic effects for nanofluid venture through composite permeable stenosed arteries with different nanosize particles. *AIP Advances, 5*(7), 077102.

Al-Abadleh, H. A., & Grassian, V. (2003). FT-IR study of water adsorption on aluminum oxide surfaces. *Langmuir, 19*(2), 341-347.

Alim, M., Abdin, Z., Saidur, R., et al. (2013). Analyses of entropy generation and pressure drop for a conventional flat plate solar collector using different types of metal oxide nanofluids. *Energy and Buildings, 66*, 289-296.

Alkaya, E., & Demirer, G. N. (2014). Sustainable textile production: a case study from a woven fabric manufacturing mill in Turkey. *Journal of Cleaner Production, 65*, 595-603.

Amrutkar, S. K., Ghodke, S., & Patil, K. (2012). Solar flat plate collector analysis. *IOSR Journal of Engineering, 2*(2), 207-213.

An, L., & Chen, R. (2016). Recent progress in alkaline direct ethylene glycol fuel cells for sustainable energy production. *Journal of Power Sources, 329*, 484-501.

Angayarkanni, S., & Philip, J. (2015). Review on thermal properties of nanofluids: recent developments. *Advances in colloid and interface science, 225*, 146-176.

Arıkan, E., Abbasoğlu, S., & Gazi, M. (2018). Experimental performance analysis of flat plate solar collectors using different nanofluids. *Sustainability, 10*(6), 1794.

Asadzadeh, F., Esfahany, M. N., & Etesami, N. (2012). Natural convective heat transfer of Fe_3O_4/ethylene glycol nanofluid in electric field. *International Journal of Thermal Sciences, 62*, 114-119.

Awang, N., Ramasamy, D., Kadirgama, K., et al. (2019). An experimental study on characterization and properties of nano lubricant containing Cellulose Nanocrystal (CNC). *International Journal of Heat and Mass Transfer, 130*, 1163-1169.

Azmi, W., Hamid, K. A., Usri, N., Mamat, R., & Mohamad, M. (2016). Heat transfer and friction factor of water and ethylene glycol mixture based TiO_2 and Al_2O_3 nanofluids under turbulent flow. *International Communications in Heat and Mass Transfer, 76*, 24-32.

Azmi, W., Sharma, K., Sarma, P., Mamat, R., & Najafi, G. (2014). Heat transfer and friction factor of water based TiO_2 and SiO_2 nanofluids under turbulent flow in a tube. *International Communications in Heat and Mass Transfer, 59*, 30-38.

Baghbanzadeh, M., Rashidi, A., Rashtchian, D., Lotfi, R., & Amrollahi, A. (2012). Synthesis of spherical silica/multiwall carbon nanotubes hybrid nanostructures and investigation of thermal conductivity of related nanofluids. *Thermochimica acta, 549*, 87-94.

Bagnold, R. A. (1954). Experiments on a gravity-free dispersion of large solid spheres in a Newtonian fluid under shear. *Proceedings of the Royal Society of London. Series A. Mathematical and Physical Sciences, 225*(1160), 49-63.

Bahrevar, M., Jahanfarnia, G., & Shayesteh, M. (2018). Thermal-hydraulic analysis of a novel design super critical water reactor with Al_2O_3 nanofluid as a coolant. *The Journal of Supercritical Fluids, 140*, 41-52.

Bai, L., Liu, Y., Ding, A., et al. (2019). Fabrication and characterization of thin-film composite (TFC) nanofiltration membranes incorporated with cellulose nanocrystals (CNCs) for enhanced desalination performance and dye removal. *Chemical Engineering Journal, 358*, 1519-1528.

Balamurugan, S., & Sajith, V. (2017). Experimental investigation on the stability and abrasive action of cerium oxide nanoparticles dispersed diesel. *Energy, 131*, 113-124.

Basavanna, S., & Shashishekar, K. (2013). CFD analysis of triangular absorber tube of a solar flat plate collector. *Int. J. Mech. Eng. & Rob. Res, 2*(1), 19-24.

Bashirnezhad, K., Bazri, S., Safaei, M. R., et al. (2016). Viscosity of nanofluids: a review of recent experimental studies. *International Communications in Heat and Mass Transfer, 73*, 114-123.

Baukal Jr, C. E., Gershtein, V., & Li, X. J. (2000). *Computational fluid dynamics in industrial combustion*: CRC press.

Bi, S.-s., Shi, L., & Zhang, L.-l. (2008). Application of nanoparticles in domestic refrigerators. *Applied Thermal Engineering, 28*(14), 1834-1843.

Blazek, J. (2015). Computational fluid dynamics: principles and applications: Butterworth-Heinemann.

BloombergNEF. (2019). Solar Investment Declined 24% in 2018, but Capacity Reached Record Levels.

Bubbico, R., Celata, G. P., D'Annibale, F., Mazzarotta, B., & Menale, C. (2015). Experimental analysis of corrosion and erosion phenomena on metal surfaces by nanofluids. *Chemical Engineering Research and Design, 104*, 605-614.

Bundesamt., S. (2014). Bruttostromerzeugung 2013.

Chandrasekar, M., Suresh, S., & Bose, A. C. (2010). Experimental investigations and theoretical determination of thermal conductivity and viscosity of Al_2O_3/water nanofluid. *Experimental Thermal and Fluid Science, 34*(2), 210-216.

Chang, H., Duan, C., Wen, K., et al. (2015). Modeling study on the thermal performance of a modified cavity receiver with glass window and secondary reflector. *Energy Conversion and Management, 106*, 1362-1369.

Chiam, H., Azmi, W., Usri, N., Mamat, R., & Adam, N. (2017). Thermal conductivity and viscosity of Al_2O_3 nanofluids for different based ratio of water and ethylene glycol mixture. *Experimental Thermal and Fluid Science, 81*, 420-429.

Choi, S. (1995). Development and applications of non-newtonian flows, Editors: DA Siginer, and HP Wang: ASME Publisher.

Chol, S. (1995). Enhancing thermal conductivity of fluids with nanoparticles. *ASME-Publications-Fed, 231*, 99-106.

Chougule, S. S., Pise, A. T., & Madane, P. A. (2012). *Performance of nanofluid-charged solar water heater by solar tracking system.* Paper presented at the Advances in Engineering, Science and Management (ICAESM), 2012 International Conference on.

Chougule, S. S., & Sahu, S. (2015). Heat transfer and friction characteristics of Al_2O_3/water and CNT/water nanofluids in transition flow using helical screw tape inserts–a comparative study. *Chemical Engineering and Processing: Process Intensification, 88*, 78-88.

Chu, S., Cui, Y., & Liu, N. (2017). The path towards sustainable energy. *Nature materials, 16*(1), 16.

Clas, S.-D., Dalton, C. R., & Hancock, B. C. (1999). Differential scanning calorimetry: applications in drug development. *Pharmaceutical science & technology today, 2*(8), 311-320.

Cruz-Peragon, F., Palomar, J., Casanova, P., Dorado, M., & Manzano-Agugliaro, F. (2012). Characterization of solar flat plate collectors. *Renewable and Sustainable Energy Reviews, 16*(3), 1709-1720.

Das, C., Gupta, S. D., & Mekjian, A. (2003). Negative specific heat in a thermodynamic model of multifragmentation. *Physical Review C, 68*(1), 014607.

Davidson, J. (2009). Nanofluid for cooling enhancement of electrical power equipment. *Department of Electrical Engineering: Vanderbilt*.

Davis, W. (1984). Hot-wire method for the measurement of the thermal conductivity of refractory materials. *Compendium of Thermophysical Property Measurement Methods., 1*, 231.

De Robertis, E., Cosme, E., Neves, R., et al. (2012). Application of the modulated temperature differential scanning calorimetry technique for the determination of the specific heat of copper nanofluids. *Applied Thermal Engineering, 41*, 10-17.

Delgado, Á. V., González-Caballero, F., Hunter, R., Koopal, L., & Lyklema, J. (2007). Measurement and interpretation of electrokinetic phenomena. *Journal of colloid and interface science, 309*(2), 194-224.

Demetzos, C. (2008). Differential scanning calorimetry (DSC): a tool to study the thermal behavior of lipid bilayers and liposomal stability. *Journal of liposome research, 18*(3), 159-173.

Dietz, K.-J., & Herth, S. (2011). Plant nanotoxicology. *Trends in plant science, 16*(11), 582-589.

Ding, Y., & Wen, D. (2005). Particle migration in a flow of nanoparticle suspensions. *Powder Technology, 149*(2-3), 84-92.

Drew, D. A., & Passman, S. L. (2006). *Theory of multicomponent fluids* (Vol. 135): Springer Science & Business Media.

Eastman, J., Choi, U., Li, S., Thompson, L., & Lee, S. (1996). *Enhanced thermal conductivity through the development of nanofluids.* Paper presented at the MRS proceedings.

Elcock, D. (2007). Potential impacts of nanotechnology on energy transmission applications and needs. Retrieved from

Eltaweel, M., & Abdel-Rehim, A. A. (2019). Energy and exergy analysis of a thermosiphon and forced-circulation flat-plate solar collector using MWCNT/Water nanofluid. *Case Studies in Thermal Engineering, 14*, 100416.

Esfahani, M. A., & Toghraie, D. (2017). Experimental investigation for developing a new model for the thermal conductivity of silica/water-ethylene glycol (40%−60%) nanofluid at different temperatures and solid volume fractions. *Journal of Molecular Liquids, 232*, 105-112.

Esfe, M. H., Arani, A. A. A., Rezaie, M., Yan, W.-M., & Karimipour, A. (2015). Experimental determination of thermal conductivity and dynamic viscosity of Ag–MgO/water hybrid nanofluid. *International Communications in Heat and Mass Transfer, 66*, 189-195.

Fan, M., You, S., Gao, X., et al. (2019). A comparative study on the performance of liquid flat-plate solar collector with a new V-corrugated absorber. *Energy Conversion and Management, 184*, 235-248.

Farajzadeh, E., Movahed, S., & Hosseini, R. (2018). Experimental and numerical investigations on the effect of Al_2O_3/TiO_2-H_2O nanofluids on thermal efficiency of the flat plate solar collector. *Renewable Energy, 118*, 122-130.

Farzaneh, H., Behzadmehr, A., Yaghoubi, M., Samimi, A., & Sarvari, S. (2016). Stability of nanofluids: Molecular dynamic approach and experimental study. *Energy Conversion and Management, 111*, 1-14.

Fernández-García, M., & Rodriguez, J. A. (2011). Metal oxide nanoparticles. *Encyclopedia of inorganic and bioinorganic chemistry*.

Feynman, R. P. (1960). There's plenty of room at the bottom. *Engineering and science, 23*(5), 22-36.

Feynman, R. P. (2011). There's plenty of room at the bottom. *Resonance-Heidelberg, 16*(9), 890.

Filipponi, L., Sutherland, D., & Center, I. N. (2010). Introduction to Nanoscience and Nanotechnologies. *NANOYOU Teachers Training Kit in Nanoscience and Nanotechnologies*, 1-29.

Ganvir, R., Walke, P., & Kriplani, V. (2016). Heat transfer characteristics in nanofluid— A review. *Renewable and Sustainable Energy Reviews*.

Gaos, Y. S., Yulianto, M., Juarsa, M., et al. (2017). The performance of solar collector CPC (compound parabolic concentrator) type with three pipes covered by glass tubes. Paper presented at the AIP Conference Proceedings.

Gertzos, K., Pnevmatikakis, S., & Caouris, Y. (2008). Experimental and numerical study of heat transfer phenomena, inside a flat-plate integrated collector storage solar water heater (ICSSWH), with indirect heat withdrawal. *Energy Conversion and Management, 49*(11), 3104-3115.

Ghaderian, J., & Sidik, N. A. C. (2017). An experimental investigation on the effect of Al_2O_3/distilled water nanofluid on the energy efficiency of evacuated tube solar collector. *International Journal of Heat and Mass Transfer, 108*, 972-987.

Ghaderian, J., Sidik, N. A. C., Kasaeian, A., et al. (2017). Performance of copper oxide/distilled water nanofluid in evacuated tube solar collector (ETSC) water heater with internal coil under thermosyphon system circulations. *Applied Thermal Engineering*, 520–536.

Ghadimi, A., & Metselaar, I. H. (2013). The influence of surfactant and ultrasonic processing on improvement of stability, thermal conductivity and viscosity of titania nanofluid. *Experimental Thermal and Fluid Science, 51*, 1-9.

Ghadimi, A., Saidur, R., & Metselaar, H. (2011). A review of nanofluid stability properties and characterization in stationary conditions. *International Journal of Heat and Mass Transfer, 54*(17), 4051-4068.

Ghanbarpour, M., Nikkam, N., Khodabandeh, R., & Toprak, M. S. (2015). Improvement of heat transfer characteristics of cylindrical heat pipe by using SiC nanofluids. *Applied Thermal Engineering, 90*, 127-135.

Ghorbani, B., Mehrpooya, M., & Sadeghzadeh, M. (2018). Developing a tri-generation system of power, heating, and freshwater (for an industrial town) by using solar flat plate collectors, multi-stage desalination unit, and Kalina power generation cycle. *Energy Conversion and Management, 165*, 113-126.

Gorji, T. B., & Ranjbar, A. (2016). A numerical and experimental investigation on the performance of a low-flux direct absorption solar collector (DASC) using graphite, magnetite and silver nanofluids. *Solar Energy, 135*, 493-505.

Gorji, T. B., & Ranjbar, A. (2017). Thermal and exergy optimization of a nanofluid-based direct absorption solar collector. *Renewable Energy, 106*, 274-287.

Goudarzi, K., Nejati, F., Shojaeizadeh, E., & Yousef-abad, S. A. (2015). Experimental study on the effect of pH variation of nanofluids on the thermal efficiency of a

solar collector with helical tube. *Experimental Thermal and Fluid Science, 60*, 20-27.

Gowda, R., Sun, H., Wang, P., et al. (2010). Effects of particle surface charge, species, concentration, and dispersion method on the thermal conductivity of nanofluids. *Advances in Mechanical Engineering, 2*, 807610.

Gunjo, D. G., Mahanta, P., & Robi, P. (2016). CFD and experimental investigation of flat plate solar water heating system under steady state condition. *Renewable Energy*.

Gunjo, D. G., Mahanta, P., & Robi, P. (2017). CFD and experimental investigation of flat plate solar water heating system under steady state condition. *Renewable Energy, 106*, 24-36.

Gupta, M., Singh, V., & Katyal, P. (2018). Synthesis and structural characterization of Al_2O_3 nanofluids. *Materials Today: Proceedings, 5*(14), 27989-27997.

Halabi, M. A., Al-Qattan, A., & Al-Otaibi, A. (2015). Application of solar energy in the oil industry—Current status and future prospects. *Renewable and Sustainable Energy Reviews, 43*, 296-314.

Hassan, M., Sadri, R., Ahmadi, G., et al. (2013). Numerical study of entropy generation in a flowing nanofluid used in micro-and minichannels. *Entropy, 15*(1), 144-155.

Hawwash, A., Rahman, A. K. A., Nada, S., & Ookawara, S. (2018). Numerical investigation and experimental verification of performance enhancement of flat plate solar collector using nanofluids. *Applied Thermal Engineering, 130*, 363-374.

Hayat, T., Muhammad, T., Alsaedi, A., & Alhuthali, M. (2015). Magnetohydrodynamic three-dimensional flow of viscoelastic nanofluid in the presence of nonlinear thermal radiation. *Journal of Magnetism and Magnetic Materials, 385*, 222-229.

He, Q., Wang, S., Zeng, S., & Zheng, Z. (2013). Experimental investigation on photothermal properties of nanofluids for direct absorption solar thermal energy systems. *Energy Conversion and Management, 73*, 150-157.

He, Q., Zeng, S., & Wang, S. (2015). Experimental investigation on the efficiency of flat-plate solar collectors with nanofluids. *Applied Thermal Engineering, 88*, 165-171.

Hossain, Z., Mustafa, G., Sakata, K., & Komatsu, S. (2016). Insights into the proteomic response of soybean towards Al_2O_3, ZnO, and Ag nanoparticles stress. *Journal of hazardous materials, 304*, 291-305.

Hottlel, H., & Whillier, A. *Evaluation of flat plate collector performance'.* Paper presented at the Transactions of the Conference on the Use of Solar Energy.

Huang, J., Wang, X., Long, Q., et al. (2009). *Influence of pH on the stability characteristics of nanofluids.* Paper presented at the Photonics and Optoelectronics, 2009. SOPO 2009. Symposium on.

Huang, Y.-W., Wu, C.-h., & Aronstam, R. S. (2010). Toxicity of transition metal oxide nanoparticles: recent insights from in vitro studies. *Materials, 3*(10), 4842-4859.

Hussein, A. K. (2016). Applications of nanotechnology to improve the performance of solar collectors–Recent advances and overview. *Renewable and Sustainable Energy Reviews, 62*, 767-792.

Ilyas, S. U., Pendyala, R., Narahari, M., & Susin, L. (2017). Stability, rheology and thermal analysis of functionalized alumina-thermal oil-based nanofluids for advanced cooling systems. *Energy Conversion and Management, 142*, 215-229.

International Renewable Energy Agency. (2017). Renewable energy investment.

Jabbari, F., Rajabpour, A., & Saedodin, S. (2017). Thermal conductivity and viscosity of nanofluids: a review of recent molecular dynamics studies. *Chemical Engineering Science, 174*, 67-81.

Jamil, M., Sidik, N. C., & Yazid, M. M. (2016). Thermal performance of thermosyphon evacuated tube solar collector using TiO_2/water nanofluid. *J. Adv. Res. Fluid Mech. Therm. Sci., 20*(1), 12-29.

Japan International Cooperation Agency. (2016). Survey on Power System Master Plan 2016, Tokyo Electric Power Company, Inc.

Jeong, J., Li, C., Kwon, Y., et al. (2013). Particle shape effect on the viscosity and thermal conductivity of ZnO nanofluids. *International Journal of Refrigeration, 36*(8), 2233-2241.

Jesko, Ž. (2008). Classification of solar collectors. *rN, 1*(21), 21.

Jia-Fei, Z., Zhong-Yang, L., Ming-Jiang, N., & Ke-Fa, C. (2009). Dependence of nanofluid viscosity on particle size and pH value. *Chinese Physics Letters, 26*(6), 066202.

Kadirgama, K., Anamalai, K., Ramachandran, K., et al. (2018). Thermal analysis of SUS 304 stainless steel using ethylene glycol/nanocellulose-based nanofluid coolant. *The International Journal of Advanced Manufacturing Technology, 97*(5-8), 2061-2076.

Kaggwa, A., Carson, J. K., Atkins, M., & Walmsley, M. (2019). The effect of surfactants on viscosity and stability of activated carbon, alumina and copper oxide nanofluids. *Materials Today: Proceedings, 18*, 510-519.

Kalogirou, S. A. (2013). Solar energy engineering: processes and systems: Academic Press.

Karunakaran, C., Anilkumar, P., & Gomathisankar, P. (2011). Photoproduction of iodine with nanoparticulate semiconductors and insulators. *Chemistry Central Journal, 5*(1), 31.

Kasaeian, A., Daneshazarian, R., & Pourfayaz, F. (2017). Comparative study of different nanofluids applied in a trough collector with glass-glass absorber tube. *Journal of Molecular Liquids*.

Kasaeian, A., Daviran, S., Azarian, R. D., & Rashidi, A. (2015). Performance evaluation and nanofluid using capability study of a solar parabolic trough collector. *Energy Conversion and Management, 89*, 368-375.

Khdher, A. M., Sidik, N. A. C., Hamzah, W. A. W., & Mamat, R. (2016). An experimental determination of thermal conductivity and electrical conductivity of bio glycol based Al_2O_3 nanofluids and development of new correlation. *International Communications in Heat and Mass Transfer, 73*, 75-83.

Khedkar, R. S., Sonawane, S. S., & Wasewar, K. L. (2012). Influence of CuO nanoparticles in enhancing the thermal conductivity of water and monoethylene glycol based nanofluids. *International Communications in Heat and Mass Transfer, 39*(5), 665-669.

Khurshid, M., & Anwar, W. (2013). Energy crisis and performance of industry of Pakistan: An empirical study of KSE listed companies.

Kim, H. J., Choi, S. M., Green, S., et al. (2011). Highly active and stable PtRuSn/C catalyst for electrooxidations of ethylene glycol and glycerol. *Applied Catalysis B: Environmental, 101*(3-4), 366-375.

Kim, K.-D., Lee, J.-B., & Kim, H. T. (2001). Synthesis of titanium dioxide nanoparticles by reversible reaction in semibatch-batch mixed method. *Journal of Industrial and Engineering Chemistry, 7*(3), 153-159.

Kim, K. (2008). High energy pulsed plasma arc synthesis and material characteristics of nanosized aluminum powder. *Metals and materials international, 14*(6), 707-711.

Kim, S., Tserengombo, B., Choi, S.-H., et al. (2019). Experimental investigation of heat transfer coefficient with Al_2O_3 nanofluid in small diameter tubes. *Applied Thermal Engineering, 146*, 346-355. doi:10.1016/j.applthermaleng.2018.10.001

Klevinskis, A., & Bucinskas, V. (2011). Analysis of a flat-plate solar collector. *Mokslas: Lietuvos Ateitis, 3*(6), 39.

Koca, H. D., Doganay, S., & Turgut, A. (2017). Thermal characteristics and performance of Ag-water nanofluid: Application to natural circulation loops. *Energy Conversion and Management, 135*, 9-20.

Koca, H. D., Doganay, S., Turgut, A., et al. (2018). Effect of particle size on the viscosity of nanofluids: A review. *Renewable and Sustainable Energy Reviews, 82*, 1664-1674.

Kodre, K., Attarde, S., Yendhe, P., Patil, R., & Barge, V. (2014). Differential scanning calorimetry: A review. *Research and Reviews: Journal of Pharmaceutical Analysis, 3*(3), 11-22.

Kole, M., & Dey, T. (2012). Thermophysical and pool boiling characteristics of ZnO-ethylene glycol nanofluids. *International Journal of Thermal Sciences, 62*, 61-70.

Kong, W., Perers, B., Fan, J., Furbo, S., & Bava, F. (2015). A new Laplace transformation method for dynamic testing of solar collectors. *Renewable Energy, 75*, 448-458.

Korada, V. S., & Hamid, N. H. (2017). Engineering Applications of Nanotechnology: From Energy to Drug Delivery: Springer.

Kumar, A., Negi, Y. S., Choudhary, V., & Bhardwaj, N. K. (2014). Characterization of cellulose nanocrystals produced by acid-hydrolysis from sugarcane bagasse as agro-waste. *Journal of Materials Physics and Chemistry, 2*(1), 1-8.

Kumar, D. D., & Arasu, A. V. (2017). A comprehensive review of preparation, characterization, properties and stability of hybrid nanofluids. *Renewable and Sustainable Energy Reviews*.

Kuno, M. K. (2005). Introduction to Nanoscience and Nanotechnology: A Workbook: faculty. ksu. edu. sa.

Lee, D., Kim, J.-W., & Kim, B. G. (2006). A new parameter to control heat transport in nanofluids: surface charge state of the particle in suspension. *The Journal of Physical Chemistry B, 110*(9), 4323-4328.

Lee, G.-J., Kim, C. K., Lee, M. K., et al. (2012). Thermal conductivity enhancement of ZnO nanofluid using a one-step physical method. *Thermochimica Acta, 542*, 24-27.

Lee, G. H., Park, J. H., Rhee, C. K., & Kim, W. W. (2003). Fabrication of Al nano powders by pulsed wire evaporation (PWE) method. *Journal of Industrial and Engineering Chemistry, 9*(1), 71-75.

Lee, J. H. (2009). Convection performance of nanofluids for electronics cooling: Stanford University.

Lee, P., Ishizaka, K., Suematsu, H., Jiang, W., & Yatsui, K. (2006). Magnetic and gas sensing property of nanosized $NiFe_2O_4$ powders synthesized by pulsed wire discharge. *Journal of Nanoparticle Research, 8*(1), 29.

Lei, W., Liu, D., Zhang, J., et al. (2009). Direct synthesis, growth mechanism, and optical properties of 3D AlN nanostructures with urchin shapes. *Crystal Growth and Design, 9*(3), 1489-1493.

Lelea, D., & Laza, I. (2014). The water based Al_2O_3 nanofluid flow and heat transfer in tangential microtube heat sink with multiple inlets. *International Journal of Heat and Mass Transfer, 69*, 264-275.

Li, X., Zhu, D., & Wang, X. (2009). Experimental investigation on viscosity of $Cu-H_2O$ nanofluids. *Journal of Wuhan University of Technology-Mater. Sci. Ed., 24*(1), 48-52.

Li, X., Zhu, D., Wang, X., et al. (2008). Thermal conductivity enhancement dependent pH and chemical surfactant for $Cu-H_2O$ nanofluids. *Thermochimica Acta, 469*(1), 98-103.

Li, X., Zou, C., Wang, T., & Lei, X. (2015). Rheological behavior of ethylene glycol-based SiC nanofluids. *International Journal of Heat and Mass Transfer, 84*, 925-930.

Li, Y., Tung, S., Schneider, E., & Xi, S. (2009). A review on development of nanofluid preparation and characterization. *Powder Technology, 196*(2), 89-101.

Lin, C.-Y., Wang, J.-C., & Chen, T.-C. (2011). Analysis of suspension and heat transfer characteristics of Al_2O_3 nanofluids prepared through ultrasonic vibration. *Applied Energy, 88*(12), 4527-4533.

Lingling, Z., Ding, Y., Povey, M., & York, D. (2008). ZnO nanofluids–A potential antibacterial agent. *Progress in Natural Science, 18*(8), 939-944.

Liu, X., Liu, H., Yu, X., Zhou, L., & Zhu, J. (2019). Solar thermal utilizations revived by advanced solar evaporation. *Current Opinion in Chemical Engineering, 25*, 26-34.

Liu, Y., Zhang, C. J., Zhao, J. C., et al. (2016). Bio-based barium alginate film: Preparation, flame retardancy and thermal degradation behavior. *Carbohydr Polym, 139*, 106-114. doi:10.1016/j.carbpol.2015.12.044

Longo, G. A., & Zilio, C. (2011). Experimental measurement of thermophysical properties of oxide–water nano-fluids down to ice-point. *Experimental Thermal and Fluid Science, 35*(7), 1313-1324.

Macosko, C. W., & Larson, R. G. (1994). Rheology: principles, measurements, and applications.

Madenci, E., & Guven, I. (2015). The finite element method and applications in engineering using ANSYS®: Springer.

Mahbubul, I., Saidur, R., & Amalina, M. (2013). Thermal conductivity, viscosity and density of R141b refrigerant based nanofluid. *Procedia Engineering, 56*, 310-315.

Mahbubul, I., Shahrul, I., Khaleduzzaman, S., et al. (2015). Experimental investigation on effect of ultrasonication duration on colloidal dispersion and thermophysical properties of alumina–water nanofluid. *International Journal of Heat and Mass Transfer, 88*, 73-81.

Mahendran, M., Lee, G. C., Sharma, K., & Shahrani, A. (2012). Performance evaluation of evacuated tube solar collector using water-based titanium oxide (TiO_2) nanofluid. *Journal of Mechanical Engineering and Sciences (JMES), 3*, 301-310.

Mahian, O., Kianifar, A., Kalogirou, S. A., Pop, I., & Wongwises, S. (2013). A review of the applications of nanofluids in solar energy. *International Journal of Heat and Mass Transfer, 57*(2), 582-594.

Mahian, O., Kianifar, A., & Wongwises, S. (2013). Dispersion of ZnO nanoparticles in a mixture of ethylene glycol–water, exploration of temperature-dependent density, and sensitivity analysis. *Journal of Cluster Science, 24*(4), 1103-1114.

Marsalek, R. (2014). Particle size and zeta potential of ZnO. *APCBEE procedia, 9*, 13-17.

Martinopoulos, G., Missirlis, D., Tsilingiridis, G., Yakinthos, K., & Kyriakis, N. (2010). CFD modeling of a polymer solar collector. *Renewable Energy, 35*(7), 1499-1508.

Mashaei, P. R., Shahryari, M., & Madani, S. (2016). Numerical hydrothermal analysis of water-Al_2O_3 nanofluid forced convection in a narrow annulus filled by porous medium considering variable properties. *Journal of Thermal Analysis and Calorimetry, 126*(2), 891-904. doi:10.1007/s10973-016-5550-3

Mazumder, Q. H. (2012). CFD analysis of single and multiphase flow characteristics in elbow. *Engineering, 4*(04), 210.

Meibodi, S. S., Kianifar, A., Niazmand, H., Mahian, O., & Wongwises, S. (2015). Experimental investigation on the thermal efficiency and performance characteristics of a flat plate solar collector using SiO_2/EG–water nanofluids. *International Communications in Heat and Mass Transfer, 65*, 71-75.

Mekhilef, S., Saidur, R., & Safari, A. (2011). A review on solar energy use in industries. *Renewable and Sustainable Energy Reviews, 15*(4), 1777-1790.

Melchior, T., Perkins, C., Weimer, A. W., & Steinfeld, A. (2008). A cavity-receiver containing a tubular absorber for high-temperature thermochemical processing using concentrated solar energy. *International Journal of Thermal Sciences, 47*(11), 1496-1503.

Moghadam, A. J., Farzane-Gord, M., Sajadi, M., & Hoseyn-Zadeh, M. (2014). Effects of CuO/water nanofluid on the efficiency of a flat-plate solar collector. *Experimental Thermal and Fluid Science, 58*, 9-14.

Mostafazade Abolmaali, A., & Afshin, H. (2019). Development of Nusselt number and friction factor correlations for the shell side of spiral-wound heat exchangers. *International Journal of Thermal Sciences, 139*, 105-117. doi:10.1016/j.ijthermalsci.2019.01.038

Muhammad, M. J., Muhammad, I. A., Che Sidik, N. A., & Muhammad Yazid, M. N. A. W. (2016). Thermal performance enhancement of flat-plate and evacuated tube solar collectors using nanofluid: A review. *International Communications in Heat and Mass Transfer, 76*, 6-15. doi:10.1016/j.icheatmasstransfer.2016.05.009

Mukherjee, S., & Paria, S. (2013). Preparation and stability of nanofluids-A Review. *IOSR Journal of Mechanical and civil engineering, 9*(2), 63-69.

Muneer, T., Asif, M., Cizmecioglu, Z., & Ozturk, H. (2008). Prospects for solar water heating within Turkish textile industry. *Renewable and Sustainable Energy Reviews, 12*(3), 807-823.

Muneer, T., Maubleu, S., & Asif, M. (2006). Prospects of solar water heating for textile industry in Pakistan. *Renewable and Sustainable Energy Reviews, 10*(1), 1-23.

Muraleedharan, M., Singh, H., Suresh, S., & Udayakumar, M. (2016). Directly absorbing Therminol-Al_2O_3 nano heat transfer fluid for linear solar concentrating collectors. *Solar Energy, 137*, 134-142.

Murshed, S., Leong, K., & Yang, C. (2008). Investigations of thermal conductivity and viscosity of nanofluids. *International Journal of Thermal Sciences, 47*(5), 560-568.

Murshed, S. S. (2012). Simultaneous measurement of thermal conductivity, thermal diffusivity, and specific heat of nanofluids. *Heat Transfer Engineering, 33*(8), 722-731.

Nadooshan, A. A., Eshgarf, H., & Afrand, M. (2018). Measuring the viscosity of Fe_3O_4-MWCNTs/EG hybrid nanofluid for evaluation of thermal efficiency: Newtonian and non-Newtonian behavior. *Journal of Molecular Liquids, 253*, 169-177.

Nagarajan, P., Subramani, J., Suyambazhahan, S., & Sathyamurthy, R. (2014). Nanofluids for solar collector applications: a review. *Energy Procedia, 61*, 2416-2434.

Namburu, P., Kulkarni, D., Dandekar, A., & Das, D. (2007). Experimental investigation of viscosity and specific heat of silicon dioxide nanofluids. *Micro & Nano Letters, 2*(3), 67-71.

Nasirov, S., & Agostini, C. A. (2018). Mining experts' perspectives on the determinants of solar technologies adoption in the Chilean mining industry. *Renewable and Sustainable Energy Reviews, 95*, 194-202.

Nguyen, C., Desgranges, F., Roy, G., et al. (2007). Temperature and particle-size dependent viscosity data for water-based nanofluids–hysteresis phenomenon. *International Journal of Heat and Fluid Flow, 28*(6), 1492-1506.

Nguyen, C. T., Desgranges, F., Galanis, N., et al. (2008). Viscosity data for Al_2O_3–water nanofluid—hysteresis: is heat transfer enhancement using nanofluids reliable? *International Journal of Thermal Sciences, 47*(2), 103-111. doi:10.1016/j.ijthermalsci.2007.01.033

Nikkam, N., Saleemi, M., Haghighi, E. B., et al. (2014). Fabrication, characterization and thermophysical property evaluation of SiC nanofluids for heat transfer applications. *Nano-Micro Letters, 6*(2), 178-189.

Noghrehabadi, A., Hajidavaloo, E., & Moravej, M. (2016). Experimental investigation of efficiency of square flat-plate solar collector using SiO_2/water nanofluid. *Case Studies in Thermal Engineering, 8*, 378-386.

Noor, M., Wandel, A. P., & Yusaf, T. (2013). *Detail guide for CFD on the simulation of biogas combustion in bluff-body mild burner.* Paper presented at the Proceedings of the 2nd International Conference of Mechanical Engineering Research (ICMER 2013).

O'Hanley, H., Buongiorno, J., McKrell, T., & Hu, L.-w. (2012). Measurement and model validation of nanofluid specific heat capacity with differential scanning calorimetry. *Advances in Mechanical Engineering, 4*, 181079.

O'neill, M. (1966). Measurement of specific heat functions by differential scanning calorimetry. *Analytical chemistry, 38*(10), 1331-1336.

Olia, H., Torabi, M., Bahiraei, M., et al. (2019). Application of nanofluids in thermal performance enhancement of parabolic trough solar collector: state-of-the-art. *Applied Sciences, 9*(3), 463.

OpenPR. (2019). Nanocellulose market is thriving worldwide with leading players like Sappi, Stora Enso, American Process Inc, FPInnovations, Kruger Inc.

Ozdil, N. F. T., Tantekin, A., & Erbay, Z. (2016). Energy and exergy analyses of a fluidized bed coal combustor steam plant in textile industry. *Fuel, 183*, 441-448.

Panchal, K. (2015). Nanofluid: A tool to increase the efficiency of solar collector. *International Journal for InnovativeEngineering and Technology, 5*(2), 350-366.

Park, S., Her, J., Cho, D., et al. (2012). Preparation of conductive nanoink using pulsed-wire-evaporated copper nanoparticles for inkjet printing. *Materials Transactions, 53*(8), 1502-1506.

Patankar, S. (2018). Numerical heat transfer and fluid flow: CRC press.

Paul, G., Chopkar, M., Manna, I., & Das, P. (2010). Techniques for measuring the thermal conductivity of nanofluids: a review. *Renewable and Sustainable Energy Reviews, 14*(7), 1913-1924.

Pazheri, F., Othman, M., & Malik, N. (2014). A review on global renewable electricity scenario. *Renewable and Sustainable Energy Reviews, 31*, 835-845.

Pointer, J. (2004). *Understanding accuracy and discretization error in an FEA model.* Paper presented at the ANSYS 7.1, 2004 Conference, Wooward Governor Company.

Pokropivny, V., Lohmus, R., Hussainova, I., Pokropivny, A., & Vlassov, S. (2007). *Introduction to nanomaterials and nanotechnology*: Tartu University Press Ukraine.

Pops, H. (1993). Importance of the conductor and control of its properties for magnet wire applications. *Wire Journal International, 26*, 66-66.

Pordanjani, A. H., Aghakhani, S., Afrand, M., et al. (2019). An updated review on application of nanofluids in heat exchangers for saving energy. *Energy Conversion and Management, 198*, 111886.

Pourmohamadian, H., Sheikhzadeh, G. A., Aghaei, A., Ehteram, H., & Adibi, M. (2019). Investigating the effect of brownian motion models on heat transfer and entropy generation in nanofluid forced convection. *Thermal Science, 23*(2).

Prajitno, D. H., & Syarif, D. G. (2014). *Corrosion of carbon steel in nanofluid containing ZrO₂ nanoparticle at different temperature.* Paper presented at the Advanced Materials Research.

Raju, B. H. S., Nath, D., & Pati, S. (2018). Effect of Prandtl number on thermo-fluidic transport characteristics for mixed convection past a sphere. *International Communications in Heat and Mass Transfer, 98*, 191-199.

Ramachandran, K., Hussein, A., Kadirgama, K., et al. (2017). Thermophysical properties measurement of nano cellulose in ethylene glycol/water. *Applied Thermal Engineering, 123*, 1158-1165.

Ramachandran, K., Kadirgama, K., Ramasamy, D., Azmi, W., & Tarlochan, F. (2017). Investigation on effective thermal conductivity and relative viscosity of cellulose nanocrystal as a nanofluidic thermal transport through a combined experimental–Statistical approach by using Response Surface Methodology. *Applied Thermal Engineering, 122*, 473-483.

Rance, G. A., Marsh, D. H., Bourne, S. J., Reade, T. J., & Khlobystov, A. N. (2010). van der Waals interactions between nanotubes and nanoparticles for controlled assembly of composite nanostructures. *ACS Nano, 4*(8), 4920-4928.

Ranjith, P., & Karim, A. A. (2016). A comparative study on the experimental and computational analysis of solar flat plate collector using an alternate working fluid. *Procedia Technology, 24*, 546-553.

Rashidi, M., Momoniat, E., Ferdows, M., & Basiriparsa, A. (2014). Lie group solution for free convective flow of a nanofluid past a chemically reacting horizontal plate in a porous media. *Mathematical Problems in Engineering, 2014*.

Rashin, M. N., & Hemalatha, J. (2014). A novel ultrasonic approach to determine thermal conductivity in CuO–ethylene glycol nanofluids. *Journal of Molecular Liquids, 197*, 257-262.

Ravisankar, R., Venkatachalapathy, V., Alagumurthy, N., & Thamizhmaran, K. (2014). A review on oxide and metallic form of nanoparticle in heat transfer. *International Journal of Engineering Science and Technology, 6*(3), 63.

Renewable Energy Policy Network. (2014). The first decade : 2004 – 2014:10 years of renewable energy progress; Renewable energy policy Network For the 21st Century, France.

Reynolds, O. (1883). XXIX. An experimental investigation of the circumstances which determine whether the motion of water shall he direct or sinuous, and of the law of resistance in parallel channels. *Philosophical Transactions of the Royal Society of London, 174*, 935-982.

Rezaei Gorjaei, A., & Shahidian, A. (2019). Heat transfer enhancement in a curved tube by using twisted tape insert and turbulent nanofluid flow. *Journal of Thermal Analysis and Calorimetry*. doi:10.1007/s10973-019-08013-1

Rodi, W. (2017). Turbulence models and their application in hydraulics: Routledge.

Ruzmaikin, A., & Byalko, A. (2015). On the relationship between atmospheric carbon dioxide and global temperature. *American Journal of Climate Change, 4*(03), 181.

Saadati, H., Hadad, K., & Rabiee, A. (2018). Safety margin and fuel cycle period enhancements of VVER-1000 nuclear reactor using water/silver nanofluid. *Nuclear Engineering and Technology, 50*(5), 639-647.

Sabiha, M., Saidur, R., Hassani, S., Said, Z., & Mekhilef, S. (2015). Energy performance of an evacuated tube solar collector using single walled carbon nanotubes nanofluids. *Energy Conversion and Management, 105*, 1377-1388.

Safari, M., Ghamari, M., & Nasiritosi, A. (2003). *Intake manifold optimization by using 3-D CFD analysis* (0148-7191). Retrieved from

Said, Z., Kamyar, A., & Saidur, R. (2013). *Experimental investigation on the stability and density of TiO_2, Al_2O_3, SiO_2 and $TiSiO_4$.* Paper presented at the IOP conference series: earth and environmental science.

Said, Z., Sabiha, M., Saidur, R., et al. (2015). Performance enhancement of a flat plate solar collector using titanium dioxide nanofluid and polyethylene glycol dispersant. *Journal of Cleaner Production, 92*, 343-353.

Said, Z., Saidur, R., & Rahim, N. (2016). Energy and exergy analysis of a flat plate solar collector using different sizes of aluminium oxide based nanofluid. *Journal of Cleaner Production, 133*, 518-530.

Said, Z., Saidur, R., Sabiha, M., Hepbasli, A., & Rahim, N. (2016). Energy and exergy efficiency of a flat plate solar collector using pH treated Al_2O_3 nanofluid. *Journal of Cleaner Production, 112*, 3915-3926.

Said, Z., Sajid, M., Alim, M., Saidur, R., & Rahim, N. (2013). Experimental investigation of the thermophysical properties of Al_2O_3-nanofluid and its effect on a flat plate solar collector. *International Communications in Heat and Mass Transfer, 48*, 99-107.

Sajid, M. U., & Ali, H. M. (2019). Recent advances in application of nanofluids in heat transfer devices: a critical review. *Renewable and Sustainable Energy Reviews, 103*, 556-592.

Samylingam, L., Anamalai, K., Kadirgama, K., et al. (2018). Thermal analysis of cellulose nanocrystal-ethylene glycol nanofluid coolant. *International Journal of Heat and Mass Transfer, 127*, 173-181.

Sarsam, W. S., Amiri, A., Kazi, S., & Badarudin, A. (2016). Stability and thermophysical properties of non-covalently functionalized graphene nanoplatelets nanofluids. *Energy Conversion and Management, 116*, 101-111.

Satti, J. R., Das, D. K., & Ray, D. (2016). Specific heat measurements of five different propylene glycol based nanofluids and development of a new correlation. *International Journal of Heat and Mass Transfer, 94*, 343-353.

Sekhar, Y. R., & Sharma, K. (2015). Study of viscosity and specific heat capacity characteristics of water-based Al_2O_3 nanofluids at low particle concentrations. *Journal of Experimental Nanoscience, 10*(2), 86-102.

Selmi, M., Al-Khawaja, M. J., & Marafia, A. (2008). Validation of CFD simulation for flat plate solar energy collector. *Renewable Energy, 33*(3), 383-387.

Serov, A., & Kwak, C. (2010). Recent achievements in direct ethylene glycol fuel cells (DEGFC). *Applied Catalysis B: Environmental, 97*(1-2), 1-12.

Shah, S. A. S., Syed, A. A. S. G., & Shaikh, F. M. (2013). Effects of wto on the textile industry on developing countries. *Revista Română de Statistică nr*, 61.

Sharifpur, M., Yousefi, S., & Meyer, J. P. (2016). A new model for density of nanofluids including nanolayer. *International Communications in Heat and Mass Transfer, 78*, 168-174.

Sharma, S., & Gupta, S. M. (2016). Preparation and evaluation of stable nanofluids for heat transfer application: a review. *Experimental Thermal and Fluid Science, 79*, 202-212.

Shoghl, S. N., Jamali, J., & Moraveji, M. K. (2016). Electrical conductivity, viscosity, and density of different nanofluids: an experimental study. *Experimental Thermal and Fluid Science, 74*, 339-346.

Shojaeizadeh, E., Veysi, F., Yousefi, T., & Davodi, F. (2014). An experimental investigation on the efficiency of a flat-plate solar collector with binary working fluid: A case study of propylene glycol (PG)–water. *Experimental Thermal and Fluid Science, 53*, 218-226.

Sidik, N. A. C., Adamu, I. M., Jamil, M. M., et al. (2016). Recent progress on hybrid nanofluids in heat transfer applications: a comprehensive review. *International Communications in Heat and Mass Transfer, 78*, 68-79.

Singh, R. K., Sharma, A. K., Dixit, A. R., Mandal, A., & Tiwari, A. K. (2017). Experimental investigation of thermal conductivity and specific heat of nanoparticles mixed cutting fluids. *Materials Today: Proceedings, 4*(8), 8587-8596.

Sivakumar, P., Christraj, W., Sridharan, M., & Jayamalathi, N. (2012). Performance improvement study of solar water heating system. *ARPN Journal of Engineering and Applied Sciences, 7*(1), 45-49.

Sivakumar, P., Raj, W. C., Malathi, N. J., & Balakrishnan, S. (2013). *Performance Analysis of Flat Plate Solar Water Heater by Changing the Heat Pipe Material.* Paper presented at the Advanced Materials Research.

Society, T. R. (2004). Nanoscience and nanotechnologies: opportunities and uncertainties; The Royal Society and the Royal Academy of engineering. 1-116.

Sorokes, J. M., Hardin, J., & Hutchinson, B. (2016). *A CFD Primer: What Do All Those Colors Really Mean?* Paper presented at the Proceedings of the 45th Turbomachinery Symposium.

Sridhara, V., Gowrishankar, B., Snehalatha, & Satapathy, L. (2009). Nanofluids—a new promising fluid for cooling. *Transactions of the Indian Ceramic Society, 68*(1), 1-17.

Stephen, E. N., Asirvatham, L. G., Kandasamy, R., Solomon, B., & Kondru, G. S. (2018). Heat transfer performance of a compact loop heat pipe with alumina and silver nanofluid. *Journal of Thermal Analysis and Calorimetry*, 1-12.

Struckmann, F. (2008). Analysis of a flat-plate solar collector (Report no. 2008MVK160). *Heat and Mass Transport.*

Suganthi, K., & Rajan, K. (2017). Metal oxide nanofluids: Review of formulation, thermo-physical properties, mechanisms, and heat transfer performance. *Renewable and Sustainable Energy Reviews, 76*, 226-255.

Suganthi, K., Vinodhan, V. L., & Rajan, K. (2014). Heat transfer performance and transport properties of ZnO–ethylene glycol and ZnO–ethylene glycol–water nanofluid coolants. *Applied Energy, 135*, 548-559.

Sun, B., Peng, C., Zuo, R., Yang, D., & Li, H. (2016). Investigation on the flow and convective heat transfer characteristics of nanofluids in the plate heat exchanger. *Experimental Thermal and Fluid Science, 76*, 75-86.

Sun, Z., Deluca, T., & Mattison, K. (2005). The size and rheology characterization of concentrated emulsions. *American laboratory, 37*(12), 8.

Sundar, L. S., Kirubeil, A., Punnaiah, V., Singh, M. K., & Sousa, A. C. (2018). Effectiveness analysis of solar flat plate collector with Al_2O_3 water nanofluids and with longitudinal strip inserts. *International Journal of Heat and Mass Transfer, 127*, 422-435.

Sundar, L. S., Ramana, E. V., Singh, M., & De Sousa, A. (2012). Viscosity of low volume concentrations of magnetic Fe_3O_4 nanoparticles dispersed in ethylene glycol and water mixture. *Chemical physics letters, 554*, 236-242.

Suresh, S., Selvakumar, P., Chandrasekar, M., & Raman, V. S. (2012). Experimental studies on heat transfer and friction factor characteristics of Al_2O_3/water nanofluid under turbulent flow with spiraled rod inserts. *Chemical Engineering and Processing: Process Intensification, 53*, 24-30.

Suresh, S., Venkitaraj, K., Selvakumar, P., & Chandrasekar, M. (2011). Synthesis of Al_2O_3–Cu/water hybrid nanofluids using two step method and its thermo physical properties. *Colloids and Surfaces A: Physicochemical and Engineering Aspects, 388*(1-3), 41-48.

Tabesh, S., Davar, F., & Loghman-Estarki, M. R. (2018). Preparation of γ-Al_2O_3 nanoparticles using modified sol-gel method and its use for the adsorption of lead and cadmium ions. *Journal of Alloys and Compounds, 730*, 441-449.

Taniguchi, N. (1974). *On the basic concept of nanotechnology.* Paper presented at the Proc. Intl. Conf. Prod. Eng. Tokyo, Part II, Japan Society of Precision Engineering.

Tawfik, M. M. (2017). Experimental studies of nanofluid thermal conductivity enhancement and applications: A review. *Renewable and Sustainable Energy Reviews, 75*, 1239-1253.

Teng, T.-P., & Hung, Y.-H. (2014). Estimation and experimental study of the density and specific heat for alumina nanofluid. *Journal of Experimental Nanoscience, 9*(7), 707-718.

Theivasanthi, T., Christma, F. A., Toyin, A. J., Gopinath, S. C., & Ravichandran, R. (2017). Synthesis and characterization of cotton fiber-based nanocellulose. *International journal of biological macromolecules*.

Tiwari, G., & Tiwari, A. (2017). *Handbook of Solar Energy*: Springer.

Tong, Y., Lee, H., Kang, W., & Cho, H. (2019). Energy and exergy comparison of a flat-plate solar collector using water, Al_2O_3 nanofluid, and CuO nanofluid. *Applied Thermal Engineering*, 113959.

Topnews. (2009). nanofluids-be-used-make-new-typescameras-microdevices-and-displays.

Trisaksri, V., & Wongwises, S. (2007). Critical review of heat transfer characteristics of nanofluids. *Renewable and Sustainable Energy Reviews, 11*(3), 512-523.

Turgut, A., Tavman, I., Chirtoc, M., et al. (2009). Thermal conductivity and viscosity measurements of water-based TiO_2 nanofluids. *International Journal of Thermophysics, 30*(4), 1213-1226.

Tyagi, H. (2008). Radiative and combustion properties of nanoparticle-laden liquids: Arizona State University.

Vadasz, P. (2010). Rendering the transient hot wire experimental method for thermal conductivity estimation to two-phase systems—theoretical leading order results. *Journal of Heat transfer, 132*(8), 081601.

Vajjha, R., Das, D., & Mahagaonkar, B. (2009). Density measurement of different nanofluids and their comparison with theory. *Petroleum Science and Technology, 27*(6), 612-624.

Vajjha, R. S., & Das, D. K. (2009). Experimental determination of thermal conductivity of three nanofluids and development of new correlations. *International Journal of Heat and Mass Transfer, 52*(21), 4675-4682.

Vajjha, R. S., & Das, D. K. (2012). A review and analysis on influence of temperature and concentration of nanofluids on thermophysical properties, heat transfer and pumping power. *International Journal of Heat and Mass Transfer, 55*(15-16), 4063-4078.

Vallejo, J., Pérez-Tavernier, J., Cabaleiro, D., Fernández-Seara, J., & Lugo, L. (2018). Potential heat transfer enhancement of functionalized graphene nanoplatelet dispersions in a propylene glycol-water mixture. Thermophysical profile. *The Journal of Chemical Thermodynamics, 123*, 174-184.

Vandsburger, L. (2009). Synthesis and covalent surface modification of carbon nanotubes for preparation of stabilized nanofluid suspensions. McGill University.

Verma, S. K., & Tiwari, A. K. (2015). Progress of nanofluid application in solar collectors: a review. *Energy Conversion and Management, 100*, 324-346.

Verma, S. K., Tiwari, A. K., & Chauhan, D. S. (2016). Performance augmentation in flat plate solar collector using MgO/water nanofluid. *Energy Conversion and Management, 124*, 607-617.

Verma, S. K., Tiwari, A. K., & Chauhan, D. S. (2017). Experimental evaluation of flat plate solar collector using nanofluids. *Energy Conversion and Management, 134*, 103-115.

Versteeg, H. K., & Malalasekera, W. (2007). An introduction to computational fluid dynamics: the finite volume method: Pearson Education.

Vezmar, S., Spajić, A., Topić, D., Šljivac, D., & Jozsa, L. (2014). Positive and negative impacts of renewable energy sources. *International Journal of Electrical and Computer Engineering Systems, 5*(2), 47-55.

Villar, N. M., López, J. C., Muñoz, F. D., García, E. R., & Andrés, A. C. (2009). Numerical 3-D heat flux simulations on flat plate solar collectors. *Solar Energy, 83*(7), 1086-1092.

Wamkam, C. T., Opoku, M. K., Hong, H., & Smith, P. (2011). Effects of pH on heat transfer nanofluids containing ZrO_2 and TiO_2 nanoparticles. *Journal of Applied Physics, 109*(2), 024305.

Wang, J. C., & Chiang, W. C. (2013). *Researches on thermo-electric properties of seawater and Al₂O₃ nanofluids.* Paper presented at the Applied Mechanics and Materials.

Wang, L., Chen, H., & Witharana, S. (2013). Rheology of nanofluids: a review. *Recent patents on nanotechnology, 7*(3), 232-246.

Wang, X.-j., & Zhu, D.-s. (2009). Investigation of pH and SDBS on enhancement of thermal conductivity in nanofluids. *Chemical physics letters, 470*(1-3), 107-111.

Wei, B., Zou, C., & Li, X. (2017). Experimental investigation on stability and thermal conductivity of diathermic oil based TiO₂ nanofluids. *International Journal of Heat and Mass Transfer, 104*, 537-543. doi:10.1016/j.ijheatmasstransfer.2016.08.078

Wei, B., Zou, C., Yuan, X., & Li, X. (2017). Thermo-physical property evaluation of diathermic oil based hybrid nanofluids for heat transfer applications. *International Journal of Heat and Mass Transfer, 107*, 281-287.

Wen, D., & Ding, Y. (2004). *Effect on heat transfer of particle migration in suspensions of nanoparticles flowing through minichannels.* Paper presented at the ASME 2004 2nd International Conference on Microchannels and Minichannels.

Wendt, J. F. (2008). *Computational fluid dynamics: an introduction*: Springer Science & Business Media.

Wenjing, C., Zou, C., & Li, X. (2017). An investigation into the thermophysical and optical properties of SiC/ionic liquid nanofluid for direct absorption solar collector. *Solar Energy Materials and Solar Cells, 163*, 157-163.

Xia, G., Liu, R., Wang, J., & Du, M. (2016). The characteristics of convective heat transfer in microchannel heat sinks using Al₂O₃ and TiO₂ nanofluids. *International Communications in Heat and Mass Transfer, 76*, 256-264.

Xian-Ju, W., & Xin-Fang, L. (2009). Influence of pH on nanofluids' viscosity and thermal conductivity. *Chinese Physics Letters, 26*(5), 056601.

Xiang-Qi, W., & Mujumdar, A. S. (2008). A review on nanofluids-part II: experiments and applications. *Brazilian Journal of Chemical Engineering, 25*(4), 631-648.

Xie, H., Wang, J., Xi, T., et al. (2002). Thermal conductivity enhancement of suspensions containing nanosized alumina particles. *Journal of Applied Physics, 91*(7), 4568-4572.

Xu, J., Bandyopadhyay, K., & Jung, D. (2016). Experimental investigation on the correlation between nano-fluid characteristics and thermal properties of Al₂O₃

nano-particles dispersed in ethylene glycol–water mixture. *International Journal of Heat and Mass Transfer, 94*, 262-268.

Xu, R. (2008). Progress in nanoparticles characterization: Sizing and zeta potential measurement. *Particuology, 6*(2), 112-115.

Yapici, K., Cakmak, N. K., Ilhan, N., & Uludag, Y. (2014). Rheological characterization of polyethylene glycol based TiO_2 nanofluids. *Korea-Australia Rheology Journal, 26*(4), 355-363.

Yılmaz, İ. H., & Söylemez, M. S. (2014). Thermo-mathematical modeling of parabolic trough collector. *Energy Conversion and Management, 88*, 768-784.

Yousefi, T., Shojaeizadeh, E., Veysi, F., & Zinadini, S. (2012). An experimental investigation on the effect of pH variation of $MWCNT–H_2O$ nanofluid on the efficiency of a flat-plate solar collector. *Solar Energy, 86*(2), 771-779.

Yousefi, T., Veisy, F., Shojaeizadeh, E., & Zinadini, S. (2012). An experimental investigation on the effect of $MWCNT-H_2O$ nanofluid on the efficiency of flat-plate solar collectors. *Experimental Thermal and Fluid Science, 39*, 207-212.

Yu, H., Hermann, S., Schulz, S. E., et al. (2012). Optimizing sonication parameters for dispersion of single-walled carbon nanotubes. *Chemical Physics, 408*, 11-16.

Yu, W., France, D. M., Choi, S. U., & Routbort, J. L. (2007). Review and assessment of nanofluid technology for transportation and other applications. Retrieved from

Yu, W., & Xie, H. (2012). A review on nanofluids: preparation, stability mechanisms, and applications. *Journal of Nanomaterials, 2012*, 1.

Yue, H., Zhao, Y., Ma, X., & Gong, J. (2012). Ethylene glycol: properties, synthesis, and applications. *Chemical Society Reviews, 41*(11), 4218-4244.

Zakomirnyi, V., Rasskazov, I., Gerasimov, V., et al. (2018). Titanium nitride nanoparticles as an alternative platform for plasmonic waveguides in the visible and telecommunication wavelength ranges. *Photonics and Nanostructures-Fundamentals and Applications, 30*, 50-56.

Zaman, K., & Abd-el Moemen, M. (2017). Energy consumption, carbon dioxide emissions and economic development: Evaluating alternative and plausible environmental hypothesis for sustainable growth. *Renewable and Sustainable Energy Reviews, 74*, 1119-1130.

Zawrah, M., Khattab, R., Girgis, L., El Daidamony, H., & Aziz, R. E. A. (2016). Stability and electrical conductivity of water-base Al_2O_3 nanofluids for different applications. *HBRC Journal, 12*(3), 227-234.

Zayed, M., Zhao, J., Du, Y., Kabeel, A., & Shalaby, S. (2019). Factors affecting the thermal performance of the flat plate solar collector using nanofluids: A review. *Solar Energy, 182*, 382-396.

Zhang, H., Zhai, C., Gao, H., Fu, N., & Zhu, M. (2019). Highly efficient ethylene glycol electrocatalytic oxidation based on bimetallic PtNi on 2D molybdenum disulfide/reduced graphene oxide nanosheets. *Journal of colloid and interface science, 547*, 102-110.

Zhang, X., Liu, X., Dong, W., et al. (2018). Corrosion behaviors of 5A06 aluminum alloy in ethylene glycol. *INTERNATIONAL JOURNAL OF ELECTROCHEMICAL SCIENCE, 13*(11), 10470-10479.

Zhou, S.-Q., & Ni, R. (2008). Measurement of the specific heat capacity of water-based Al_2O_3 nanofluid. *Applied Physics Letters, 92*(9), 093123.
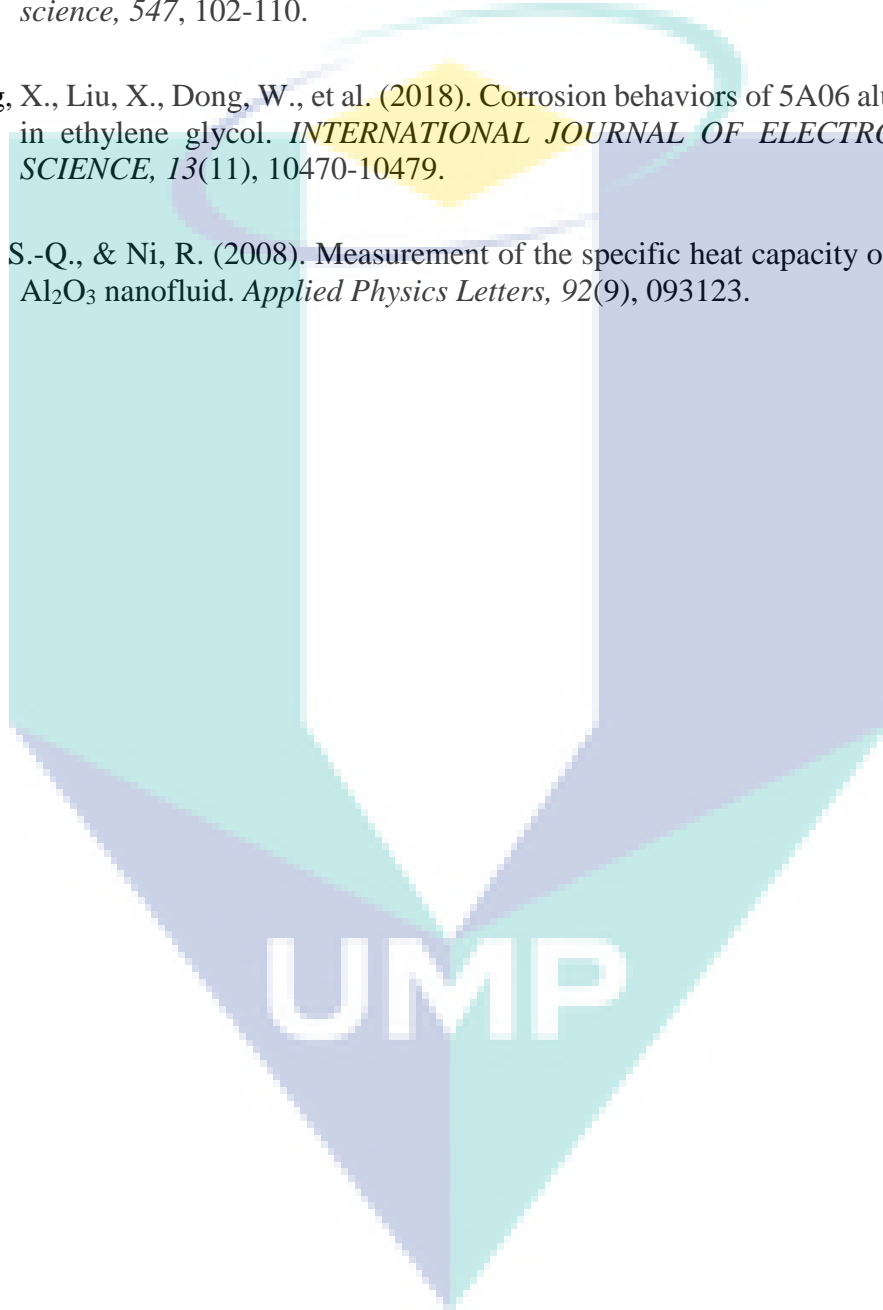
Construction of experimental setup

FLIR thermographic camera

Preparation of experimental work
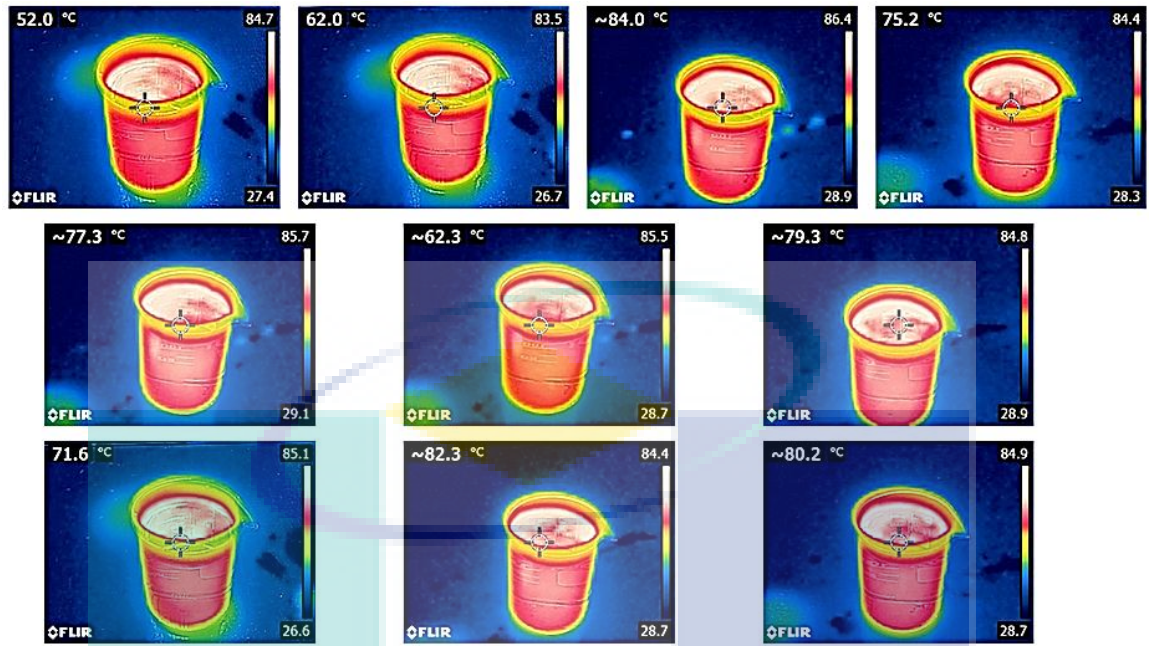
Images of calibration of thermal camera with hot water

APPENDIX B
IMAGES OF EQUIPMENT AND FLUID BEHAVIOUR

IMAGES OF EQUIPMENT OF CHARACTERIZATION

FTIR equipment of UMP (CARIFF)
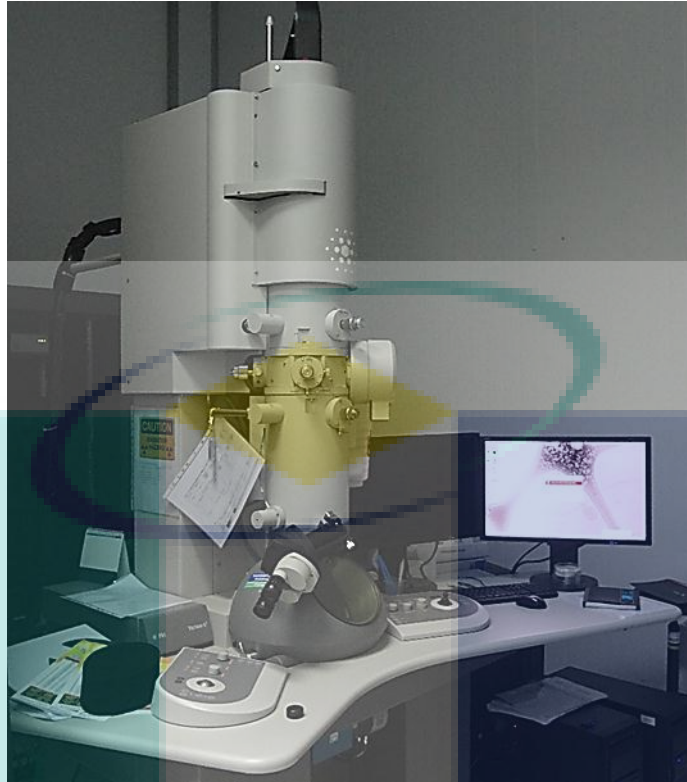
TEM equipment of UMP (CARIFF)

FESEM and FESEM-EDX equipment of UMP (Central Lab)

GRAPHICAL PRESENTATION OF VISCOSITY BEHAVIOUR OF NANOFLUIDS
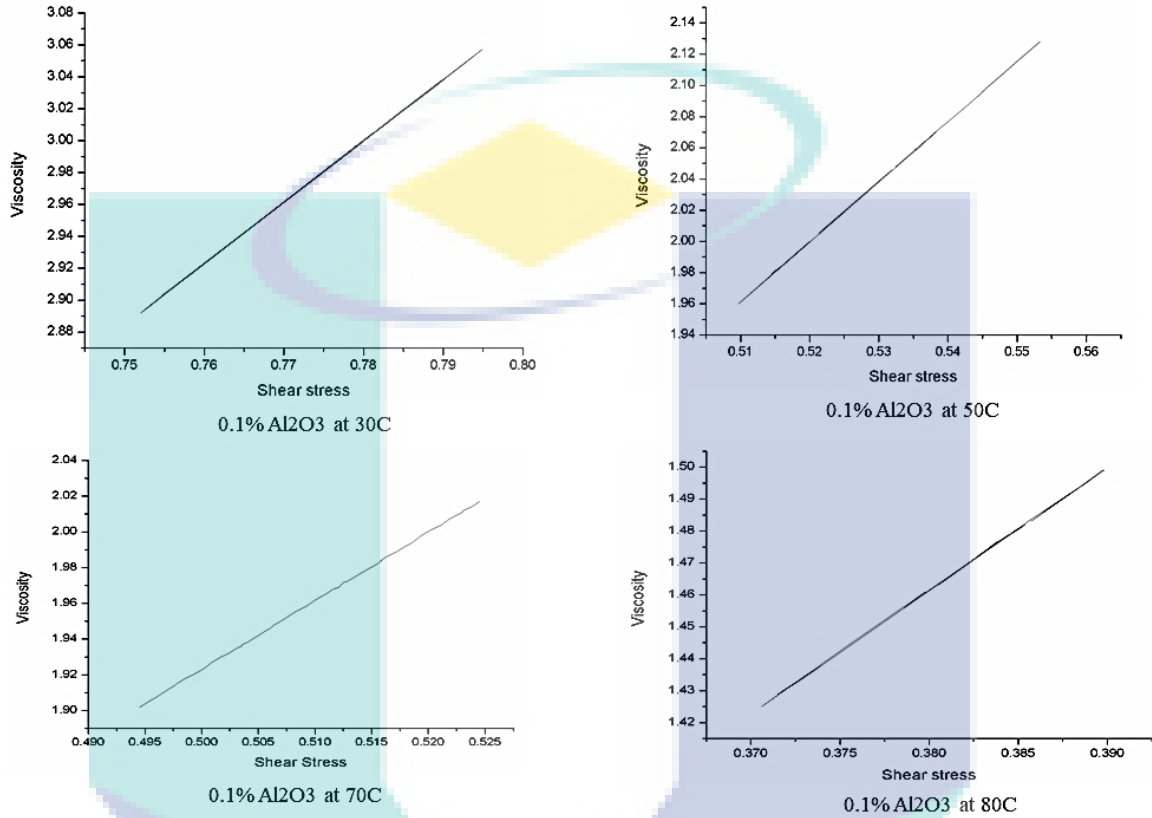
Viscosity behaviour of 0.1% Al_2O_3 nanofluid

0.3% Al2O3 at 30C

0.3% Al2O3 at 50C

0.3% Al2O3 at 70C

0.3% Al2O3 at 80C
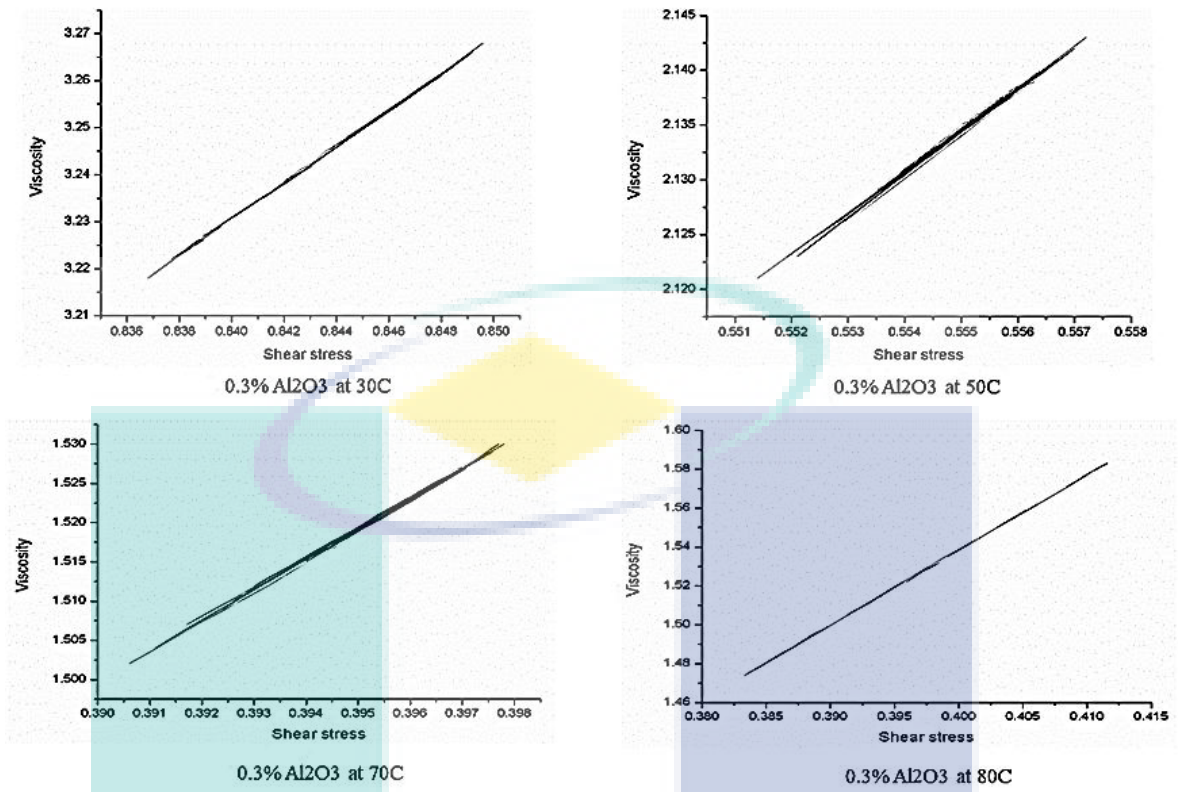
Viscosity behaviour of 0.3% Al_2O_3 nanofluid
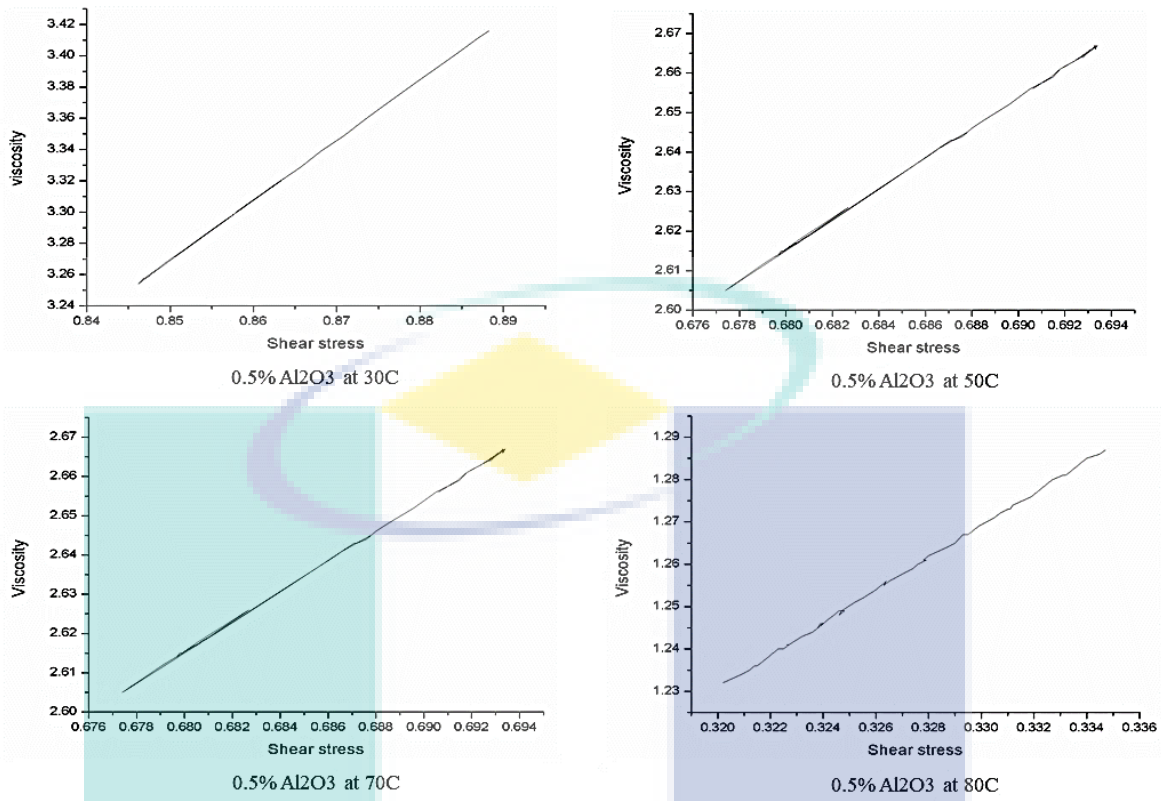
Viscosity behaviour of 0.5% Al$_2$O$_3$ nanofluid

0.1% CNC at 30C

0.1% CNC at 50C

0.1% CNC at 70C

0.1% CNC at 80C
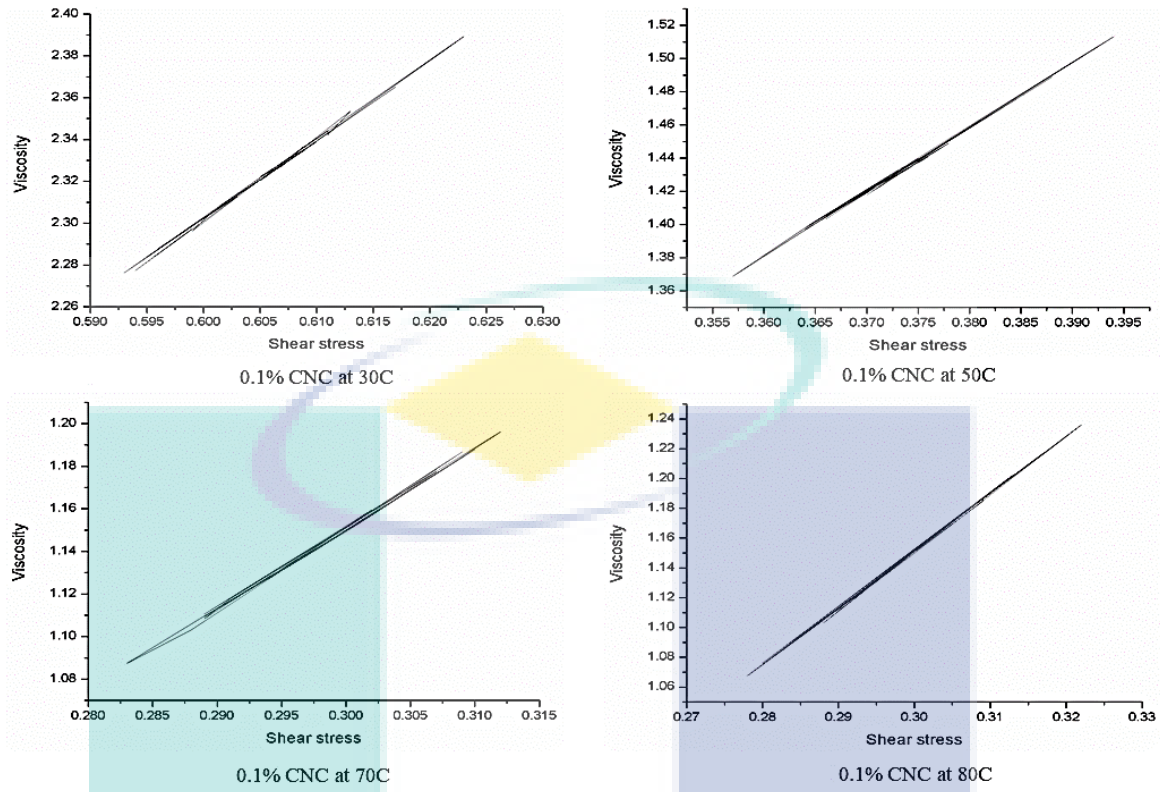
Viscosity behaviour of 0.1% CNC nanofluid
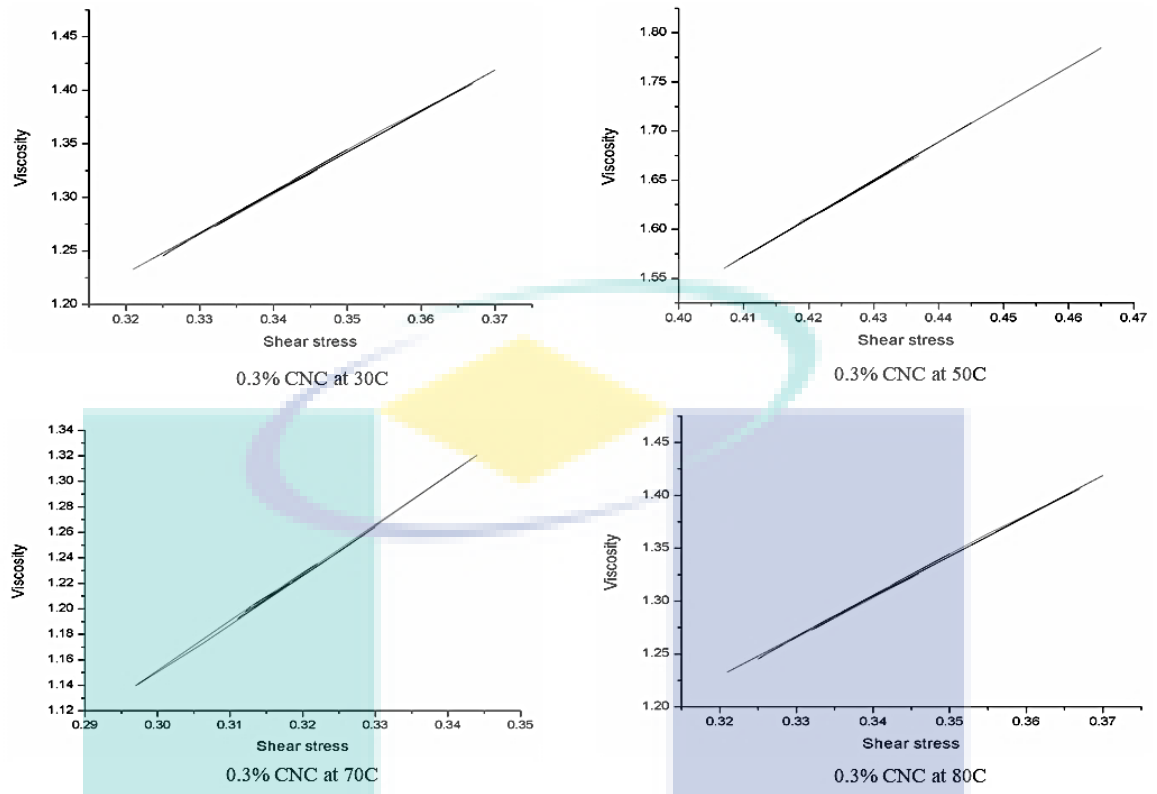
Viscosity behaviour of 0.3% CNC nanofluid

0.5% CNC at 30C

0.5% CNC at 50C

0.5% CNC at 70C

0.5% CNC at 80C
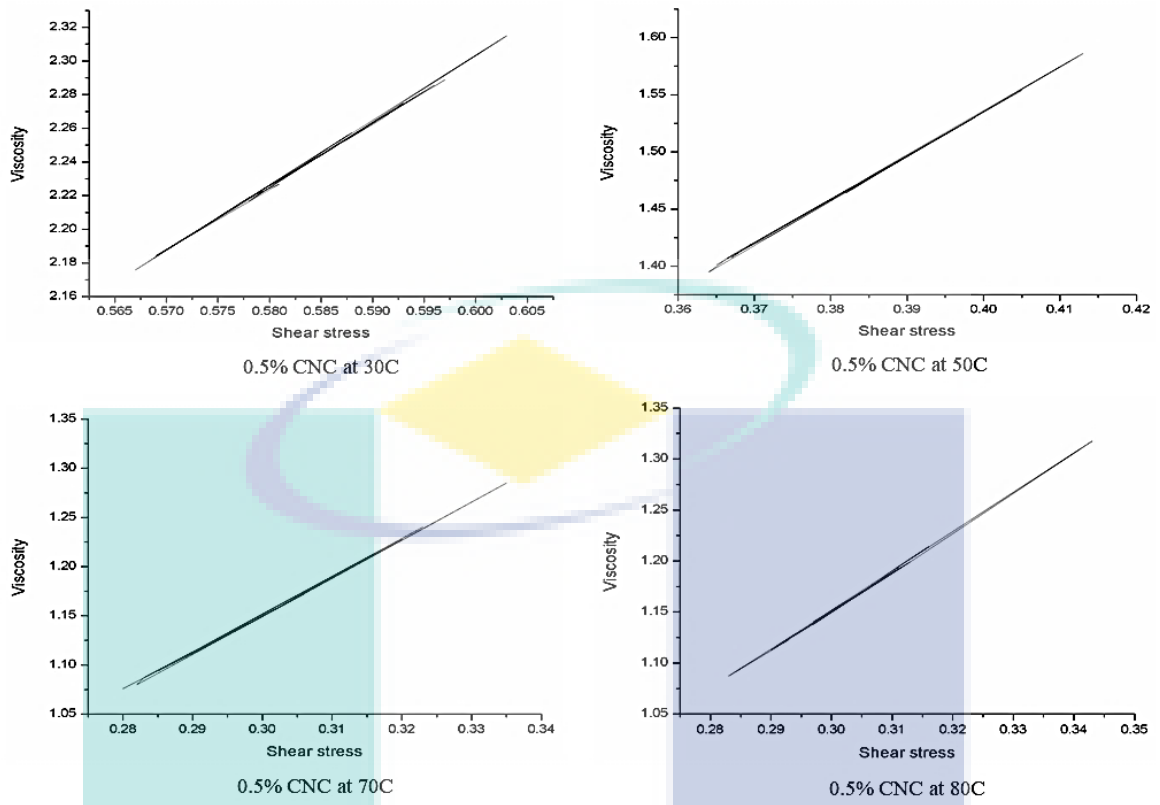
Viscosity behaviour of 0.5% CNC nanofluid

THERMAL CONDUCTIVITY

Experimental and ASHRAE Standard thermal conductivity (W/m-K) data of base fluid

Temperature (°C)	Base fluid	
	Experimental data	ASHRAE Standard data
30°C	0.407	0.412
50°C	0.433	0.425
70°C	0.463	0.434
80°C	0.452	0.438

Average thermal conductivity (W/m-K) of the base fluid and Al_2O_3 nanofluids at different temperature (°C).

Temperature (°C)	Base fluid	Volume concentration of Al_2O_3		
		0.1%	0.3%	0.5%
30°C	0.407	0.429	0.443	0.454
50°C	0.433	0.444	0.462	0.462
70°C	0.463	0.522	0.524	0.528
80°C	0.452	0.586	0.539	0.550

Average thermal conductivity (W/m-K) of the base fluid and CNC nanofluids at different temperature (°C).

Temperature (°C)	Base fluid	Volume concentration of CNC		
		0.1%	0.3%	0.5%
30°C	0.407	0.422	0.414	0.410
50°C	0.433	0.428	0.443	0.491
70°C	0.463	0.454	0.496	0.475
80°C	0.452	0.481	0.567	0.525

DYNAMIC VISCOSITY

Experimental and ASHRAE Standard viscosity (cP) data of base fluid

Temperature (°C)	Base fluid	
	Experimental data	ASHRAE Standard data
30°C	2.08	2.26
50°C	1.33	1.43
70°C	1.16	0.97
80°C	1.21	0.82

Average viscosity (cP) of the base fluid and Al_2O_3 nanofluids at different temperature (°C).

Temperature (°C)	Base fluid	Volume concentration of Al_2O_3		
		0.1%	0.3%	0.5%
30°C	2.08	2.99	3.24	3.27
50°C	1.33	2.04	2.13	2.65
70°C	1.16	1.96	1.52	1.86
80°C	1.21	1.46	1.48	1.27

Average viscosity (cP) of the base fluid and CNC nanofluids at different temperature (°C).

Temperature (°C)	Base fluid	Volume concentration of CNC		
		0.1%	0.3%	0.5%
30°C	2.08	2.32	2.58	2.23
50°C	1.33	1.43	1.64	1.46
70°C	1.16	1.14	1.17	1.15
80°C	1.21	1.14	1.32	1.17

SPECIFIC HEAT

Specific heat (J/(g-K)) of the base fluid and Al_2O_3 nanofluids at different temperatures (°C).

Temperature (°C)	Base fluid	Volume concentration of Al_2O_3		
		0.1%	0.3%	0.5%
30°C	0.83	0.73	0.11	-0.18
50°C	0.88	0.88	0.65	0.38
70°C	0.68	0.91	0.9	0.87
80°C	0.53	0.87	0.91	0.98

Specific heat (J/(g-K)) of the base fluid and CNC nanofluids at different temperatures (°C).

Temperature (°C)	Base fluid	Volume concentration of CNC		
		0.1%	0.3%	0.5%
30°C	0.83	-1.28	-1.26	-2.08
50°C	0.88	-1.16	-1.09	-1.91
70°C	0.68	-1.42	-1.42	-3.94
80°C	0.53	-1.61	-1.69	-5.29

DENSITY

Experimental and ASHRAE Standard density (g/m^3) data of base fluid

Temperature (ºC)	Base fluid	
	Experimental data	ASHRAE Standard data
30ºC	1.0505	1.05539
50ºC	1.0390	1.04535
70ºC	1.0217	1.03337
80ºC	1.0118	1.02665

Density (g/m^3) of the base fluid and Al$_2$O$_3$ nanofluids at different temperatures (ºC).

Temperature (ºC)	Base fluid	Volume concentration of Al$_2$O$_3$		
		0.1%	0.3%	0.5%
30ºC	1.0505	1.0492	1.0501	1.0517
50ºC	1.0390	1.0385	1.0392	1.0405
70ºC	1.0217	1.0250	1.0263	1.0269
80ºC	1.0118	1.0146	1.0094	1.0100

Density (g/m^3) of the base fluid and CNC nanofluids at different temperatures (ºC)

Temperature (ºC)	Base fluid	Volume concentration of CNC		
		0.1%	0.3%	0.5%
30ºC	1.0505	1.0509	1.0511	1.0506
50ºC	1.0390	1.0398	1.0399	1.0393
70ºC	1.0217	1.0241	1.0250	1.0260
80ºC	1.0118	1.0138	1.0157	1.0136

pH

The pH of the base fluid and Al$_2$O$_3$ nanofluids at different temperatures (ºC)

Temperature (ºC)	Base fluid	Volume concentration of Al$_2$O$_3$		
		0.1%	0.3%	0.5%
30ºC	6.9	3.4	3.8	3.3
50ºC	7.4	3.3	3.4	3.0
70ºC	6.5	3.2	3.2	2.8
80ºC	6.7	3.1	3.1	2.7

The pH of the base fluid and CNC nanofluids at different temperatures (ºC)

Temperature (ºC)	Base fluid	Volume concentration of CNC		
		0.1%	0.3%	0.5%
30ºC	6.9	6.6	6.9	7.1
50ºC	7.4	5.6	7.4	6.1
70ºC	6.5	5.7	5.7	6.9
80ºC	6.7	6.0	5.6	5.8

REYNOLDS NUMBER

List of Reynolds number of different fluids

Types of fluids	Temperature (ºC)	Reynolds number (Re)
Base fluid (W:EG 60:40)	30ºC	575.5
	50ºC	859.3
	70ºC	968.9
	80ºC	919.8
0.3% Al_2O_3	30ºC	356.5
	50ºC	366.7
	70ºC	742.7
	80ºC	750.2
0.5% Al_2O_3	30ºC	353.8
	50ºC	431.9
	70ºC	607.9
	80ºC	874.8
0.3% CNC	30ºC	448.1
	50ºC	677.5
	70ºC	963.7
	80ºC	846.4
0.5% CNC	30ºC	518.3
	50ºC	783
	70ºC	981.4
	80ºC	953

CONVECTION HEAT TRANSFER COEFFICIENT

Data of forced convection heat transfer coefficient of different fluids

Types of fluids	Heat flux, q (W/m^2)	Temperature difference (K)	Forced convection heat transfer coefficient, h (W/m^2-K)
0.3% Al_2O_3	830	4.26	194.835
0.5% Al_2O_3		3.37	246.29
0.3% CNC		2.79	297.49
0.5% CNC		4.98	166.67

ZETA POTENTIAL VALUE OF NANOFLUIDS

Zeta potential values of Al_2O_3 and CNC nanofluids

Volume concentrations	Al_2O_3	CNC
0.1%	27	-13.8
0.3%	36.1	-21.6
0.5%	33.6	-17.2

PRANDTL NUMBER

List of Prandtl number (predicted and experimental) of different fluids

Types of fluids	Temperature (ºC)	Predicted	Experimental
Base fluid	30	4.24	4.24
(W:EG 60:40)	50	2.70	2.70
	70	1.70	1.70
	80	1.41	1.42
0.3% Al_2O_3	30	0.805	0.805
	50	2.97	2.97
	70	2.61	2.55
	80	2.50	2.56
0.5% Al_2O_3	30	1.29	1.29
	50	2.18	2.18
	70	3.06	3.06
	80	2.26	2.62
0.3% CNC	30	7.85	7.85
	50	4.04	4.04
	70	3.35	3.35
	80	3.77	3.77
0.5% CNC	30	11.31	11.31
	50	5.67	5.68
	70	9.53	9.53
	80	11.79	11.79

PROPERTIES OF MATERIALS

List of properties of different materials (used as nanoparticles).

Properties	TiO_2	Solid CNC	Al_2O_3
Specific heat (J/kg-K)	692	1300	773
Density (kg/m^3)	4230	1050	3960
Thermal conductivity (W/m-k)	8.4	0.9	40
Viscosity (kg/m.s)	-	-	-

ELEMENTAL PROPORTION OF NANOPARTICLES

Elemental proportion of Al_2O_3 nanoparticles

Elements	60 µm		20 µm		10 µm	
	Weight%	Atomic%	Weight%	Atomic%	Weight%	Atomic%
O	53.85	59.53	43.21	53.80	49.49	59.73
Al	33.63	22.05	52.14	38.49	45.90	32.85

Elemental proportion of CNC nanoparticles

Elements	60 µm		20 µm		10 µm	
	Weight%	Atomic%	Weight%	Atomic%	Weight%	Atomic%
C	47.38	54.53	47.22	54.37	49.37	56.50
O	52.62	45.47	52.78	45.63	50.63	43.50

APPENDIX D
EXPERIMENTAL CALCULATION

MASS FLOW RATE

$$\dot{m} = \rho v A$$

$$v = \frac{Q}{A}$$

$$A = \frac{\pi D^2}{4}$$

Where,

$\dot{m}$ = ? = 0.0108 (kg/s)

ρ = Density of water = 998.2 (kg/m³)

v = Velocity =? = 0.088 (m/sec)

Q = Volume flow rate =0.00065 (m³/min) (for liquid)

A = Cross-sectional area of the tube =? = 0.000123 (m²)

D = Inside diameter of the tube = 0.0125 (m)

ENERGY GAIN

$$Q_u = \dot{m} \, C_p (T_{out} - T_{in})$$

Where,

Q_u = ? = 20.1096 (kW)

$\dot{m}$ = Mass flow rate =0.0108 (kg/s)

C_p = Specific heat of 0.5% Al_2O_3 at 80°C temperature = 980 (J/kg-K)

T_{out} = Outlet temperature = 45.1°C = 318.25 (K)

T_{in} = Inlet temperature = 43.2°C = 316.35 (K)

EFFICIENCY

$$\eta = \frac{Q_u}{I_t A_c}$$

Where,

$\eta = ? = 2.48\%$

Q_u = Energy gain = 20.1096 (kW)

I_t = Solar radiance = 830 (W/m^2)

A_c = Total surface area of the tubes = 0.97526 (m^2)

REYNOLDS NUMBER

$$R_e = \frac{\rho D v}{\mu}$$

Where,

$R_e = ? = 356.5$

ρ = Density of individual fluid; assume, 0.3% Al_2O_3 at 30°C temperature = 1050.1(kg/m^3)

D = Characteristics length = Inner diameter of the tube = 0.0125 (m)

v = Velocity = 0.088 (m/s)

μ = Dynamic viscosity of individual fluid; assume, 0.3% Al_2O_3 at 30°C temperature = 0.00324 (kg/m. s)

NUSSELT NUMBER

$$N_u = \frac{hL}{k}$$
$$h = \frac{q}{\Delta T}$$

Where,

N_u= ? = 8.98

h = ? = Force convection heat transfer coefficient of 0.3% CNC at 30ºC temperature = 297.49 (W/m²-K)

L = Characteristics length = Inner diameter of the tube = 0.0125 (m)

k = Thermal conductivity of individual fluid; assume 0.3% CNC at 30ºC temperature = 0.414 (W/m-K)

q = Heat flux = 830 (W/m²)

ΔT = Temperature difference between the solid surface and surrounding fluid area = (Avg. surface temperature – outlet temperature) = (320.74 – 317.95) (K) = 2.79 (K)

PRANDTL NUMBER

$$P_r = \frac{\mu C_p}{k}$$

Where,

P_r = ? = 1.29

μ = Dynamic viscosity of individual fluid; assume, 0.5% Al₂O₃ at 30ºC temperature = 0.00327 (kg/m. s)

C_p = Specific heat of individual fluid; assume, 0.5% Al₂O₃ at 30ºC temperature = 180 (J/kg-K)

k = Thermal conductivity of individual fluid; assume, 0.5% Al₂O₃ at 30ºC temperature = 0.454 (W/m-K)

AREA OF TUBES

The total surface area of tubes:

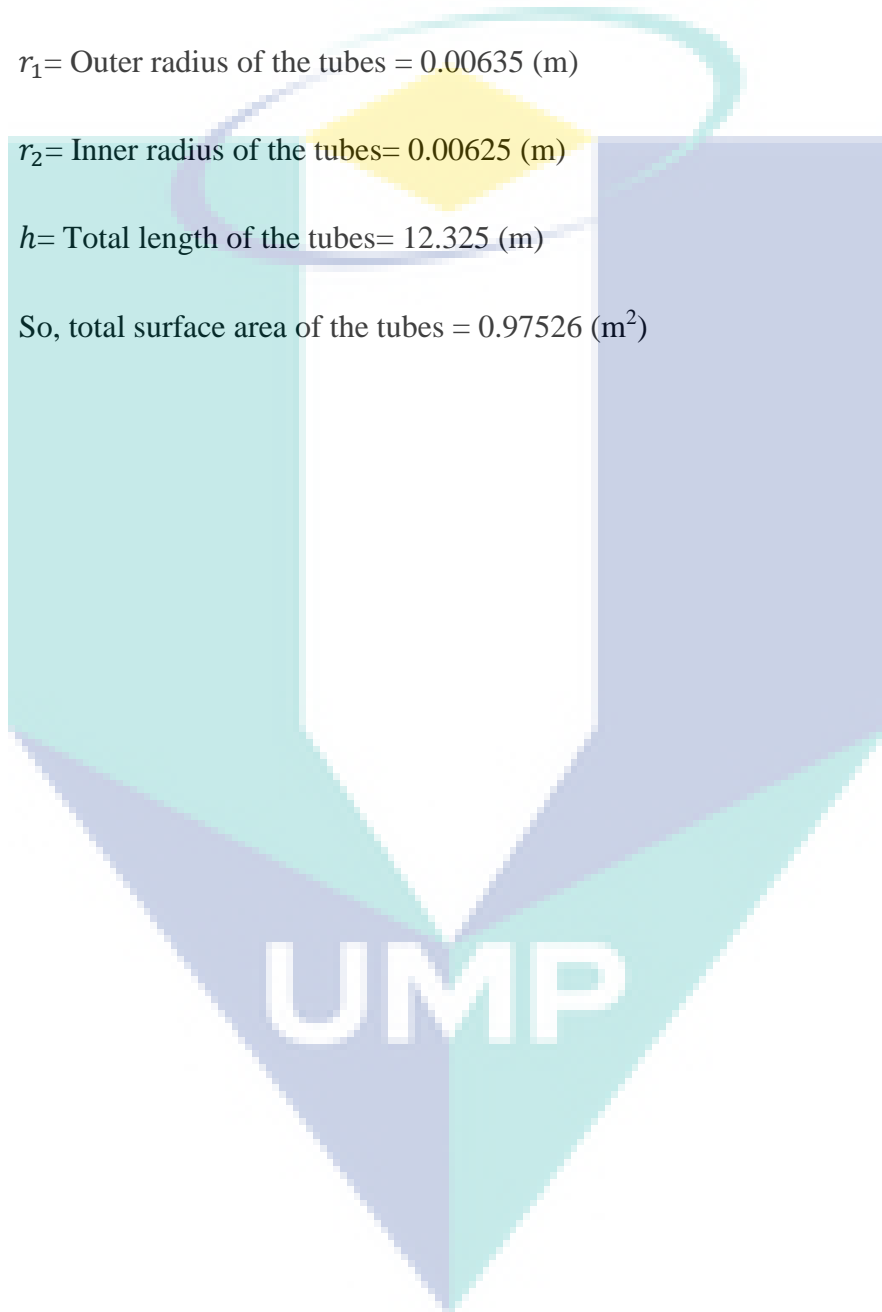$$2\pi[(r_1 + r_2)(r_2 - r_1 + h)]$$

Where,

r_1= Outer radius of the tubes = 0.00635 (m)

r_2= Inner radius of the tubes= 0.00625 (m)

h= Total length of the tubes= 12.325 (m)

So, total surface area of the tubes = 0.97526 (m^2)

APPENDIX E
LIST OF PUBLICATIONS

1. Improvement in the performance of solar collectors with nanofluids— A state-of-the-art review. Nano-Structures & Nano-Objects 18 (2019) 100276 (published).

2. Significance of Alumina in Nanofluid Technology – An Overview. Journal of Thermal Analysis and Calorimetry (2019), 26 April 2019, (published).

3. CFD modelling of different properties of nanofluids in header and riser tube of flat plate solar collector. Scopus, 2019 (published).

4. Internal energy analysis with nanofluids in header and riser tube of flat plate solar collector by CFD modelling. Scopus, 2019 (published).

5. Analysis of non-dimensional numbers of fluid flowing inside tubes of flat plate solar collector. Scopus, 2019 (accepted).

6. The present scenario of textile industry in Malaysia (under review).

7. Experimental studies on thermo-physical properties of nanocellulose–aqueous ethylene glycol nanofluids (under review).

8. Analysis of efficiency enhancement of flat plate solar collector using nanofluids (submitted).

9. Global textile industries, energy consumption, environmental impact and implementation of renewable energy resources (submitted).

10. Energy Crisis: Impact on textile industries in Bangladesh (submitted).

Improvement in the performance of solar collectors with nanofluids — A state-of-the-art review

K. Farhana [a,d], K. Kadirgama [a,b,c], M.M. Rahman [a], D. Ramasamy [a], M.M. Noor [a], G. Najafi [e,*],
M. Samykano [a], A.S.F. Mahamude [f]

[a] Faculty of Mechanical Engineering, Universiti Malaysia Pahang, 26600 Pekan, Pahang, Malaysia
[b] Center of Excellence for Advanced Research in Fluid Flow (CARIFF), Universiti Malaysia Pahang, 26600 Pekan, Pahang, Malaysia
[c] Department of Manufacturing and Materials Engineering, Faculty of Engineering, International Islamic University of Malaysia, Jalan Gombak,
Selangor Darul Ehsan, 50728 Kuala Lumpur, Malaysia
[d] Department of Apparel Manufacturing Engineering, Bangladesh University of Textiles, 92 Shaheed Tajuddin Ahmed Avenue, Tejgaon Industrial
Area, Dhaka 1208, Bangladesh
[e] Tarbiat Modares University, Tehran, Iran
[f] Faculty of Chemical & Natural Resources Engineering, Universiti Malaysia Pahang, 26300 Gambang, Pahang, Malaysia

GRAPHICAL ABSTRACT
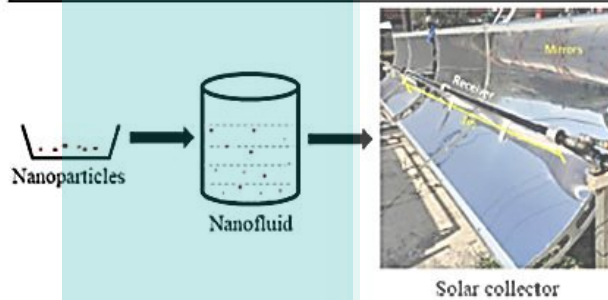
ARTICLE INFO

ABSTRACT

The upward energy demand along with the depletion of conventional energy sources demands improved utilization of renewable energy resources. Among many energy resources, solar energy is the most appropriate alternative to conventional energy sources owing to its inexhaustibility and green property. Solar collectors are the devices which convert the solar radiation into heat or energy. Solar collector's efficiency should be improved by nanofluids. The importance and significance of nanofluid on the performance of solar collectors especially on thermal properties are extensively described here.

Significance of alumina in nanofluid technology

An overview

K. Farhana[1] · K. Kadirgama[1] · M. M. Rahman[1] · M. M. Noor[1] · D. Ramasamy[1] · M. Samykano[1] ·
G. Najafi[2] · Nor Azwadi Che Sidik[3] · F. Tarlochan[4]

Abstract

Nanotechnology has emerged to be an essential aspect of science and technology. The growth of this field has been enormous specifically in the development of nanomaterials. Till date, numerous nanomaterials have been developed and designed to suit various applications from mechanical to biomedical. Among the developed nanomaterial, alumina (Al) has been subject of interest due to its notable chemical and physical properties. Specifically, in thermal properties, Al has been shown to have superior thermal conductivity, convective heat transfer coefficient and heat transfer coefficient properties. As such, Al has been utilized in different forms in various fields of applications and verified for its importance, significance and efficiency. Though it had shown outstanding results in the field engineering and sciences, their effect towards the environment and human health is yet to be explored extensively. The present paper aims to review the significance of Al nanoparticle addition in mono- and hybrid nanofluids. Also, this paper intends to provide the reader with an overview of the works that have been carried out using Al nanoparticles and their findings.

Keywords Alumina nanoparticle · Mono-nanofluid · Hybrid nanofluid · Thermal conductivity

List of symbols

TEM	Transmission electron microscopy	DC	Direct current
XRD	X-ray diffraction	nHTF	Nano-heat transfer fluid
SEM	Scanning electron microscopy	EG	Ethylene glycol
FESEM	Field emission scanning electron microscopy	CNT	Carbon nanotube
		MWCNT	Multi-walled carbon nanotube
		SWCNT	Single-walled carbon nanotube
CHF	Critical heat flux	NP	Nanoparticle

173

Internal energy analysis with nanofluids in header and riser tube of flat plate solar collector by CFD modelling

K Farhana [*1,3], A S F Mahamude [2], K Kadirgama [1], M M Rahman [1], M M Noor [1], D Ramasamy [1]

[1]Faculty of Mechanical Engineering, Universiti Malaysia Pahang, 26600 Pekan, Pahang, Malaysia
[2]Faculty of Chemical & Natural Resources Engineering, Universiti Malaysia Pahang, 26300 Gambang, Pahang, Malaysia
[3]Department of Apparel Manufacturing Engineering, Bangladesh University of Textiles, Dhaka 1208, Bangladesh

[*]Corresponding author: kanizfar7@gmail.com

Abstract. In this study, Computational Fluid Dynamics (CFD) modelling of internal energy with different nanofluids (TiO_2 and crystal nano cellulose) studied. The modelling was three dimensional under Viscous Laminar model. The base fluid for nanoparticles was 60% water+40% ethylene glycol along with individual water and ethylene glycol fluids. Volume fraction of nanofluids was 0.5% and single-phase model used. The diameter of inlet and outlet was fixed of individual model and three kinds of designing model used here. The diameter of both header and riser tubes varied whereas the number of tubes varied only for riser. The results revealed that diameter and number of tubes (riser) do not affect on the internal energy. Since internal energy only depends on different properties of the inside fluids.

1. Introduction

Solar energy is the most promising renewable energy due to its extensibility and abundant in nature. Negative impact and depletion of fossil fuels enslaved forcefully to realize alternative sources of energy [1, 2]. Green technology revolution has been trying to minimize these burning issues by implementing renewable energies in place of fossil energies. Academic and industrial enterprises participated to build

CFD modelling of different properties of nanofluids in header and riser tube of flat plate solar collector

K Farhana [1,3*], K Kadirgama[1], M M Noor[1], M M Rahman[1], D Ramasamy[1], and A S F Mahamude[2]

[1]Faculty of Mechanical Engineering, Universiti Malaysia Pahang, 26600 Pekan, Pahang, Malaysia
[2]Faculty of Chemical & Natural Resources Engineering, Universiti Malaysia Pahang, 26300 Gambang, Pahang, Malaysia
[3]Department of Apparel Manufacturing Engineering, Bangladesh University of Textiles, Dhaka 1208, Bangladesh

*Corresponding author: kanizfar7@gmail.com

Abstract. This paper aimed to evaluate the state of three different flow parameters of nanofluids and hybrid nanofluids flowing through inside header and riser tube of flat plate solar collector. This research work studied with Computational fluid dynamics (CFD) modelling method using nanofluids (Al_2O_3, TiO_2, ZnO) and hybrid nanofluids ($Al_2O_3+TiO_2$, TiO_2+ZnO, $ZnO + Al_2O_3$). The modelling was three dimensional under k-epsilon turbulence model, which was set with Standard and Standard Wall Functions. Besides, Absolute reference frame and calculative intensity percentage was fixed. The base fluid was water as well as volume fraction of nanofluids and hybrid nanofluids was 0.1%. Single-phase viscous model with energy equation used. Three types of design models (Model A, B and C) used with fixed inlet and outlet diameter. The number of header tubes fixed with two, but the number of riser tube varied such as two, seven and twelve. Maximum dynamic pressure increased in model B for both nanofluid and hybrid nanofluid of about 48% and 16% respectively. Velocity magnitude enhanced in maximal for both nanofluid and hybrid nanofluid in model B. Besides, highest turbulence kinetic energy achieved in model A (5.5%) for nanofluids and in model B (18%) for hybrid nanofluids. Model B perform better comparing with model A and model C.

MUCET2019 notification for paper 128

Dear K. Farhana

Thank you for your submission of the paper entitled "Analysis of Non-Dimensional Numbers of Fluid Flowing Inside Tubes of Flat Plate Solar Collector" (Paper ID: 128) to the 11th Malaysian Technical Universities Conference on Engineering and Technology 2019 (MUCET 2019). Based on reviewer's remarks, we are pleased to inform that your submission has been ACCEPTED CONDITIONALLY to be published in LNME subject to addressing the reviewers' comments and suggestions adequately. Please prepare the "Camera Ready Paper' according to the respective publisher's template that is available via the following link (http://bit.ly/MUCET2019_template). Reviewers comments are appended at the end of this notification email for your information and necessary action.